ISTANBUL TECHNICAL UNIVERSITY ★ GRADUATE SCHOOL

FUNCTIONAL ALKYNYL-LINKED MONO AND DOUBLE-DECKER METAL PHTHALOCYANINES FOR MULTI-DISCIPLINARY BIOLOGICAL AND PHOTOCONDUCTIVE APPLICATIONS

DOCTORATE THESIS

Javaria AFTAB

Department of Chemistry

Chemistry Programme

NOVEMBER 2022

ISTANBUL TECHNICAL UNIVERSITY ★ GRADUATE SCHOOL

FUNCTIONAL ALKYNYL-LINKED MONO AND DOUBLE-DECKER METAL PHTHALOCYANINES FOR MULTI-DISCIPLINARY BIOLOGICAL AND PHOTOCONDUCTIVE APPLICATIONS

DOCTORATE THESIS

Javaria AFTAB
(509182274)

Department of Chemistry

Chemistry Programme

Thesis Advisor: Prof. Dr. Zehra ALTUNTAŞ BAYIR

NOVEMBER 2022

ISTANBUL TEKNİK ÜNİVERSİTESİ ★ LİSANSÜSTÜ EĞİTİM ENSTİTÜSÜ

FARKLI BİYOLOJİK VE FOTO İLETKEN UYGULAMALARI İÇİN FONKSİYONEL ALKİNİL GRUPLARI İÇEREN MONO VE SANDVİÇ METALLİ FTALOSİYANİNLER

DOKTORA TEZİ

Javaria AFTAB
(509182274)

Kimya Anabilim Dalı

Kimya Programı

Tez Danışmanı: Prof. Dr. Zehra ALTUNTAŞ BAYIR

KASIM 2022

Javaria AFTAB, a Ph.D. student of ITU Graduate School student ID 509182274, successfully defended the thesis entitled "FUNCTIONAL ALKYNYL-LINKED MONO AND DOUBLE-DECKER METAL PHTHALOCYANINES FOR MULTI-DISCIPLINARY BIOLOGICAL AND PHOTOCONDUCTIVE APPLICATIONS", which she prepared after fulfilling the requirements specified in the associated legislations, before the jury whose signatures are below.

Thesis Advisor :	**Prof. Dr. Zehra ALTUNTAŞ BAYIR** Istanbul Technical University	.....
Jury Members :	**Prof. Dr. Ayfer KALKAN BURAT** Istanbul Technical University	.....
	Prof. Dr. Esin HAMURYUDAN Istanbul Technical University	.....
	Prof. Dr. Atıf KOCA Marmara University	.....
	Prof. Dr. Yasemin KURT Istanbul University-Cerrahpaşsa	.....

Date of Submission : 22.08.2022
Date of Defense : 04.11.2022

To my spouse and son,

FOREWORD

I would like to express my sincere appreciation to my Chief Supervisor, Prof. Dr. Zehra ALTUNTAŞ BAYIR, for her constant guidance and encouragement throughout my work. For her constant support, I am utterly grateful.

I would like to express my heartful gratitude to Dr. Nazli FARAJZADEH. Without her motivation, support and help, the successful completion of this work would not have been possible. It was a great chance to work with her extraordinary and calm personality with a positive energy. Also, I want to thank Assoc. Prof. Dr. Yasemin YENILMEZ for her gracious help and guidance throughout my thesis work.

This thesis study was supported by the Scientific and Technological Research Council of Turkey TÜBİTAK 118Z731 under the title of: "Foto Transistör Uygulamaları İçin Yakın Infrared Bölgede De Absorpsiyon Bandına Sahip Ftalosiyaninlerin Sentezi ve Karakterizasyonu" and T.C. İstanbul Teknik Üniversitesi Bilimsel Araştırma Projeleri Koordinasyon Birimi TDK-2021-42932 with the title: "Sübstituye Ftalosiyaninlerin Sentezi ve Özelliklerinin İncelenmesi".

Finally, I would like to thank my husband (Asst. Prof. Dr. Jawad RASHEED) and son (Muhammad Jasim RASHEED) for being my love and moral support the whole time.

August 2022

Javaria AFTAB
(Chemist)

TABLE OF CONTENTS

Page

ABBREVIATIONS

^{13}C-NMR **:** Carbon-13 nuclear magnetic resonance
^{1}H-NMR **:** Proton nuclear magnetic resonance
ALD **:** Atomic layer deposition
AuNPs **:** Gold nanoparticles
CV **:** Crystal violet
CVD : Chemical vapor deposition
DBU **:** 1,8-Diazabicyclo(5.4.0)undec-7-ene
DCM **:** Dichloromethane
DMAE **:** Dimethylaminoethanol
DMF **:** Dimethylformamide
DMSO **:** Dimethylsulfoxide
DNA **:** Deoxyribonucleic acid
DPPH **:** 2,2-diphenyl-1-picrylhydrazyl
EtOH **:** Ethyl alcohol
FT-IR **:** Fourier transform infrared spectroscopy
GQDs **:** Graphene quantum dots
H_2Pc **:** Metal-free phthalocyanine
HOMO **:** Highest occupied molecular orbital
IR **:** Infrared spectroscopy
LSPR **:** Localized surface plasmon resonance
LUMO **:** Lowest unoccupied molecular orbital
MALDI-TOF: Matrix-assisted laser desorption ionization time-of-flight
MeOH **:** Methyl alcohol
MIC **:** Minimum inhibition concentration
MNPs **:** Metal nanoparticles
M.P. **:** Melting point
MPc **:** Metal Phthalocyanine
NPs **:** Nanoparticles
NLO **:** Non-linear optics
OAc **:** Acetate

OFET **:** Organic field-effect transistors

PDT **:** Photodynamic therapy

Pc **:** Phthalocyanine

Pcs **:** Phthalocyanines

PS **:** Photosensitizer

PSs **:** Photosensitizers

ROS **:** Reactive oxygen species

Sub-PC **:** Sub-phthalocyanine

Super-Pc **:** Super-phthalocyanine

THF **:** Tetrahydrofuran

TLC **:** Thin layer chromatography

UV-Vis **:** Ultraviolet-visible spectrophotometry

SYMBOLS

A	**:** Current
V	**:** Voltage
Ω	**:** Impedance (resistance)
ε	**:** Molar absorptivity
I_{DS}	**:** Drain-Source current
V_{DS}	**:** Drain-Source voltage
V_{GS}	**:** Gate-Source voltage

LIST OF TABLES

Page

LIST OF FIGURES

Page

FUNCTIONAL ALKYNYL-LINKED MONO AND DOUBLE-DECKER METAL PHTHALOCYANINES FOR MULTI-DISCIPLINARY BIOLOGICAL AND PHOTOCONDUCTIVE APPLICATIONS

SUMMARY

Phthalocyanines (Pcs) and their metal correlatives (MPcs) have attained great significance lately because of the unique, planar and stable structural arrangement, optical, electronic and catalytic aspects they hold. Traditionally, phthalocyanine macrocycles were demanded as pigments and dyestuff, but they have found wide usage in different scientific and technological fields such as catalysis, liquid crystals, chemical sensors, photodynamic therapy, solar energy conversion, phototransistor, OFET and various biological applications in recent times. High redox character of metal phthalocyanines (MPcs) is a principal behind their extraordinary performance for these functions. All these features can be altered simply by modifying metal centers or side chains. More recently, much research have been done to analyze the antioxidant, antimicrobial, microbial DNA cleavage and enzyme inhibition activities of MPcs molecules conjugated with nanoparticles. In this essence, MPcs/ nanoparticle hybrids to attain high antimicrobial activity has become important in view of extensive consumption of man-made antibiotic medications following to subsequent drug resistance.

In order to attain good results in all the above mentioned applications, attaining a good solubility in a wide range of organic solvents for phthalocyanines is a crucial stage. Limitations in high solubility arises due to the π stacking (clustering) between planar macrocycles. Therefore, unsubstituted phthalocyanines are insoluble or poorly soluble in organic solvents and water, prohibiting their application areas. Substitution at peripheral or axial sites of macrocycles increases the distance between their 18π-electron conjugated systems. Thus aggregation reduces and an increased solubility in various solvents is observed tending to improve their optical properties. Insertion of large side groups and longer alkyl chains helps enhancing the solubility and thus the optical properties of phthalocyanines. For gaining proper solubility and substantiality in MPcs, the terminal alkynyl group (C≡C) serves as an exemplary substituent and is known to provide excellent rigidity and significance in many optical related properties.

In the span of this thesis work, 15 phthalocyanine compounds were prepared out of which four are asymmetrical, 5 symmetrical peripherally tetra-substituted and 6 are symmetrical peripherally octa-substituted metal phthalocyanines. These synthesized compounds were investigated for their potential use in photoconductive and biological applications. For this purpose, the phthalonitriles synthesized in this study for subsequent MPc substitution are; 4-(thiophen-3-ylethynyl) phthalonitrile **(2)**, 4-[(4-pentylphenyl)ethynyl] phthalonitrile **(3)**, of 4-{[4-(N,N-Dimethylamino)phenyl]ethynyl}phthalonitrile **(5)**, Synthesis of 4,5-bis{[3,5 bis(trifluoromethyl)phenyl]ethynyl}phthalonitrile **(6)** and 4,5-bis((4-(dimethylamino)phenyl)ethynyl)phthalonitrile **(7)**.

For asymmetrical MPcs preparation, 4-(thiophen-3-ylethynyl) phthalonitrile **(2)** and 4-[(4-pentylphenyl)ethynyl] phthalonitrile **(3)** were reacted in statistical condensation fashion with 1,2-Dicyano-3,4,5,6-tetrafluorobenzene to attain A_3B type push-pull type asymmetrical tetra-substituted Co and Zn MPcs. Latterly, symmetrical peripherally tetra-substituted MPcs (M= Co, Zn, Mn, Fe and Lu) were shaped from the prepared phthalonitrile derivative **(5)**. Whereas, from the phthalonitriles **(6)** and **(7)** symmetrical peripherally octa-substituted phthalocyanines were gathered containing Co, Zn and Lu metal ions. To attain high purity of all the newly synthesized phthalonitrile derivatives and related phthalocyanines, they were subjected to thin layer, preparative and column chromatography. Furthermore, all of their structures were examined through distinct spectroscopic techniques such as FT-IR, NMR, MALDI-TOF and UV-vis spectroscopy.

Electronic UV-vis spectra of the newly synthesized symmetrical phthalocyanines were reported in DMSO and THF solvent while for asymmetrical MPcs only THF was employed. Moreover, the effect of concentration and type of solvent (THF) on the spectral and aggregating properties of newly synthesized **PcOFLu** was investigated, as well.

Photovoltaic cells consisting of ITO/PEDOT:PSS/Pc/Ag layers were designed from synthesized asymmetric phthalocyanines of phtahlonitrile **(2)** and **(3)** for photoconductive analysis are also a part of this thesis study.

Phthalonitriles **(5)** and **(7)** and their respective Co and Zn MPcs were subjected to conjugation with gold nano particles (AuNPs) and assessed through the TEM analysis to elucidate the size and shape of these hybrid particles. All the synthesized MPc/AuNP hybrids, phthalonitrile **(5)** & **(7)** along with their related Co and Zn Pcs and AuNPs were analyzed for several biological studies including, anti-oxidant activity, biofilm inhibition, anti- microbial activity, microbial cell viability inhibition and DNA cleavage activity. All these studies concluded that using the MPc/AuNP hybrids for these biological applications gave better results for all the above mentioned biological applications rather than employing AuNPs alone.

FARKLI BİOLOJİK VE FOTO İLETKEN UYGULAMALARI İÇİN FONKSİYONEL ALKİNİL GRUPLARI İÇEREN MONO VE SANDVİÇ METALLİ FTALOSİYANİNLER

ÖZET

Ftalosiyaninler (Pcs) yeşil/mavi renkli bileşikler; ilk olarak 1907'de mavi renkli bir yan ürün olarak elde edilmiştir. 1930'da, Linstead ve çalışma arkadaşları tarafından yürütülen araştırmalar, bu bileşiğin yapısal özelliklerini ortaya çıkardı. Genel olarak ftalosiyaninler, 18 π-elektronik sistemler taşıyan tetrapirol makrosiklik bileşiklerle ve 1 ve 3 pozisyonundaki aza köprüleri aracılığıyla konjuge dört izoindol üniteden oluşmuşlar.

Bu olağanüstü nitelikler ve yüksek konjugasyon, kimyasal ve termal değişikliklere karşı dirençli kılar. Ftalosiyaninler sentetik olarak sentezlenmiş yapılardır ve doğal olarak bulunmazlar.

Ftalosiyaninler pigment ve boyar madde olarak kullanılr. Son yıllarda kataliz, sıvı kristaller, kimyasal sensörler, fotodinamik terapi, güneş enerjisi dönüşümü, fototransistör, OFET ve biyolojik uygulamalar gibi farklı bilimsel ve teknolojik alanlarda kullanım potansiyelleri araştırlmaktadır.

Halka boşlukları metal iyonları içerebilir ve yaklaşık 70 metal ile kararlı kompleksler oluşturabilirler.

Ftalik anhidrit, ftalonitril, diiminoizoindolin, ftalimid ve ftalik asit, Pc sentezi için uygun öncü olarak kullanmaktadır. Ayrıca, metal içermeyen ftalosiyanin molekülünün merkezindeki iki hidrojen atomunun çeşitli metal iyonu ile yer değiştirmesi metal ftalosiyaninlerin sentezine yol açabilir.

Ftalosiyaninler UV-vis spektroskopisinde gözlenen Q ve B bantları sayesinde kolaylıkla karakterize edilebilir. Genellikle bu bantlar, Q bandı için 600-700 nm ve B bandı için 300-400 nm aralığında görünür.

Aynı substituye ftalonitrilin siklotetramerizasyonundan simetrik ftalosiyaninler elde edilirken, farklı sübstitüentler içeren ftalosiyaninler asimetrik bileşikler olarak tanımlanır. Simetrik Pc'lerin sentezi için, siklotetramerizasyon yoluyla, yani metal iyonunun şablon etkisi ile uyumlu olarak yürütülürken, asimetik ftalosiyaninler genellikle istatistiksel yoğunlaştırma, subftalosiyanin veya polimer destekli yöntemi kullanılarak elde edilir.

Metal ftalosiyaninlerin yüksek redoks karakteri, çeşitli işlevler için olağanüstü performanslarına neden olur. Tüm bu MPc özellikleri, metal merkezler ve/veya yan zincirler değiştirilerek kolaylıkla değiştirilebilir. Son yıllarda araştırmacılar, nanopartiküller ile kojuge edilmiş MPcs moleküllerinin antioksidan, antimikrobiyal, mikrobiyal DNA parçalanması ve enzim inhibisyon aktivitelerini de incelemişler.

Yüksek antimikrobiyal aktivite elde etmek için MPcs/nanopartikül hibritleri, ilaç direncine neden olan sentetik antibiyotik ilaçların yoğun tüketimi nedeniyle önemli

hale gelmiştir.

Yukarıda bahsedilen tüm uygulamalarda iyi sonuçlar elde etmek için, ftalosiyaninlerin çeşitli organik çözücülerde çözünürlüğünün iyi olması gerekiyor. Yüksek çözünürlükteki sınırlamalar, düzlemsel makro döngüler arasındaki π yığını (kümelenme) nedeniyle ortaya çıkar. Bu nedenle sübstitüe edilmemiş ftalosiyaninler, organik çözücüler ve su içinde çözünmezler veya az çözünürler, bu da kullanım alanlarını engeller. Makrosiklerin çevresel substituentler veya eksenel bölgelerindeki ligantlar, 18π elektronlu konjuge sistemleri arasındaki mesafeyi arttırır. Böylece topaklaşma azalır ve optik özelliklerini iyileştirme eğiliminde olan çeşitli çözücülerde artan bir çözünürlük gözlenir. Hacimli yan grupların ve uzun alkil zincirlerinin eklenmesi, çözünürlüğün ve dolayısıyla ftalosiyaninlerin optik özelliklerinin arttırılmasına yardımcı olur.

MPcs'de iyi çözünürlük ve stabilite elde etmek için, terminal alkinil grubu (C≡C) substituye edilir. Alkinil grupları içeren MPc'ler için mükemmel optiksel özellikler gözlenmiştir. Sonogashira çapraz bağlama reaksiyonunun uygun koşallarından dolayı, MPc'nin alkilasyonu rahatlıkla yapılır.

Flor atomu periyodik tablodaki tüm elementler arasında en yüksek elektronegatifliğe sahiptir. Ftalosiyanin üzerinde flor içeren grupların substituye edilmesi, florlu Pc'nin dikkate değer elektron transferi, manyetik ve ışığa duyarlı özellikleri ile sonuçlanır. Ayrıca, flor içeren Pc'ler yüksek termal direnç, kimyasal kararlılık ve daha iyi çözünürlük gösterir. Bu bileşiklerin sentezi, çeşitli uygulamalar için malzemelerin geliştirilmesine yardımcı olabilir.

Bu tez kapsamında, asimetrik, simetrik tetra-sübstitüe ve okta-sübstitüe simetrik metal ftalosiyanin olmak üzere 15 ftalosiyanin bileşikleri hazırlanmıştır. Sentezlenen bu bileşiklerin fotoiletkenlik ve biyolojik özellikleri araştırıldı. Bu amaçla, çalışmada 4-(tiyofen-3-iletinil)ftalonitril **(2)**, 4-[(4-pentilfenil)etinil] ftalonitril **(3)**, of 4-{[4-(N,N-Dimetilamino)fenil]etinil}ftalonitril **(5)**, 4,5-bis{[3,5 bis(triflorometil)fenil]etinil}ftalonitril **(6)** ve 4,5-bis((4-(dimetilamino)fenil)etinil)ftalonitril **(7**) sentezlenip metal eşliğinde siklotetramerizasyon ile hedeflenen metal ftalosiyaninler hazırlandı.

Asimetrik MPcs sentezi için 4-(tiyofen-3-iletinil) ftalonitril **(2)** ve 4-[(4-pentilfenil)etinil] ftalonitril **(3)**, 1,2-Dicyano-3,4,5, 6-tetraflorobenzen ile istatistiksel kondenzasyon yöntemiyle sentezlendi. A_3B tipi asimetrik tetra sübstitüe Co ve Zn ftalosiyaninler elde edildi.

Son olarak hazırlanan ftalonitril türevinden **(5)** simetrik periferik tetra-sübstitüe MPcs (M= Co, Zn, Mn, Fe ve Lu) sentezlendi. **(6)** ve **(7)** nolu ftalonitrillerden simetrik periferik okta substituye Co, Zn ve Lu ftalosiyaninler sentezlendi. Yeni sentezlenen tüm ftalonitril türevleri ve ilgili ftalosiyaninlerin yüksek saflığını elde etmek için ince tabaka ve kolon kromatografisine tabi tutuldular. Ayrıca tüm yapıları çeşitli spektroskopik yöntemlerle (FT-IR, NMR, MALDI-TOF ve UV-vis) incelendi.

Yeni sentezlenen simetrik ftalosiyaninlerin elektronik spektrumları DMSO ve THF solventinde rapor edilirken, asimetrik MPcs THF içinde UV-vis spektrometresi kullanılarak oda sıcaklığında incelendi. Ayrıca, konsantrasyonun ve çözücünün PcOF'nin spektral ve agregasyon özelliklerine etkisi araştırıldı.

(2) ve **(3)** nolu ftalonitrillerden sentezlenmiş asimetrik ftalosiyaninler kullanılarak ITO/PEDOT:PSS/Pc/Ag katmanlar oluşturuldu ve elde edilen fotovoltaik hücreler fotoiletkenlik analizi için kullanıldı.

(5) ve **(7)** nolu ftalonitriller ve bunların ilgili Co ve Zn Pc'leri altın nano partiküller (AuNP'ler) ile kojugasyona tabi tutuldu ve bu partiküllerin boyut ve şeklini TEM analizi ile değerlendirildi. Sentezlenen tüm MPc/AuNP hibritleri, **(5)** ve **(7)** nolu ftalonitrillerden oluşan simetrik Co ve Zn ftalosiyanin/altın nanohibritlei, antioksidan aktivite, biyofilm inhibisyonu, antimikrobiyal aktivite, mikrobiyal hücre canlılığı inhibisyonu ve DNA klevaj aktivitesi dahil olmak üzere çeşitli biyolojik özellikleri incelendi. AuNP'lerin metal ftalosiyaninler ile modifakasyonu altın nanopartiküllerin biyolojik özelliklerini iyileştirdi.

1. INTRODUCTION

1.1 General Properties of Phthalocyanines

Phthalocyanine (Pc), is an extraordinary transition metal macrocyclic complex that belongs to a highly planar and symmetrical class of tetrapyrrolic compounds. This remarkable macrocycle is composed of four imino-isoindoline units conjugated via nitrogen bridges (Figure 1.1). Furthermore, it has 18 π aromatic delocalized cloud system that provides thermal and chemical flexibility and stability to these metallized organic heterocycles. A wide range of incredible applications of these macrocycles in material sciences is from this electronic delocalization ability.

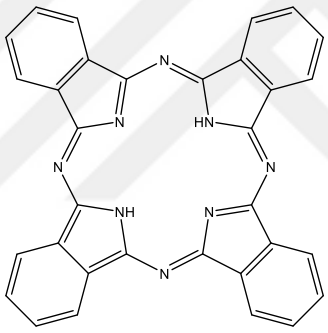

Figure 1.1: Typical phthalocyanine structure.

The Greek origin of phthalocyanine mean naphtha (rock oil); cyanine (dark blue) had been given in 1933 by Professor Linstead as he explained this category of organic compounds (Nalwa, 2001).

First ever synthesis of Pc was an accidental discovery in 1907 (metal-free Pc) and 1927 (copper Pc) during the chemical reactions of some ortho-(1,2)-substituted benzene derivatives (Figure 1.2) ((Braun & Tcherniac, 1907; Soppok, 1979; Thomas, 1990).

The real structure of phthalocyanines, coincidently discovered became certain between 1933 and 1940 as a result of Linstead's investigations in 1929 and later Robertson's X-ray studies (Bekaroğlu, 2001). Commercial production of phthalocyanines has been started since 1934. Addition of numerous substituents to the peripheral and non-peripheral sites of phthalocyanines, several outstanding properties could be attained.

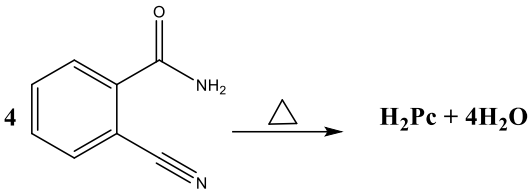

Figure 1.2: Production of metal-free phthalocyanine during ortho-cyanobenzamide synthesis.

1.2 Structural Properties of Phthalocyanines

Phthalocyanines are 16-membered (8 carbon and 8 nitrogen atoms) macrocyclic compounds with an exceptionally stabilized 18 π-electron system, bivalent best-known derivatives of tetraazaporphyrins (Figure 1.3).The macrocyclic structure of phthalocyanines is very much alike porphyrin derivatives and their close analogues, porphyrazine and tetrabenzoporphyrins (Figure 1.4) (K. Kadish et al., 2000).

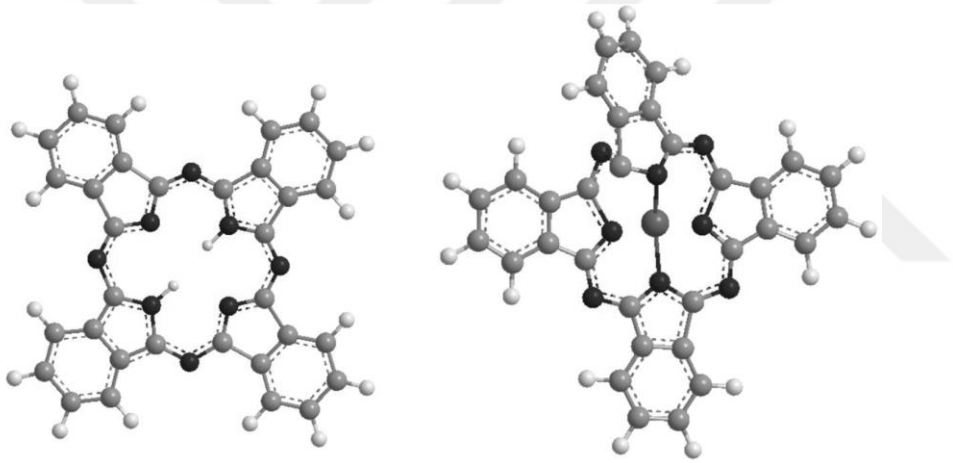

Figure 1.3: Structure of metal and metal-free phthalocyanine.

Even though phthalocyanines fundamental structure is very much like the porphyrins, they are not found naturally like hemoglobin, chlorophyll A and vitamin B12, they are completely synthetic products. The structural difference between Pc and porphyrin is that the nitrogen atoms in the meso position change the bond angles. The bonds forming the 16-membered inner macro ring are shorter than the bonds in porphyrin, that is, the bridge over the meso-nitrogen atoms significantly reduced the bonds (Moser & Thomas, 1983). Two H- atoms situated in the central chamber of phthalocyanine macrocycle could be interchanged by nearly all the available metal cations, thus metallized phthalocyanine derivative are synthesized. Today, nearly 70 metal cations have been placed in metal phthalocyanines.

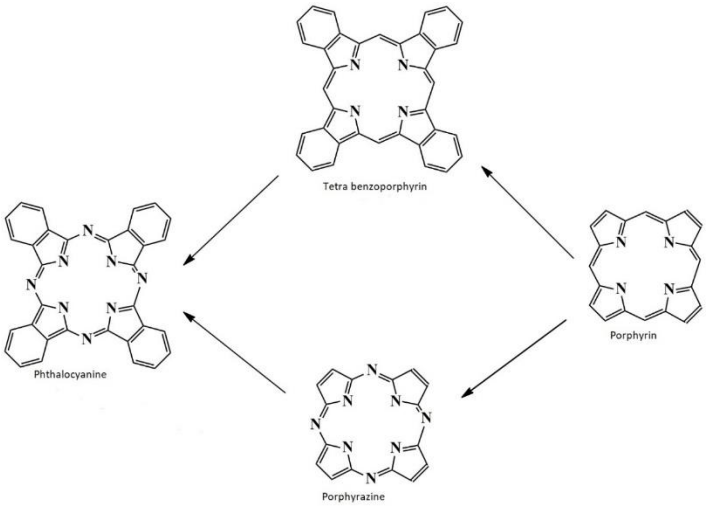

Figure 1.4: Analogues of pthalocyanine.

Phthalocyanine macrocycles generally form square-plane complexes with a coordination number of four. They can also form square pyramid or octahedral structures with metal cations that prefer high coordination numbers. Phthalocyanine compounds are highly coordinated with rare earth elements, actinides and can also form complexes in sandwiched form double-decker (Pc_2M) or triple-decker (Pc_3M_2) manner. (Figure 1.5) (Gao et al., 2009; Geyer et al., 1996; M. B. Koçak et al., 2003). Few actinide phthalocyanines have been synthesized due to their radioactive nature and difficulty in obtaining them. The sandwich-structured Pcs have significance as electrochromic and organic semiconductors (Day et al., 1975).

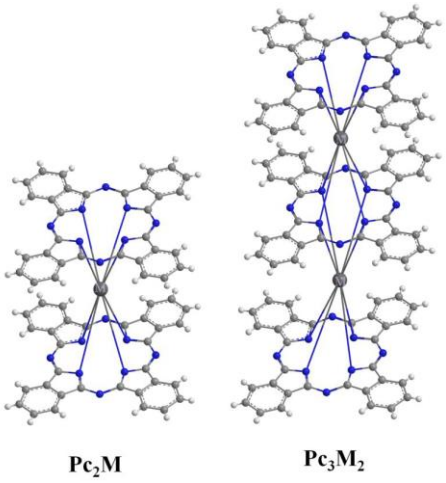

Figure 1.5: Double and triple decker Pc.

In addition to phthalocyanines consisting of four isoindole units, there are also sub-phthalocyanines (SubPc) consisting of a boron cation and three isoindole units

attached to it, and superphthalocyanines (SuperPc) consisting of a uranium cation and five isoindole units attached to it in the center (Figure 1.6). Sub-phthalocyanines have delocalized 14π-electrons while superphthalocyanines are conjugated macrocycles with 22π-electrons. While the metal-nitrogen bond length is approximately 1.85-2.05 ºA in most phthalocyanines, the uranyl-nitrogen bond length is approximately 2.5-2.6 ºA in superphthalocyanines (Day et al., 1975; Marks & Stojakovic, 1978).

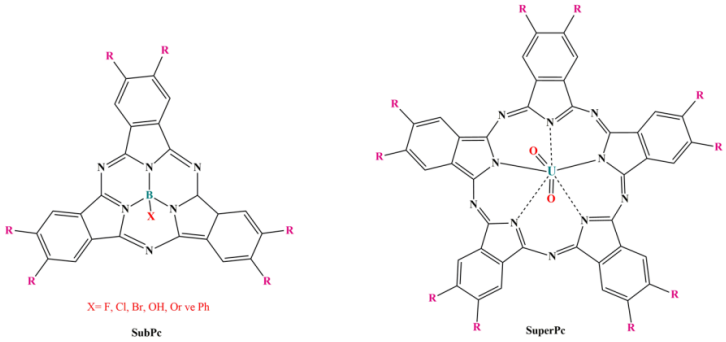

Figure 1.6: Sub and super- phthalocyanine.

1.3 Physical and Chemical Properties of Phthalocyanines

Metallic phthalocyanines containing metal cations (such as Zn, Pt, Cu, Co) with +2 oxidation state as the central atom are generally found in a square planar structure, having D4h symmetry, and have four coordination numbers. Phthalocyanines containing metals with an oxidation state greater than +2 (such as Ga, Sn and In), the central atom can coordinate with one or two axial ligands (such as acetate, pyridine, chlorine, alkyl, aryl or water, etc.). Thus, structures with square pyramid and octahedral geometry are formed (Figure 1.7) (Templeton et al., 1971).

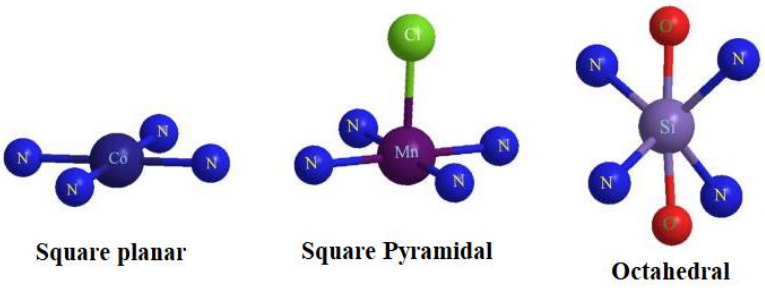

Figure 1.7: Possible molecular geometries of the metal phthalocyanine molecule.

High stability and color are the two most important physical properties of phthalocyanine compounds. The color of most phthalocyanines varies from blue to green, according to their chemical and crystalline arrangements. For instance, copper

phthalocyanine complex changes from bluish to greenish color as the number of substituted Cl-atoms starts to increase.

MPc's central atom has a great impact on the chemical features of phthalocyanines. The molecule is stable if the diameter of the metal cation corresponds to the diameter of the phthalocyanine core. Transition metals with ionic radii of 0.7 and 0.8 °A and +2 oxidation states can sit in the space in the middle of the phthalocyanine molecule. When the metal cation's diameter gets smaller or greater than gap diameter of 1.35 °A, the metal cations are easily separated from the phthalocyanine nucleus. This is the case for the Pb^{2+} cation with an ionic radius of 1.75 °A, the metal goes outside the macrocyclic plane (Gürek, 1996; C. C. Leznoff & Lever, 1989; Mckeown, 1998).

Metallic phthalocyanine compounds are divided into two types; covalent and electrovalent. Phthalocyanines containing alkali and alkaline earth metals are called electrovalent phthalocyanines and are generally soluble in organic solvents. When treated with dilute inorganic acids, aqueous alcohol and water, the metal ion is easily separated to obtain metal-free phthalocyanine. Unlike other metallic phthalocyanines, lithium phthalocyanine dissolves in alcohol at room temperature and when reacted with other metal salts, a new metallized phthalocyanine is obtained by replacing the cation of the salt with lithium (Birsöz, 2013). The covalent type phthalocyanine complexes are more stable as compared to the electrovalent ones, due to their strong bond with the metal in their structure. It is difficult to remove the metal in the ring by treating such phthalocyanine complexes with acids (C. C. Leznoff & Lever, 1989). They are partially soluble in solvents such as quinoline and chlornaphthalene

The solubility of phthalocyanine derivatives without substituents in organic solvents and water is low. This is due to the fact that Pc molecules cluster easily due to their bulky and planar structure. The substitution of the peripheral positions of the macro ring with long alkyl chains or bulky groups or the addition of axial ligands to the central atom increases the distance between the macrocyclic layers, prevents aggregation, and thus the dissolution of Pcs in organic solvents can be enhanced (Duruk et al., 2015; Kurt, Koca, et al., 2015; Kurt, Özçeşmeci, et al., 2015; Ma et al., 2007; Nar et al., 2018).

Similarly, by adding sulfonic acid, carboxylic acid or quaternary ammonium groups to peripheral positions, phthalocyanine compounds are dissolved in aqueous solutions

in a wide pH range (Bayır, 2005; Choi et al., 2004; Güzel et al., 2013; Kurt, Koca, et al., 2015; Kurt, Özçeşmeci, et al., 2015; Pekbelgin Karaoğlu et al., 2008).

While tetra- and octasubstituted phthalocyanines are compared in the literature, it has been observed that tetrasubstituted phthalocyanines dissolve at a higher rate than their octasubstituted analogues (Diesbach & Von der Weid, 1927). The sense behind this is that tetrasubstituted phthalocyanines are isolated as a combination of four constitutional isomers and symmetrical octasubstituted phthalocyanines are more ordered in solid state (Beck et al., 1991; Durmuş et al., 2006; Hanack et al., 1993). The 2,3- and 1,4 tetra- and octa-substituted phthalocyanines are named due to the substituents placed at positions 2,3,9,10,16,17,23,24 or 1,4,8,11,15,18,22,25 (Figure 1.8).

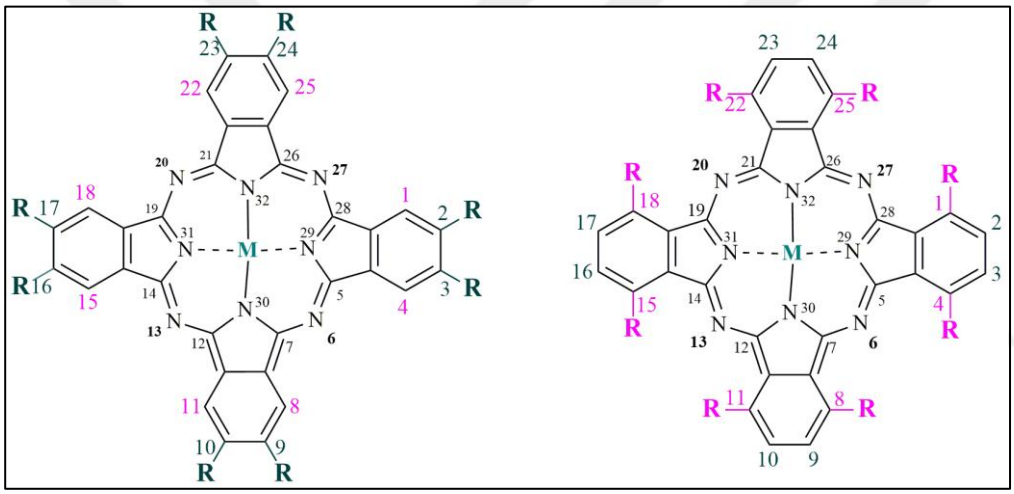

Figure 1.8: 2,3- and 1,4- substituted phthalocyanines

1.4 Basic Synthesis Routes for Phthalocyanines

The most commonly used starting materials for phthalocyanine synthesis are listed in Figure 1.9.

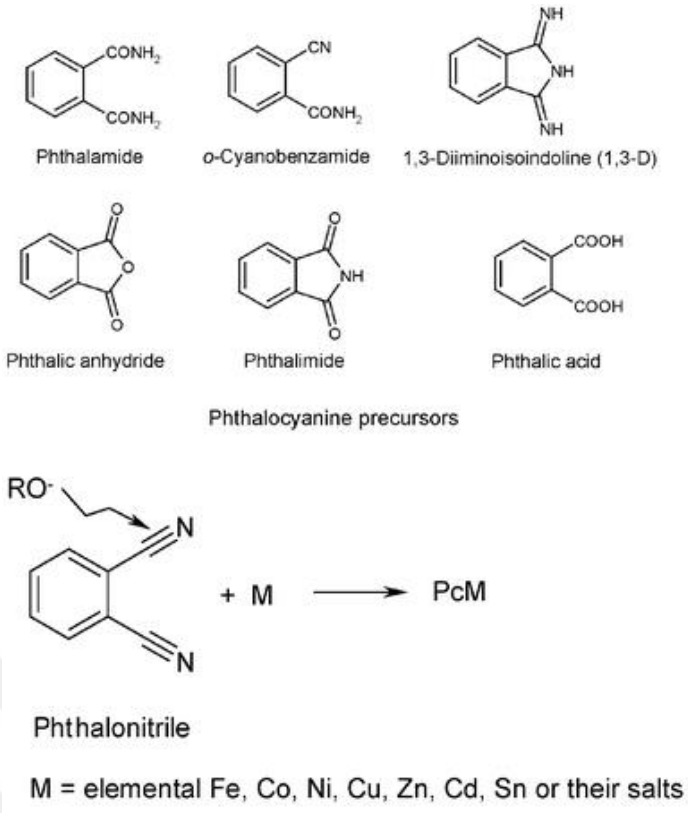

Figure 1.9: Precursors for phthalocyanine synthesis (Kharisov et al., 2005).

In order for phthalocyanine compounds to be synthesized, the substitution must be done at the ortho position of the starting material and presence of a double bond is essential between the atoms bearing functional groups, if not, a regulation mechanism is necessary to ensure the formation of double bonds during the condensation reaction. Since synthesis from phthalic anhydride derivative is cheaper to prepare phthalocyanine compounds industrially, it is the most commonly used method. However, in scientific research, phthalonitrile derivatives are the most widely applied starting materials for the production of substituted phthalocyanines, as it offers much better reaction yields, less by-products and allows structural modifications (Snow, 2003).

1.4.1 Synthesis of metal phthalocyanines

Metallic phthalocyanine can be synthesized from a phthalonitrile derivative or diiminoisoindoline molecule accompanied by a metal salt help in arranging the process of cyclotetramerization. In addition, MPc can be obtained using phthalic anhydride or phthalimide supported by a metal ion (salt) and a nitrogen gas source (urea). In addition, MPc can be formed utilizing H_2Pc or Li_2Pc in the presence of a metal salt in

aromatic solvents having a high boiling point such as chlornaphthalene or quinoline (Thompson et al., 1993). As a different approach, MPc preparation can also be performed using sub-phthalocyanine or super-phthalocyanine. The schematic methods are mentioned in Figure 1.10.

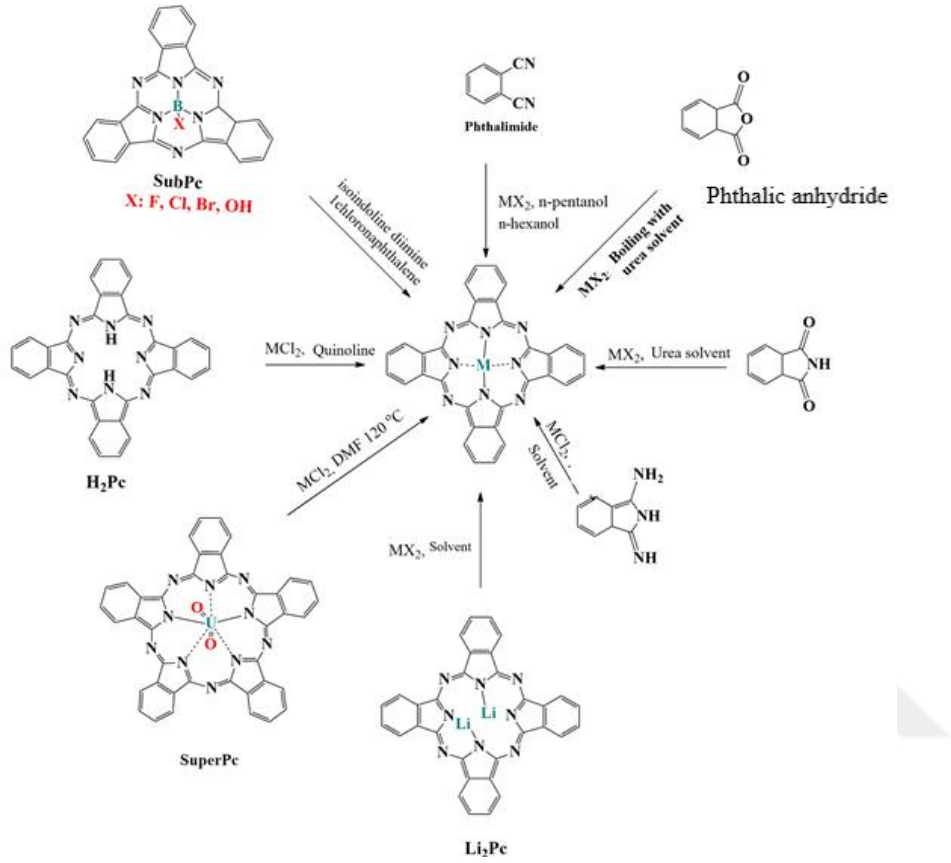

Figure 1.10: Synthesis routes for metallophthalocyanines.

1.4.2 Synthesis of substituted phthalocyanines

Substituted MPcs can be synthesized either by proper substitution of phthalonitrile derivatives or via desired replacement in the phthalocyanine ring. Thus, generating tetra or octa substituted phthalocyanines

1.4.2.1 Synthesis of tetra-substituted phthalocyanines

Among different types of substituted phthalocyanines, the most researched ones are tetra-substituted. Particularly, tetra-substituted phthalocyanines are have greater solubility than their equivalent octa-substituted counterparts. Mainly, it is due to the reason that these tetra-substituents offer isomers constitution and high dipole moment due to their unsymmetrical arrangement at the peripheral region of Pc ring (Beck et al., 1991; Eberhardt & Hanack, 1997; Tau & Nyokong, 2006). The high solubility

helps with their applications in many electrochemical, physiological, chemical, biological areas**.**

Tetra substituted phthalocyanines are classified as peripheral and non-peripherally substituted phthalocyanines correspondent to the substituent's position on Pc ring. Non-peripherally substituted phthalocyanines are developed where the starting material is 3-substituted phthalonitrile derivatives, while peripherally substituted phthalocyanines are synthesized starting from phthalonitriles substituted at 4th position (Figure 1.11).

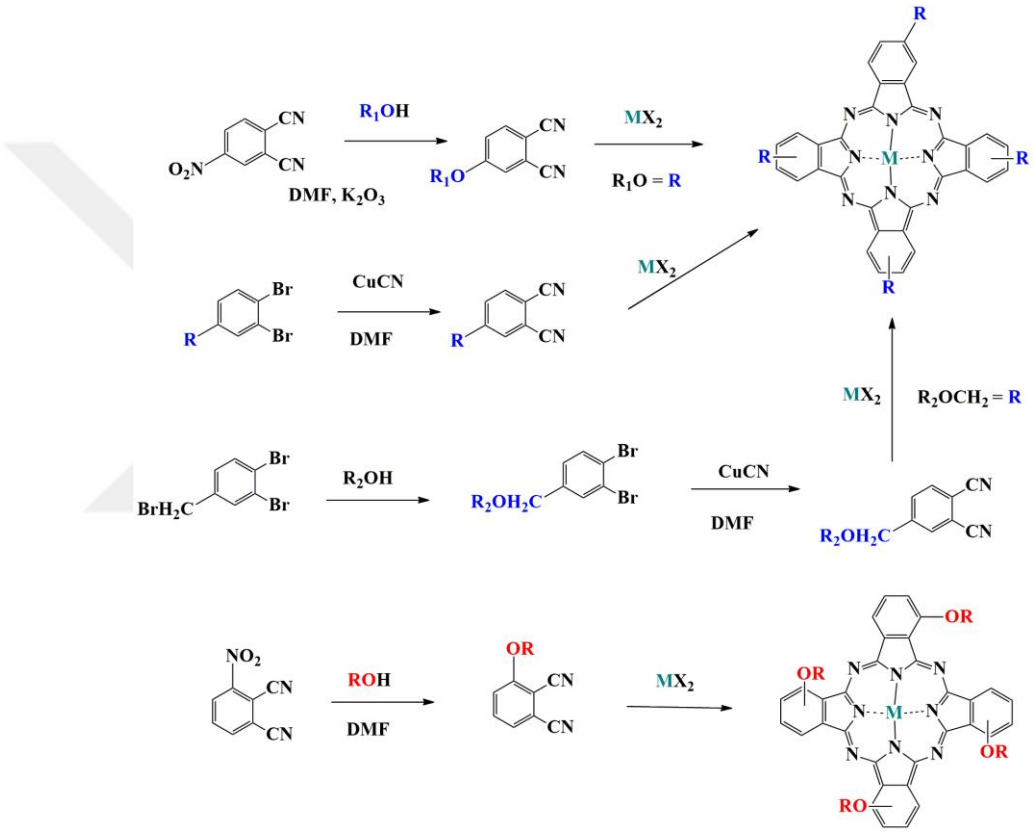

Figure 1.11: Synthesis of tetrasubstituted Pc starting from 3- and 4-substituted phthalonitrile.

In order to obtain peripherally substituted Pcs, the method used is to synthesize 4-nitrophthalonitrile from phthalimide in a three step nucleophilic displacement reaction (figure 1.10) (Young & Onyebuagu, 1990). 4-nitrophthalonitrile submerged in highly polar dissolving agents like DMF and DMSO can easily operate with certain nucleophilic groups. Nucleophile's acidic H^+ can be separated by either sodium or potassium carbonate compounds. The nitro group is replaced as sodium nitrate when nucleophile reacts with the ring.(C. C. Leznoff & Lever, 1989; Mckeown, 1998).

Non-peripherally tetrasubstituted phthalocyanines are very new as compared to peripheral derivatives and 3-nitrophthalonitrile is the starting material that usually serves the purpose of initiating the synthesis reaction (Figure 1.11) (Culhane & Woodward, 1927; George & Snow, 1995; Nicolet & Bender, 1927)

For tetrasubstituted phthalocyanines assemble, the starting compounds utilized are actually the mono-substituted phthalonitriles. After the synthesis is completed via cyclotetramerization, the symmetries of the obtained MPcs are D_{2h}, C_{4h}, C_{2v}, C_s whereas the arithmetic classification for these isomeric congeners is defined as 4:2:1:1 respectively (Figure 1.12). In pursuance to attempt segregation of these extracted isomers, the basic chromatography techniques are usually applied but the dissolution and accumulation of retrieved isomers is very much alike making the separation very challenging. Only few examples are found for these isomeric separations (Hanack et al., 1993).

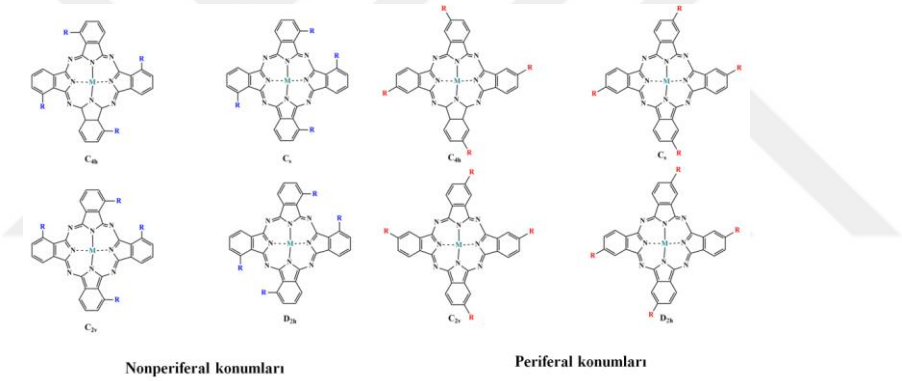

Figure 1.12: Structural isomers of non-peripheral and peripheral tetra-substituted phthalocyanines.

1.4.2.2 Synthesis of octa-substituted phthalocyanine

Generally applied in most cases, the two available methods in order to get phthalocyanines bearing 8 peripheral substituents are mentioned below;

The route describes to use 4,5-dichlorophthalonitrile which is synthesized in four stages starting from 4,5-dichloro-1,2-benzenedicarboxylic acid. (Figure 1.13). This method is more preferred because the reaction efficiency is much higher. To obtain additional derivatives of 4,5- di-substituted phthalonitrile, the reaction must be carried out with the nucleophiles like 4-nitrophthalonitrile and specific reaction conditions are required (Karaoğlu et al., 2012; Wöhrle et al., 1993).

The second method is the assembling of 4,5-dibromo-o-xylene achieved by bromination of o-xylene, and then 1,2-bromomethyl-4,5-dibromobenzene is obtained as a result of bromination with N-bromosuccinimide (Figure 1.14). Then, the primal alkyl groups are replaced with appropriate nucleophiles, and finally the Bromo units on the aromatic ring are transformed into nitriles through Rosenmund-Von Braun reaction (Sharman & Van Lier, 2003).

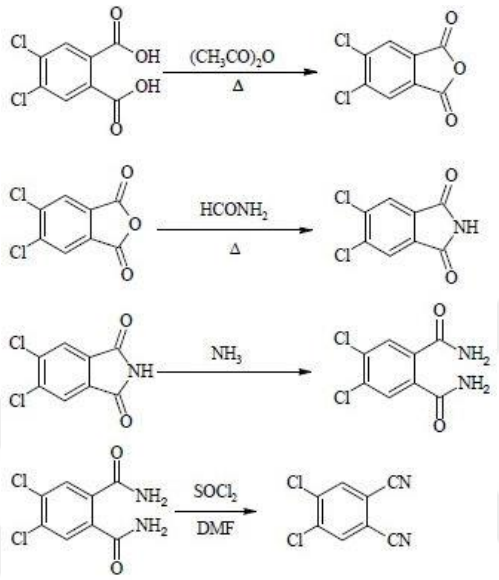

Figure 1.13: Synthetic procedure of 4,5- dichlorophthalonitrile.

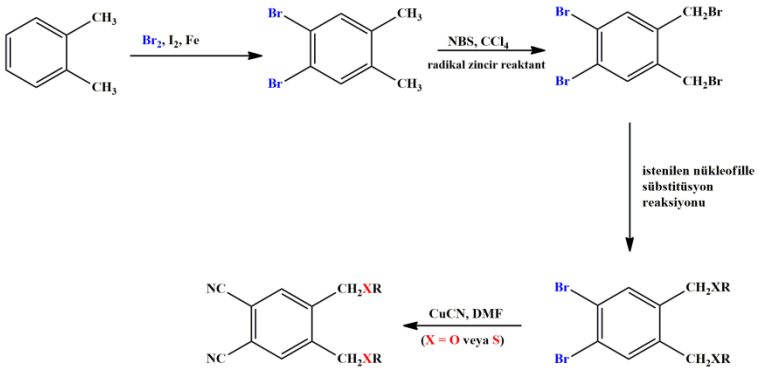

Figure 1.14: Synthetic pathway for a required phthalonitrile derivative from o-xylene compound.

Cook and coworkers established a pair of new schemes for obtaining nonperipheral octa-substituted phthalocyanine (MPc onp C_n). 3,6 dialkylphthalonitriles are obtained from suitable 2,5 dialkyl furan or thiophene as starters (Figure 1.15). As a consequence of Diels Alder ring addition of fumaronitrile and five-ringed heterocycle, suitable dinitrile derivatives are synthesized. While the thiophene pathway is more efficient for the synthesis of simple MPc onp C_{ns}, the furan pathway is more flexible and allows

the preparation of phthalonitriles containing functionally suitably protected carboxylic acid or alcohol groups. This route can also be used in the synthesis of asymmetric phthalocyanine. (McKeown et al., 1990).

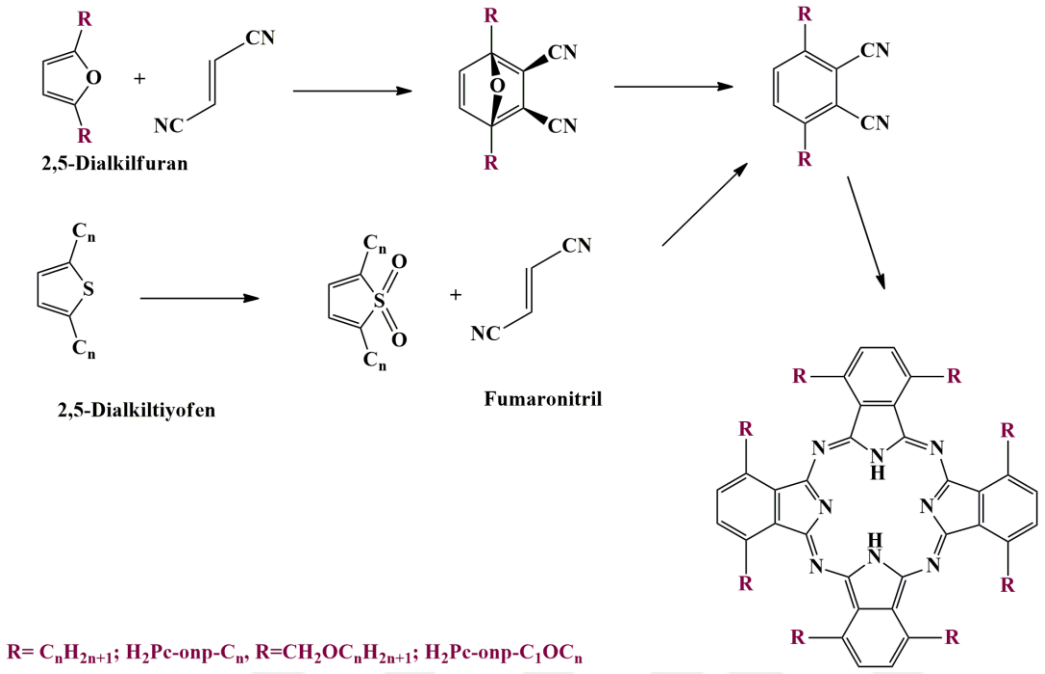

Figure 1.15: Synthetic pathway for non-peripheral octa-substituted phthalocyanines (H_2Pc-onp-C_n).

1.4.2.3 Synthesis of asymmetric phthalocyanines

Statistical condensation method, sub-phthalocyanine approach and polymer assisted synthesis methods are employed for synthesizing asymmetrically substituted phthalocyanine. In the condensation approach, asymmetric phthalocyanines are synthesized starting from two different phthalonitrile compounds. Since selectivity cannot be achieved in this method, six different phthalocyanine compounds are obtained in statistical ratios (Figure 1.16).

After synthesis, the desired product can be separated from other products by using chromatography. By reacting two different phthalonitrile compounds with similar reactivity at a ratio of 3:1, AAAB 44%, AAAA 33% and other cross-condensation products 23% are obtained (Erdem et al., 2021; Farajzadeh et al., 2020; Nemykin et al., 2014)

Another method in asymmetric Pc synthesis is the subphthalocyanine method. In this method, AAAB type asymmetric Pc is synthesized. In this method, which was reported by Kobayashi et al. in 1990, subphthalocyanine is reacted with an iminoisoindoline

derivative containing a different substituted group in DMSO:chloronaphthalene (2:1) at 90 °C (Figure 1.17) (Kobayashi et al., 1990)

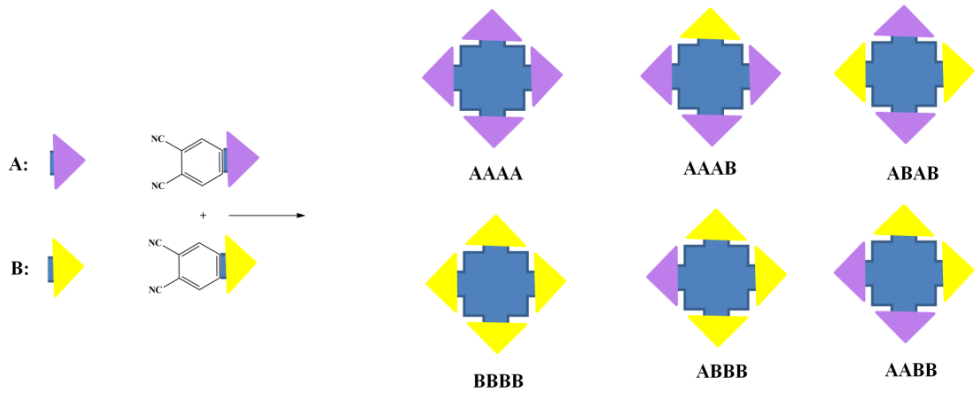

Figure 1.16 Synthesis of asymmetric phthalocyanine using two different isoindole units.

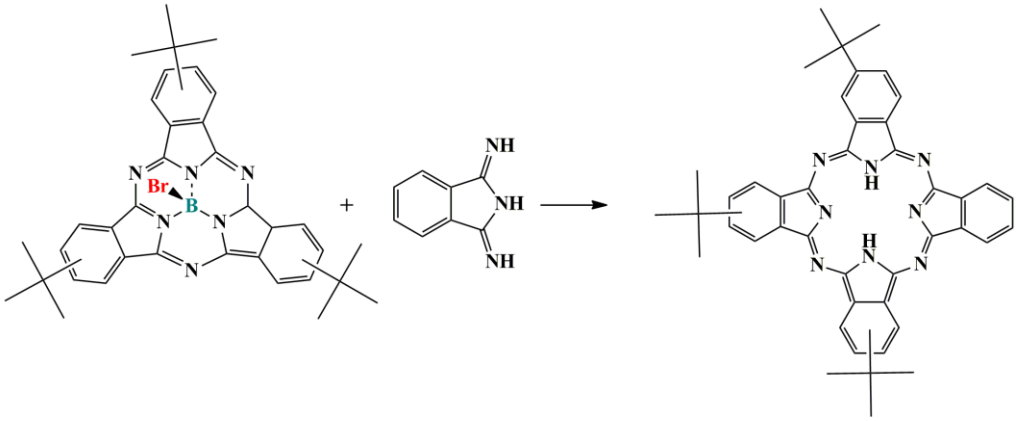

Figure 1.17: Synthesis of asymmetric phthalocyanine by subphthalocyanine method.

A method used for the synthesis of asymmetric phthalocyanines in the AAAB structure was developed by Leznoff and Hall (Figure 1.17). In this method, a diiminoisoindoline or phthalonitrile (B) is bound to an unsolvable polymer and reacted with another diiminoisoindoline unit (A). Then, the targeted asymmetric structure is detached from the polymer support, and the efficiency is around 20-25% (Figure 1.18) (C. C. Leznoff & Hall, 1982).

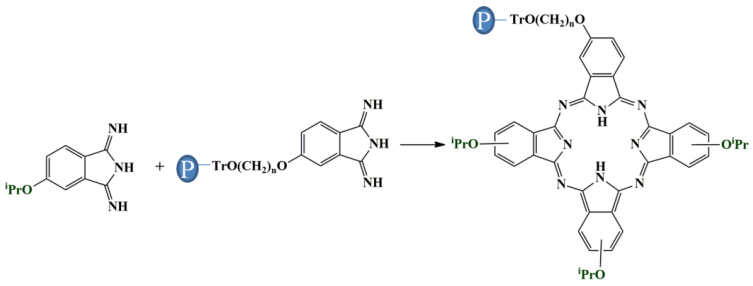

Figure 1.18: Example of polymeric synthesis of asymmetric phthalocyanine.

1.5 UV-vis Spectra and Electronic Absorption in Phthalocyanines

Pc's spectral properties are justified from its 18π-electron system and all its chemical and electronic properties are generally investigated through examining their spectra (Figure 1.19). Ordinarily, Pcs ground state optical absorptions is represented by two dominant absorption series in the visible or near infrared (IR) (670 – 1000 nm) and the UV (325 – 370 nm) area of the electromagnetic spectrum named as the Q (600-800 nm) and B band (300-400 nm) (Gouterman, 1978).

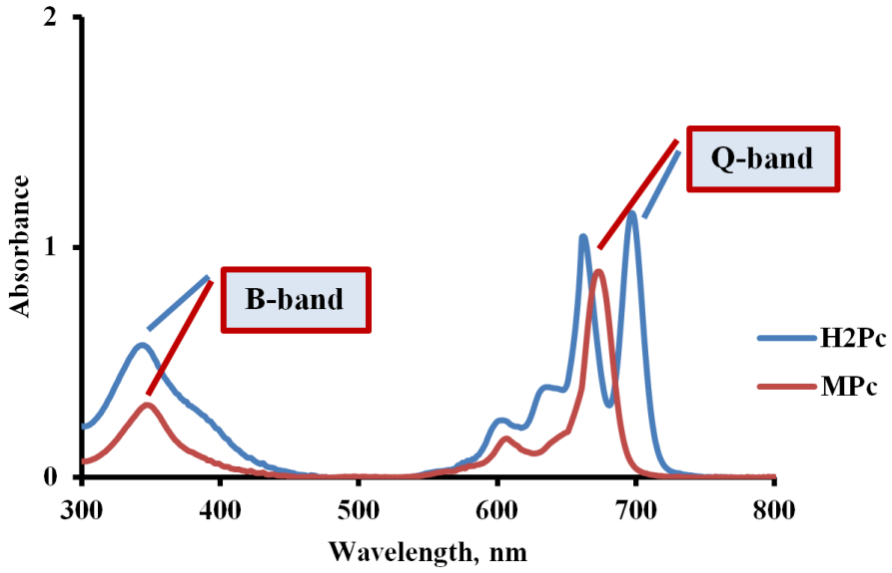

Figure 1.19: Metal and metal free phtalocyanines.

As evident (Figure 1.20), the Q and B bands are designated in correspondence to Gouterman's four-orbital model (Gouterman, 1978; Schaffer et al., 1973) where Q band (Q_{00}) is generally interpreted by a high molar extinction coefficient (ε) of usually 10^5 $M^{-1}.cm^{-1}$, along with a coinciding vibrational band (Q_{01}) (Figure 1.20). The Q band's high intensity is noticeable related to B band which situated at significant

higher energy values around 350 nm.

The Q-band in Pcs is due to π – π* transitions from the highest occupied molecular orbital (HOMO) to the lowest vacant molecular orbital (LUMO). For typical Pcs, the B-band can be specified to the transition from the a_{2u} orbital (HOMO-1) to the e_{gx} and e_{gy} (LUMO and LUMO + 1) orbitals. A decrease in the symmetry of these compounds from D_{4h} to D_{2h} causes the Q-band to be bisected. In general, the lacking of metal ion in the metal-free Pc causes disruption in the regulation of the Pc ring. Also, large metal ions in the cavity cause the same impacts (Figure 1.21).

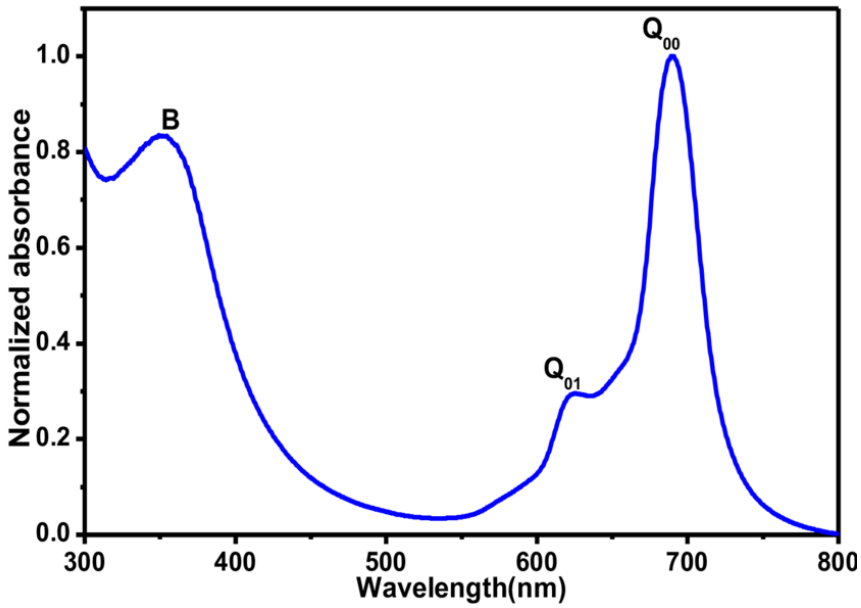

Figure 1.20: Electronic ground state absorption spectrum of MPc.

The occupancy of metal ion in the Pc's vicinity, gives rise to a single intense Q band owing to D_{4h} symmetry causing π-π* transition from the a_{1u} of the HOMO to e_g of LUMO within the MPc core (Fig. 1.21). The Q band for H_2Pcs is cleaved into Q_x and Q_y bands due to reduction of symmetry to D_{2h} resulted from transitions of a_{1u} HOMO to the non-degenerate b_{2g} and b_{3g} of LUMO respectively (Fig. 1.21). Whereas, the B bands develops as a result of shifts from a_{2u} and b_{2u} to e_g.

UV–vis absorption spectra of MPcs can vary depending on many factors, like existence of contrasting metal, derivatives and solvent system as compared to metal-free Pcs. Compared to electron donating groups, electron accepting groups cause Q-bands to deviate more towards the red region. In addition, the presence of a substituent at a non-peripheral location results in a shift to longer wavelengths as compared to when the same substitution occurs at the peripheral site. Also, the extended Q-band

alteration to the red side is also due to the high refraction index of the solvent. Therefore, a linear relationship has been observed amidst the Q-band's location in the electromagnetic spectrum and the rising refractive index of the solvent dispensed (K. M. Kadish et al., 2003; C. C. Leznoff & Lever, 1989; McKeown, 1983).

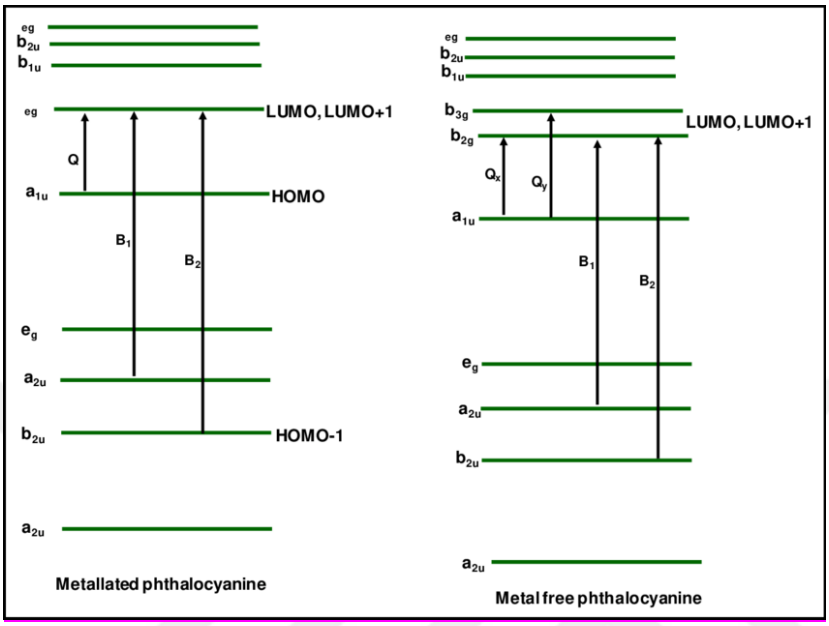

Figure 1.21: Simplified energy diagram of metallic and non-metallic phthalocyanines.

1.6 Aggregation Behaviors of Phthalocyanines

When two or more of the planar monomer molecules in solution come together and interact through intermolecular forces, dimerization or oligomerization is called aggregation (Figure 1.22). The bioavailability of aggregation, its in vivo sequence and singlet oxygen generation efficiency has a vital significance on the optical and photodynamic qualities of highly displaced π-electron systems (Kessel & Lier, 1990). Hence, varying concentration, solvent, substituent type/size/location and/or temperature are means to overcome the cluster formation. Considering any development in electronic state sequence results from intermolecular forces is then traced by modification of spectral properties, examination of UV-vis spectra can aid in clustering identification and control (C. C. Leznoff & Lever, 1989; McKeown, 1983; Torre et al., 2010).

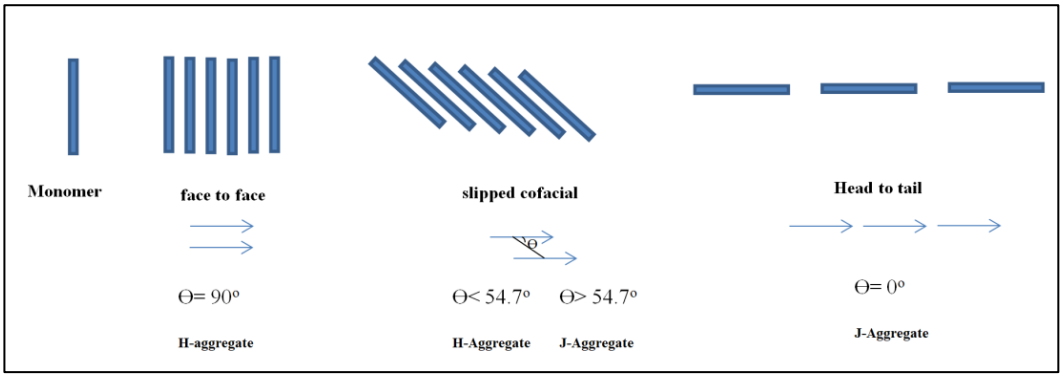

Figure 1.22: Aggregation manner in MPcs.

1.7 Main Application Areas of Phthalocyanines

Phthalocyanines and their metal derivatives have attracted great interest in recent years owing to their special properties related to optics, electronics, catalysis and structural properties. Traditionally, phthalocyanines have been used as dyeing agents, but recently they have found wide application in numerous methodic and research fields such as catalysis, liquid crystals, chemical sensors, photodynamic therapy, solar energy conversion, optical data storage, semiconductors, and nonlinear optics (C. C. Leznoff & Lever, 1989; McKeown, 1983).

1.7.1 Biological applications of phthalocyanines

The biological characteristics of Pc molecules have been the object of many studies including PDT studies (Ogunsipe et al., 2008), antimicrobial (M. S. Ağırtaş et al., 2014), antioxidant (Yıldırım et al., 2017) and enzyme inhibition activities have been studied in detail. Reactive oxygen species (ROS) are resulted via several mechanisms in living cells metabolisms, and then readily react with most of the cellular biomolecules, reducing an organism's normal defense mechanisms (Patra et al., 2015). Synthesizing new phthalocyanines with antimicrobial abilities becomes important as to the excessive use of antibiotic drugs gives resistance to microbes against commercial antibiotics

1.7.2 Photophysical and photochemical applications of phthalocyanines

Photodynamic therapy (PDT) is a definitely favorable and intensively studied approach in tumor diagnosis and treatment. Photosensitizer (PS), visible light and oxygen are required for the PDT method. To date, only hematoporphyrin related compounds (hpd) and photofrin have been employed as first generation

photosensitizers for clinical photodynamic therapy. A photosensitizer to be used generally for photodynamic therapy of cancer; It should have strong photo stability, immense percipience towards cancerous cells, show strong reception in the 600 to 850 nm region where tissue light transmittance is high, and the triplet state should have a long lifetime. This method involves by firstly applying a photosensitizing operator and then continued by exposing the cancer growth to visible light source. In the treatment course, some chemotherapeutic reactive oxygen species mainly singlet oxygen, are radiochemically formed and eliminated the aimed cancer cells (Chauke et al., 2007).

MPcs exhibit strong electronic absorption due to delocalized π bonds and are efficient as photosensitizers. For these reasons, phthalocyanines are important compounds with properties that can be exploited as second-generation photosensitizers in cancer therapy with PDT. Usually zinc phthalocyanines are employed as second generation PS in PDT applications and are seen as promising compounds due to their strong and extended wavelength absorption (mainly in the beneficial range of 650-800 nm), high PDT effect, and low skin photosensitivity. Aluminum, gallium, indium and silicon phthalocyanines, which can make axial substitution through their central atom, have been preferred as photosensitizers (PS) in PDT in recent years due to their low intermolecular interactions, non-agglomeration and good solubility. Among various substituted MPcs, the ones containing alkoxy- and alkylthio- groups show excellent photosensitizer (PS) properties (Durmuş & Nyokong, 2007; Erdoğmuş & Nyokong, 2010). It has also been reported that fluorinated phthalocyanines show more effective photosensitizer properties compared to derivatives that do not contain fluorine (Durmuş & Nyokong, 2007; Güzel et al., 2017; Ogunsipe et al., 2007; Sen et al., 2019).

1.7.3 Electrochemical and spectrolectrochemical applications of phthalocyanines

Metallic phthalocyanines are widely employed as operators in varied electrochemical methods such as electrocatalytic, electrochromic screens as well as for sensory purposes (Durmuş et al., 2006; Hanack & Lang, 1994; Zagal, 1992; Zagal et al., 2010). The redox abundancy of metal phthalocyanines plays the fundamental role for their applicability in these areas, and these attributes can be adapted conveniently via changing central metals and/or substituent groups.

The redox properties of phthalocyanine derivatives and the electrochromic properties directly related to these properties are very interesting. Electrochromic materials,

including phthalocyanines, generally exhibit three types of color change behavior with the electroactive species they form as a result of their optical properties. The first type of electrochromic materials show a single color transition from transparent (colorless) as a result of their optical transmittance and are suitable for absorption/transmission type applications such as smart windows. The second type of electrochromic materials, on the other hand, respond with two visible colors of varying intensity under different constant potential applications. Application of polythiophene-based materials in image technologies is an example of this type. As the last type, polyelectrochromic materials that show more than two redox processes and these events are accompanied by multiple color transitions are reversible. It is evaluated between the absorption/transmittance optical changes and the sought-after materials of the future. Phthalocyanines are among this group of materials with their polyelectrochromic properties. The electrochemical properties of phthalocyanine complexes are mainly due to the interactions between the central metal cation and the 18π-electron system and the effects of different substituents on these interactions. Phthalocyanine complexes with conjugated 18π-electron systems are prone to chemical and electrochemical oxidation and reduction, thereby changing their electrical and optical properties. These complexes give up to four ring-centered reduction and two oxidation reactions in many electrochemical systems. In addition, the conditions of redox reactions can be changed by changing the redox active metal centers along with their side- chain groups (type, position and number). These electrochemical activities of phthalocyanine compounds are one of the main factors that ensure their usability in electrochromic imaging systems and smart material production. The fact that the reduced or oxidized derivatives of phthalocyanine complexes are in different colors enables these complexes to be used as electrochromic materials (Kurt, Koca, et al., 2015; Kurt, Özçeşmeci, et al., 2015).

1.8 Nanomaterials and Metallophthalocyanines

As mentioned earlier, a number of Pc properties can be tuned via addition at peripheral, nonperipheral positions or incorporating different metal ions to the core. The association of metal nanoparticles (MNPs) with MPcs can be achieved with either peripheral, non-peripheral or axial ligand substitution (Ashokkumar et al., 2014; Castro-Latorre et al., 2020; Cheng et al., 2019; Fashina et al., 2013; Hong et al., 2018;

Matlou et al., 2019; Mpeta et al., 2020; Mphuthi et al., 2017; Zasedatelev et al., 2016). In the following sections a brief introduction to general nanomaterials has been described.

1.8.1 Introduction to nanomaterials

By definition, nanometer is 10^{-9} or one-billionth of a meter and therefore, nanotechnology is referred as particles bearing a size less than 100 nanometers. Owing to their small magnitude they exhibit new chemical and physical attributes. (Brechignac et al., 2007; Whitesides, 2005). It has been reported by (Morachevskii & Beloglazov, 2006; Poole Jr. & Owens, 2003; Whitesides, 2005) that the electronic network, conductive and mechanical properties, reactiveness and other structural attributes and behaviours show immense shifts when particles size become evidently smaller in comparison to the bulk state of the same particle. One of the fundamental speciality of nanosubstances is that they must have larger surface to volume ratio which differs them from their bulk kinds. This aspect enables these nanostructured materials to work more efficiently and show high performance while dealing with high recative species in contrast to their bulk counterparts. Different types of nanomaterials include, carbon nanotubes, graphene quantum dots (GQDs) and metal- nanoparticles (MNPs).

Our main focus in this thesis work is to prepare metallic nanoparticles (MNPs) especially the gold-nano particles and conjugate them with MPcs to evaluate their potential applications. The subsequent section will demonstrate the basic properties and synthetic routes specifically for MNPs.

1.8.2 Metallic-nano partlces (MNPs)

MNPs have received wide interest in the last decade due to their utilization for biological properties, like drug delivery (Lee et al., 2011), biological and chemical sensing applications (Malekzad et al., 2017), catalysis (L. Liu & Corma, 2018), gas sensing (Rawal & Kaur, 2013) , surface-enhanced plasmon resonance (SPR) (Pereira et al., 2019).

Until this day, numerous classes of nanoparticles have been chemically integrated and studied especially the ones containing semiconducting metal oxides, magnetic and ferroelectric compounds or noble metals like silver, platinum or gold. In this domain,

metallic nanoparticles have superior and distinguished potential applications for dye formulations due to their intrinsic photocatalytic aspects. Additionally, they have promising sensory functionalities as they have exceeding surface-enhanced Raman scattering (SERS) attributes when applied as electrode for capacitors. Furthermore, the metallic nanoparticles could be employed in food depositories thanks to their anti-fungal and anti- bacterial properties to extend the food's shelf life (Ghosh, 2017).

As far as the optical properties of these MNPs are concerned, a noble progress by Zijlstra et. al., demonstrated the development of a DVD of a ~10 terabytes storage capacity owing to the optical character of gold nanorods implemented in the process (Zijlstra et al., 2009). For the photothermal performance of these metallic nanoparticles, they carry an aggregate of free surface electrons vacillating at a precise frequency known as the famous 'plasmon frequency'. When these nanoparticles begin fluctuating at this specific value of plasmon frequency, the free electrons at their surface will begin to vibrate at a higher extent playing a vital role to adopt them in imaging technologies for biolabeling functions, in bio-filters and chemosensory equipment (Abbasi et al., 2014; Amendola & Meneghetti, 2009).

Few conditions like adjusting the dimensions and structure of the nanoparticles play a vital part while deciding the properties of the surface electrons. Presently, the main approaches named as physical and chemical modes are available to prepare metal nanoparticles. For each of the techniques, some pros and cons have been observed in terms of value and reliability. The first one named as bottom-up chemical method is regulated by the atom-by-atom formation of the nanoparticles irrespective of the medium i.e, it could be executed under either the solid, gas or liquid phase. Whereas, for the physical method it is essential for the photochemical reactions to be carried out at high temperature and special vacuum conditions. So, it turns out to be quite costly and in need of sophisticated equipment. While, the chemical one is more affordable and require simpler equipment (Ghosh, 2017).

1.8.3 Gold nano particles (AuNPs)

In the class of noble-metal nanoparticles, gold nanoparticles (AuNPs) containing materials have attained tremendous significance in biomedical fields especially related to cancer therapy. Miscellaneous shapes of AuNPs's materials implemented in various areas differ from each other due to the formulation procedures and reaction perquisites.

These include AuNPs in nano-rod, caged, shell, star, boxes, cubes, crystals, triangular bipyramids or spherical modeled formulations (Khlebtsov & Dykman, 2010; Kim et al., 2010; C. Li et al., 2008; M. Liu & Guyot-Sionnest, 2005; Murphy et al., 2011; Nehl et al., 2006; Ye et al., 2009). The electronic and magnetic characteristics of gold nanoparticles (AuNPs) are extraordinary as compared to other MNPs.

A strong Localized surface plasmon resonance (LSPR) observed in AuNPs make their utilization in bio-imaging, drug-delivery systems, cancer-theronastics as well in cosmetics formulations. This property emerges from the excitation of AuNPs when incident photons of specific wavelength cause the vibrations of electrons in the conduction band at a specific resonant frequency range (Mukherjee et al., 2001; Shankar et al., 2004). Another interesting property associated with AuNPs is that they exhibit a variety of different colors according to their shape, magnitude and extent of particles aggregation (Daniel & Astruc, 2004).

1.8.3.1 Synthesis of AuNPs

Numerous techniques have been presented so far the formation of noble metal nano particles of gold and silver. These include synthesis via chemical reduction (Suriati et al., 2014), electrochemical (Kalska-Szostko, 2012), an atomic layer deposition (ALD) (Lei et al., 2013) and chemical vapor deposition (CVD) process (T. V. Basova et al., 2019).

Chemical reduction is the mostly employed to obtain silver and gold nanoparticles. The steps leading to formation of NPs include the reduction of metallic (Ag/Au) acidic solution in the presence of an relevant reducing and stabilizing operative to prevent any aggregation or contamination (Kumari et al., 2019). Particle size usually falls in the range of 5-30 nm and relies on several factors like the concentration of precursor and stabilizer solution, temperature, reaction period etc. (T. Basova et al., 2014; L. Li et al., 2019). On the other hand, CVD and ALD offer the nanoparticles synthesis in a superior way with high metal fraction (up to 100%) excluding either surfactant or stabilizing agents (Klyamer et al., 2020). The rudimentary method generally employed to assemble AuNPs explains as to immediately reduce the gold ions containing aqueous solution where citrate compound acts as the reducing agent (Brust et al., 1995; Schulz et al., 2014) is known as the ‘Turkevich method’ and was employed first in 1951 (Turkevich et al., 1951). In detailed procedure, citrate solution is slowly added

to chloroauric acid solution once it starts boiling with continuous whisking. This facile reaction reduced Au^{3+} ions to neutral Au atoms which later precipitates and delivers nanometer-sized gold particles known as AuNPs. The end result is the formation of wine-red colloidal suspension of AuNPs which can be stored at a specific temperature for long-term use (Turkevich et al., 1951, 1953).

The reaction equation of Au nanoparticles synthesis using citrate is written below (Equation 1.1) (Ghosh, 2017):

$$2HAuCl_4 + 3C_6H_8O_7 \rightarrow 2Au + 3C_5H_6O_5 + 8HCl + 3CO_2 \quad (1.1)$$

In this context, the size of the Au nanoparticles is varied by altering the temperature, reagent concentration, etc. (Uppal et al., 2010).

Among other reducing agents used for this synthetic procedure include compounds like aminoboranes or borohydrides, hydrazines, hydroxylamines, CH_2O, polyols, some sugars, saturated or unsaturated alcohols, H_2O_2 gas, citric and oxalic acid, CO gas, sulfites, acetylene or H_2 gas (Park & Shumaker-Parry, 2014; Sardar et al., 2009; Westerlund & Bjørnholm, 2009). To improve the stability of this AuNPs colloidal solution for longer periods, some stabilizers such as phosphorus ligands, trisodium citrate dihydrate, N, O and S based ligands, branched polymers and surfactants are also used (Boisselier & Astruc, 2009; Sperling et al., 2008). In order to get the nano-particles of different size range (15 to 150 nm) Frens revised the original Turkevich procedure by altering the concentration ratios of gold acidic solution and trisodium citrate (Park & Shumaker-Parry, 2014).

1.8.4 Conjugational hybrids of MNPs and MPcs

Metal phthalocyanines (MPcs) conjugated to metal nanoparticles (MNPs) leads to the formation of hybrid MPcs/MNPs materials which have been proved highly efficient in various medicinal, biological, electrochemical and sensory fields. Phthalocyanines and Au nanoparticles hybrids have been addressed for enhanced drug delivery functions (Camerin et al., 2010; Hone et al., 2002; Wieder et al., 2006) by many researchers in the literature. A profound study has been published by (Majeed et al., 2020) that highlights conjugation mechanisms between MPcs and Ag/Au MNPs along with several characterization techniques.

1.8.5 Synthesis of MNPs and MPcs hybrids

There are two main concepts involved while considering these conjugation reactions; First one is the self-assembly approach which is established when a ligand exchange occurs on the NP's periphery creating a linear electrostatic link to the sulphur and/or nitrogen of MPc molecule. Whereas the second method involves a covalent linking amide bond development amidst carboxylic and amino groups (Majeed et al., 2020).

To aid the conjugation phenomenon in self-assembly procedures, single solvent or a mixture of solvents can be utilized. For example, dimethyl sulfoxide (DMSO) has been used by (D'Souza et al., 2015; Khoza & Nyokong, 2014; Lokesh et al., 2009). The subsequent purification of the developed MPc/MNPs nanoconjugate can be performed by adding methanol in the resultant product followed by centrifugation to segregate MNPs (Bankole et al., 2016; Bankole & Nyokong, 2016; Dubinina et al., 2018; Nwaji et al., 2017, 2018; Nwaji & Nyokong, 2017; Oluwole et al., 2016, 2017).

1.8.6 Biological applications of MNPs and MPcs hybrids

Not long ago, the application span of MPcs have been spread to photosensitizers (PSs) in photodynamic therapy (PDT) besides their usage as blue-green colorants. In particular, the analysis of MPcs as promising PDT operant has gained a lot of recognition. The properties of phthalocyanine complexes which make them excellent second generation photosensitizers include their non-toxic response towards healthy cells, excellent photochemical attributes, and higher accumulating efficiency specifically into the target cells. Regardless of all these exceptional attributes, the most common problem face by many Pc photosensitizers is their familiar hydrophobic and aggregate forming nature while working within aqueous systems. These shortcoming effectively reduce their photosensitizing efficacy in PDT trials. The answer to solve these issues lies holds within nano technology which has shown best PDT agents for clinical applications (Jia & Jia, 2012).

AuNPs have been acknowledged as optimal drug vehicles for cancer treatment due to their multivalent structure, chemically inert behavior and minimal toxicity towards normal cells (Connor et al., 2005)

Nguyen and co-workers have published a detailed and beneficial review about the size- and shape-controlled growth and performance of AuNPs to synthesize gold

nanoprobes and their possible relevancy in biological aspects such as nucleic acid/protein detection and cell imaging (Nguyen et al., 2011).

Many scientists have worked to enhance this coordinated relation between metal phthalocyanines and metal nanoparticles and explained the effect of MNPs on biological properties especially the PDT of MPcs (Nyokong & Antunes, 2013). Phthalocyanine-AuNP hybrids were demonstrated as favorable photodynamic therapeutic agents by many scientists in literature (Doubrovsky et al., 2010). Ghosh et al. and Hone et al. assessed noble AuNPs nanoparticles offset with MPcs generated 50% higher quantum yield of singlet oxygen species alongwith greater hydrophobic MPc solubility as compared to free MPc (GHOSH et al., 2008; Hone et al., 2002).

Similarly, subsequent tumor depletion results were narrated with the ZnPc-gold nanoparticle conjugates by (Camerin et al., 2010; Manthe et al., 2010). Wieder et al. have suggested ZnPc derivatives as hydrophobic PDT photosensitizers where their delivery was aided for cancer cell destruction by the Pc-Np conjugates as they showed greater solubility in polar medium. Cancer cells exposed to these conjugates indicated massive extermination due to singlet oxygen production with double productivity as compared to the Pcs without nano conjugates (Wieder et al., 2006).

Another work by Chen et al. explained using a complex containing plasmonic gold nanorods and sulfonated aluminum Pc (AlPcS- AuNRs) which displayed facile transfer to human liver cancer cells and enhanced cancer cell diagnosis and their subsequent eradication via PDT (L. Li et al., 2010). Another research employing non-intrusive AlPcS-AuNRs conjugate for near-infrared fluorescence prediction and subsequent cancer treatment via PTT/PDT. These complexes illustrated four times higher drug transfer within cells and enhanced in vitro phototoxicity compared to the cells cured with AlPcS alone. As a consequence of the PDT treatment, the tumor reduced 79% and up to 95% when PTT and PDT was employed together (Jang et al., 2011).

Stuchinskaya and co-workers explained the formation of a conjugate of four constituents; antibody, phthalocyanine, polyethylene glycol and gold nanoparticles, employed for PDT targeted against breast cancer cells (Stuchinskaya et al., 2011). Barmin et al. presented hybrid conjugates comprised of albumin-coated gold nanoparticles with Zn Pc and indocyanine green dye to attain multimodal diagnostics and potential PDT applications (Barmin et al., 2021).

In another work, Dube and group reported the synthesis zinc(II) complex connected to AuNPs like gold nanorods and nanospheres via self-assembly procedure. These complexes exhibited superior PDT/PTT activities in response to the epithelial breast cancer cells (Dube et al., 2018).

Among other biological aspects, the antimicrobial activity of phthalocyanine-bearing MNPs composites acting as nano photosensitizers for creating promising antibacterial nanotherapeutic operators against bacteria was illustrated by Mondal et. al (Mondal & Bera, 2014).

Our thesis research process followed the Turkevich method for AuNPs synthesis and DMSO for the conjugation of MPc and AuNPs for nanoparticle/MPc hybrids which are further evaluated for biological applications listed in subsequent sections.

2. AIM AND SCOPE OF THESIS

This thesis is intended to synthesize new symmetric phthalocyanines containing 4-{[4-(dimethylamino)phenyl]ethynyl, 4,5-bis{[3,5-bis(trifluoromethyl)phenyl]ethynyl}, 4,5-bis[(4-(dimethylamino)phenyl)ethynyl] groups and push-pull asymmetric phthalocyanines bearing 4-[(4-pentylphenyl)ethynyl], 4-(thiophen-3-ylethynyl) groups.

These substituents are present in different numbers and positions onto the Pc ring to determine their possible application areas in medicine, biology and other physical technological fields. New tetra-substituted and octa metals Pcs (M= Zn, Co, Fe, Mn, and Lu) soluble in polar and apolar organic solvents substituted with peripheral substituents are synthesized that show effective biological, electrochemical and optical properties.

Co and Zn tetra substituted 4-{[4-(dimethylamino)phenyl]ethynyl , and octa-substituted Co, and Zn MPc having 4,5-bis[(4-(dimethylamino)phenyl)ethynyl] substituents were subjected to the gold nano nanoparticles synthesis and evaluated for their biological applications. Moreover, the statistical condensation method was applied to prepare A_3B type Co and Zn asymmetric phthalocyanines bearing 4-[(4-pentylphenyl)ethynyl] and 4-(thiophen-3-ylethynyl) phthalonitrile ligands. Subsequently, the synthesis, characterization and phototransistor related applications of metallophthalocyanines containing both electron-accepting and electron-donating groups (push-pull) new asymmetrical phthalocyanines are reported.

The structural aspects of the obtained compounds were analyzed through spectral approaches such as FT-IR ^{1}H-NMR (except for paramagnetic phthalocyanines), ^{13}C NMR, mass and UV-vis spectroscopy.

Co and Zn tetra substituted 4-{[4-(dimethylamino)phenyl]ethynyl , and octa-substituted Co, and Zn MPc having 4,5-bis[(4-(dimethylamino)phenyl)ethynyl] substituents were conjugated to the gold nano nanoparticles to obtain MPc-nanohybrids. The bioavailability of these synthesized symmetrical phthalocyanines along with their nanoparticles was analyzed for biological properties such as

antimicrobial, antioxidant, tyrosinase inhibition activities, and the photophysical and photochemical properties in order to investigate their usability in PDT and SPDT. The effects of both the quantity of the substituted group and the selection of the coordinated metals on the antioxidant, antimicrobial, tyrosinase-inhibited activity, electrochromic, photophysical and photochemical properties were examined.

In addition, photoconductive measurements of asymmetrical phthalocyanines substituted with alkynyl groups were determined by different electrochemical, photoconductive analysis methods. Within the scope of the project, their potential for use in photoconductive devices was investigated.

3. DEVICES AND MATERIALS USED

3.1 Devices

FT-IR spectra were cataloged at room temperature employing a Perkin-Elmer Spectrum spectrometer in the 4000-400 cm^{-1} range. NMR spectra were obtained using an Agilent VNMRS 500 MHz spectrometer and chemical shifts (δ) are recorded in ppm. Electronic absorption spectra were reported utilizing a Scinco Lab Pro Plus UV-vis spectrophotometer. Whereas, the mass spectral analysis was done through a Perkin-Elmer Clarus 500 GC-MS and a Bruker Microflex MALDI-TOF mass spectrometer. TEM analysis was carried out through High Resolution TEM, (RTEM) Jeol JEM 2100F HRTEM, 200kV at ODTÜ Merlab.

3.2 Materials

The high purity materials used in this study were purchased from commercial suppliers. Nitrogen gas, acetic acid, hydrochloric acid (HCl), acetone, dichloromethane (DCM), dimethyl formamide (DMF), diethylether, dimethyl sulfoxide (DMSO), ethyl alcohol, ethylacetate, hexane, chloroform ($CHCl_3$), methyl alcohol, 1- pentanol, 1-hexanol, toluene, tetrahydrofuran (THF), diethylether, dimethylaminoethanol (DMAE), 1,8-diazabicyclo [5. 4. 0] undec-7-ene (DBU), potassium carbonate (K_2CO_3), sodium sulfate (Na_2SO_4), 3-nitrophthalonitrile zinc(II)acetate [$Zn(OAc)_2$], palladium(II)acetate [$Pd(OAc))_2$], cobalt(II) chloride ($CoCl_2$), copper(II) chloride ($CuCl_2$), Manganese(II) chloride ($MnCl_2$), Iron(II) acetate ($Fe(CO_2CH_3)_2$), lutetium (III) acetate [$Lu(OAc)_3$], 1,2-dicyano-3,4,5,6-tetrafluorobenzene, 1-ethynyl-4-pentylbenzene, 3-ethynylthiophene, 4-(N,N-Dimethylamino)phenylethylene.

4. EXPERIMENTS AND METHODS PERFORMED

This section summarizes the experiments conducted in order to obtain desired asymmetrical and symmetrical metal phthalocyanines starting from preparing the precursor materials which were later transformed into tetra and octa-substituted phthalocyanines.

4.1 Synthesis of Precursor Materials

4.1.1 Synthesis of 4-iodo phthalonitrile (1)

The procedure followed consisted of five steps is stated in detail.

4.1.1.1 Synthesis of 4-nitrophthalimide

In a balloon flask, 200 mL H_2SO_4 with 50 mL fuming HNO_3 was added and stirred. The temperature of the reaction was brought down to 0 ºC by using an ice bath with continuous stirring. As the time passed the temperature was lowered to 0 ºC, 38 g (0.26 mol) phthalimide was then mixed into the reaction mixture in small quantities over a time span of 1.5 hour keeping the temperature below10 ºC. Once the phthalimide addition was completed, the mixture was left to be stirred over ice bath for further half an hour. Later on, the ice bath was removed the reaction mixture was heated up to 35 °C and the yellow bits begin to dissolve away in the solution. Finally, the mixture was left to be mixed stirred for 1 more hour. After that the reaction was stopped and the contents were left to be cooled and later emptied onto water and ice mixture.

The yellow colored 4-nitrophthalimide thus obtained was first precipitated and percolated. Later it was washed and vacuum filtered several times with water and checked until the precipitate became neutral to litmus paper. Precipitate thus gathered was crystallized with approx.900 mL of hot ethanol. Crystals appeared to be bright yellow in color were filtered and washed off with cold ethanol. The obtained crystals were then left in a vacuum oven with temperature set to 80-90 °C (Figure 4.1). Molecular formula: $C_8H_4N_2O_4$. Molecular weight: 192.13g/mol. Yield: 35.6g (72%). M.P: 195 °C.

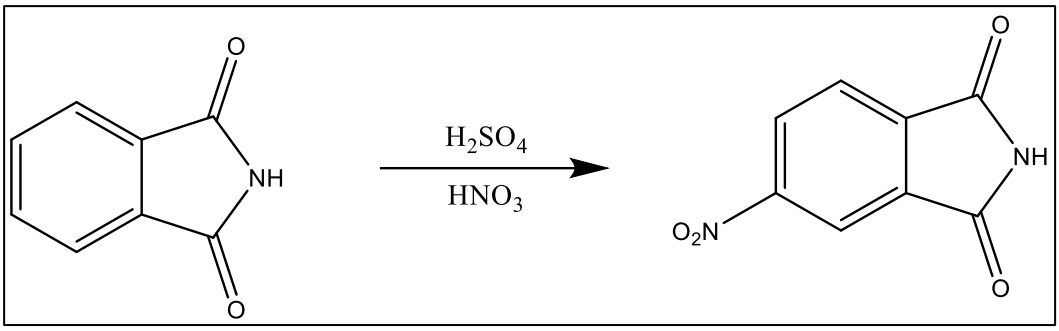

Figure 4.1: Synthetic pathway to 4-nitrophthalimide.

4.1.1.2 Synthesis of 4-nitrophthalamide

32 g (0.166 mol) 4-nitrophthalimide was combined with 168 mL of 32% NH_3 solution and continuously stirred for 24 hours. After 24h, the products are filtered then washed using cold water and then with THF solvent. At start of the reaction, the phthalimide reactant was yellow in color and products turned white until the reaction completed (Figure 4.2).

Molecular formula: $C_8H_7N_3O_4$. Molecular weight: 209.16g/mol. Yield: 26 g (74.63%). M.P: 197 °C.

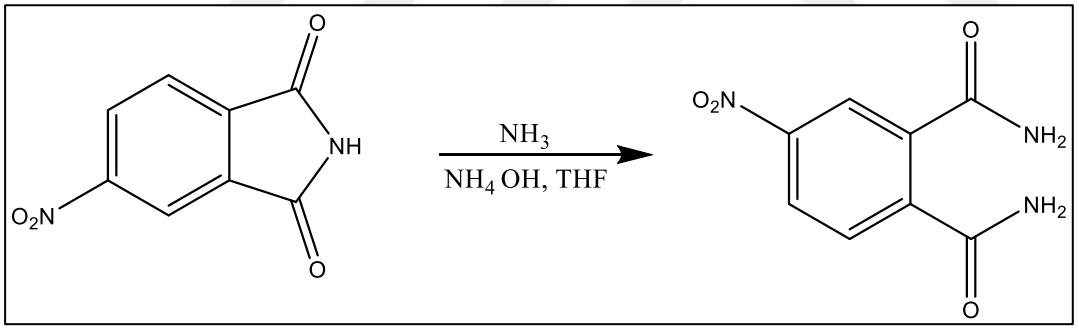

Figure 4.2: Synthetic pathway to 4-nitrophthalamide.

4.1.1.3 Synthesis of 4-nitrophthalonitrile

For 4- nitrophthalonitrile preparation, the procedure was followed as stated in (Young & Onyebuagu, 1990). In a reaction flask, firstly 70 mL of dry dimethylformamide (DMF) was poured and the temperature was lowered to 0 °C while N_2 gas flowed. Then, 7.3 mL of thionyl chloride was mixed in the DMF and the temperature was kept below 5 °C with the help of ice bath. Once the thionyl chloride was incorporated, the nitrogen gas source was removed and a $CaCl_2$ plug was installed on the flask's opening. As the reaction proceeded, the color of the reactants turned yellowish. Next, 10 g (0.048 mol) of 4- nitrophthalamide was slowly mixed and reaction temperature

was maintained around 5 °C. Then, the contents were left to be stirred over ice bath for one more hour. After one hour, ice bath was removed and the reaction was further stirred at room temperature for another 2 hours and finally poured over ice-water mixture. Filtration and successive washing of the precipitate was completed with water, 250 mL 5% sodium hydrogencarbonate and left to be dried in vacuum oven at 110-120°C temperature (Figure 4.3).

Molecular formula: $C_8H_3N_3O_2$. Molecular weight: 173.13g/mol. Yield: 7.0g (85%). M.P: 141°C.

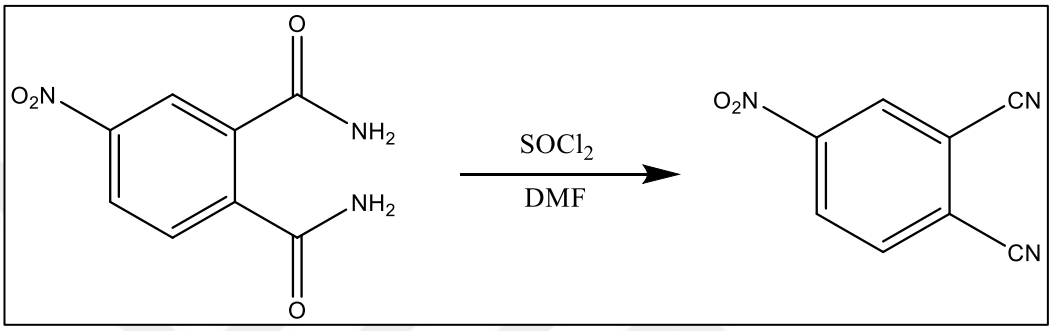

Figure 4.3: Synthesis of 4-nitrophthalonitrile.

4.1.1.4 Synthesis of 4-aminophthalonitrile

45 mL MeOH with 9.6 mL conc. HCl and 2.0 g (145 mmol) of 4-nitrophthalonitrile were reacted in a reaction vessel and heated until boiling. The reflux helps 4-nitrophthalonitrile to be dissolved. Later, Fe powder (2.21 g, 39.2 mmol) was incorporated portion wise over an hour time. Gradually, the solution's color tuned brown from yellow. The reaction products were left to get cooled and later precipitated and washed in distilled water (Figure 4.4).

Molecular formula: $C_8H_5N_3$. Molecular weight: 143.15g/mol. Yield: 1.4 g (84%).

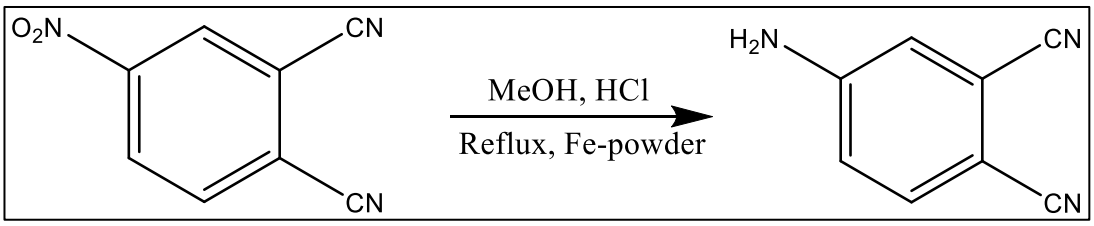

Figure 4.4: Synthesis of 4-aminophthalonitrile.

4.1.1.5 Synthesis of 4-iodophthalonitrile (1)

The compound 4-iodophthalonitrile **(1)** was synthesized as explained in literature (Marcuccio et al. 1985). The reactants combined as 1.40 g (9.78mmol) of 4-

aminophthalonitrile diluted in 22.4 mL of 2.5 M H_2SO_4 and stirred at 0 °C. Later on, 0.850 g (12.32 mmol) $NaNO_2$ mixed in 3.5 mL of water was added to the reactants and stirred for half an hour. Then, 2.00 g (12.05 mmol) KI solution was poured and the reaction solution kept on stirring for 45 minutes at 25 °C. At the end, the brown precipitate formed was filtered and washed with copious amounts of water and left to be dried. Finally, it was extracted over a super saturated solution of $Na_2S_2O_3$ and then ran through column filled with silica gel and separated by dichloromethane eluent (Figure 4.5).

Molecular formula: $C_8H_3IN_2$. Molecular weight: 254.03 g/mol. Yield: 2.01 g (81%).

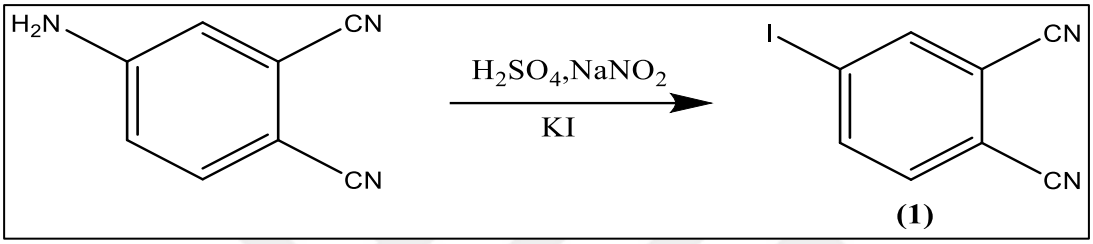

Figure 4.5: Synthesis of 4-iodophthalonitrile **(1)**.

4.1.2 Synthesis of 4-(thiophen-3-ylethynyl) phthalonitrile (2)

A reaction solution of 0.290 g 4-iodophthalonitrile **(1)** (1.14 mmol), 7mL TEA, 3 mL THF, (1.37 mmol) 0.148 g of 3-ethynylthiophene, (0.005 mmol) 0.001 g copper iodide and (0.011 mmol) 0.008 g bis(triphenylphosphine) palladium (II) chloride was subjected to continuous magnetic stirring at 50ºC under N_2 gas for 48 hours (Figure 4.6). After the time interval passed, the solvent was removed under pressure.

The precipitate was then rinsed with hot MeOH and purified afterwards. Higher purification was achieved via column chromatographic method with DCM as mobile phase and silica as stationary phase (Kumral et al., 2020).

Molecular formula: $C_{14}H_6N_2S$. Molecular weight: 234.28g/mol. Yield: 0.181g (68%), M.P. 125 °C, FT-IR υ_{max} (cm^{-1}): 3096-3043 (Ar-H), 2233 (C≡N), 2204 (C≡C), 1591 (Ar C=C). ^{1}H-NMR (500 MHz, $CDCl_3$): δ ppm 7.91 (1H, s, S-CH), 7.82-7.78 (2H, q, Ar-H), 7.66 (1H, d, S-CH), 7.38-7.37 (1H, d, Ar-H), 7.23-7.22 (1H, d, CH).^{13}C-NMR (500 MHz; $CDCl_3$): δ ppm 142.34, 141.93, 135.74, 133.36, 130.99, 129.55, 126.06, 120.35, 116.20 (C≡N), 115.08 (C≡N), 114.65, 114.00, 91.91, 85.45.

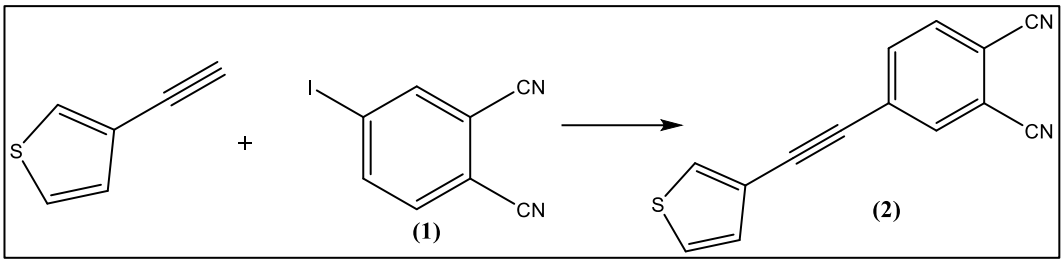

Figure 4.6: Synthesis of 4-(thiophen-3-ylethynyl) phthalonitrile **(2)**.

4.1.3 Synthesis of 4-[(4-pentylphenyl)ethynyl] phthalonitrile (3)

The reaction started combining 1.14 mmol (0.290 g) 4-iodophthalonitrile **(1)** in a 10 ml solution consisting TEA:THF in 7:3 ratio alongside 0.011 mmol (0.008 g) $PdCl_2(PPh_3)_2$, 0.005 mmol (0.001 g) CuI and 1.37 mmol (0.236 g) 1-ethynyl-4-pentylbenzene (Figure 4.7). This amalgam was refluxed at 50°C temperature and stirred for 48h with N_2 gas effect. The precipitate collected after drying solvent was purified via CH_2Cl_2:ethyl acetate (2:1) eluent in vertical chromatographic separation resulted in a dark yellow colored compound (Yenilmez et al., 2021).

Molecular formula: $C_{21}H_{18}N_2$. Molecular weight: 298.39g/mol. Yield: 0.23 g (73.5%). M.P. 77°C. FT-IR: υ_{max} (cm^{-1}): 3067-3039 (Ar–H), 2935-2857 (alkyl C-H), 2236 (C≡N), 2207 (C≡C). ^{1}H- NMR (500 MHz, $CDCl_3$): δ, ppm 7.91 (1H, s, Ar-H), 7.82-7.77 (2H, m, Ar-H), 7.48-7.46 (2H, d, Ar-H), 7.23-7.21 (2H, d, Ar-H), 2.66-2.63 (2H, t, CH_2), 1.67-1.61 (2H, m, CH_2), 1.35-1.32 (4H, m, CH_2–CH_2), 0.92-0.89 (3H, s, CH_3).^{13}C- NMR (500 MHz, $CDCl_3$): 145.40, 135.90, 135.42, 133.44, 131.92, 131.42, 129.64, 129.02, 128.68, 118.39, 116.26 (C≡N), 115.24 (C≡N), 114.81, 113.94, 97.26, 85.38, 35.97, 31.41, 30.83, 22.50, 14.00.

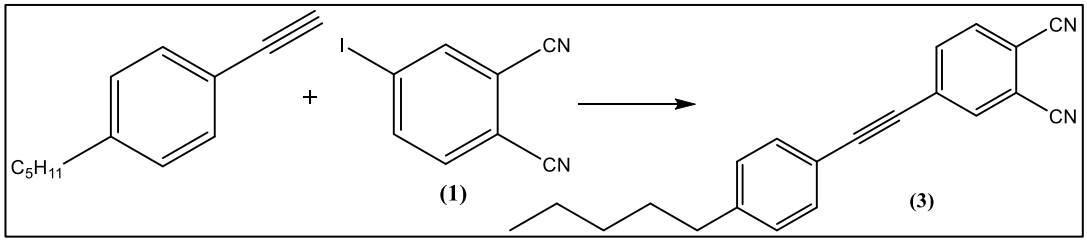

Figure 4.7: Synthesis of 4-[(4-pentylphenyl)ethynyl] phthalonitrile **(3)**.

4.1.4 Synthesis of 4,5-Dichlorophthalonitrile (4)

It was synthesized in 4 steps starting from 4,5-Dichloro-1,2-benzenedicarboxylic acid (Wöhrle et al., 1993)

4.1.4.1 Synthesis of 5,6-Dichloro-1,3-isobenzofurandione

30 g (0.127 mol) of 4,5-Dichloro-1,2-benzenedicarboxylic acid were refluxed in an oil bath for 12 hours with 70 mL of acetic anhydride (Figure 4.8). After this time, the precipitate formed in the reaction mixture was chilled to room conditions, precipitated and cleansed initially with 2-methylpentane and subsequently with ethyl ether. Finally, white product obtained was dried in vacuum at 100 °C.

Molecular formula: $C_8H_4Cl_2O_3$. Molecular weight: 219.02g/mol. Yield: 25.7 g (93%). M.P: 184-186°C.

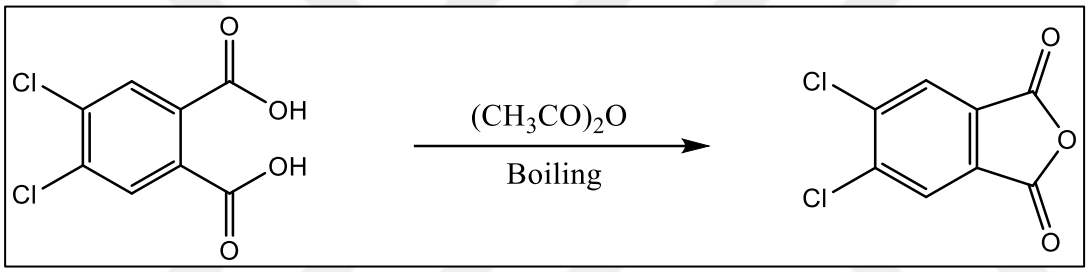

Figure 4.8: Synthesis of 5,6-Dichloro-1,3-isobenzofurandione.

4.1.4.2 Synthesis of 5,6-Dichloro-1H-isoindole-1,3-(2H)-dione

22 g (0.1 mol) of 5,6-Dichloro-1,3-isobenzofurandione reacted in 30 mL formamide continued for 6 hours. After the reaction completion, the product solution cooled and precipitated in plenty of water. Resultant white product was desiccated at 100 °C (Figure 4.9).

Molecular formula: $C_8H_3Cl_2NO_2$. Molecular weight: 216.02g/mol. Yield: 21.2 g (98%). M.P: 193-195ºC.

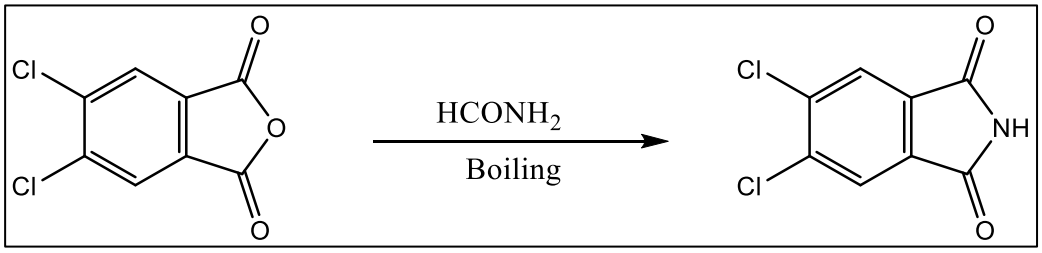

Figure 4.9: Synthesis of 5,6-Dichloro-1H-isoindole-1,3-(2H)-dione.

4.1.4.3 Synthesis of 4,5-Dichloro-1,2-benzenedicarboxamide

21 g (0.1 mol) 5,6-Dichloro-1H-isoindole-1,3-(2H)-dione mixed alongside 300 mL 25% NH_4OH at 25 °C for a 48 h time period (Figure 4.10). Resultant precipitate retrieved in a light yellow color later strained and cleansed with distilled water till came neutral to litmus test. Lastly, the precipitate gave white crystals with ethanol which were dried at 100 °C.

Molecular formula: $C_8H_6Cl_2N_2O_2$. Molecular weight: 233.05g/mol. Yield: 18 g (77%). M.P: 245-247°C.

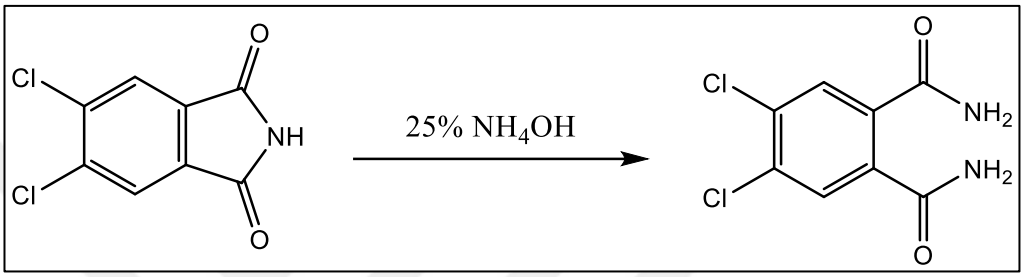

Figure 4.10: Synthesis of 4,5-Dichloro-1,2-benzenedicarboxamide.

4.1.4.4 Synthesis of 4,5-Dichloro-1,2-dicyanobenzene (4)

70 mL of $SOCl_2$ was slowly mixed with dry DMF chilled to 0 °C and proceeded under N_2 atmosphere. 18 g (0.086 mol) of 4,5-Dichloro-1,2-benzenedicarboxamide was blended into to this solution for 2 hours such that thermal reading should not exceeds 5 °C. The mixture was shaken at temperature range of 0-5 °C for 5 hours interval and then at 25 °C for another 12 hour period. Eventually, the obtained yellow precipitates was slowly incorporated to 700 mL of iced water. Later, resultant crude product was sieved and rinsed repeatedly with water and crystallized with methyl alcohol. White crystalline substance thus obtained was dried in vacuum at 100 °C (Figure 4.11).

Molecular formula: $C_8H_2Cl_2N_2$. Molecular weight: 197.02g/mol. Yield: 13 g (76%). M.P.182-184 °C.

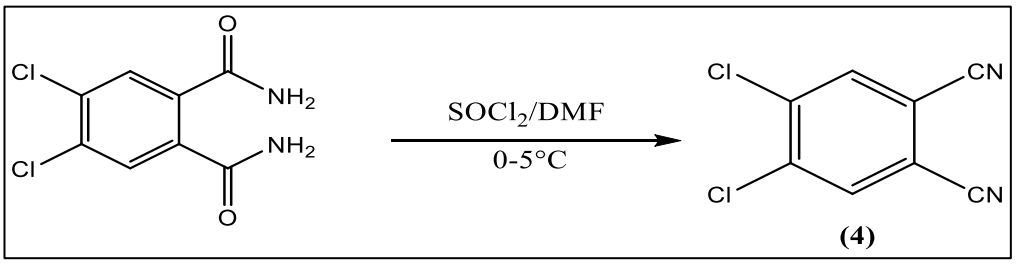

Figure 4.11: Synthesis of 4,5-Dichloro-1,2-dicyanobenzene **(4)**.

4.1.5 Synthesis of 4-{[4-(N,N- Dimethylamino)phenyl]ethynyl}phthalonitrile (5)

The procedure for this phthalonitrile synthesis is followed from (Maya et al., 2000). 4-iodo phthalonitrile **(1)** (1 g, 3.93 mmol) and 4-(N,N-Dimethylamino)phenylethylene (0.66 g, 4.6 mmol) were dissolved in a solvent mixture of THF:triethylamine (20:16). Copper(I) iodide (3.7 mg, 0.019 mmol) along with bis(triphenylphosphine)palladium(II) chloride (28 mg, 0.039 mmol) catalysts were added and stirred under nitrogen gas for 12 hours at room temperature (Figure 4.12). Later, liquid part of product solution was removed under vacuum. Resultant product was dispersed in CH_2Cl_2 and water rinsed over and over again with water and dried and finally clarified with using silica gel column chromatography with CH_2Cl_2:hexane (2:3) mobile phase.

Molecular formula: $C_{18}H_{13}N_3$. Molecular weight: 271.32g/mol. Yield: 0.60 g (56%). M.P:118 °C. FT-IR υ_{max} (cm^{-1}): 3088 (aromatic C-H), 2904 (aliphatic C-H), 2194 (C≡N), 2125 (C≡C), 1585, 1522, 1364, 1227, 1180, 1136. ^{1}H- NMR (500 MHz; DMSO-d6): δ (ppm) 8.25-8.23 (1H, s, Ar-H), 8.12-8.09 (1H, d, Ar-H), 7.95-7.91 (1H, d, Ar-H), 7.43-7.39 (2H, d, Ar-H), 6.76-6.72 (2H, d, Ar-H), 2.99-2.97 (6H, s, CH_3). ^{13}C-NMR (500 MHz; DMSO-d6): δ (ppm) 40.30, 85.91, 98.94, 106.91, 112.28, 112.78, 116.21 (C≡N), 129.63, 133.60, 134.64, 135.75, 135.99, 151.35.

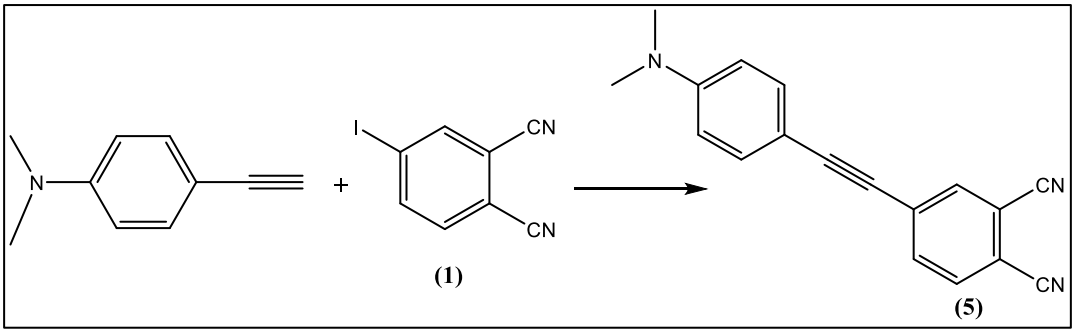

Figure 4.12: Synthesis of 4-{[4-(N,N-Dimethylamino)phenyl]ethynyl}phthalonitrile **(5)**.

4.1.6 Synthesis of 4,5-bis{[3,5-bis(trifluoromethyl)phenyl]ethynyl}phthalonitrile (6)

4,5-dichloro-phthalonitrile **(4)** (0.500g, 2.5mmol) and 1-Ethynyl-3,5-bis(trifluoromethyl)benzene (0.500g 1.67mmol) were dissolved in a THF:triethylamine (20:10) solvent mixture. Copper(I) iodide (3.7 mg, 0.019 mmol) and bis(triphenylphosphine)palladium(II) chloride (28 mg, 0.039 mmol) compounds

were added as catalysts and stirred at 70°C for 24 hours under nitrogen gas (Figure 4.13). After the 24 hours' time, the solvent was vacuum extracted and the product was diluted in chloroform and went through water extraction. For purification, the reaction precipitate was refined by means of silica filled column with chloroform solvent.

Molecular formula: $C_{28}H_8F_{12}N_2$. Molecular weight: 600.37 g/mol. Yield: 0.7 g (46%). M.P: 112 °C. FT-IR $\nu_{max}(cm^{-1})$: 3080 (aromatic C-H), 2124 (C≡C), 2238 (C≡N), 2982 (aliphatic C-H). ^{1}H-NMR (500 MHz; DMSO-d6): δ (ppm) 8.26 (2H, s, Ar-H), 8.20 (4H, s, Ar-H), 8.15 (2H, s, Ar-H). ^{13}C-NMR (500 MHz; DMSO-d6): δ (ppm) 94.3, 110.79, 115.00, 115.30 (C≡N), 124.80, 129.23, 132.14, 136.03, 137.96, 138.50.

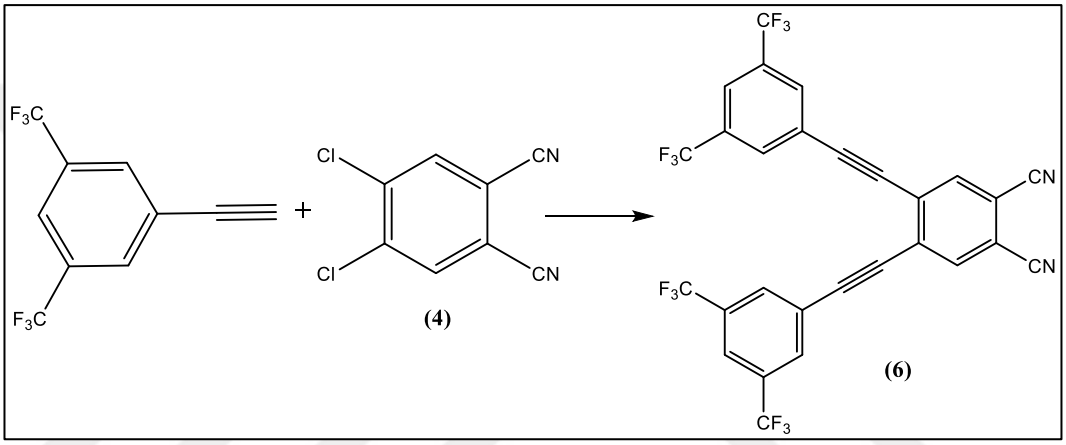

Figure 4.13: Synthesis of 4,5-bis{[3,5 bis(trifluoromethyl)phenyl]ethynyl}phthalonitrile **(6)**.

4.1.7 Synthesis of 4,5-bis[(4-(dimethylamino)phenyl)ethynyl]phthalonitrile (7)

The procedure follows Sonogashira Pd/Cu-catalyzed cross-coupling. It's started by starting with a mixture consisting of 4-Ethynyl-N,N-dimethylaniline (1.47 g, 10.15 mmol) and 4,5- dichlorophthalonitrile **(4)** (1 g, 5.08 mmol) dissolved in triethylamine:THF (4:5) solution. Moreover, [Pd $(PPh_3)_2Cl_2$] (53.44 mg, 0.076 mmol) and CuI (7.73 mg, 0.041 mmol) acted as the reaction catalyzing agents (Figure 4.14). The mixture refluxed at 80 ºC and blended beneath inert air for a 24 hour period. After the completion, the solvent removal under reduced pressure was followed by dissolution in dichloromethane and extraction in water. For purifying the resulting compound, silica filled column and hexane: dichloromethane (3:2) mixture acted as mobile phase. The pure product was obtained in orange colored powdered form.

Molecular formula: $C_{28}H_{22}N_4$. Molecular weight: 414.51g/mol. Yield: 1.30 g (62%). M.P. > 168 °C. FT-IR υ_{max} (cm^{-1}): 3083 (aromatic C-H), 2924 (aliphatic C-H), 2194

(C≡N), 2158 (C≡C), 1577, 1526, 1223, 1142. ^{1}H-NMR (500 MHz; DMSO-d6): δ (ppm) 8.47 (1H, s, Ar-H), 8.38 (1H, s, Ar-H), 7.44-7.33 (4H, d, Ar-H), 6.79-6.76 (4H d, Ar-H), 2.99-2.95 (12H, s, CH_3). ^{13}C-NMR (500 MHz; DMSO-d6): δ (ppm) 152.77 149.99, 148.00, 145.23, 141.46, 140.83, 140.46, 137.97, 136.02, 133.79, 115.29 (C≡N), 115.00, 113.46, 107.40, 105.92, 94.38-91.02, 39.46-40.47.

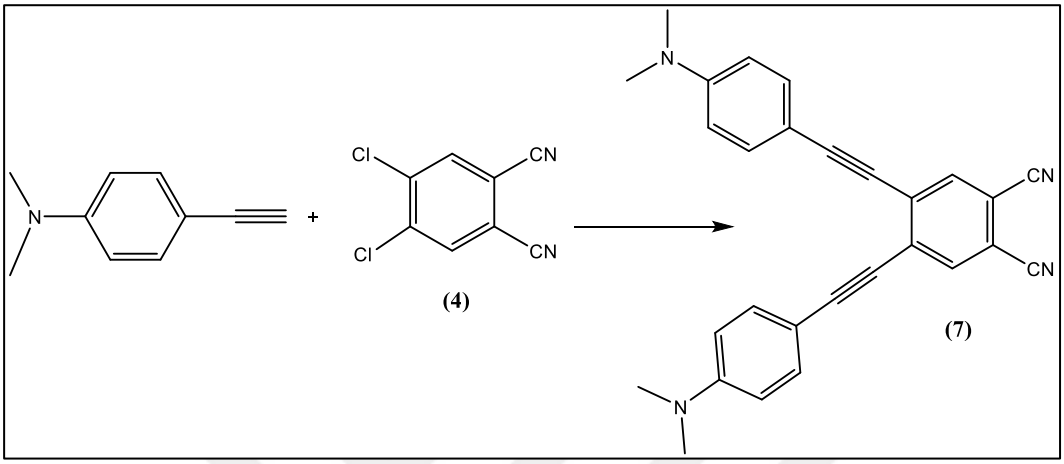

Figure 4.14: Synthesis of 4,5-bis((4-(dimethylamino)phenyl)ethynyl)phthalonitrile **(7)**.

4.2 Synthesis of Asymmetric Metal Phthalocyanines

4.2.1 Synthesis of 2-(3-ethynyl thiophene)-8, 9, 10, 11, 15, 16, 17, 18, 22, 23, 24, 25 - dodecafluoro phthalocyaninato cobalt (II) (PcAsCo-1)

A mixture consisting of 4-(thiophen-3-ylethynyl) phthalonitrile **(2)** (0.032 g, 0.14 mmol), 1,2-dicyano-3,4,5,6-tetrafluorobenzene (0.080 g, 0.40 mmol), $CoCl_2$ salt (0.022 g, 0.17 mmol) dissolved in 1.5-2 mL 1-Chloronaphthalene solvent was reacted for 48 hours at 180°C under N_2 atmosphere (Figure 4.15). The obtained product was precipitated and then washed with methanol. First, two isomers were separated with a combination of hexane:dioxane (5:1.5) on a silica-loaded column, then the desired isomer was purified with a solvent mixture of hexane:dioxane (5:0.5) by preparative chromatography method. UV-vis, FT-IR and MALDI-TOF analysis of the compound are attached.

Molecular formula: $C_{38}H_6CoF_{12}N_8S$. Molecular weight: 893.49 g/mol. Yield: 0.006 g (3%). M.P. >200 ºC. FT-IR υ_{max} (cm-^{1}): 3056-3067 (aromatic C-H), 2113-2114 (C≡C). (MALDI-TOF): m/z $[M]^+$ calculated 893.5 found 892.0 $[M-H]^+$.

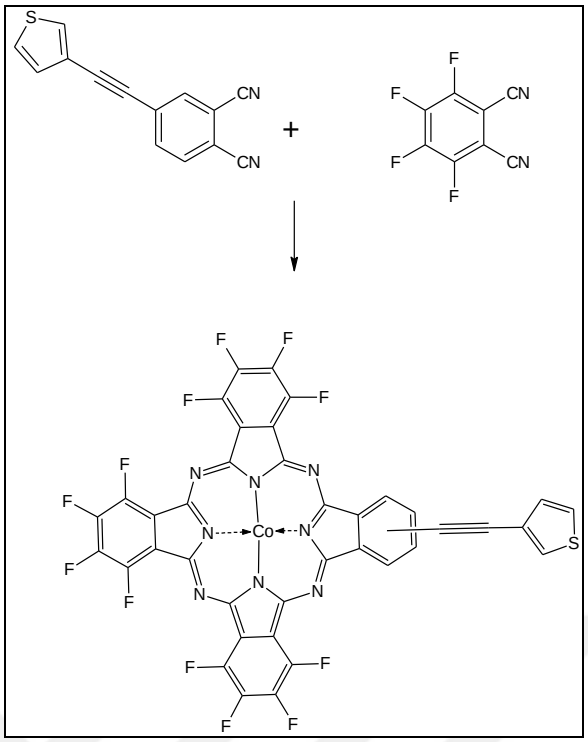

Figure 4.15: 2-(3-ethynyl thiophene)-8, 9, 10, 11, 15, 16, 17, 18, 22, 23, 24, 25 - dodecafluoro phthalocyaninato cobalt (II) **(PcAsCo-1)**.

4.2.2 Synthesis of 2-(3-ethynyl thiophene)- 8, 9, 10, 11, 15, 16, 17, 18, 22, 23, 24, 25 - dodecafluoro phthalocyaninato zinc (II) (PcAsZn-1)

The procedure started with combining 4-(thiophen-3-ylethynyl)phthalonitrile **(2)** (0.032g, 0.14 mmol), 1,2-dicyano-3,4,5,6-tetrafluorobenzene (0.080g ,0.40 mmol) and $Zn(OAC)_2$ (0.031g, 0.17 mmol), and 2 mL 1-Chloronaphthalene stirred under N_2 gas at 180°C for 48 hours (Figure 4.16). The obtained product was first precipitated and subsequently washed with methanol. First, two isomers were isolated using a solution of hexane:dioxane (5:1.5) loaded onto column filled with silica and desired isomer was then purified later using an eluent mixture of hexane:dioxane (5:0.5) via preparative chromatography. ^{1}H-NMR, FT-IR, MALDI-TOF and UV-vis analysis graphs of PcAsZn-1 are presented.

Molecular Formula: $C_{38}H_6F_{12}N_8SZn$. Molecular weight: 899.96 g/mol. Yield: 0.008 g (%7). M.P. >200 ºC. FT-IR υ_{max} (cm^{-1}): 3056-3067 (aromatic C-H), 2113-2114 (C≡C). (MALDI-TOF): m/z calculated $[M]^+$ 899.96 found 899.44 $[M]^+$. ^{1}H-NMR (500 MHz; DMSO-d6): δ (ppm) 7.68- 7.70 (1H, d, S-CH), 6.87 (1H, s, CH-S), 6.58-6.64 (4H, m, Ar-H).

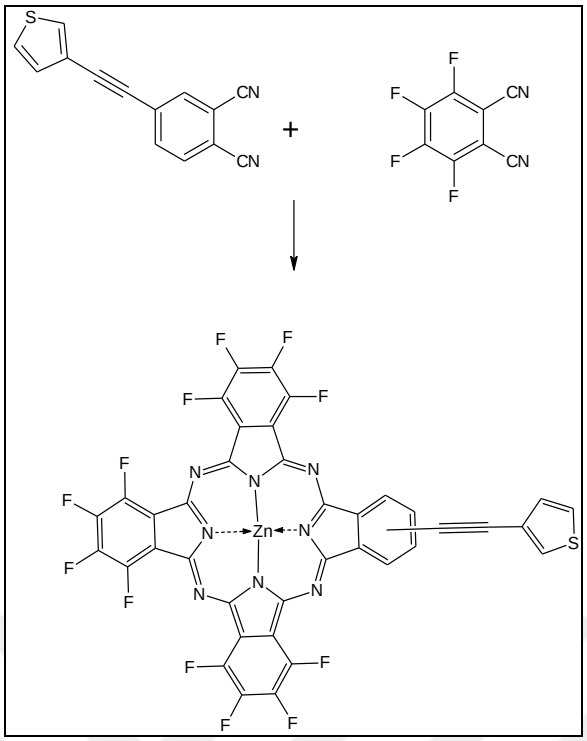

Figure 4.16: 2-(3-ethynyl thiophene)- 8, 9, 10, 11, 15, 16, 17, 18, 22, 23, 24, 25 - dodecafluoro phthalocyaninato zinc (II) **(PcAsZn-1)**.

4.2.3 Synthesis of 2-(4- pentylphenyl)ethynyl-8, 9, 10, 11, 15, 16, 17, 18, 22, 23, 24, 25- dodecafluoro phthalocyaninato cobalt (II) (PcAsCo-2)

4-[(4-pentylphenyl)ethynyl] phthalonitrile **(3)** (0.037 g, 0.14 mmol), 1,2-Dicyano-3,4,5,6-tetrafluorobenzene (0.080 g , 0.40 mmol) and $CoCl_2$ (0.022 g, 0.17 mmol) was dissolved in 2 mL 1-Chloronaphthalene solvent and left to react under N_2 pressure at 180 °C and lasted 48h (Figure 4.17). After completion, the product was cooled and precipitated then washed with a copious amount of methyl alcohol. At first, the two isomers of Pc compound were separated via column chromatography by hexane:dioxane (5:1.5) solvent mixture then the desired isomer was purified through hexane:dioxane (5:0.5) mixture by preparative chromatography. UV-vis, MALDI-TOF spectra of synthesized compound have been presented.

Molecular formula: $C_{45}H_{18}CoF_{12}N_8$. Molecular weight: 957.59 g/mol. Yield: 0.0012 g (%9). M.P. >200 ºC. FT-IR υ_{max} (cm^{-1}): 3066-3056 (aromatic CH), 2963-2854 (aliphatic CH), 2210 (C≡C). (MALDI-TOF): m/z calculated $[M]^+$ 957.59 found 957.49 $[M]^+$.

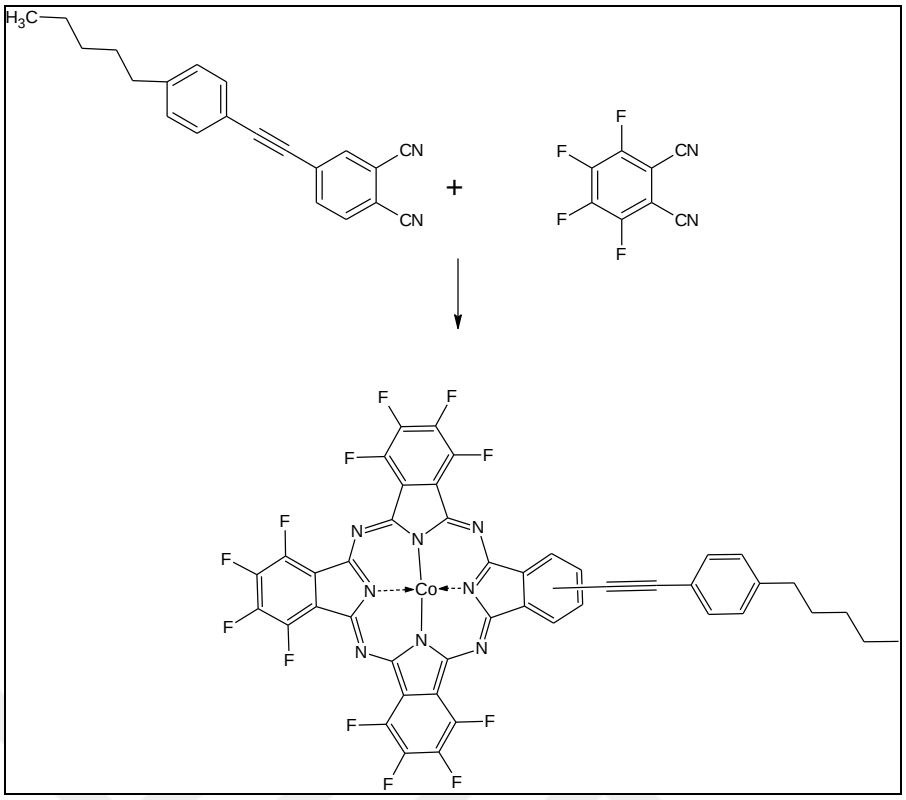

Figure 4.17: 2-(4- pentylphenyl)ethynyl-8, 9, 10, 11, 15, 16, 17, 18, 22, 23, 24, 25 - dodecafluoro phthalocyaninato cobalt (II) **(PcAsCo-2)**.

4.2.4 Synthesis of 2-(4-pentyl phenyl)ethynyl- 8, 9, 10, 11, 15, 16, 17, 18, 22, 23, 24, 25 - dodecafluoro phthalocyaninato zinc (II) (PcAsZn-2)

4-[(4-pentylphenyl)ethynyl] phthalonitrile (3) (0.037g, 0.14 mmol) with 1,2-dicyano-3,4,5,6-tetrafluorobenzene (0.080g , 0.40 mmol) and $Zn(OAc)_2$ (0.031g, 0.17 mmol), mixed with 2 mL 1-Chloronaphthalene boiled beneath N_2 gas and stirred for 48 hours at 180°C temperature (Figure 4.18). The product was initially precipitated and later washed with methanol. Initially, the two isomers were segregated on chromatographic silica column with hexane:dioxane (5:1.5) and then the desired isomer was isolated via solvent mixture of hexane:dioxane (5:0.5) using preparative chromatography. UV-vis, Mass and FT-IR spectra analysis of compound have been presented.

Molecular formula: $C_{45}H_{18}F_{12}N_8Zn$. Molecular weight: 964.07 g/mol. Yield: 0.006 g (%5). M.P. >200 ºC. FT-IR υ_{max} (cm^{-1}): 3066-3056 (aromatic CH), 2963-2854 (aliphatic CH), 2114 (C≡C). ^{1}H-NMR (500 MHz; DMSO-d6): δ (ppm) 8.18 (1H, s, Ar-H), 8.03 (1H, d, Ar-H), 7.95 (1H, d, Ar-H), 7.71-7.67 (2H, m, Ar-H), 7.51 (2H, m, Ar-H), 1.25 (8H, m, Aliphatic CH_2), 0.87-0.84 (3H, m, Aliphatic CH_3). (MALDI-TOF): m/z calculated $[M]^+$ 964.07 found 962.26 $[M-2H]^+$.

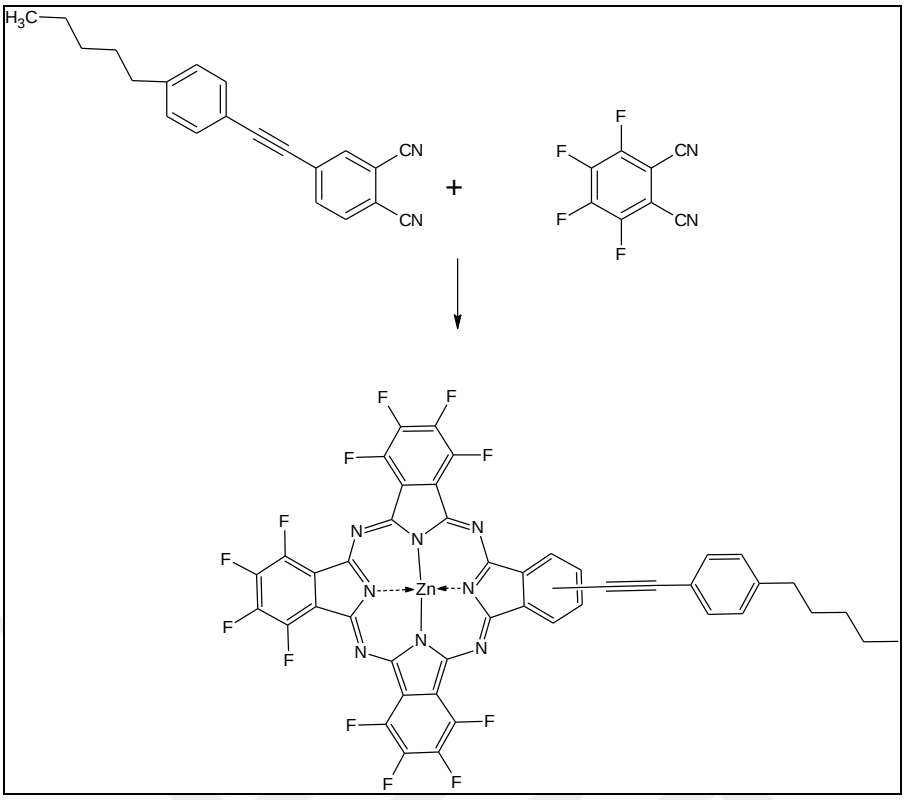

Figure 4.18: Synthesis of 2-(4-pentyl phenyl)ethynyl- 8, 9, 10, 11, 15, 16, 17, 18, 22, 23, 24, 25 - dodecafluoro phthalocyaninato zinc (II) **(PcAsZn-2)**.

4.3 Synthesis of New Peripherally Tetra-Substituted Symmetrical Phthalocyanine Derivatives

Metal substituted Pcs were synthesized by cyclotetramerization of the related dinitrile derivative in a high boiling point solvent. Tetra-substituted phthalocyanines are obtained as a combination of 4 structural isomers and hardly any examples in the literature are available as their separation is very difficult by the normal chromatographic method. Hereof, no separation method was applied for these isomeric structures.

4.3.1 Tetra substituted metal Pcs of 4-{[4 (dimethylamino)phenyl]ethynyl}phthalonitrile derivative (5)

Metal phthalocyanines synthesis was administered by cyclotetramerization of 4-{[4-(N,N-Dimethylamino)phenyl]ethynyl}phthalonitrile **(5)** (136mg, 0.50mmol) with anhydrous $CoCl_2$ (0.020 g, 0.15 mmol), $Zn(OAc)_2$ (0.030 g, 0.16 mmol), $MnCl_2$ (0.020 g, 0.15 mmol), $Fe(OAc)_2$ (0.287 mmol) respectively in 3mL N,N-dimethylaminoethanol solvent stirred at 135ºC temperature under inert atmosphere

(Figure 4.19-4.22). The crude products were precipitated and washed using hexanol, methanol and water and later purified via column chromatography working with THF as mobile and silica gel as static phase. The procedure for LuPc synthesis follows by first dissolving Lutetium (III) acetate salt (5.8mg, 0.016mmol) and (5) phthalonitrile (136mg, 0.50mmol) in 1.5mL of 1-pentanol and also few drops of DBU are added to make the reaction medium basic and then boiled upto165 ºC and continued for 24h with nitrogen gas atmosphere (Figure 4.23). Obtained product mixture is then cooled down and precipitated in water/ethanol (1:1), filtered off and left to dry. Sandwich lutetium Pc product is separated through DCM: THF (1:1) solution on chromatographic column. The products are usually isolated as a mixture of isomers. Solubility: DCM, THF and methanol. All these synthesized metal phthalocyanines went through characterization via MALDI-TOF, UV-vis, and FT-IR spectroscopy. Moreover, the ZnPc went under additional ^{1}H NMR spectroscopy.

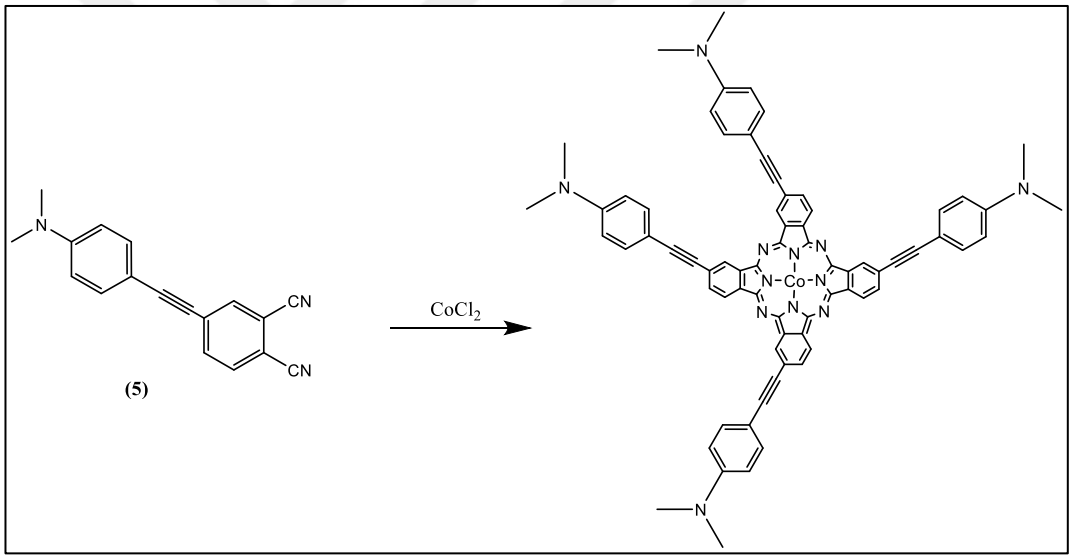

Figure 4.19: Synthesis of {2(3),9(10),16(17),23(24)-Tetrakis-2-(4-(N,N-Dimethylamino)phenyl)ethynyl] phthalocyaninato cobalt (II) **(PcTACo)**.

Molecular formula: $C_{72}H_{52}CoN_{12}$. Molecular weight: 1144.23g/mol. Yield: 0.090 mg (66%). M.P. > 250 °C. FT-IR υ_{max} (cm^{-1}): 3070 (C-H aromatic), 2929 (C-H aliphatic), 2188 (C≡C), 1599 (C=C aromatic), 1091 (C-N), 1357, 812. (MALDI-TOF): m/z calculated $[M]^{+}$ 1114.20 found 1145.59 $[M+2H_2O-4H]^{+}$.

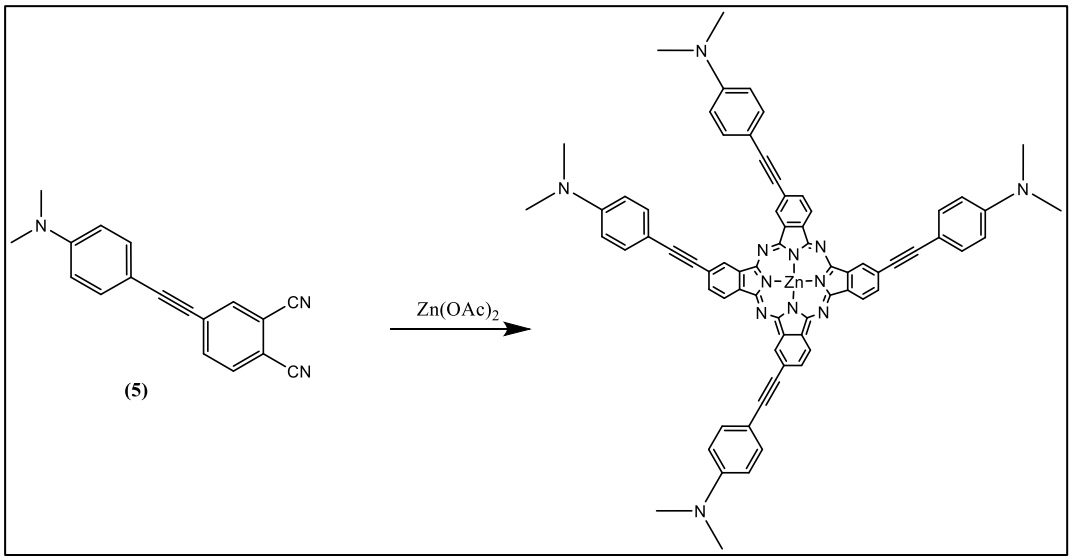

Figure 4.20: Synthesis of {2(3),9(10),16(17),23(24)-Tetrakis2-(4-(N,N-Dimethylamino)phenyl)ethynyl] phthalocyaninato zinc (II) **(PcTAZn)**.

Molecular formula: $C_{72}H_{52}N_{12}Zn$. Molecular weight: 1150.67g/mol. Yield: 0.082 g (60%). M.P. > 250 °C. FT-IR υ_{max} (cm^{-1}): 3002 (C-H aromatic), 2920 (C-H aliphatic), 2213 (C≡C), 1043 (C-N), 1306, 953.^{1}H-NMR (500 MHz; DMSO-d6): δ (ppm) 6.96-6.91 (10H, m, Ar-H), 6.88-6.85 (10H, m, Ar-H), 6.74-6.72 (4H, d, Ar-H), 6.64 (4H, d, Ar-H), 3.13-3.08 (24H, s, N-CH_3). (MALDI-TOF): m/z calculated $[M]^+$ 1150.64 found $[M]^+$ 1151.17.

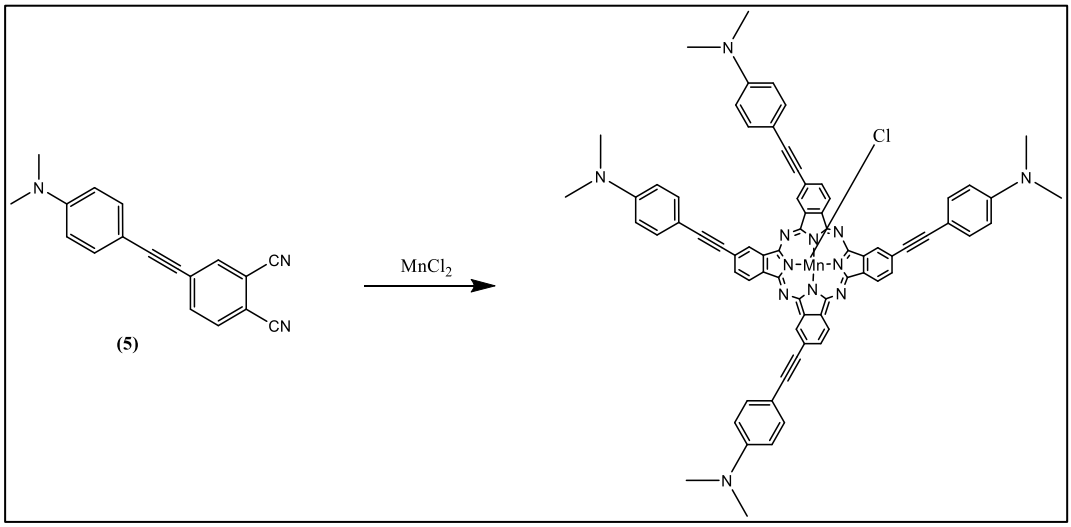

Figure 4.21: Synthesis of {2(3),9(10),16(17),23(24)-Tetrakis2-(4-(N,N-Dimethylamino)phenyl)ethynyl] phthalocyaninato manganese (II) **(PcTAMn)**.

Molecular formula: $C_{72}H_{52}ClN_{12}Mn$. Molecular weight: 1175.68g/mol. Yield: 0.070g (50%). M.P. > 250 °C. FT-IR υ_{max} (cm^{-1}): 3035 (C-H aromatic), 2918 (C-H aliphatic), 2178 (C≡C), 1314, 1013 (C-N), 951. (MALDI-TOF): m/z $[M]^+$=1175.718 found

1160.540 $[M\text{-}CH_3]^+$, 1125.520 $[M\text{-}2C_2H_6N\text{+}2H_2O\text{+}2H]^+$, 1091.234 $[M\text{-}6CH_3\text{+}6H]^+$, 982.111 $[M\text{+}2DIT\text{-}3C_2H_6N\text{+}3H_2O]^{+2}$, 838.553 $[M\text{+}DIT\text{+}3Na]^{+2}$.

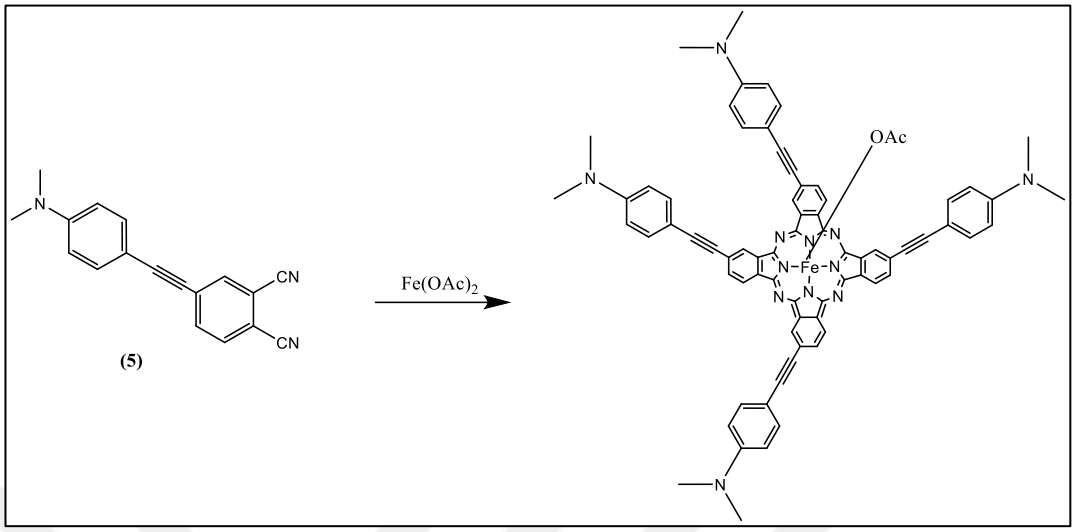

Figure 4.22: Synthesis of {2(3),9(10),16(17),23(24)-Tetrakis-2-(4-(N,N-Dimethylamino)phenyl)ethynyl] phthalocyaninato iron(II) **(PcTAFe)**.

Molecular Formula: $C_{74}H_{55}FeN_{12}O_2$. Molecular Weight: 1200.18g/mol. Yield: 0.055g (45.21%). FT-IR υ_{max} (cm^{-1}): 3009 (C-H aromatic), 2919 (C-H aliphatic), 2187 (C≡C), 1315, 1013 (C-N), 951. (MALDI-TOF): m/z calculated $[M]^+$=1200.68 found 1078 $[M\text{-}4C_2H_6N\text{+}3H_2O]^+$, 785.586 $[M\text{-}4CH_3\text{-}2H\text{+}DIT]^{2+}$, 700.783 $[2M\text{-}8C_2H_6N\text{+}3H_2O]^{3+}$, 1346.104 $[M\text{+}4Na\text{+}3H_2O]$, 898.459 $[M\text{+}DIT\text{+}4Na\text{+}4H_2O]$.

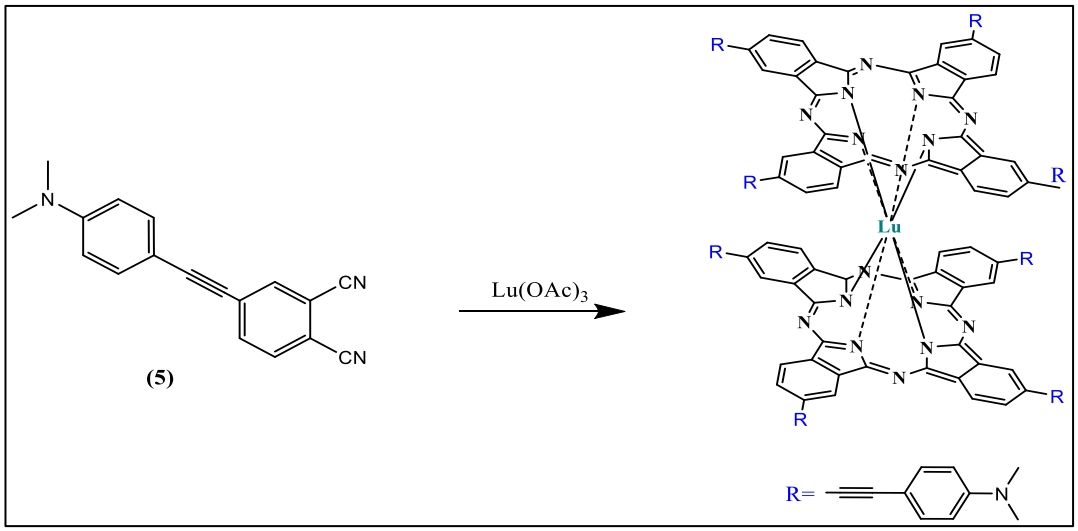

Figure 4.23: Synthesis of Bis-[{2(3),9(10),16(17),23(24)-Tetrakis-2-(4-(N,N-dimethylamino)phenyl)ethynyl] phthalocyaninato} lutetium (III) **(PcTALu′).**

Molecular formula: $C_{144}H_{104}LuN_{24}$. Molecular Weight: 2345.55g/mol. Yield: 0.050g (35.59%). FT-IR υ_{max} (cm^{-1}): 3030 (C-H aromatic), 2954 (C-H aliphatic), 2181(C≡C),

1362, 1234 (C-N). (MALDI-TOF): m/z calculated $[M]^{+}$= 2345.55 found 956.018 $[M+DIT+3Na+H_2O+H]^{3+}$, 1160.551 $[M-2CH_3+4H]^{2+}$.

4.4 Synthesis of New Symmetrical Peripherally Octa-Substituted Phthalocyanine Derivatives

Symmetrical peripheral octa-substituted phthalocyanines were synthesized from 4,5-bis{[3,5-bis(trifluoromethyl)phenyl]ethynyl}phthalonitrile **(6)** and 4,5-bis((4-(dimethylamino)phenyl)ethynyl)phthalonitrile **(7)**.

4.4.1 Octa substituted metal Pcs of 4,5-bis{[3,5-bis(trifluoromethyl)phenyl]ethynyl}phthalonitrile (6) derivative

Octa substituted MPcs were developed by combining 0.100 g (0.17mmol) 4,5-bis{[3,5-bis(trifluoromethyl)phenyl]ethynyl}phthalonitrile **(6)** with anhydrous $CoCl_2$ (0.020g, 0.15 mmol), anhydrous $Zn(OAc)_2$ (0.030 g, 0.16 mmol) respectively dissolved in 3 mL of 2-(dimethylamino ethanol) in an airtight vessel refluxed at 137 °C under nitrogen atmosphere and continued 24 hours (Figure 4.24-4.25).Once the process finished, the product has been cooled then precipitated by water treatment and washed thoroughly with methanol, water and hexane and desiccated. Later on, pure compound was obtained with chromatographic process on a column filled with silica and THF as eluent. While, the LuPc synthesis follows starting with dissolving Lutetium (III) acetate salt (5.8mg, 0.016mmol) and **(6)** phthalonitrile (100mg, 0.17mmol) in 1.5mL 1-pentanol solvent along with few drops of DBU, then heated upto165 ºC for 24h under nitrogen gas pressure (Figure 4.26). After 24h, the product mixture is cooled down and precipitated by dissolving in water/ethanol (1:1) solution and filtered. The mono product is separated via THF on silica gel column. The products are present as a mixture of isomers. Solubility: DCM, acetone, THF, methanol. Characterization of these all these octa MPcs has been executed through ^{1}H-NMR (paramagnetic MPcs), FT-IR, MALDI-TOF (mass) and UV-vis spectroscopy.

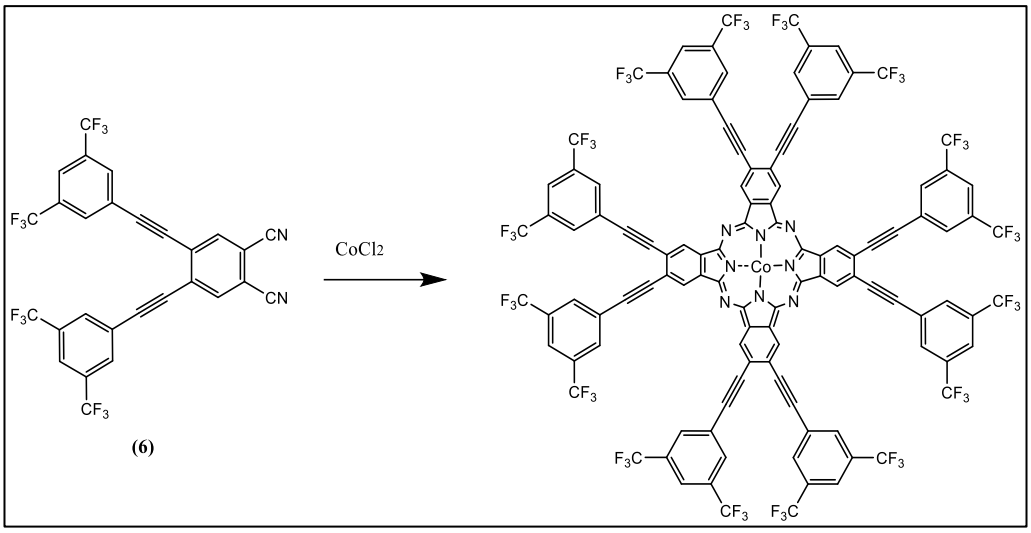

Figure 4.24: Synthesis of {2(3),9(10),16(17),23(24)-octakis-{[3,5 bis(trifluoromethyl)phenyl]ethynyl}phthalocyaninato} cobalt (II) **(PcOFCo)**.

Molecular formula: $C_{112}H_{32}CoF_{48}N_8$. Molecular weight: 2460.40g/mol. Yield: 0.068 g (66.37%). M.P. > 250 ºC. FT-IR υ_{max} (cm^{-1}): 3022 (C-H aromatic), 2952 (C-H aliphatic), 2204 (C≡C), 1364, 1026 (C-N), 941. (MALDI-TOF): m/z calculated $[M]^+$=2460.40 found 1154.304 $[M+Na+5H_2O+10H-6CF_3]^{2+}$, 866.645 $[M+8H_2O-3H]^{3+}$, 782.015 $[M+H_2O-2CF_3]^{3+}$.

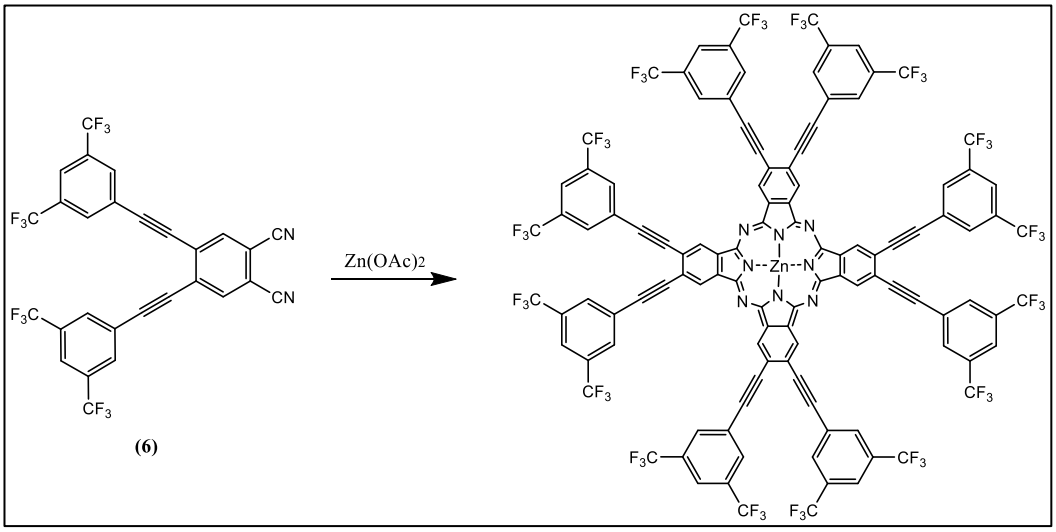

Figure 4.25: Synthesis of {2(3),9(10),16(17),23(24)-octakis-{[3,5 bis(trifluoromethyl)phenyl]ethynyl}phthalocyaninato} zinc (II) **(PcOFZn)**.

Molecular formula: $C_{112}H_{32}ZnF_{48}N_8$. Molecular weight: 2466.86g/mol. Yield: 0.066g (64%). M.P. > 250 ºC. FT-IR υ_{max} (cm^{-1}): 3022 (C-H aromatic), 2952 (C-H aliphatic), 2204 (C≡C), 1364, 1026 (C-N), 941. (MALDI-TOF): m/z calculated $[M]^+$=2466.86 found 956.239 $[M+3H_2O+Na+DIT-3CF_3+8H]^{3+}$, 922.200 $[M+8H_2O+DIT-4CF_3]^{3+}$,

853.701 $[M+5H_2O+2H]^{3+}$, 715.878 $[M+3Na+H_2O+4H-6CF_3]^{3+}$. ^{1}H-NMR (500 MHz; DMSO-d6): δ (ppm) 8.11 (8H, s, Ar-H), 7.81 (16H, s, Ar-H), 7.37 (8H, s, Ar-H).

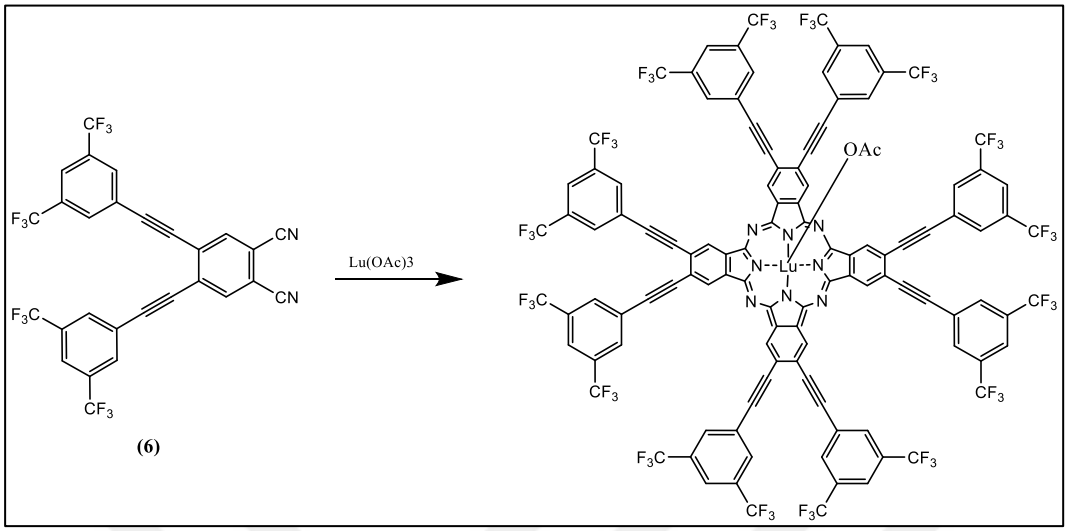

Figure 4.26: Synthesis of {2(3),9(10),16(17),23(24)-octakis-{[3,5 bis(trifluoromethyl)phenyl]ethynyl}phthalocyaninato}lutetium (III) **(PcOFLu)**.

Molecular formula: $C_{114}H_{35}F_{48}LuN_8O_2$. Molecular weight: 2635.48g/mol. Yield: 0.043g (39%). M.P. > 250 ºC. FT-IR υ_{max} (cm^{-1}): 3022 (C-H aromatic), 2952 (C-H aliphatic), 2204 (C≡C), 1364, 1026 (C-N), 941. (MALDI-TOF): m/z calculated $[M]^+$=2635.491 found 1121 $[M-6CF_3+H_2O+2H]^{2+}$, 660 $[M+4H]^{4+}$.^{1}H-NMR (500 MHz; DMSO-d6): δ (ppm) 7.66-7.72 [24H, m, Ar-H (CH-CF_3)], 6.86 [8H, s, Ar-H(CHC≡C)], 1.86 (3H s, O-CH_3).

4.4.2 Octa substituted metal Pcs of 4,5-bis((4-(dimethylamino)phenyl)ethynyl)phthalonitrile (7) derivative

Phthalonitrile derivative (**7)** 's (100mg, 0.24mmol) cyclotetramerization administered the development of respective octa-substituted metal phthalocyanines in the presence of cobalt(II)chloride (0.008g, 0.060 mmol) as well as zinc(II)acetate (0.011g, 0.060 mmol) salts submerged in 3mL of 2-dimethylaminoethanol respectively and stirred at 135 ºC with N_2 gas (Figure 4.27-4.28). The phthalocyanines produced were then precipitated with hexanol, water and methanol and firther subjected to chromatographic technique where a silica gel and THF filled column retrieved purified products. Whereas, for LuPc, Lutetium (III) acetate salt (5.8mg, 0.016mmol) and **(7)** phthalonitrile (100mg, 0.24mmol) was solvated in 1.5mL of 1-pentanol with few DBU drops stirred at 165 ºC for 24h under N_2 gas pressure in a closed tube (Figure 4.29).

When finished, the produced compound was left to be cooled down and precipitated with a water/ethanol (1:1) mixture. After filtering the greenish blue product, it was then rinsed with hot hexane thus cleaning any organic pollutants and then dried. The product is purified running DCM then THF on chromatographic column and extracted isomeric mixtures. Solubility: DCM, THF, methanol. Characterization of these all octa MPcs was done via FT-IR, Mass, ^{1}H-NMR and UV-vis spectroscopic approaches.

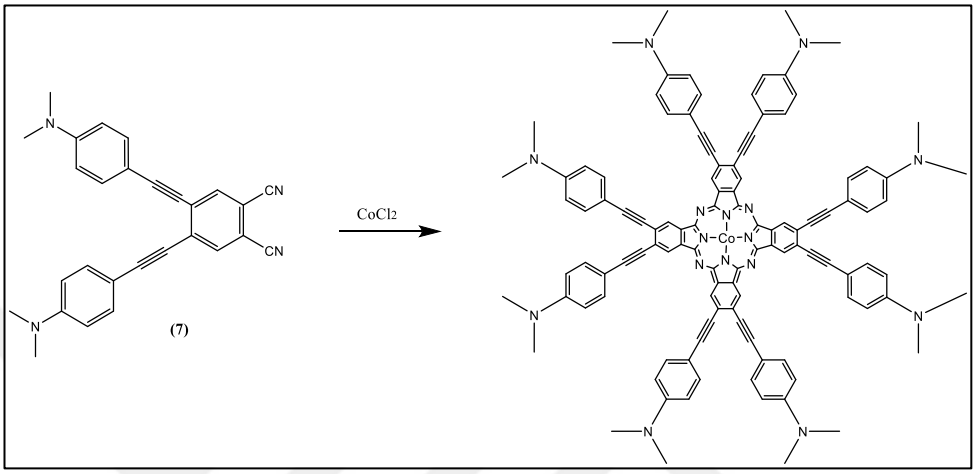

Figure 4.27: Synthesis of {2(3),9(10),16(17),23(24)-octakis-{[34,5-bis((4-(dimethylamino)phenyl)ethynyl)}phthalocyaninato}cobalt (II) **(PcOACo)**.

Molecular formula: $C_{112}H_{88}CoN_{16.}$ Molecular weight: 1716.98 g/mol. Yield: 43mg (41.5%). M.P > 250 °C. FT-IR υ_{max} (cm^{-1}): 3054 (C-H aromatic), 2916 (C-H aliphatic), 2116 (C≡C), 1597 (C=C aromatic), 1516 (C-C aromatic), 1360, 1229-1164 (C-N). (MALDI-TOF): m/z calculated $[M]^{+}$= 1716.94 found 1154.30 $[2M+Na+5H]^{3+}$.

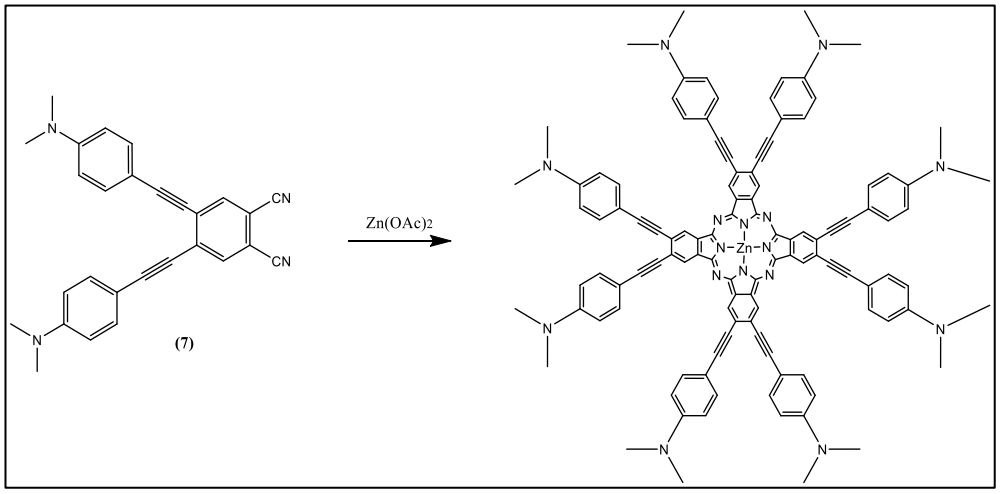

Figure 4.28: Synthesis of {2(3),9(10),16(17),23(24)-octakis-{[34,5-bis((4-(dimethylamino)phenyl)ethynyl)}phthalocyaninato}zinc (II) **(PcOAZn)**.

Molecular formula: $C_{112}H_{88}N_{16}Zn$. Molecular weight: 1723.43g/mol. Yield: 35 mg (34%). M.P. > 250 °C. FT-IR υ_{max} (cm^{-1}): 3046 (C-H aromatic), 2929 (C-H aliphatic), 2141 (C≡C), 1599-1516 (C-C aromatic), 1360, 1227-1164 (C-N). ^{1}H-NMR (500 MHz; DMSO-d6): δ (ppm) 8.33-8.29 (20H, m, Ar-H), 5.76-5.73 (20H, m, Ar-H), 4.12-4.09 (48H, m, N-CH_3). (MALDI-TOF): m/z calculated $[M]^+$= 1723.38 found 1289.26 [M-3($C_{10}H_{10}N$)-2H]$^+$.

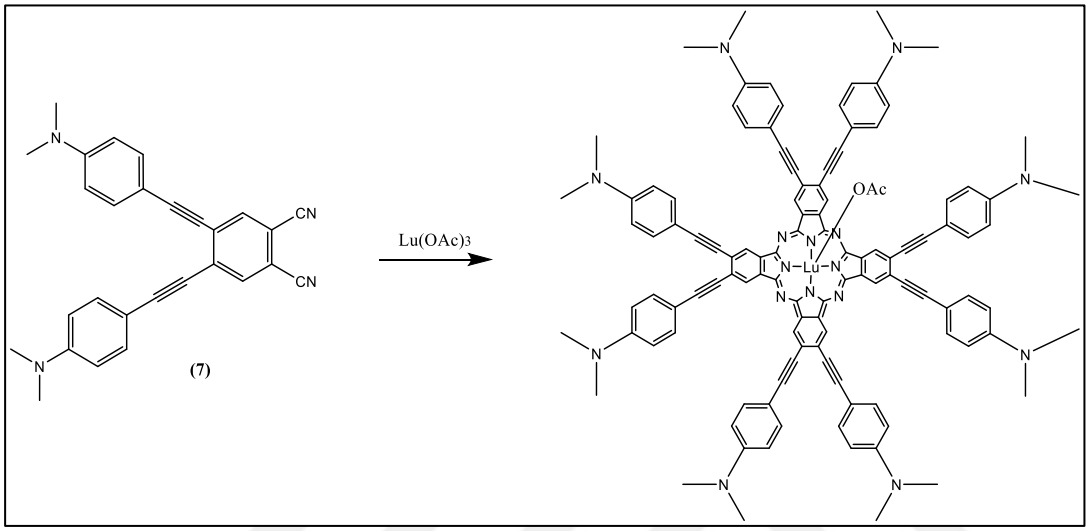

Figure 4.29: Synthesis of {2(3),9(10),16(17),23(24)-octakis-{[34,5-bis((4-(dimethylamino)phenyl)ethynyl)}phthalocyaninato}lutetium (III) acetate **(PcOALu).**

Molecular formula: $C_{114}H_{91}N_{16}LuO_2$. Molecular weight: 1892.06g/mol. Yield: 35 mg (30%). M.P. > 250 °C. FT-IR υ_{max} (cm^{-1}): 3022 (C-H aromatic), 2952 (C-H aliphatic), 2141 (C≡C), 1602-1520 (C-C aromatic), 1364, 1245 (C-N). ^{1}H-NMR (500 MHz; DMSO-d6): δ (ppm) 7.66-7.71 (40H, m, Ar-H), 2.533 (48H, s, N-CH_3), 2.17 (3H, s, O-CH_3). (MALDI-TOF): m/z calculated $[M]^+$= 1892.04 found 1976.124 [M-$N(CH_3)_2$+CHCA-CH_3COO^-+$2H^+$]$^+$, 2084.720 [M+CHCA+$3H^+$]$^+$, 2119.520 [M+CHCA+$2H_2O$+$2H^+$]$^+$, 2228.348 [M-CH_3COO^-+OH^-+2CHCA]$^+$.

4.5 Synthesis of Metal Pcs–Metal NanoParticles Conjugates

The synthesis of Metal Pcs–Nanoparticles conjugates is achieved in two-steps. Firstly, the desired metal-nanoparticles **(AuNPs)** are prepared and later conjugated to Metal Pcs **(PcTACo&Zn, PcOACo &Zn)**.

4.5.1 Synthesis of gold nanoparticles (AuNPs)

Spherical AuNPs were prepared according to the Turkevich procedure (Turkevich et

al., 1951)(Turkevich et al., 1953) with some modifications described in reference (Nguyen et al., 2011).

4.5.2 Synthesis of AuNPs-MPc conjugates

Conjugation of AuNPs was conducted with phthalonitriles **(5)** & **(7)** and their respective Co and Zn Pcs in DMSO and combined with gold nanoparticles (AuNPs) solution (Figure 4.30-4.31). The TEM analysis of the acquired AuNPs-MPcs conjugates **(AuNP- PcTACo &Zn, AuNP-PcOACo &Zn)** was carried out to observe the size and shape of these particles. All these MPc/AuNP hybrids along with phthalonitrile **(5)** & **(7)** and their respective Co and Zn Pcs were subjected to investigate several biological studies explained in the subsequent section.

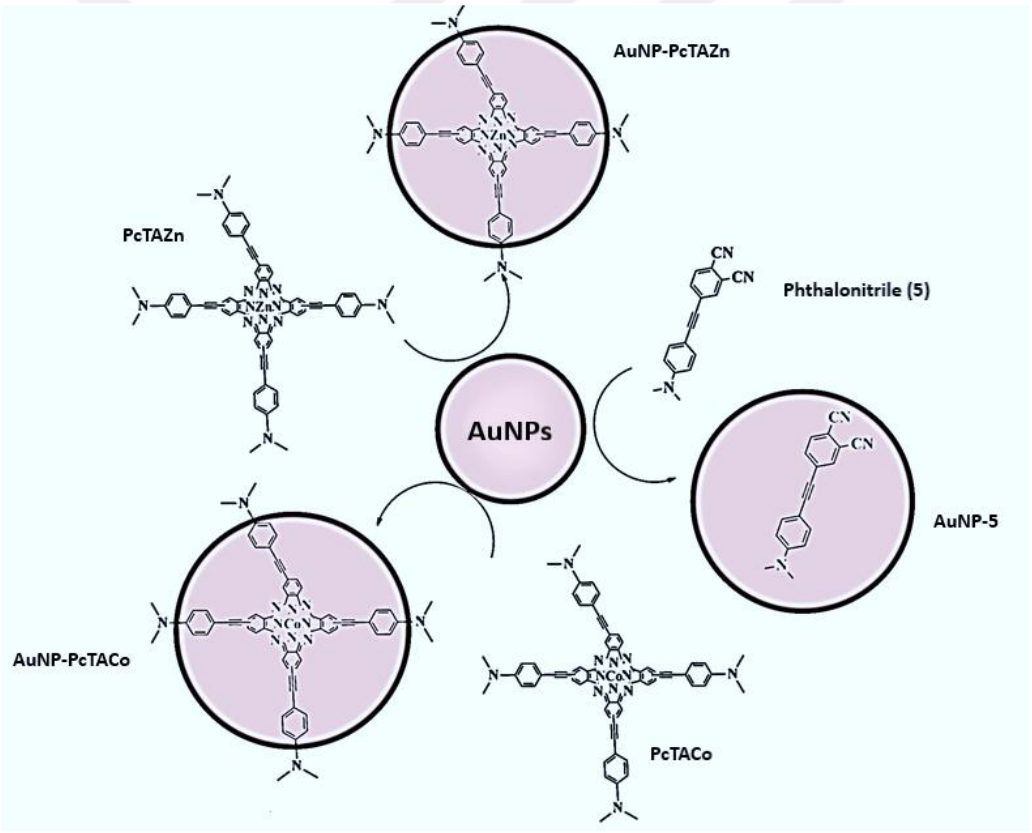

Figure 4.30: Synthesis of AuNPs-MPcs conjugates for phthalonitrile **(5)** and its subsequent MPcs.

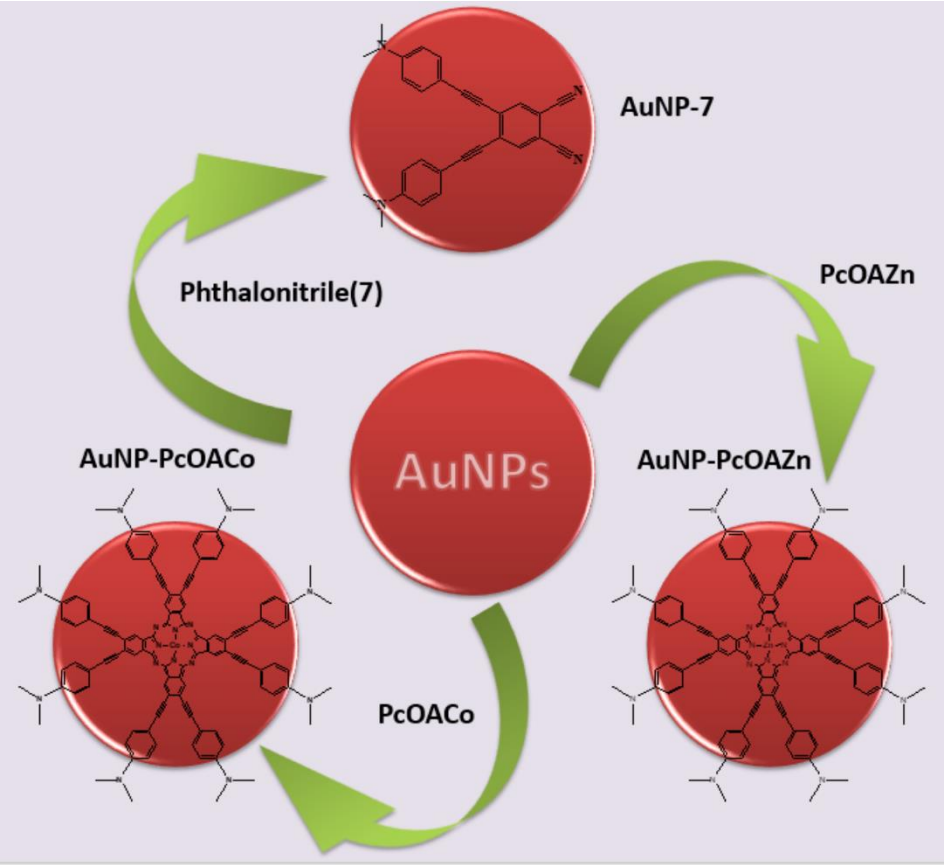

Figure 4.31: Synthesis of AuNPs-MPcs conjugates for phthalonitrile **(7)** and its subsequent MPcs.

4.6 Biological Studies of the AuNPs-MPc conjugates

4.6.1 DPPH radical scavenging activity

Oxidative stress is a process that occurs naturally in all living organisms. It results due to the irregularities regarding the presence of free radicals and antioxidants in the body systems. These free radicals are produced as a part of natural metabolic process occurring inside different organs and can damage cell organelles leading to eventual cell and tissue deterioration thus known as oxidative damage (Valko et al., 2006). Development of certain chronic and neurodegenerative illnesses are linked to oxidative stress like Alzheimer's and Parkinson's disorders, hypertension, diabetes, obesity, asthma, cancer etc.(Rahman et al., 2012). Several personal and environmental factors such as diet rich in fats and processed carbohydrates, exposure to UV radiations and pollution can also advance the damaging process.

The protection mechanisms responsible for natural eradication of these free radicals from the body could follow either an endogenous enzymatic (superoxide dismutase,

glutathione peroxidases, glutathione, catalase and glutathione reductase) or non-enzymatic path (uric acid, bilirubin, melatonin) and exogenous antioxidant nutrients are among the few known defense functions to encounter the free radical damages(Fang et al., 2002; Prior & Cao, 1999).

The free radical inhibition of the compounds (**5, PcTACo&Zn, AuNPs, AuNP-5, AuNP-PcTACo&Zn**) towards the DPPH radical in this thesis was investigated as quoted in (Prior & Cao, 1999). The sample tubes consisted of 500 µL solution of various concentrations of the above mentioned compounds along with 2.0 mL of DPPH solution and were left in the incubator with 25 ºC conditions for 30 min. Herein, Trolox and Ascorbic acid were control compounds and followed the same incubation process. After finishing, the free radical inhibition ability was recorded via spectrophotometer at a wavelength of 517 nm. The free radical inhibition ability was determined with following equation (4.1).

For the antioxidant activities calculation of compounds **(7, PcOACo&Zn, AuNPs, AuNP-7, AuNP-PcOACo&Zn)** the DPPH radical scavenging method applied is mentioned in ref. (Prior & Cao, 1999). The sample test tubes contained 250 µL solution of 6.25 to 100 mgL^{-1} concentrations of examined compounds and 1000 µL DPPH solution. All the solutions were prepared in distilled water. Sample contents were homogenized and placed for 30 mins into incubator at room temperature and dark conditions. Identical conditions were imitated for standards; ascorbic acid and Trolox materials. Afterwards, the absorbance was calculated at 517 nm with a spectrophotometer equipment and the radical scavenging performance was computed by the below mentioned eqn (4.1).

$$\text{DPPH activity (\%)} = \left(\frac{Abs(control) - Abs(sample)}{Abs(sample)}\right) \times 100 \qquad (4.1)$$

Here, Abs (control) stands for absorbance of control substance and Abs(sample) implies the absorbance readings of the tested compounds and DPPH following 30 minutes time duration.

4.6.2 DNA cleavage activity

The importance of DNA (deoxyribonucleic acid) as a macromolecular target for the treatment of genetic and microbial infectious illnesses is well known. Because DNA molecules are responsible for storing all genetic information related to biological

processes, they perform a critical function while developing anticancer and antibacterial medicines. DNA is the principal objective of anticancer medicines since it regulates most biochemical activities in cellular systems. Regulatory processes involving DNA include gene expression, gene regulation, aberration, and carcinogenesis. Most chemotherapeutic drugs neutralize cancerous cells by adhering to or modifying DNA due to its predominant function in cellular multiplication (Ozturk et al., 2012). The ability to predict the rate of cancer obliteration in tumor therapeutics (Amitha & Vasudevan, 2020) and pathogenic microorganism elimination in antimicrobial response can be aided by understanding the DNA binding/cleavage activities of medications and their processes. Because of the possible purposes of nucleic acid chemistry, materials that are ideal for adhering to and sequencing DNA have gained wide popularity (Ayala et al., 2005). The study of DNA's interaction with small molecules is critical in the development of new pharmaceutical compounds (Tabassum et al., 2014).

The capacity of prepared compounds (**5, PcTACo&Zn, AuNPs, AuNP-5 and AuNP-PcTACo&Zn**) to cleave DNA was tested using agarose gel electrophoresis technique. The testing DNA molecule was *E. coli*'s plasmid DNA. PCR tubes were filled with various concentrations of all of the above mentioned chemicals and strands of target DNA molecule. For 60 minutes, these mixes were cultivated at 37 º Cand later placed in agarose gel wells and the electrophoresis procedure lasted 90 minutes at 100V. Negative control was the untreated DNA and a transilluminator tracked the DNA cleavage efficiency of investigated compounds.

Similarly, the effects of phthalonitrile compound **(7), PcOACo&Zn, AuNPs, AuNP-7 and AuNP-PcOACo&Zn** on DNA were studied using *Escherichia coli* bacterial DNA. Herein, the negative control was plasmid DNA that had not been treated with any of the studied chemical products. In the test tubes three different proportions of testing compounds along with control DNA was placed, blended uniformly and later processed in incubator for 60 minutes at 37 °C. The negative control and test samples were then put into the agarose gel for electrophoresis for 90 minutes at 80 volts and 120 amps. Subsequently, using a transilluminator, DNA molecules were observed.

4.6.3 Antimicrobial activity

For prepared substances **(5, PcTACo&Zn, AuNPS, AuNP-5,** and **AuNP-PcTACo&Zn)**, antimicrobial properties were assessed with microdilution method. Microbial tested strains were *Enterococcus faecalis* (ATCC 29212), *Enterococcus hirae* (ATCC 10541), *Staphylococcus aureus* (ATCC 25923), *Legionella pneumophila subsp. pneumophila* (ATCC 33152), *Pseudomonas aeruginosa* (ATCC 27853), and *Escherichia coli* (ATCC 25922). To begin, serial two-fold (1: 2) dilutions of the compounds at known concentrations ranging from 1024 to 1 mg mL^{-1} were carried out. The microbes were injected onto the well plates and incubated at 37°C for 24 hours. The antibacterial ability was then assessed using minimum inhibitory concentration (MIC) values, which is defined as the lowest concentrations at which microbial growth is inhibited. The antibacterial activity of the compounds **(5, PcTACo&Zn, AuNPS, AuNP-5,** and **AuNP-PcTACo&Zn)** was further investigated using a disc diffusion experiment, as described in literature (Amitha & Vasudevan, 2020).

The antibacterial activity of substances (**7), PcOACo&Zn, AuNPs, AuNP-7** and **AuNP-PcOACo&Zn** was tested using the microdilution method. The strains that were employed are named as*: Candida parapisilosis* (ATCC 22019) and *Candida tropicalis* (ATCC 750) [fungal strains], *Enterococcus faecalis* (ATCC 29212), *Staphylococcus aureus* (ATCC 25923), *Enterococcus hirae* (ATCC 10541) [Gr +ve strains], *Escherichia coli* (ATCC 25922), *Pseudomonas aeruginosa* (ATCC 27853) and *Legionella pneumophila subsp. pneumophila* (ATCC 33152) [Gr −ve strains]. Compounds to be tested were serially diluted twice to prepare a series of samples in microplates with concentrations form 1024 mg L^{-1} to 1 mg L^{-1} and incubated at 37 °C temperature for 24 h. Later, the plates were analyzed and MIC measurements were reported as the lowest concentration that constrained microbial production.

4.6.4 Microbial cell viability inhibition

The microbe Escherichia coli (ATCC 10536) was used to study the chemical agents **(5), PcTACo&Zn, AuNPs, AuNP-5,** and **AuNP-PcTACo&Zn** for their capacity to reduce bacterial cell survival. E. coli was injected into the fermented colony, which was then shaken for 24 hours at 37 ºC at 150 rpm and later recovered via centrifuging at 5000 rpm lasting for 5 minutes. To remove any remaining fermentation media, the E. coli was washed and placed in 10 mL of 0.9 % NaCl solution. The microbe

survivability treatment was conducted using the above prepared bacterial solution. For 90 minutes at 37 ºC, *E. coli was* cultured with varied amounts of the compounds (**5), PcTACo&Zn, AuNPs, AuNP-5,** and **AuNP-PcTACo&Zn**. Finally, the bacterial groups were numerated to estimate the bacterial cell viability via equation (4.2)

Escherichia coli (ATCC 10536) was utilized to test the inhibitory action of prepared substances **(7), PcOACo&Zn, AuNPs, AuNP-7** and **AuNP-PcOACo&Zn** on microbial cells vitality. The microbe was injected into growth media and shaken for 24 hours at 37 °C at 150 rpm and later spun for 5 minutes at 5000 rpm to extract the sediment. The bacterial pellet was then washed with 0.9 percent disinfecting NaCl to eliminate any remaining culture medium. Disinfected *E. coli* was washed and suspended in 10 mL of 0.9 percent NaCl solution. This sterile microbial slurry was used to inhibit bacteria cell growth. *E. coli* was incubated for 90 minutes at 37 °C with compounds **(7), PcOACo&Zn, AuNPs, AuNP-7** and **AuNP-PcOACo&Zn** at doses of 100 and 200 mg L^{-1}. The very same approach was used for antimicrobial photodynamic treatment activity after irradiating compounds **(7), PcOACo&Zn, AuNPs, AuNP-7** and **AuNP-PcOACo&Zn** to LED source for approx. 20 minutes. The solutions were prepared in various amounts, injected on NB agar then placed in incubator at 37 °C for 24 hours. Finally, colonies were enumerated, to determine cell viability of bacteria using the following equation 4.2:

$$\text{Cell viability (\%)} = \left(\frac{A_{control} - A_{samplel}}{A_{control}}\right) \times 100 \qquad (4.2)$$

4.6.5 Biofilm inhibition

Pathogenic microorganisms have a significant negative influence on human health, producing illnesses and endangering human life. The rise of drug-immune bacterial species has exacerbated the complexity of this situation. Antibiotic drug treatment is the generally used approach for treating harmful bacteria. As a result, bacterial germs can develop immunity against antibacterial treatments with the help of a protection mechanism. Incorrect antibiotic usage obscures the cure leading to the generation of bacteria biofilm at the infection site (Doron & Gorbach, 2008). Bacterial cells are generated in environment as planktonic or as microbial communities that grow after adhering to a biological or abiotic surface (Costerton et al., 1999). These colonies may constitute a single microbe type or a variety of species (Costerton et al., 1999). Biofilm

structure is a syntrophic consortium created by microbe groups. Biofilms are bacterial colonies that attach to the area and develop further. Such network arrangement is essential for bacteria in enhancing their virulent factors by promoting microbial population and renders it resistive to unfavorable environmental factors such as pH shifts, nutritional shortage, and chemical agents such as antibiotics and antiseptics. This biofilm structure is an elaborate and progressive system made up of several constituents such as polysaccharide, protein, extracellular DNA, liquid and minerals (Fleming & Rumbaugh, 2017; Marcinkiewicz et al., 2013). This matrix works as a cover for bacteria within the biofilm, protecting them from host cell immune responses and antibacterial agent penetration (Packiavathy et al., 2014). Because of this, they now become far more insusceptible to antibiotics (Mah, 2012).

The 24 well plates containing crystal violet (CV) dyeing approach was employed to investigate the biofilm inhibition efficiency of compounds **(5, PcTACo&Zn, AuNPS, AuNP-5** and **AuNP-PcTACo&Zn)**. *P. Aeruginosa* and *S. Aureus* bacterial samples were employed to test the prepared compounds' antibiofilm activity. Before the test method began, bacterial cultures were grown for 1080 minutes. The bacterial cells were then injected into well plates at 2.9×10^8 CFU per mL and cultured in well plates with varied doses of the compounds to be examined (**5, PcTACo&Zn, AuNPS, AuNP-5** and **AuNP-PcTACo&Zn)** for 72 hours at 37 ºC. The plate's wells were unloaded and cleansed in two steps using distilled water than dried in an oven at 70 ºC for 15 minutes. After that, the well plated were treated with CV dye for a half an hour that dyed the biofilms purple. Later, CV was extracted and discs were progressively cleaned with tap water two times. To retrieve the soaked CV, the plates were allowed to sit in ethanol for 30 minutes. Subsequently, the absorbance reading was taken at 595 nm wavelength to test the anti-biofilm action. The positive controls employed were only the bacterial strain-containing wells along with medium. Equation 4.3 was used to determine the anti-biofilm efficiency.

Biofilm inhibition performance of compounds **(7), PcOACo&Zn, AuNPs, AuNP-7,** and **AuNP-PcOACo&Zn** on the *S. Aureus* and *P. Aeruginosa*'s colonial growth was analyzed via 24-well plates employing crystal violet (CV) tinting procedure. Concisely, the procedure initiated by cultivating bacterial samples one night prior the examination phase. Cultured strains were injected in well plates along with 2.9×10^8 CFU mL^{-1} solution. Soon after, the bacterial samples were processed in incubator for

72 h at 37 °C containing different concentrations of compounds **(7), PcOACo&Zn, AuNPs, AuNP-7** and **AuNP-PcOACo&Zn**. Subsequently, the wells media was carefully and repeatedly cleansed with purified water without cracking the biofilms while removing the floating bacteria on plates. The wells discs were then dried in an oven for 25 minutes at 75 °C. Afterwards, CV stain was assimilated for 40 minutes to infuse the color within the bacterial biofilms and later removed smoothly by repeated rinsing. Ethanol was mixed to retrieve the absorbed CV while the plate was stirred in incubator for 15 min. Biofilm inhibition was analyzed by a spectrophotometer that calculated absorbance at 595 nm. S. Aureus and *P. Aeruginosa* containing media wells discs were employed in positive controls place. Biofilm inhibition was calculated by applying equation (4.3) below;

$$\text{Anti-biofilm activity (\%)} = \frac{Abs(control) - Abs(sample)}{Abs(sample)} \times 100 \qquad (4.3)$$

The next section entails the results gathered from different characterization techniques for all the synthesized materials

5. RESULTS AND DISCUSSION

In this study, the phthalonitriles synthesized for MPc substitution are listed as; 4-(thiophen-3-ylethynyl) phthalonitrile **(2)**, 4-[(4-pentylphenyl)ethynyl] phthalonitrile **(3)**, 4-{[4-(N,N-Dimethylamino)phenyl]ethynyl}phthalonitrile **(5)**, 4,5-bis{[3,5 bis(trifluoromethyl)phenyl]ethynyl}phthalonitrile **(6)** and 4,5-bis((4-(dimethylamino)phenyl)ethynyl)phthalonitrile **(7)**.

4-(thiophen-3-ylethynyl) phthalonitrile **(2)**, 4-[(4-pentylphenyl)ethynyl] phthalonitrile **(3)** were used to synthesize push-pull type new asymmetric cobalt and zinc phthalocyanines containing A_3B type extra-ring triple bonds via statistical condensation method. Moreover, peripheral tetra-substituted metal (Zn, Co, Mn, Fe and Lu) symmetrical phthalocyanines were assembled from the obtained phthalonitrile derivative **(5)**. Moreover, from the phthalonitrile derivative **(6)** and **(7)** the symmetrical peripherally octa-substituted phthalocyanines created had metals Co, Zn and Lu in their cores. The purity of newly synthesized phthalonitrile derivatives and phthalocyanines was followed by thin layer, preparative and column chromatography and their structures were elucidated using spectroscopic methods (FT-IR, NMR, MALDI-TOF and UV-vis).

5.1 Synthesis of Phthalonitrile Derivatives (2) and (3) and Related Asymmetric Metal-Phthalocyanines

The 4-(thiophen-3-ylethynyl) phthalonitrile **(2)** was obtained according to the procedure explained in literature (Kumral et al., 2020). Whereas, 4-[(4-pentylphenyl)ethynyl] phthalonitrile **(3)** was synthesized relevant to the one mentioned in (Yenilmez et al., 2021). Fundamental synthetic procedure followed for the **(2)** and **(3)** was Palladium catalyzed Sonogashira cross-coupling strategy mentioned in (Sonogashira, 2002). For **(2)**, the first round of synthesis is the reaction between alkynyl starting material 3-ethnyl thiophene and 4- iodophthalonitrile **(1)** and for **(3)** 1- ethynyl-4-pentylbenzene and 4-iodo-phthalonitrile **(1)** combined under inert atmosphere and palladium halides perform catalysis to provide basis establishing the

carbon-carbon triple bond respectively (Figure 5.1).

Asymmetric phthalocyanine derivatives were synthesized through the reaction of **(2)** or **(3)** with 1,2-Dicyano-3,4,5,6-tetrafluorobenzene in a 3:1 ratio. Primarily, it was determined from the mass result of the isomer that the reactive fluorine groups reacted with the solvent when synthesis was done using and N,N-dimethyl amino ethanol solvent. Later, 1-chloronaphthalene was used employed as the solvent. The yield of the isomeric mixtures obtained from this reaction is very low due to the reactivity of the fluorine groups. Literally, the procedure progressed for asymmetrical A_3B type Pcs of zinc and cobalt via statistical condensation reaction of two corresponding phthalonitriles (Kalkan et al., 2004; Sastre et al., 1995) i.e., 1,2-dicyano-3,4,5,6-tetrafluorobenzene with both 4-(thiophen-3-ylethynyl) phthalonitrile **(2)** and 4-[(4-pentylphenyl)ethynyl] phthalonitrile **(3)** along with corresponding metal salts under nitrogen source and a high boiling solvent 1-Chloronaphthalene occurred at 180 ºC. The reaction's end products were firstly purified from symmetrical isomers through hexane:dioxane (5:1.5) solvent mixture on a silica chromatographic column and later the desired isomer was separated via hexane:dioxane (5:0.5) mixture on preparative chromatography. The structures of novel asymmetrical Pcs for both **(2)** and **(3)** were illustrated and fully characterized with the routine spectroscopic methods.

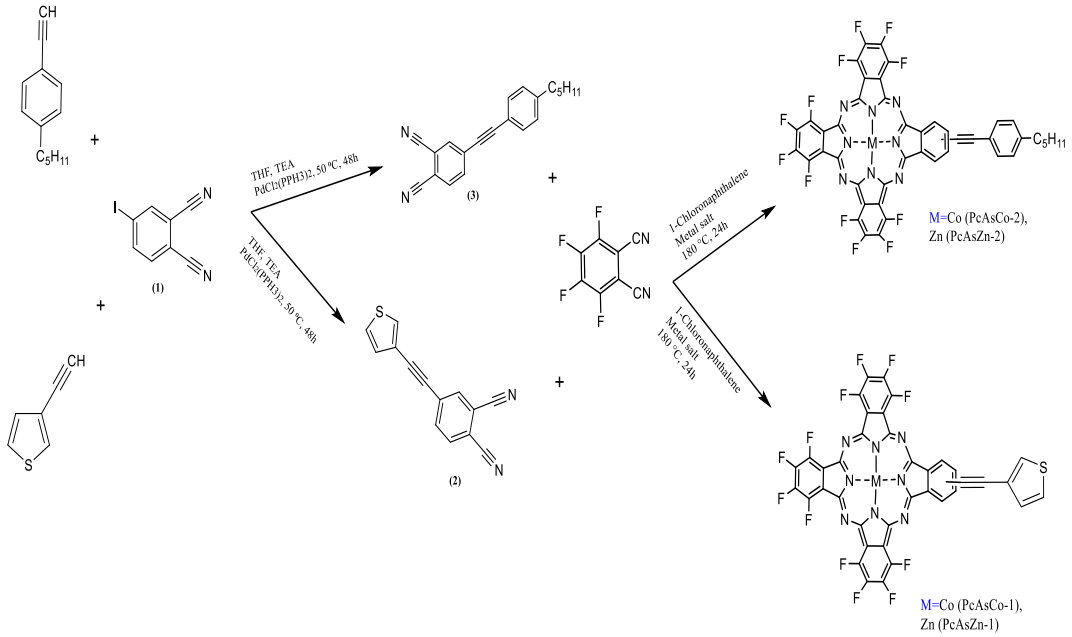

Figure 5.1: Synthesis of phthalonitrile derivatives **(2)** and **(3)** and related asymmetric metal-phthalocyanines.

5.1.1 Dc Measurement analysis of PcAsCo-1 and PcAsZn-1 asymmetric phthalocyanines

Photoconductivity behaviors of these compounds were determined by measuring I-V characteristics in dark and lighting conditions. Figure 5.2 shows the I-V characteristics of this group of compounds recorded under dark and lighting conditions.

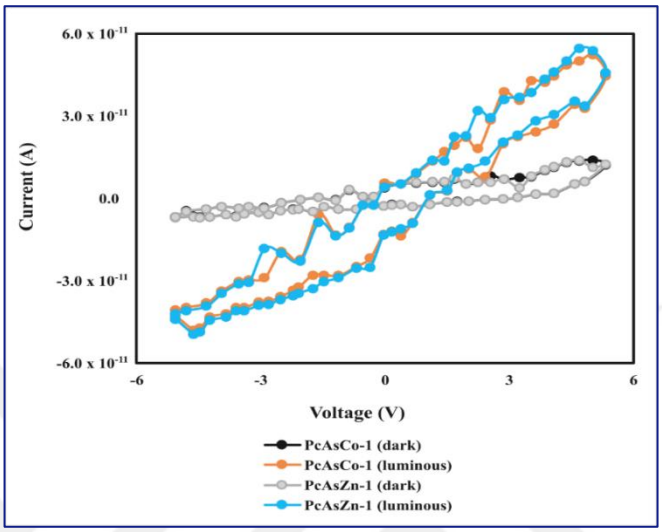

Figure 5.2: I-V characteristics of phthalocyanines in dark and light conditions.

From the I-V characteristics of the compounds, it was observed that the current values observed in the films increased linearly with the applied voltage. Herein, I-V characteristics also suggested that the hysteresis effect was quite dominant in the I-V characteristics of the compounds in both dark and lighting conditions. It is clearly seen from Figure 5.2 that the conductivity values observed in the compounds under lighting conditions are higher than the conductivity values observed in the dark environment. It has also been observed that the I-V behaviors observed in both dark and lighting conditions in the compounds are quite similar to each other.

Studies on the electrical properties of phthalocyanine compounds show that the compounds exhibit ohmic behavior for low values of applied voltage, and their electrical conductivity in this voltage range is directly proportional to the charge carrier density and the mobility of these carriers (Schultz et al., 1990). At high values of the electric field, between the current density (J) and the applied voltage (V), with n > 2:

$$J = V^n \tag{5.1}$$

In this group of compounds, the hysteresis width was observed to vary between 0.63 V and 1.32 V in illuminated and non-illuminated films. It is known that in order to explain the difference in hysteresis behavior of films under dark and lighting conditions, many physical mechanisms such as live charge density and polarization effect should be considered. The hysteresis effect observed in the I-V characteristics is highly dependent on the distribution of these trap levels as well as the filling-discharging rates of the trap levels that occur inevitably in the structure. The distribution of trap levels in the structure, the trapping and re-release of carriers during charge transitions is one of the most important reasons for the hysteresis effect observed in I-V characteristics. The high hysteresis effect observed in asymmetric phthalocyanines was attributed to the high impurity rate in the compounds in question. As it is known, one of the most important problems in asymmetric phthalocyanines is the separation. It has been concluded that the photoconductivity values of asymmetric phthalocyanines vary between 6.31×10^{-9} S/cm and 7.18×10^{-9} S/cm.

5.1.2 Photoconductivity measurements analysis of PcAsCo-2 & PcAsZn-2 asymmetric phthalocyanines

Photoconductivity behaviors of asymmetric compounds **PcAsCo-2** and **PcAsZn-2** were investigated by two different methods, dc and ac. The impedance spectra of the compounds measured under dark and light conditions are shown in Figure 5.3.

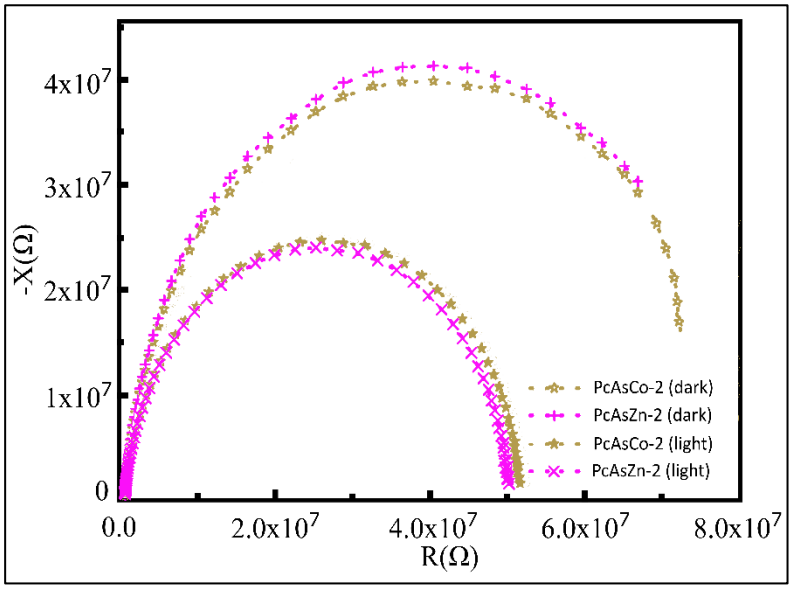

Figure 5.3: Impedance spectra of asymmetric phthalocyanines **PcAsCo-2** and **PcAsZn-2**.

As can be clearly seen from the analysis of Figure 5.3, the impedance spectra measured in the dark environment consist of curves that tend to form semi-circles, while the spectra measured in the illuminated environment consist of semi-circles whose center is not on the real axis. While the maximum impedance was observed in the **PcAsZn-2** compound from the impedance spectra measured in the dark environment but for lighting conditions minimum impedance was observed in the **PcAsZn-2**.

Again, from the Figure 5.3, it was seen that both the imaginary part and the real part of the impedance decreased (the radii of the semicircles became smaller) under lighting conditions. The observed impedance spectra are interpreted as the structure can be represented by a resistor connected in parallel with a capacitor. As mentioned before, many basic physical parameters should be considered in the interpretation of the impedance spectra obtained. Impedance spectra obtained in both dark and bright environments have been explained as both grains and grain boundaries play a role in load transmission in the structure.

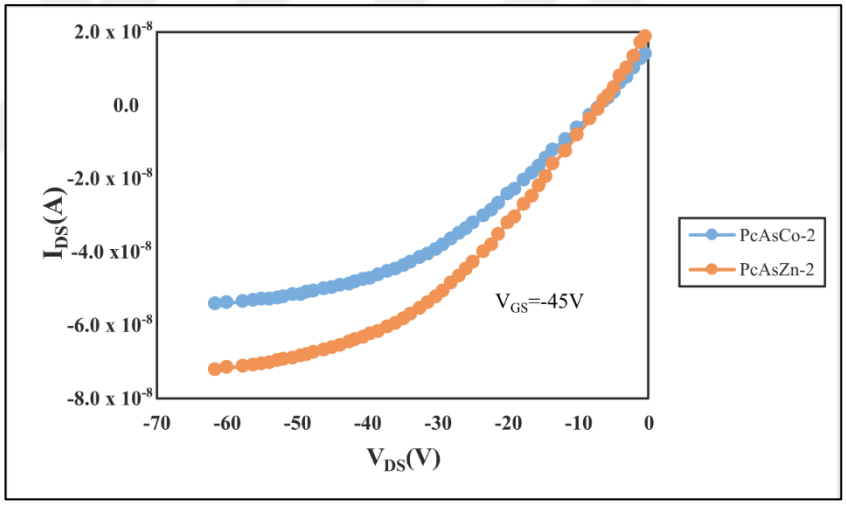

Figure 5.4: Output characteristics of devices using asymmetric phthalocyanines **PcAsCo-2** and **PcAsZn-2**.

The performance of asymmetric compounds as active layers in field-effect transistors was also determined. Figure 5.4 shows the dependence (output characteristics) of the channel current ID on the voltage applied between the source and the channel under 6.4 mW/cm^2 lighting conditions of the manufactured devices. During the measurement of the output characteristics of the devices, the source-gate voltage was changed between 0 and -60 V. For comparison purposes, the illumination measurements are recorded as well. The output of the monochromator is set to 720 nm for measurements

under lighting conditions. As can be seen from Figure 5.4, all devices exhibit field effect transistor characteristics under lighting conditions. That is, the current between the source and the channel region in the devices can be controlled by the voltage applied between the gate and the source under lighting conditions. As in Figure 5.4, the channel-source current increases with increasing gate-source voltage in the negative direction. As can be seen from the examination of the two output characteristics, for each value of the source-gate voltage, the maximum channel-source current was observed in the device where PcAsZn-2 was used as the active layer. For the gate source voltage - 45 Volts, the channel source voltage - 60 V, the saturation value of the channel source current observed in the device where PcAsZn-2 is used as the active layer is 72 nA. In field effect transistors, where these compounds are used as active layers, these currents are observed as 7.3 nA and 11.4 nA, respectively. This shows that the channel current increases in all devices when the devices are illuminated with 720 nm wavelength light.

Compared to other compounds, the high current observed in the device using the compound PcAsZn-2 was interpreted as high charge mobility and low injection barrier in the compound in question. As mentioned in the previous sections, photoconductivity and photovoltaic events are effective in the behavior observed under lighting conditions. As it is known, the electron-hole pairs formed as a result of absorption that are responsible for the photoconductivity phenomenon and the separation of these pairs as free carriers by the effect of the voltage applied between the channel and the source. Therefore, it is expected that the number of photo carriers formed as a result of photon absorption is not dependent on the gate voltage. On the other hand, the photovoltaic phenomenon, which means that a voltage is generated under lighting conditions, results from the presence of a rectifier junction, including the generation potential, between the metal and the semiconductor. In a photo field-effect transistor, when incident light is absorbed by the active layer in the device, charge carriers created by the absorbed photons cause the potential barrier at the metal-semiconductor interface to drop, which means a channel region with a larger cross-sectional area for charge carriers. It has been concluded that both the photovoltaic phenomenon and the photoconductivity mechanism play a role in the channel current in the lighting conditions in the devices in which the said compounds are used as the active layer.

5.1.3 UV-vis spectra of asymmetric metal phthalocyanines of phthalonitriles (2) and (3)

The UV-vis spectra of synthesized asymmetric MPcs are recorded in THF, the Q- band was observed as a single peak at 664 and 677nm. B-bands of **PcAsCo-1**, **PcAsZn-1**, **PcAsCo-2** and **PcAsZn-2** were analyzed at 333, 357, 342 and 352nm respectively (Table 5.1 and Figure 5.5).

Table 5.1: UV-vis spectral values of asymmetrical tetra-substituted metal-phthalocyanines of phthalonitriles **(2)** and **(3).**

Name of the Compound	B-Band λ_{max}(log Ɛ)	Q-Band λ_{max} (log Ɛ)
PcAsCo-1	333	664
PcAsCo-2	342	664
PcAsZn-1	357	667
PcAsZn-2	352	667

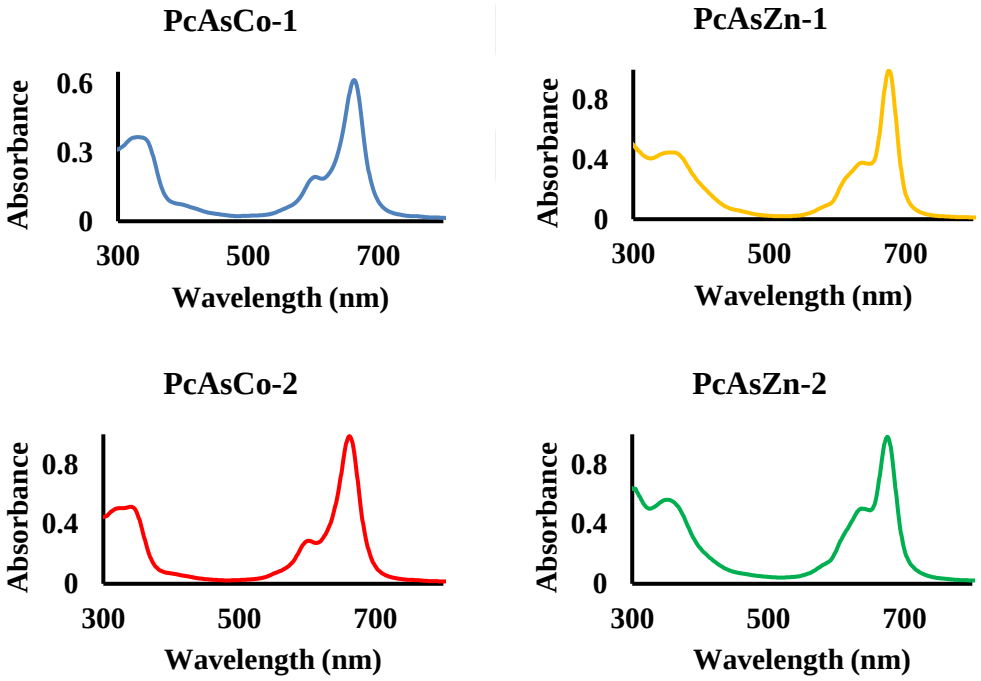

Figure 5.5: UV-vis spectra of asymmetric metal-phthalocyanines of phthalonitriles **(2)** & **(3)**.

5.2 Synthesis of Phthalonitrile Derivative (5) and Related Peripheral Symmetrically Tetra-substituted Metal-Phthalocyanines and Derived AuNPs Conjugates

The synthetic procedure followed for the preparation of phthalonitrile **(5)** is as mentioned in (Maya et al., 2000). 4-ethynyl-N,N-dimethylaniline and 4-iodophthalonitrile **(1)** are linked together via Sonogashira coupling reaction (Sonogashira 2002) where palladium compounds served as catalysts under a N_2 source.

Subsequently, the related metal phthalocyanines containing Co, Zn, Fe and Mn metals were prepared by cyclotetramerization of compound **(5)** in DMAE medium and 1-Pentanol for Lu with suitable metal salts at boiling temperature and nitrogen source (Figure 5.6). Later, the MPc derivatives were purified with THF as the mobile phase on column chromatography.

Characterization of these newly synthesized MPcs was executed using a list of spectroscopic modes such as UV-vis, FT-IR, ^{1}H-NMR and MALDI-TOF. All the gathered data from spectroscopic results coreesponds to the prepared phthalocyanines structures.

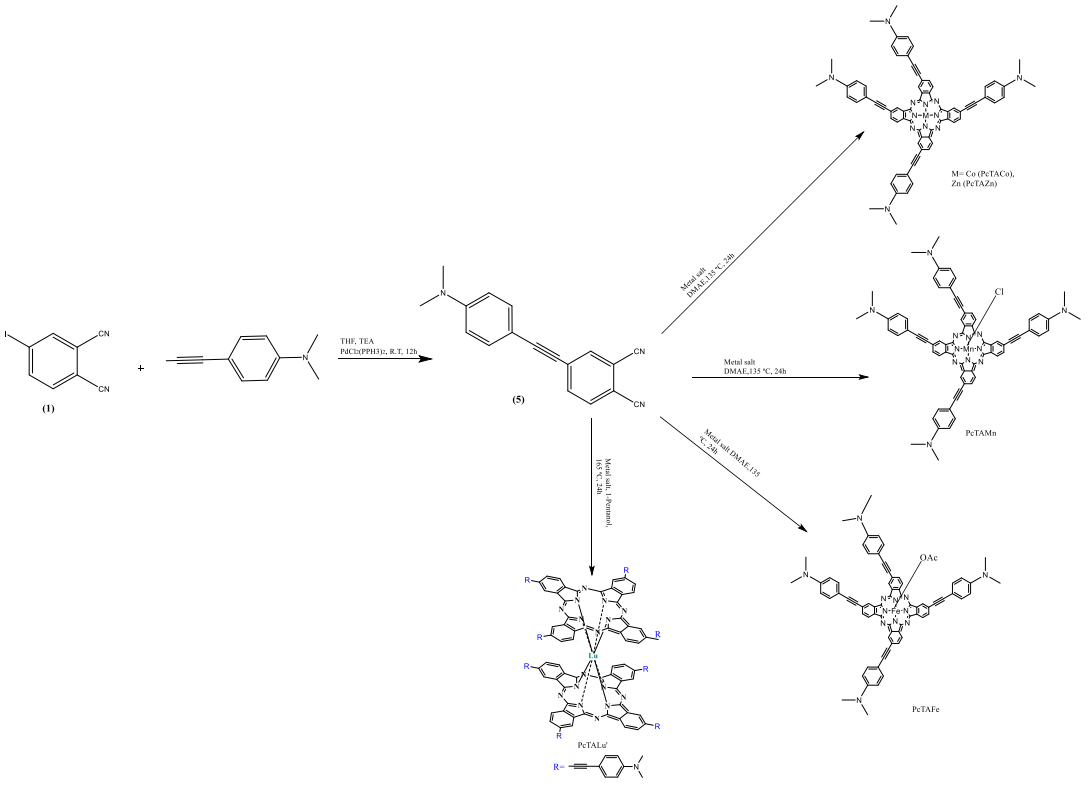

Figure 5.6: Synthesis of phthalonitrile derivative **(5)** and related symmetrical tetra-substituted metal-phthalocyanines.

5.2.1 UV-vis spectra of phthalonitrile (5) related symmetrically tetra-substituted metal phthalocyanines

In this study, the UV-vis spectra of the compounds **(PcTACo, Zn, Fe, Mn and Lu')** were obtained in DMSO and THF (for FePc few pyridine drops) at room temperature. The respective B, vibronic and Q-bands observed for all the compounds are illustrated in Table 5.2. and Figure 5.7 (Byliss, 1950; Özçeşmeci et al., 2013; Evren et al, 2014).

Table 5.2: UV-vis spectral values of symmetrical tetra-substituted metal-phthalocyanines of phthalonitrile **(5)**.

Name of the Compound	B-Band λ_{max}(nm) (log Ɛ)	Vibronic Band λ_{max} (nm) (log Ɛ)	Q-Band λ_{max} (nm) (log Ɛ)
Phthalonitrile (5)	276 (5.59)	-	406 (5.47)
PcTACo-DMSO	355 (5.15)	623 (4.37)	690 (4.75)
PcTACo-THF	347 (5.16)	629 (4.56)	697 (5.18)
PcTAZn-DMSO	357 (5.30)	627 (4.12)	693 (4.70)
PcTAZn-THF	355 (5.00)	616 (4.57)	679 (5.29)
PcTAFe-DMSO	350 (4.74)	642 (4.89)	727 (5.07)
PcTAFe-THF-Pyridine	390 (5.58)	-	676 (4.89)
PcTAMn-DMSO	351(5.74)	634 (4.93)	728 (5.07)
PcTAMn-THF	338 (5.48)	-	627 (5.07)
PcTALu′-DMSO	269 (5.77)	617 (4.92)	677 (5.31)

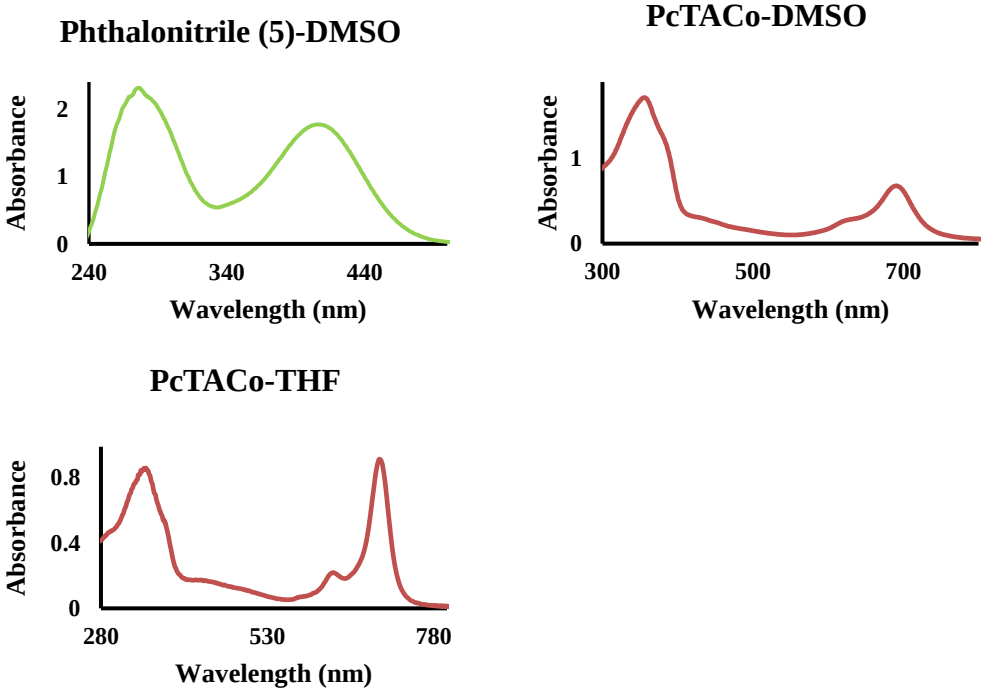

Figure 5.7 (continued): UV-vis spectra of phthalonitrile derivative **(5)** and related symmetrical tetra-substituted metal-phthalocyanines.

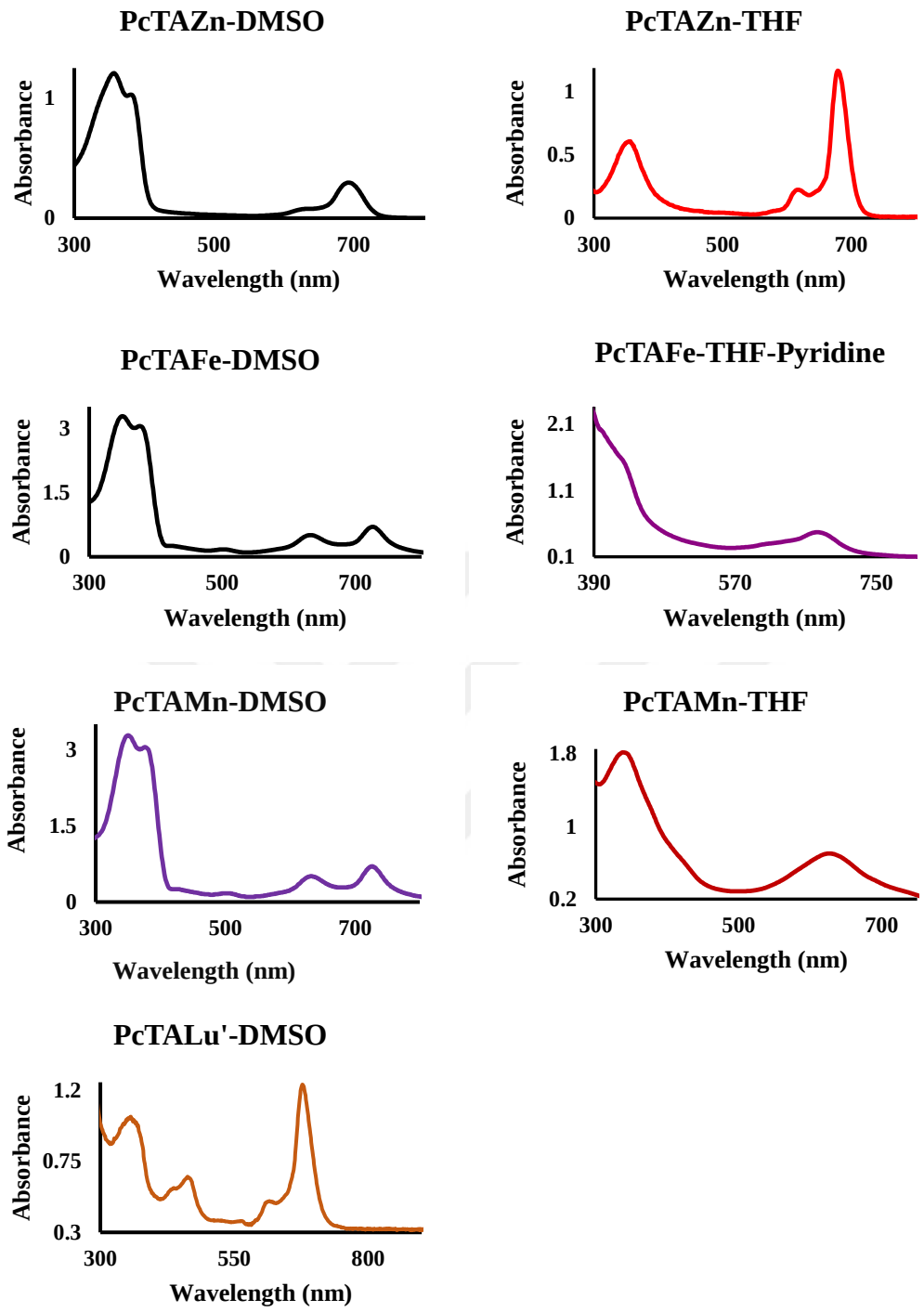

Figure 5.7 (continued): UV-vis spectra of phthalonitrile derivative **(5)** and related symmetrical tetra-substituted metal-phthalocyanines.

5.2.2 AuNPs conjugates of phthalonitrile (5) and related MPcs

Additionally, the gold nanoparticles were adjoined with compounds **(5)**, **PcTACo** & **PcTAZn**. Electrostatic interactions between the compounds **(5)**, Co and Zn MPc and AuNPs directed the self-assembly and conjugation of the prepared compounds on the

nanoparticles surface while formulated a monolayer on the AuNPs (Hone et al. 2002).The hybrid compounds are **AuNP-5, AuNP-PcTACo** and **AuNP-PcTAZn**. These gold nano particles and their MPc hybrids were subjected to biological applications and characterized via UV-vis and TEM techniques arementioned further.

5.2.3 Biological Studies

5.2.3.1 DPPH radical scavenging activity

In this thesis, the DPPH radical scavenging approach was utilized to analyze the antioxidant activities of the compounds **(5, PcTACo&Zn, AuNPS, AuNP-5** and **AuNP-PcTACo&Zn)**. The DPPH radical scavenging activities of the studied compounds are illustrated in Table 5.3 and Figure 5.8.

Consequently, analyzed compounds featured exceptional free radical scavenging activity values. Compounds **5, PcTACo&Zn** exhibited greater free radical scavenging action than compounds **AuNP-5** and **AuNP-PcTACo&Zn**. An increase in the DPPH inhibition activity was recognized once the concentrations of the compounds (**5, PcTACo&Zn, AuNPS, AuNP-5** and **AuNP-PcTACo&Zn**) increased from 50 mg L^{-1} to 100 mg L^{-1}. As evident from Figure 5.8 and Table 5.3, the maximum DPPH inhibition value of 100.00% was achieved for compounds (**5)** and **AuNP- PcTACo** at 100 mg L^{-1} concentration and for **PcTACo** at 200mg L^{-1}.

Similar results have been published in literature. For example, Barut and Demirbas reported DPPH scavenging strengths of metal-free, Ni and Cu phthalocyanines containing triclosan at non-peripheral sites (Barut & Demirbaş, 2020). Furthermore, Korkut et al. stated the synthesis and antioxidant activities of Zn phthalocyanine containing tetranitroxide moieties (Korkut et al., 2021).

The DPPH radical inhibition capacity of the newly synthesized compound investigated in this thesis displayed variations. As compared to the literature, the prepared compounds presented exemplary radical scavenging activity and can be employed as alternate antioxidant operative following additional toxicological evaluation.

Table 5.3: %DPPH activity of **(5), AuNP-5, PcTACo&Zn, AuNP-PcTACo&Zn** and **AuNPs** at different concentrations.

Compounds	12.5mg/L	25 mg/L	50 mg/L	100 mg/L	200 mg/L
(5)	86.60%	91.85%	98.65%	100%	100%
AuNP-5	51.36%	62.88%	71.15%	78.43%	79.84%
PcTACo	82.92%	87.31%	90.71%	96.78%	100%
AuNP-PcTACo	78.29%	85.67%	87.45%	100%	100%
PcTAZn	67.26%	75.57%	84.98%	90.39%	97.36%
AuNP-PcTAZn	59.90%	64.55%	68.21%	75.81%	96.13%
AuNPs	42.23%	54.79%	59.31%	60.87%	65.35%

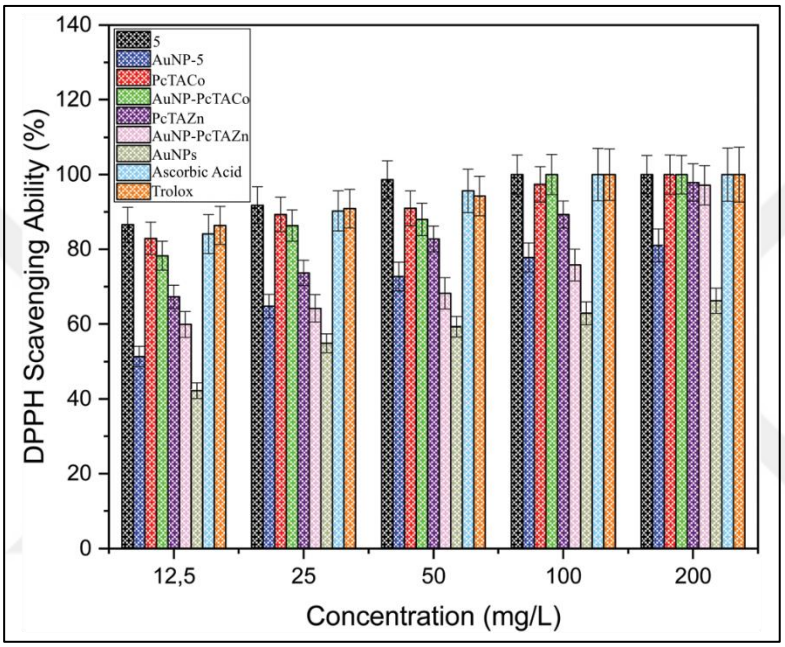

Figure 5.8: DPPH activity of **(5), AuNP-5, PcTACo&Zn, AuNP-PcTACo&Zn** and **AuNPs**.

5.2.3.2 DNA cleavage activity

This study examined the DNA cleavage activities of the compounds (**5, PcTACo &Zn, AuNPs, AuNP-5** and **AuNP-PcTACo&Zn** was analyzed while reciprocating these compounds with DNA samples with subsequent electrophoresis in agarose gel. Compounds **(5)** and **PcTAZn** demonstrated single-strain DNA cleavage activity at 100 and 200 mgL^{-1}, but no DNA cleavage activity at 50 mgL^{-1}. **PcTACo** and **AuNP-Co**, on the other hand, fully fabricated DNA particles. Furthermore, compounds **AuNP-5** and **PcTAZn** were able to cleave single strain DNA, whereas **AuNPs** did not show DNA cleavage activity at any analyzed concentration. According to literature, Vasudevan and Amitha synthesized a variety of phthalocyanines and evaluated their DNA fastening and cleaving capabilities. DNA cleavage activity was seen in all of the

prepared phthalocyanines (Amitha & Vasudevan, 2020). Yalazan et al. examined the DNA cleavage activities of fabricated tetra substituted Zn MPcs with tosylated 4-morpholinoaniline entities on peripheral locations (Yalazan et al., 2020).

The aforementioned observations back up the findings presented in this study. The newly manufactured complexes were reported to bind to the major or minor groove of DNA or make exterior contact (electrostatic binding). These comparable strategies can be used to explain the DNA cleavage activity of newly produced substances in this study (Figure 5.9). As a result of their chemical nuclease capabilities, compounds **(5), PcTACo&Zn, AuNP-5** and **AuNP-PcTACo&Zn**, and especially **PcTACo** and **AuNP-5**, can be employed for tumour therapeutics and antimicrobial activity research in the health industry.

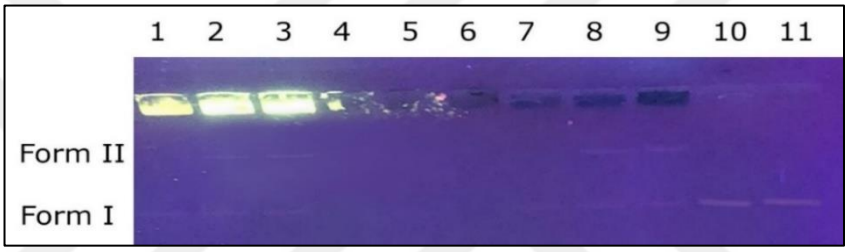

(a)

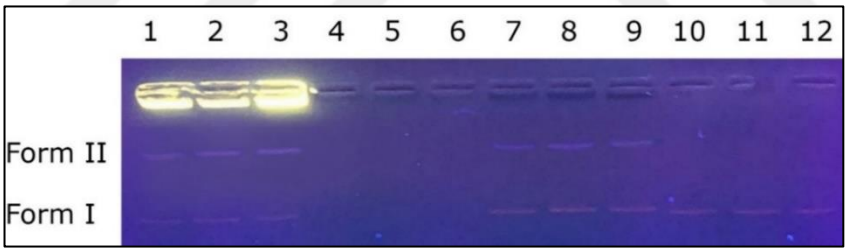

(b)

Figure 5.9: DNA cleavage activity of **(5), PcTACo&Zn, AuNP-5, AuNP-PcTACo&Zn** and **AuNPs**. (a) Lane 1, pBR 322 DNA; + 50 mg of (5); Lane 2, pBR 322 DNA + 100 mg of (5); Lane 3, pBR 322 DNA + 200 mg of (5); Lane 4, pBR 322 DNA + 50 mg of PcTACo; Lane 5, pBR 322 DNA + 100 mg/L PcTACo; Lane 6, pBR 322 DNA + 200 mg/L PcTACo; Lane 7, pBR 322 DNA + 50 mg of PcTAZn; Lane 8, pBR 322 DNA + 100 mg/L PcTAZn; Lane 9, pBR 322 DNA + 200 mg/L PcTAZn; Lane 10, pBR 322 DNA; Lane 11, pBR 322 DNA + DMSO; (b) Lane 1, pBR 322 DNA; + 50 mg of AuNP-5; Lane 2, pBR 322 DNA + 100 mg of AuNP-5; Lane 3, pBR 322 DNA + 200 mg of AuNP-5; Lane 4, pBR 322 DNA + 50 mg of AuNP-PcTACo; Lane 5, pBR 322 DNA + 100 mg/L of AuNP-PcTACo; Lane 6, pBR 322 DNA + 200 mg/L of AuNP-PcTACo; Lane 7, pBR 322 DNA + 50 mg of AuNP-PcTAZn; Lane 8, pBR 322 DNA + 100 mg/L of AuNP-PcTAZn; Lane 9, pBR 322 DNA + 200 mg/L of AuNP-PcTAZn; Lane 10, pBR 322 DNA + 50 mg/L of AuNPs; Lane 11, pBR 322 DNA + 100 mg/L of AuNPs; Lane 12, pBR 322 DNA + 200 mg/L of AuNPs.

5.2.3.3 Antimicrobial activity

Antibacterial activity of the compounds **(5, PcTACo&Zn, AuNPs, AuNP-5** and **AuNP-PcTACo&Zn)** was examined utilizing micro dilution protocol, while the results were interpreted using minimum inhibitory concentrations (MIC). Anti - microbial activity was observed in all of the substances examined as demonstrated in Table 5.4.

The antibacterial activity of **AuNPs** against the microorganisms turned out to be the lowest. Compounds **AuNP-5** and **AuNP-PcTACo&Zn** resulting from the combination of gold nanoparticles with compounds **(5), PcTACo&Zn** have stronger antibacterial activity than compounds **(5), PcTACo &Zn** and **AuNPs** due to the combined impact of compounds **(5) and PcTACo &Zn** with gold nanoparticles. The antimicrobial inhibition activity of the compounds **(5, PcTACo&Zn, AuNPs, AuNP-5** and **AuNP-PcTACo&Zn)** was examined using a disc diffusion assay and the results are listed in Table 5.5. In the light of obtained observations, *E. faecalis* was the most susceptible whereas the most invulnerable microorganism was *E. Hirae*.

Similar investigations have been described in the literature. Maliszewska et al. developed sulfonated hydroxyl aluminum phthalocyanine-biogenic Au/ Ag alloy nanoparticles and tested their antibacterial efficacy. Reported compounds displayed considerable antimicrobial efficiency (Maliszewska et al., 2020). The antibacterial properties of ZnPc-epolylysine conjugated Au and Ag nanoparticles were examined versus S. Aureus by Nombona et al. (Nombona et al., 2012).

The antibacterial properties of a variety of zinc phthalocyanines implanted on silver (Ag)-NP modified silica nanofibers were investigated by Mapukata et al. Because of the cooperation between AgNPs and phthalocyanines, the Pc@Ag-SiO_2 NFs had the maximum antibacterial action (Mapukata et al., 2021).

In this thesis study, the antibacterial activity of the MPcs conjugated with AuNPs **(AuNP-5 and AuNP-PcTACo&Zn)** was found to be more effective than that of **(5), PcTACo &Zn** and **AuNPs**. These findings are similar to a work published recently (Mapukata et al., 2021). As a consequence, compound **(5), PcTACo &Zn**, particularly **AuNP-5** and **AuNP-PcTACo&Zn**, could potentially be used as antibacterial agents upon future research.

Table 5.4: MIC values of compounds **(5), PcTACo&Zn, AuNP-5, AuNP-PcTACo&Zn** and **AuNPs**.

Microorganisms	(5)	PcTA Co	PcTA Zn	AuNP-5	AuNP-PcTACo	AuNP-PcTAZn	AuNPs
E. coli	128	64	128	64	32	32	512
P. Aeruginosa	128	128	128	32	64	64	512
L. pneumophila subsp. pneumophila	256	64	128	64	64	32	1024
E. hirae	256	128	128	128	64	64	512
E. fecalis	256	128	256	64	64	128	1024
S. Aureus	256	128	256	128	64	64	1024
C. parapisilosis	256	256	128	128	128	64	512
C. tropicalis	128	128	128	64	64	32	512

Table 5.5: Inhibition zones of compounds **(5), PcTACo&Zn, AuNP-5, AuNP-PcTACo&Zn** and **AuNPs.**

Microorganisms	(5)	PcTA Co	PcTA Zn	AuNP-5	AuNP-PcTACo	AuNP-PcTAZn	AuNPs
E. coli	8	11	11	9	13	12	ND
P. Aeruginosa	7	9	12	9	12	13	7
L. pneumophila subsp. pneumophila	7	10	12	8	13	12	ND
E. hirae	7	8	11	8	10	12	ND
E. fecalis	12	14	14	14	15	16	7
S. Aureus	7	9	12	10	12	14	ND
C. parapisilosis	10	11	12	12	13	15	ND
C. tropicalis	8	11	12	12	15	16	ND

5.2.3.4 Microbial cell viability inhibition

Using *E. coli*, a Gram-negative bacteria as testing microbe, the effect of the compounds **(5, PcTACo&Zn, AuNPs, AuNP-5** and **AuNP-PcTACo&Zn)** on microbial viability inhibitory activities was investigated. This model microbe has a peptidoglycan and lipopolysaccharide-based double cell envelope. The viable cells inhibition action of varied concentration ratios of the substances was tested against *E. coli* in this investigation are demonstrated in Table 5.6, Figures 5.10 and 5.11 as the final results.

As indicated, all of the examined compounds, particularly **AuNP-5** and **AuNP-PcTACo&Zn**, had a high suppression level of microbial cell viability. At 500 mg L^{-1}, all of the tested substances completely suppressed *E. coli* growth.

Relatively similar studies have been reported in the literature. The group of Ali et al. created metallic nanoparticles (MNPs) stuffed on CS/zinc phthalocyanine (ZnPc-CS)

hybrid fibers. MNPs packed on ZnPc-CS composite fibers have better antibacterial properties than ZnPc-CS composite fibers against *E. coli*, the lethal bacteria species examined in the study. In detail, the nanoparticles can interact with bacterial cell membrane while altering the accessibility, hence block the nutritional molecules from entering the bacterial cell. An additional source of further inhibition in the presence of these metallic nanocomposites could be their ability to produce highly reactive ions like hydrogen/superoxide radicals or H_2O_2. By adhering to proteids, DNA, and/or cellular membrane, these radicals can decrease cell survival (Ali et al., 2017). It became evident that newly synthesized chemicals have the potential to be used in sewage disposal since they can suppress harmful micro-organisms.

Table 5.6: Microbial cell viability inhibition of compounds **(5)**, **PcTACo&Zn**, **AuNP-5, AuNP-PcTACo&Zn** and **AuNPs**.

Compounds	125mg/L	250 mg/L	500 mg/L
(5)	95.43%	98.02%	100%
AuNP-5	100%	100%	100%
PcTACo	99.12%	100%	100%
AuNP-PcTACo	96.78%	100%	100%
PcTAZn	99.19%	100%	100%
AuNP-PcTAZn	100%	100%	100%
AuNPs	90.36%	96.41%	100%

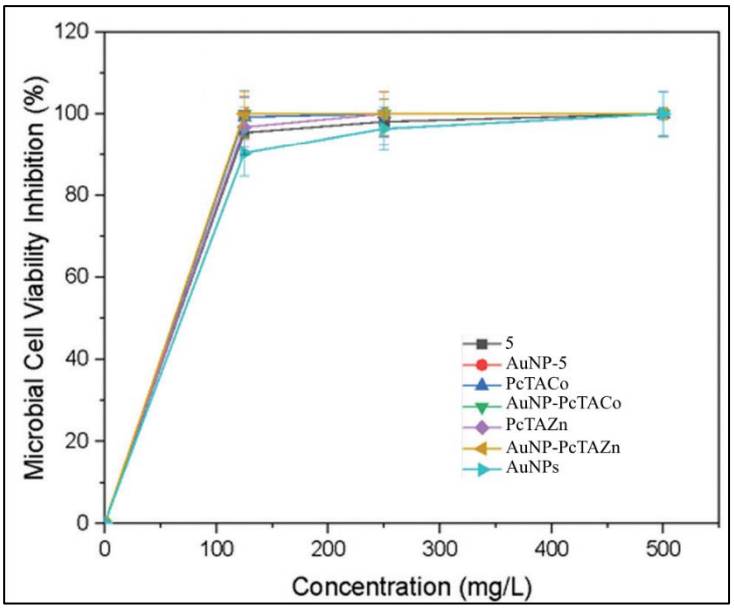

Figure 5.10: Microbial cell viability inhibition of compounds **(5), PcTACo&Zn, AuNP-5, AuNP-PcTACo&Zn** and **AuNPs**.

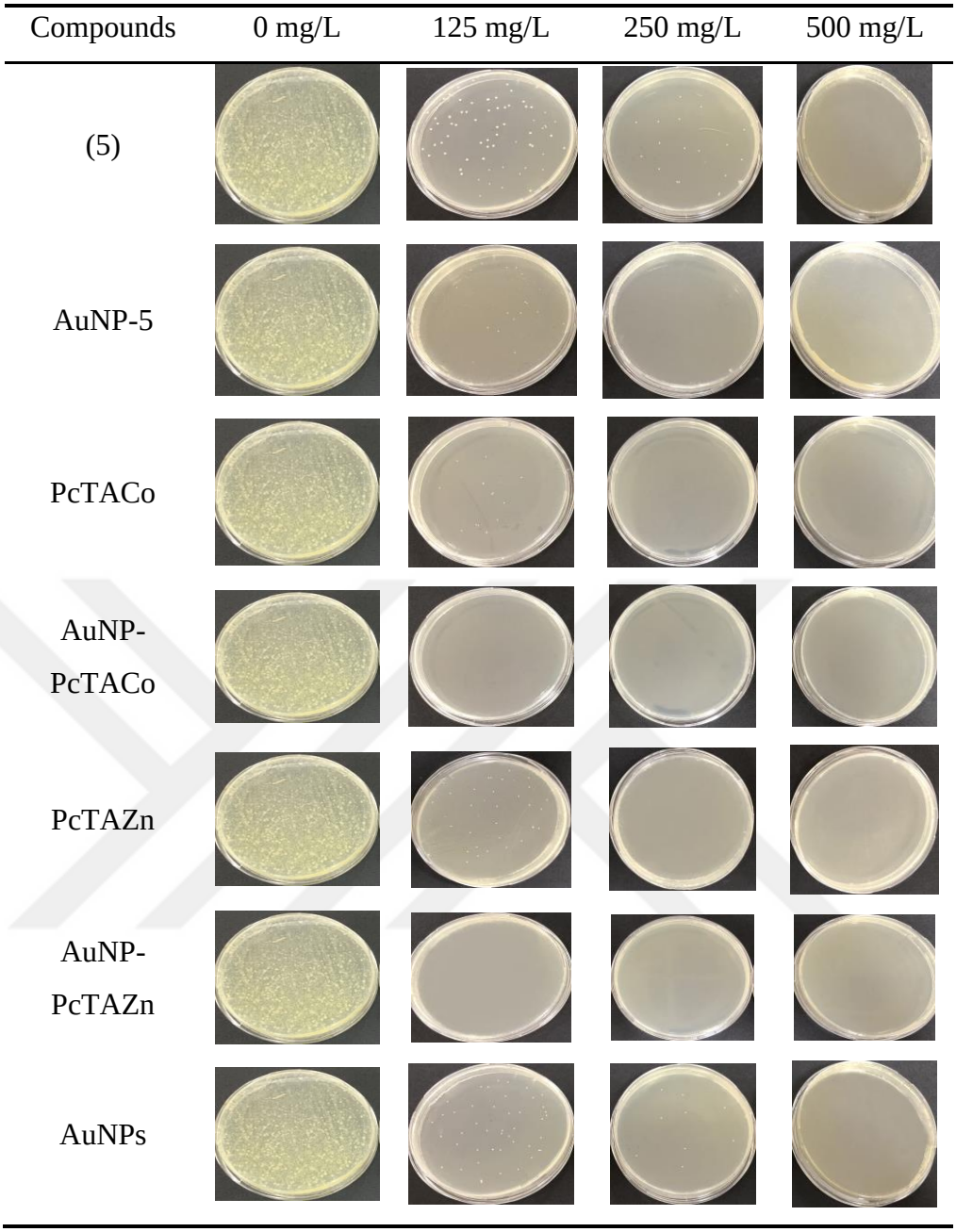

Figure 5.11: Microbial cell viability inhibition of compounds **(5)**, **PcTACo&Zn**, **AuNP-5, AuNP-PcTACo**&**Zn** and **AuNPs.**

5.2.3.5 Biofilm inhibition

The anti-biofilm effectiveness of the substances **(5, PcTACo&Zn, AuNPS, AuNP-5** and **AuNP-PcTACo&Zn)** was investigated on *S. Aureus* and *P. Aeruginosa* in this research. Table 5.7, Figures 5.12 (a) and (b) depict biofilm inhibition against *S. Aureus* while Table 5.8, Figures 5.13 (a) and (b) illustrate biofilm inhibition capabilities for *P. Aeruginosa*. Anti-biofilm action was quantity depending, according to these findings. The results indicated that anti-biofilm activity in related to the concentration. The

effect of the examined compounds on *P. Aeruginosa* biofilm inhibition was found to be greater than their effect on *S. Aureus* biofilm inhibition. At 500 mg L^{-1}, the largest biofilm inhibitions were obtained: 96.48 percent against *S. Aureus* and 98.13 percent against *P. Aeruginosa*.

Several analyses are presented in the literature that are significant in this manner. For example, Cavalcante et al. used chitosan nanoparticles treated with chloro aluminum phthalocyanines to suppress Streptococcus mutans biofilm. The investigated material inhibited biofilms effectively (Cavalcante et al., 2020). By using the crystal violet technique, Openda and Nyokong manufactured protonated phthalocyanine-detonation nanodiamonds and studied their impact on biofilm inhibition. They dramatically reduced S. Aureus and E. coli biofilm development (Openda & Nyokong, 2021). Compared to the found literature, chemicals **(5), PcTACo&Zn, AuNP-5** and **AuNP-PcTACo&Zn**, particularly **AuNP-5** and **AuNP-PcTACo&Zn**, can be employed as biofilm inhibitors in the pharmaceutical and biotechnological sectors

Table 5.7: Biofilm inhibition activity % of compounds **(5)**, **PcTACo&Zn**, **AuNP-5**, **AuNP-PcTACo&Zn** and **AuNPs** using *S. Aureus*.

Compounds	125mg/L	250 mg/L	500 mg/L
(5)	53.33%	65.77%	79.98%
AuNP-5	58.55%	75.66%	94.16%
PcTACo	43.15%	80.04%	89.83%
AuNP-PcTACo	82.56%	90.55%	92.21%
PcTAZn	58.08%	85.05%	90.15%
AuNP-PcTAZn	63.11%	89.08%	96.48%
AuNPs	45.11%	56.55%	66.66%

Table 5.8: Biofilm inhibition activity % of compounds **(5)**, **PcTACo&Zn**, **AuNP-5, AuNP-PcTACo&Zn** and **AuNPs** using *P. Aeruginosa*.

Compounds	125mg/L	250 mg/L	500 mg/L
(5)	80.69%	83.69%	90.17%
AuNP-5	75.75%	92.43%	98.13%
PcTACo	82.39%	86.31%	85.90%
AuNP-PcTACo	85.79%	95.47%	95.36%
PcTAZn	82.66%	84.56%	86.56%
AuNP-PcTAZn	81.77%	95.56%	95.66%
AuNPs	53.23%	54.37%	70.05%

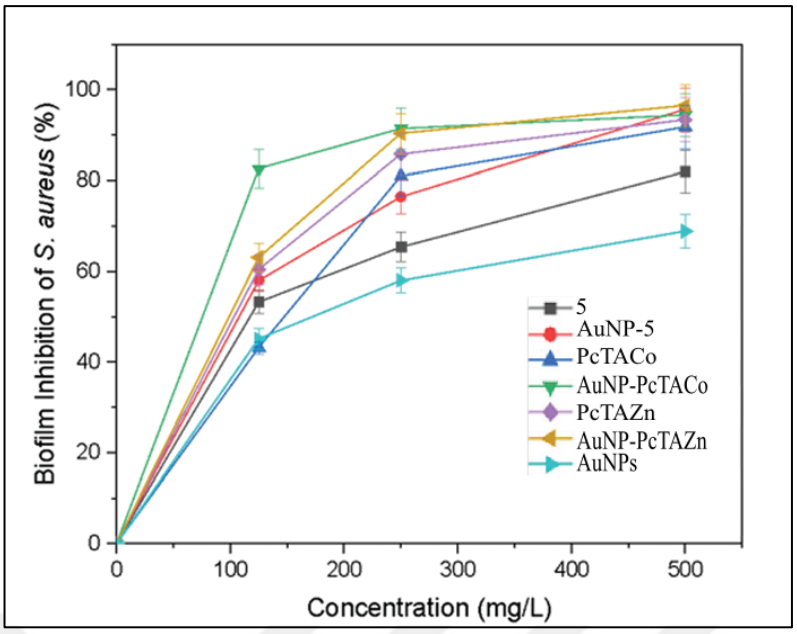

Figure 5.12 (a): Biofilm inhibition of the compounds (**5, PcTACo&Zn, AuNP-5, AuNP-PcTACo&Zn** and **AuNPs)** using *S. Aureus*.

Compounds	0 mg/L	125 mg/L	250 mg/L	500 mg/L
(5)				
PcTACo	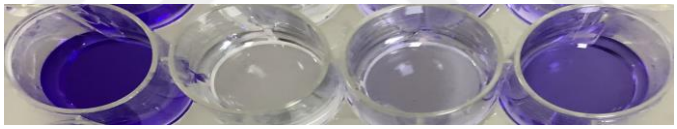			
PcTAZn	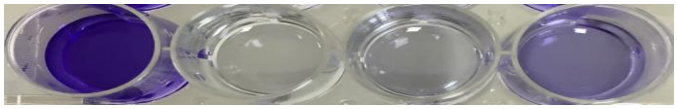			
AuNP-5				
AuNP-PcTACo				
AuNP-PcTAZn	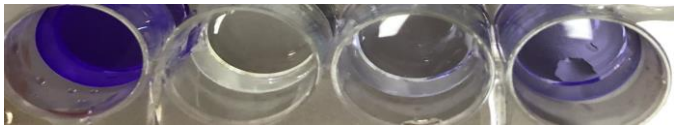			

Figure 5.12 (b): Biofilm inhibition of the compounds (**5, PcTACo&Zn, AuNP-5, AuNP-PcTACo&Zn** and **AuNPs)** using *S. Aureus*.

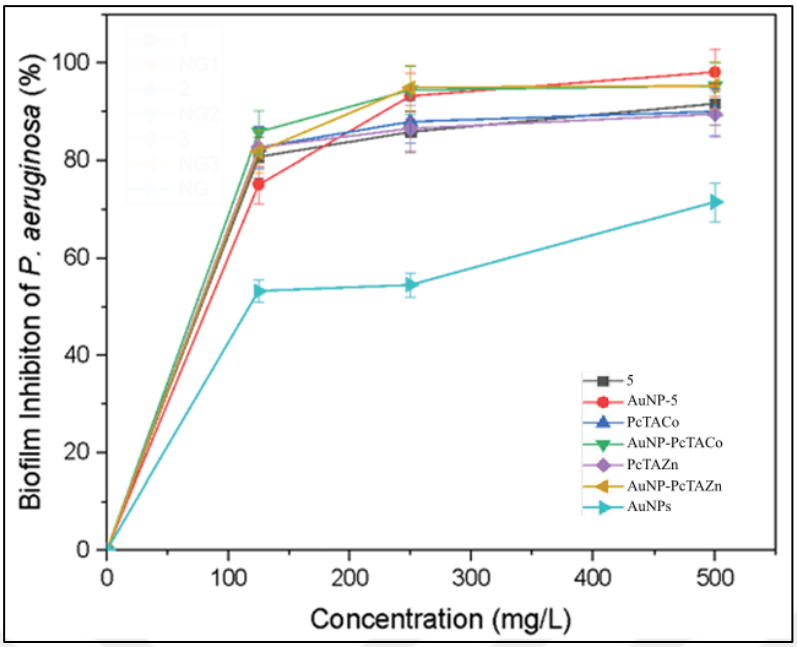

Figure 5.13 (a): Biofilm inhibition of the compounds (**5, PcTACo&Zn, AuNP-5, AuNP-PcTACo&Zn** and **AuNPs)** using *P. Aeruginosa*.

Compounds	0 mg/L	125 mg/L	250 mg/L	500 mg/L
(5)				
PcTACo				
PcTAZn				
AuNP-5				
AuNP-PcTACo				
AuNP-PcTAZn				
AuNPs				

Figure 5.13 (b): Biofilm inhibition of the compounds (**5, PcTACo&Zn, AuNP-5, AuNP-PcTACo&Zn** and **AuNPs)** using *P. Aeruginosa*.

5.2.4 UV-vis spectra of AuNPs-MPc conjugates of symmetrical tetra-substituted metal-phthalocyanines of phthalonitrile derivative (5)

In this study, the UV-vis spectra of the **AuNP-PcTACo&Zn** were obtained in DMSO at room temperature and are illustrated in Figure 5.14 and Table 5.9. Moreover, the surface plasmon resonance (SPR) absorption band of AuNPs (15–20 nm) appeared at a wavelength of 517 nm (Figure 5.14 and Table 5.9). As expected, the conjugation of phthalocyanines with the gold nanoparticle and their assembly onto the AuNPs surface led to the hypsochromic shift of the Q-bands of derived compounds **AuNP-PcTACo&Zn** in comparison to that of their related phthalocyanine precursors **PcTACo&Zn** (Mthethwa & Nyokong, 2015).

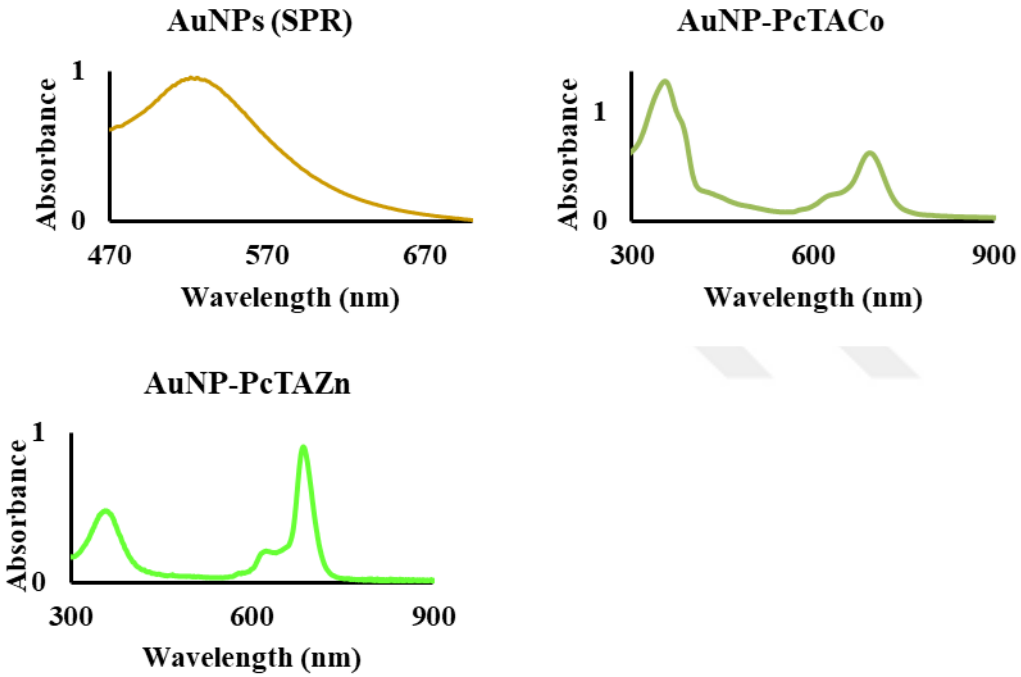

Figure 5.14: UV-vis spectra of AuNPs conjugates of symmetrical tetra-substituted metal-phthalocyanines of phthalonitrile derivative **(5).**

Table 5.9: UV-vis spectral values of AuNPs-MPc conjugates of symmetrical tetra-substituted metal-phthalocyanines of phthalonitrile derivative **(5).**

Name of the Compound	B-Band λ_{max}(nm) (log Ɛ)	Vibronic Band λ_{max} (nm) (log Ɛ)	Q-Band λ_{max} (nm) (log Ɛ)
AuNPs	(SPR)517nm	-	-
AuNP-PcTACo	354 (5.06)	623 (4.30)	687 (4.71)
AuNP-PcTAZn	358 (4.60)	630 (4.22)	685 (4.88)

5.2.5 TEM analysis of AuNPs-MPc conjugates of symmetrical tetra-substituted metal-phthalocyanines of phthalonitrile derivative (5)

Transmission electron microscopy (TEM) is a most used technique to analyze the size and structural characteristics of metallic nanoparticles. Results in TEM analysis are received in the form of TEM images when a beam of electrons passes through a sample compound (D'Souza et al., 2015). Ordinarily, when metallic nanoparticles are conjugated with MPcs, resulting hybrids have a larger size than the original nanoparticles, as π– π interactions between MPcs macrocycles causes H-aggregation (Bankole & Nyokong, 2017; Nwaji & Nyokong, 2017). Herein, conjugation of AuNPs to Metal Pcs (PcTACo and Zn) resulted in increment of size of the **AuNPs** (Ashjari et al., 2015; Moon et al., 2010). In actual, π– π stacking between MPcs and newly developed cooperation with adjoined AuNPs produced large sized single or paired molecules (Bankole & Nyokong, 2017; Moon et al., 2010). TEM images of AuNPs and **AuNP-PcTAZn** are shown in Figures 5.15 (a) and (b). Figure 5.15 (a) confirmed the synthesized gold nanoparticles diameters in the range of 15–20 nm that increased approximately 4 nm after the conjugation with compound **PcTAZn** (Figure 5.15. b).

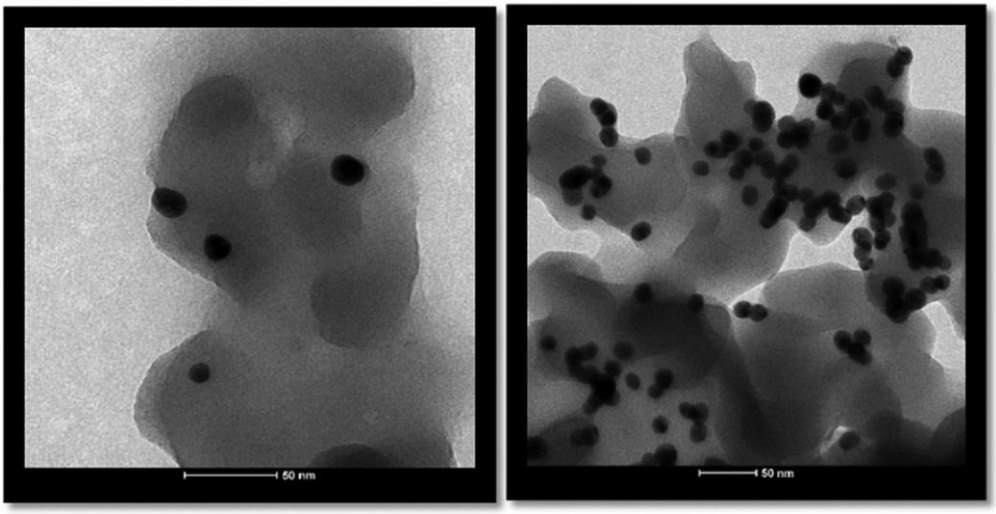

Figure 5.15: TEM images of **AuNPs** (a) and **AuNP-PcTAZn** (b).

5.3 Synthesis of Phthalonitrile Derivative (6) and Related Peripheral Symmetrically Octa-substituted Metal-Phthalocyanines

The pursued procedure mentioned for the 4,5-bis{[3,5 bis(trifluoromethyl)phenyl]ethynyl}phthalonitrile **(6)** synthesis is similar to the procedure employed by Bayir and coworkers for preparation of 4-((3,5-

Difluorophenyl)ethynyl)phthalonitrile (Ertunç et al., 2015). 4,5-dichloro-phthalonitrile **(4)** and 1-Ethynyl-3,5-bis(trifluoromethyl)benzene underwent Sonogashira coupling reaction (Sonogashira, 2002). The method uses alkynes and organic halides to introduce carbon– carbon triplet bonds to the resulting phthalonitrile. Afterwards, the template cyclotetramerization of the dintrile derivative **(6)** in collaboration of anhydrous metal salts for Co & Zn in DMAE and Lutetium acetate in 1-Pentanol for Lu gave octa-substituted metallophthalocyanine derivatives substituted at peripheral positions (Figure 5.16).

Furthermore, the octa- substituted MPcs were separated with THF as the mobile phase via column chromatography. Characterization measurements of these newly synthesized phthalocyanines were achieved using UV-vis, FT-IR, ^{1}H NMR and MALDI-TOF techniques and results corresponds strongly to the prepared compounds' structures.

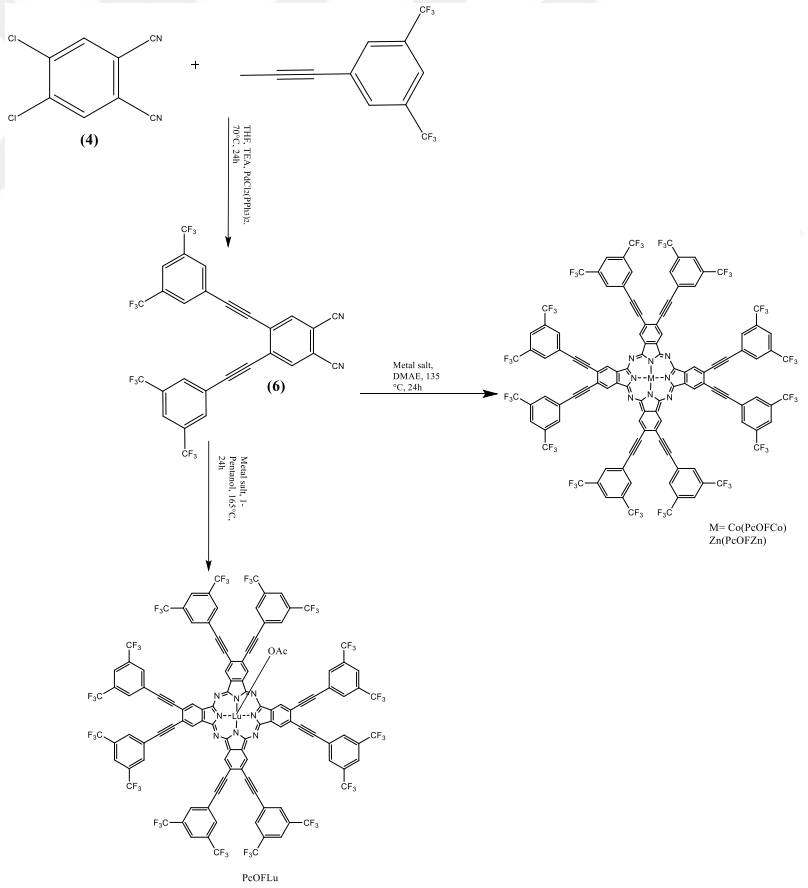

Figure 5.16: Synthesis of phthalonitrile derivative **(6)** and related symmetrical octa-substituted metal-phthalocyanines.

5.3.1 UV-vis spectra of symmetrically octa-substituted metal phthalocyanines of phthalonitrile (6)

As mentioned before, the phthalocyanine ring structure is generally distinguished through strong absorption bands obtained via UV-vis spectrometer appearing in the 300-700 nm range. The spectra are recoded in DMSO and THF (few pyridine drops) (Table 5.10 and Figure 5.17).

Herein, the effects of ethynyl and fluorine groups' presence, within the same Pc molecule, on UV-vis spectra values must be taken into consideration. Some literature mentions bathochromic shift (red region) of the Q-bands of MPcs bearing alkynyl groups in the periphery (Kalkan et al., 2004; D. Koçak & Gonca, 2010; Özçeşmeci et al., 2013). Aside from this, fluorine containing Pc compounds are known to cause hypsochromic shift towards the blue region (Wei 2003; L. Gao and Qian 2001).

Although in this study, the obtained Q-bands of the resulting octa-CF3 containing Pc molecules did not show bathochromic shift (appear before 700nm) (Table 5.10 and Figure 5.17) corresponding to the alkynyl moieties present. This analysis led to believe the strongly electron-withdrawing effect of 48 fluorine atoms on the Pc periphery have a much substantial effect on Q band wavelength position rather than the associated triple bonds (Sevim et al., 2013).

Moreover, the PcOFLu (DMSO) exhibit vibronic bands around 614nm and PcOFZn (THF-Pyridine) around 650nm.

DMSO is an aprotic polar solvent and unable to maintain effective axial coupling with Co and Zn metal ions, not able to make a significant decrease in π–π interactions hence leading to aggregation (Alvarez, 2020; Díaz-Torres & Alvarez, 2011; Słota & Dyrda, 2003). Due to this, the UV–vis spectra measured in DMSO appeared broad and aggregated (Cong et al., 2015; Loosli et al., 2005; Voronina et al., 2015). However, this aggregation phenomenon was overcome as observed in the lutetium Pc due to the presence of axial acetate group and DMSO integrated well with the metal ion and much sharper B and Q bands are seen (Figure 5.17).

Furthermore, Co and Zn MPcs spectra are also recorded in THF added with few pyrdine drops providing better solubility and resulted in sharper UV-vis Q and B band peaks (Figure 5.17).

Table 5.10: UV-vis spectral values of symmetrical octa-substituted metal-phthalocyanines of phthalonitrile **(6)**.

Name of the Compound	B-Band λ_{max}(nm) (log Ɛ)	Vibronic Band λ_{max}(nm) (log Ɛ)	Q-Band λ_{max}(nm) (log Ɛ)
PcOFCo-DMSO	373 (5.22)	-	634 (4.90)
PcOFCo-THF-Pyr	430 (5.43)	-	667 (5.31)
PcOFZn-DMSO	354 (5.10)	-	635 (4.23), 679 (4.87)
PcOFZn-THF-Pyr	346 (5.37)	650 (5.18)	678 (5.29)
PcOFLu	354 (5.01)	614 (4.69)	682 (5.23)

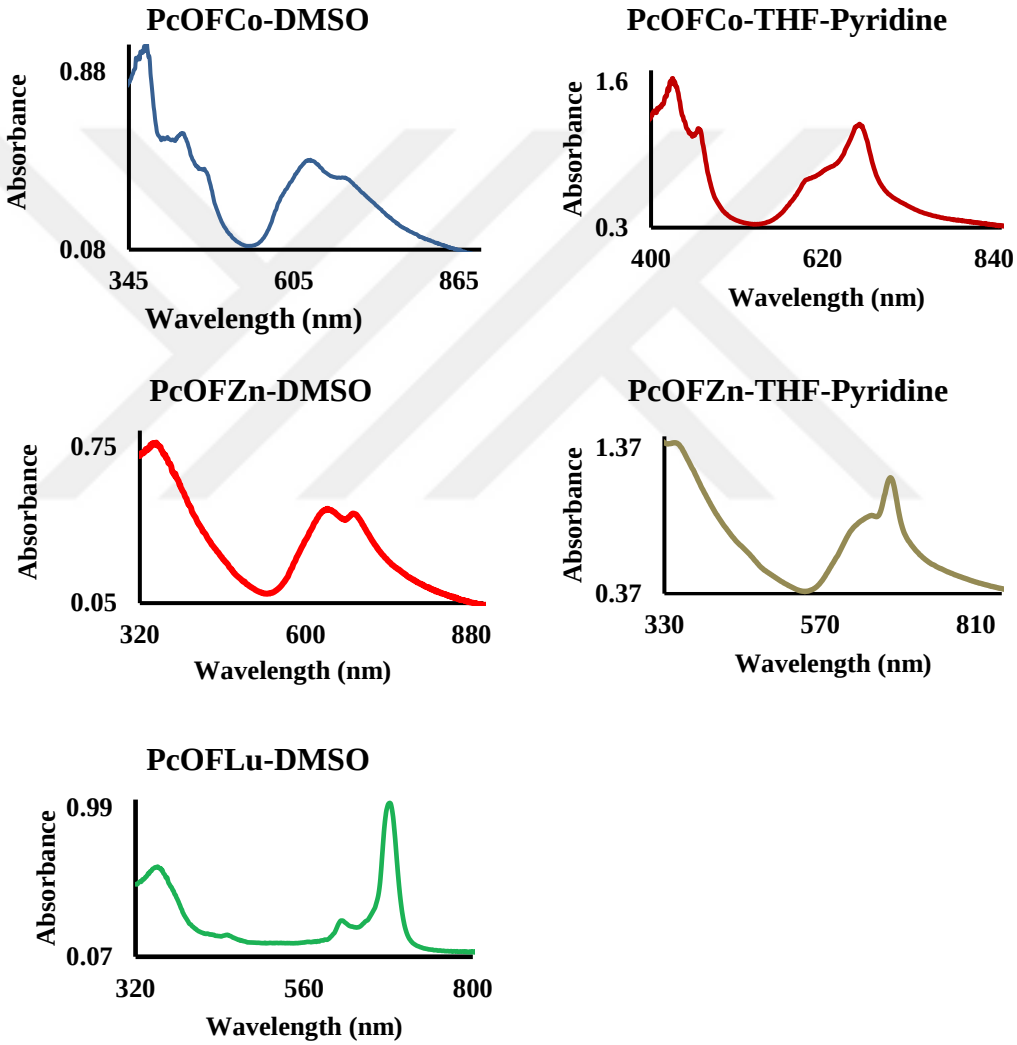

Figure 5.17: UV-vis spectra of symmetrical octa-substituted metal-phthalocyanines of phthalonitrile **(6)**.

5.3.2 Aggregation studies of PcOFLu

In this study, the aggregation behavior of **PcOFLu** compound was investigated in THF at different concentrations. The increase in the concentration of **PcOFLu** phthalocyanine was followed by an increase in the absorption intensity of the Q-band, and no new bands originating from the clustered species were observed (Figure 5.18). Due to its non-clustering behavior, **PcOFLu** complied with Lambert – Beer law at different concentrations in THF ranging from 4×10^{-6} to 14×10^{-6} M (Figure 5.19) (Karaoğlu et al., 2018).

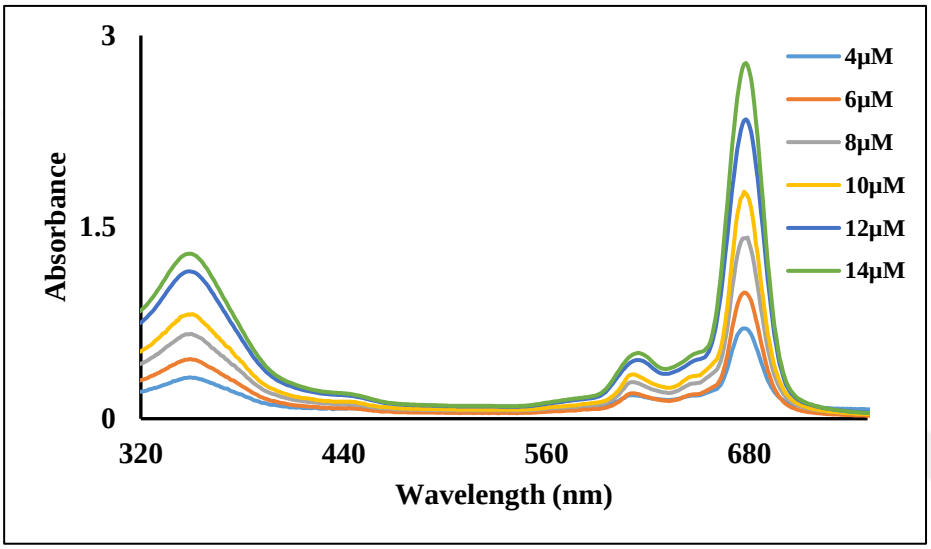

Figure 5.18: UV-vis spectra of compound **PcOFLu** at different concentrations between 4×10^{-6}–14×10^{-6} M in THF.

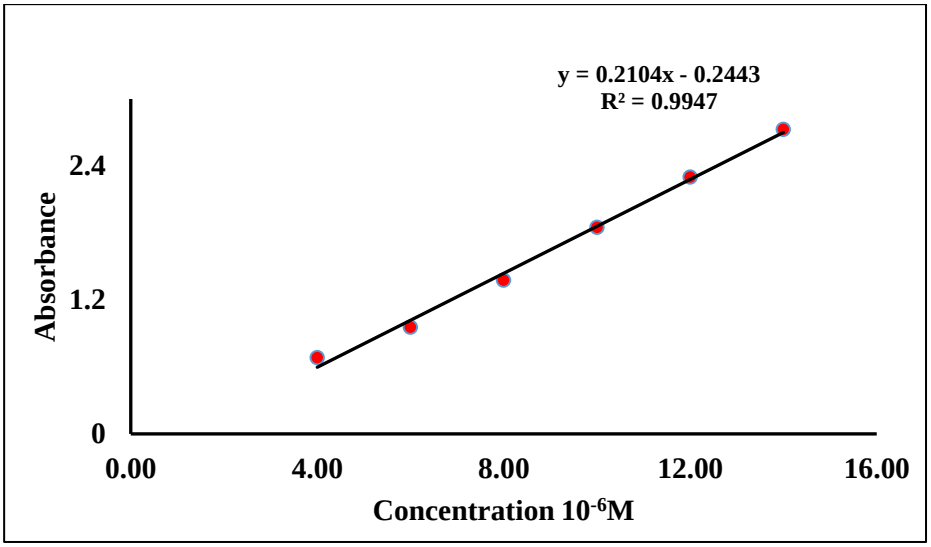

Figure 5.19: Graph of compound **PcOFLu** absorbance versus concentrations (THF).

5.4 Synthesis of Phthalonitrile Derivative (7) and Related Peripheral Symmetrically Octa-substituted Metal-Phthalocyanines and Derived AuNPs Conjugates

Organic compounds containing amines or related aromatic nitrogen derivatives have found considerable significance in disciplines related to agriculture, dyes and paints, and biological and therapeutic applications (Magro et al., 2007; S. A. Lawrence, 2004; Seayad et al., 2002; Vollhardt & Schore, 1999). Organic amines residing in the vicinity of phthalocyanine ring has a noticeable effect on the rings conductivity and energy properties which in turn can be profited in diverse photo dissociation, electrolytic and sensory (Bala et al., 2013; Linares-Flores et al., 2015; Yang et al., 2012). While, presence of acetylene group on the same compound can also have immense pharmaceutical and biological importance (Broggi et al., 2014; Diederich et al., 2005; Zhou et al., 2015).

As the primary element of aromatic stability is π-expansion abilities of these compounds, that is highly practiced in molecular electronics engineering, sensors, organic photovoltaic solar devices and pharmaceutical adaptations (Chanteau & Tour, 2001; Inouye et al., 1999; Mohajer et al., 2021). Therefore, the synthesis of such diverse heterocyclic compounds containing alkyne groups is utterly advantageous. In the light of these benefits, this thesis emphasized on preparing alkynyl-aniline containing metal phtahlocyanines and their subsequent fabrication with AuNPs evaluated for valuable biological applications.

Dinitrile compound **(7)** was synthesized through the Sonogashira halide catalyzed cross-coupling reaction (Sonogashira, 2002) when 4-ethynyl-N,N-dimethylaniline and 4,5-dichlorophthalonitrile (4) dissolved in TEA:THF mixture was stirred at 80 °C and purified on silica column eluted by hexane : dichloromethane (3 : 2) (Figure 5.20). The prepared phthalonitrile was characterized by UV-vis, FT-IR, ^{1}H-NMR, and ^{13}C-NMR spectroscopic techniques. Subsequent metal mediated cyclotetramerization of phthalonitrile **(7)** in 2-dimethylaminoethanol for PcOACo and Zn and 1-pentanol solvent for PcOALu resulted in the synthesis of derived MPc compounds. The coarse phthalocyanines thus obtained were purified via chromatographic silica ran with THF eluent. Further characterization was carried out testing via FT-IR, UV–vis, and MALDI-TOF and ^{1}H- NMR spectroscopy.

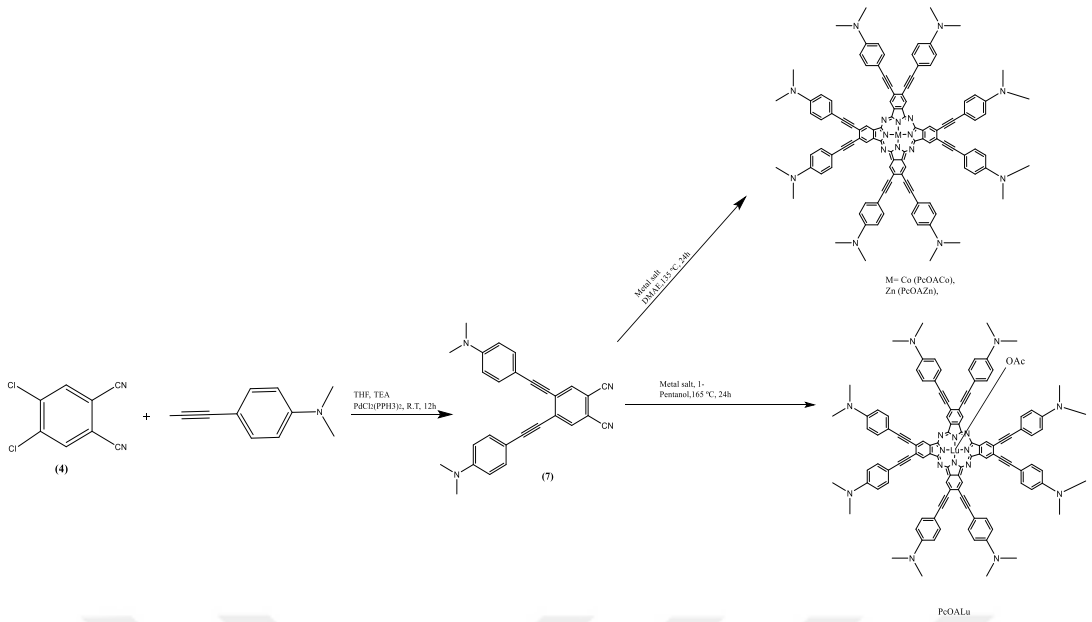

Figure 5.20: Synthesis of phthalonitrile derivative **(7)** and related peripheral symmetrically octa-substituted metal-phthalocyanines.

5.4.1 UV-vis spectra of phthalonitrile (7) related symmetrically octa-substituted metal phthalocyanines

UV–vis spectra of phthalonitrile **(7)** and all its related MPc compounds were conducted in DMSO and THF (with drops of pyridine) at room temperature (Figure 5.21). The respective B, vibronic and Q-band values are illustrated in Table 5.11. Relative intense B-band as compared to Q-band corresponds to the presence of peripheral substituents is evident from the UV-vis spectra of phthalonitrile **(7)**.

Due to DMSO's inability to show efficient axial integration with the metal ion, no significant decrease in π–π interactions was observed between the rings leading to aggregation (Alvarez, 2020; Díaz-Torres & Alvarez, 2011; Słota & Dyrda, 2003). As a consequence, the UV–vis spectra taken in DMSO appeared wide (Cong et al., 2015; Loosli et al., 2005; Voronina et al., 2015). The aggregation was minimized in the lutetium Pcs due to the presence of axial acetate attached to Lu-metal ion and DMSO correlated efficiently with the M-ion and hence sharp Band Q bands are observed.

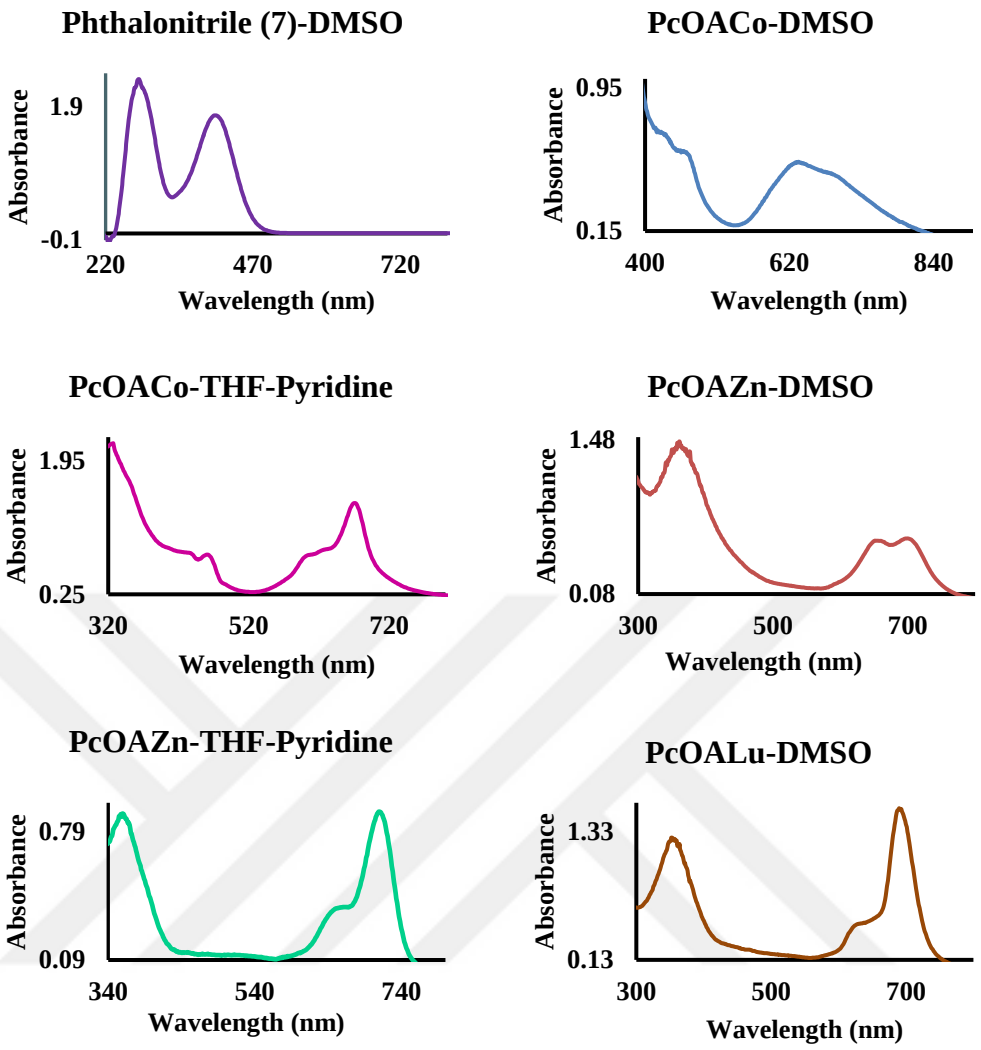

Figure 5.21: UV-vis spectra of symmetrical octa-substituted metal-phthalocyanines of phthalonitrile **(7).**

Table 5.11: UV-vis spectral values of symmetrical octa-substituted metal-phthalocyanines of phthalonitrile **(7).**

Name of the Compound	B-Band λ_{max}(log Ɛ)	Vibronic Band λ_{max} (log Ɛ)	Q-Band λ_{max} (log Ɛ)
Phthalonitrile **(7)**- DMSO	272 (5.61)	-	426 (5.42)
PcOACo-DMSO	359 (5.37)	-	634 (4.95)
PcOACo-THF-Pyr	327 (5.56)	-	671 (5.37)
PcOAZn-DMSO	357 (5.25)	650 (4.97)	698 (4.98)
PcOAZn-THF-Pyr	359 (5.17)	668 (4.80)	712 (5.18)
PcOALu-DMSO	356 (5.34)	-	689 (5.30)

5.4.2 AuNPs conjugates of phthalonitrile (7) and related MPcs

Moreover, Co and Zn MPcs of **(7)** were self-assembled on gold nanoparticles surface (AuNPs) through electrostatic interactions (D'Souza et al. 2015). Herein, the gold

nanoparticles were adjoined with prepared compounds **(7), PcOACo & Zn**. Electrostatic interactions between the compounds **(7), PcOACo & Zn** and **AuNPs** directed the self-assembly and conjugation of the prepared compounds on the nanoparticles surface while formulated a monolayer on the AuNPs (Hone et al. 2002).

Biological studies, UV-Vis and TEM recordings conducted for the prepared AuNPs and their conjugated MPcs of phthalonitrile **(7)** are illustrated in the subsequent section.

5.4.3 Biological studies

5.4.3.1 DPPH radical scavenging activity

In this thesis study, the DPPH radical inhibition capacity of compounds **(7), PcOACo&Zn, AuNPs, AuNP-7** and **AuNP-PcOACo&Zn** was evaluated and the results are shown in Table 5.12 and Figure 5.22. All the studied compounds depicted extraordinary DPPH scavenging activities. Herein, the highest 100% value was given by compounds **(7), AuNP-7, PcOACo** and **AuNP-PcOACo** at 100 mg L^{-1}. The antioxidant ability of Pcs is directly related to the π-electrons resonance. Many other aspects like the type of substituent as well as the electrovalent character of the metal ion have a primary intake on the magnitude of π-electron character (C. Leznoff & Lever). Other researchers have also quoted related results. For instance, Saki et al. reported synthesis and antioxidant activities of novel In and Ga Pcs using the DPPH approach. (Saki et al., 2018). Moreover, Aydın et al. evaluated the DPPH scavenging activity of tetra-substituted MPcs containing (4-(methylthio)phenylthio) substituents and reported maximum 54% DPPH radical inhibition for Co phthalocyanine at concentration of 500 mg L^{-1} (Aydın et al., 2017). As compared to the related literature, our synthesized compounds showed greater DPPH radical ability.

Table 5.12: DPPH scavenging activity of **(7), AuNP-7, PcOACo&Zn, AuNP-PcOACo&Zn** and **AuNPs.**

Compounds	6.25mg/L	12.5 mg/L	25 mg/L	50 mg/L	100 mg/L
(7)	76.32%	86.37%	97.53%	100%	100%
AuNP-7	68.47%	81.62%	90.46%	97.67%	100%
PcOACo	71.96%	83.43%	92.56%	99.89%	100%
AuNP-PcOACo	69.18%	81.39%	90.27%	96.35%	100%
PcOAZn	64.25%	76.43%	85.09%	93.59%	98.37%
AuNP-PcOAZn	59.64%	70.26%	78.91%	85.77%	92.58%
AuNPs	29.29%	43.65%	58.07%	68.45%	70.43%

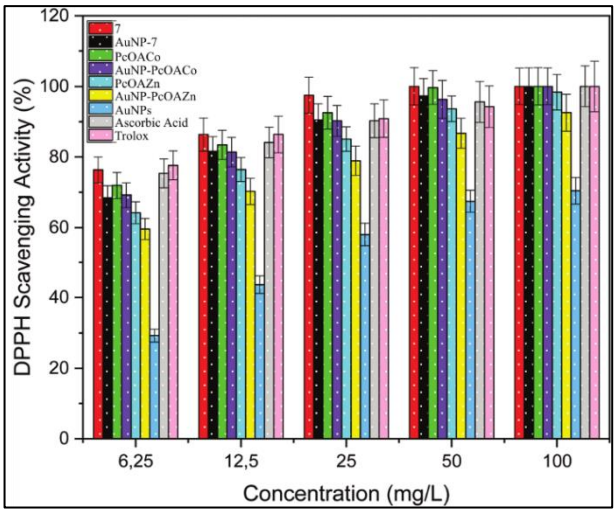

Figure 5.22: DPPH scavenging activity of **(7), AuNP-7, PcOACo&Zn, AuNP-PcOACo&Zn** and **AuNPs**.

5.4.3.2 DNA clevage activity

The transformation of DNA from Form I (superhelical form) to Form II (broken circular form) or Form III (non-superhelical form) was used to assess the DNA cleavage activity of **(7), PcOACo&Zn, AuNPs, AuNP-7** and **AuNP-PcOACo&Zn.** The studies were done by inoculating varying concentrations of the examined substances with DNA to detect their DNA nuclease ability. Figure 5.23 (a) and (b) illustrates the influence of all compounds on DNA cleavage activity. Herein, AuNPs lacked DNA cleavage capability.

Similar findings have been addressed in the literature. Xiao et al. created fluorinated dendritic silicon(IV) phthalocyanines-polyethylene glycol monomethyl ethet-polycaprolactone-NPs and investigated their DNA cleavage activities, finding that the resulting compounds had single-strand DNA cleavage power (Xiao et al., 2021). Moreover, DNA cleavage activity of various phthalocyanines was examined by Baş et al. The phthalocyanines were seen to be capable of cleaving plasmid DNA (Baş et al., 2019). Following additional examination and correlation to the literature, it was realized that phthalonitrile compound **(7), PcOACo&Zn, AuNP-7** and **AuNP-PcOACo&Zn** can be employed as DNA targeting molecules in treatment of cancer and microbiological studies.

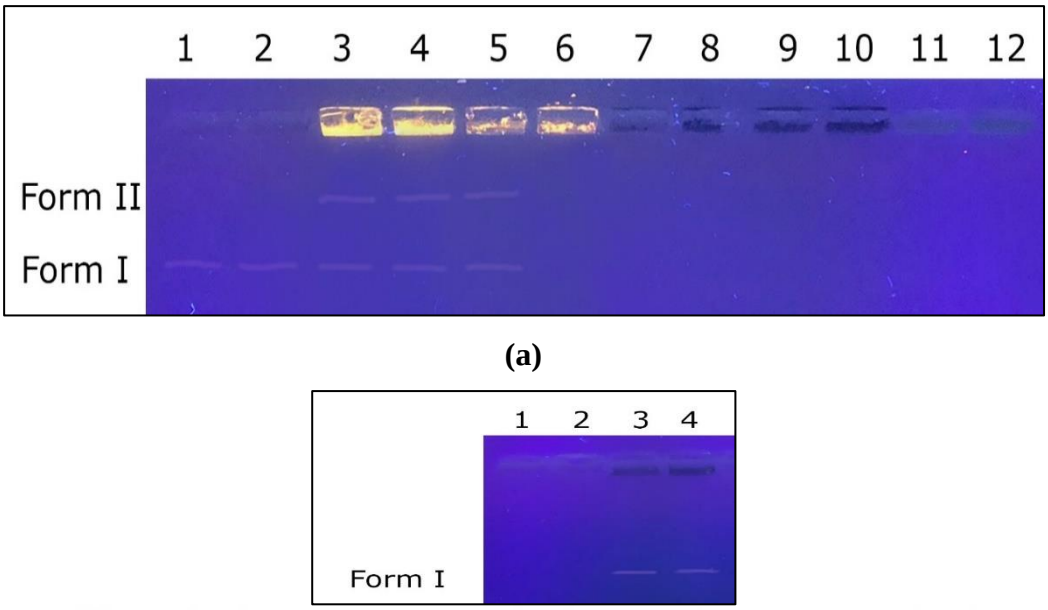

(a)

(b)

Figure 5.23: DNA cleavage activity of **(7), PcOACo&Zn, AuNP-7, AuNP-PcOACo&Z** and **AuNPs**. (a) Lane 1, pBR 322 DNA; Lane 2, pBR 322 DNA + DMSO; Lane 3, pBR 322 DNA + 100 mg of **(7)**; Lane 4, pBR 322 DNA + 200 mg of **(7)**; Lane 5, pBR 322 DNA + 100 mg/L of **AuNP-7**; Lane 6, pBR 322 DNA + 200 mg/L of **AuNP-7**; Lane 7, pBR 322 DNA + 100 mg of **PcOACo**; Lane 8, pBR 322 DNA + 200 mg/L of **PcOACo**; Lane 9, pBR 322 DNA + 100 mg/L of **AuNP-PcOACo**; Lane 10, pBR 322 DNA + 200 mg/L of **AuNP-PcOACo**; Lane 11, pBR 322 DNA + 100 mg/L of **PcOAZn**; Lane 12, pBR 322 DNA + 200 mg/L of **PcOAZn**; (b) Lane 1, pBR 322 DNA + 100 mg/L of **AuNP-PcOAZn**; Lane 2, pBR 322 DNA + 200 mg/L of **AuNP-PcOAZn**; Lane 3, pBR 322 DNA + 100 mg/L of **AuNPs**; Lane 4, pBR 322 DNA + 200 mg/L of **AuNPs.**

5.4.3.3 Antimicrobial activity

Utilizing micro dilution method, the antimicrobial properties of substances **(7), PcOACo&Zn, AuNPs, AuNP-7** and **AuNP-PcOACo&Zn** was explored. The antibacterial activity of the samples were determined as MIC (minimum inhibition concentration) values using this procedure, which involved preparing 2-fold dilutions of the specimens.

Table 5.13 shows a summary of the findings. As a result, compounds **AuNP-7 and AuNP-PcOACo&Zn** outperformed compounds **(7), PcOACo&Zn** and **AuNPs** in terms of antibacterial activity. The most effective antibacterial efficacy against the studied microbes was **AuNP-PcOAZn**, while **AuNPs** had the least efficient antimicrobial activity.

Furthermore, evaluated especially in comparison to Gram-negative bacteria, the investigated complexes had far more potent antibacterial activity towards Gram-

positive bacteria. Gr(+) bacteria are far more susceptible to light activation by various colors than Gr(-) bacteria, according to Huang and group (Huang et al., 2012).

Similar investigations have been presented. Artaş et al. synthesized new phthalocyanines with poly-hydroxyl groups and used the microdilution method to test their antibacterial activity.

Antimicrobial activity was shown in all of the complexes against Gram-positive bacteria, Gram-negative bacteria, and micro fungus. Copper(II) phthalocyanine, according to their in vitro antimicrobial studies, had the best antibacterial activity against *P. Aeruginosa*, with a MIC value of 8 mg L^{-1} (M. Ağırtaş et al., 2021). Unsymmetrical zinc phthalocyanine coupled to silver (Ag) nanoparticles and iron oxide (FeO) nanoparticles was produced by Mapukata et al. They also looked at the antibacterial properties of the materials, as well as phthalocyanine-modified Ag nanoparticles and phthalocyanine-modified FeO nanoparticles, which have antimicrobial properties (Mapukata et al., 2020).

Our results are supported with previous analyses when compared to the previous research. Following numerous toxicological testing, it was discovered that compounds **(7), PcOACo&Zn**, and especially **AuNP-7** and **AuNP-PcOACo&Zn** can be employed as antibacterial agents in the nano pharmaceutical sector.

Table 5.13: Antimicrobial activity of **(7), AuNP-7, PcOACo&Zn, AuNP-PcOACo&Zn** and **AuNPs**.

Microorganisms	(7)	AuNP-7	PcOACo	AuNP-PcOACo	PcOAZn	AuNP-PcOAZn	AuNPs
E. coli	128	64	64	32	64	16	512
P. Aeruginosa	128	64	32	16	64	16	512
L. pneumophila subsp. pneumophila	128	64	64	32	32	16	1024
E. hirae	64	32	32	16	32	16	512
E. fecalis	64	32	64	32	32	8	1024
S. Aureus	128	32	64	32	16	8	1024
C. parapisilosis	64	16	64	16	32	16	512
C. tropicalis	32	16	32	16	32	16	512

5.4.3.4 Microbial cell viability inhibition

Using Escherichia coli as a reference microbe, the inhibitory effects of substances **(7), PcOACo&Zn, AuNPs, AuNP-7** and **AuNP-PcOACo&Zn** on bacteria cell survival was investigated. The outcomes are shown in Figure 5.24 (a) & (b) and Table 5.14. All of the chemicals tested were efficient at inhibiting microbial cell life. In addition,

when compared to compounds **(7), PcOACo&Zn, and AuNPs, AuNP-7** and **AuNP-PcOACo&Zn** showed more potent microbial inhibitory action. Compounds **(7), PcOACo&Zn,** and **AuNPs** had respective microbial cell inhibition activities of 92.34 percent, 94.86 percent, 91.47 percent, and 90.69 percent at 100 mg L^{-1}, while compounds **AuNP-7** and **AuNP-PcOACo&Zn** had respective microbial cell inhibition activities of 97.61 percent, 98.67 percent, and 98.56 percent at 100 mg L^{-1}.

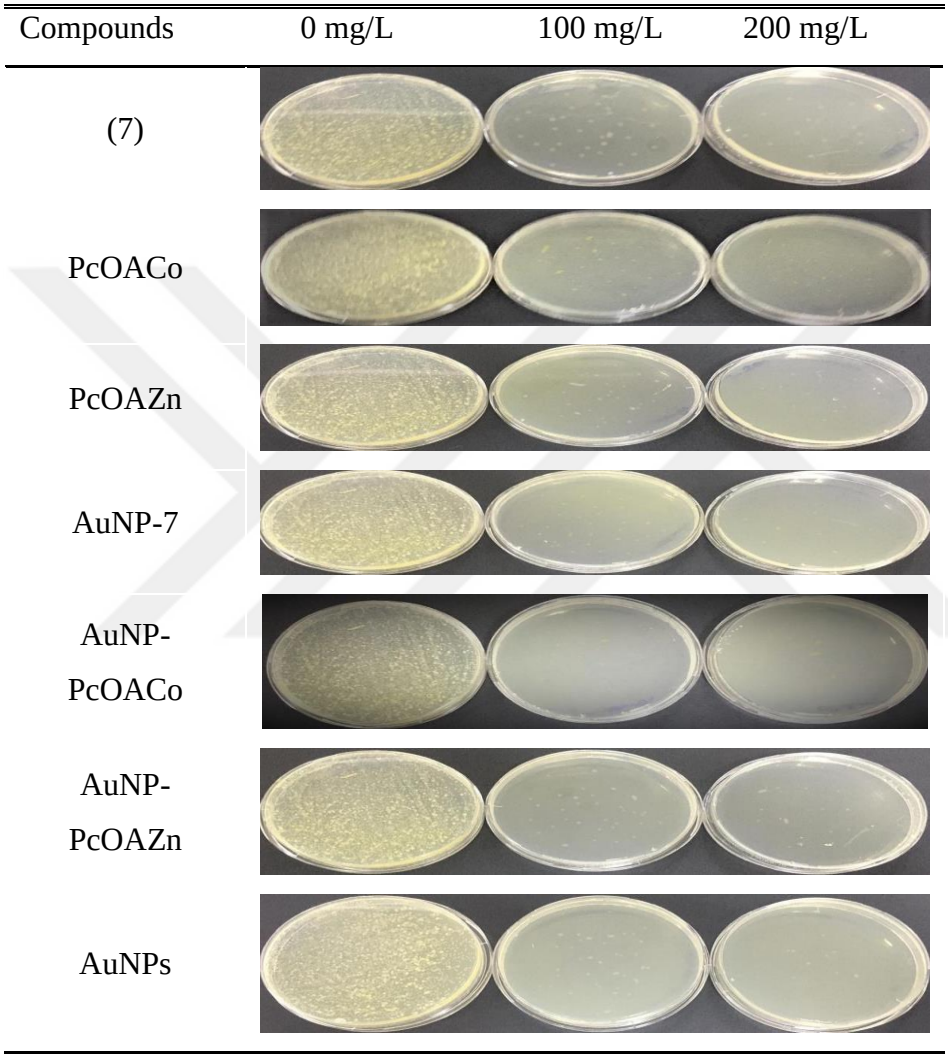

Figure 5.24 (a): Microbial cell viability inhibition of compounds **(7)**, **AuNP-7**, **PcOACo&Zn**, **AuNP-PcOACo&Zn** and **AuNPs.**

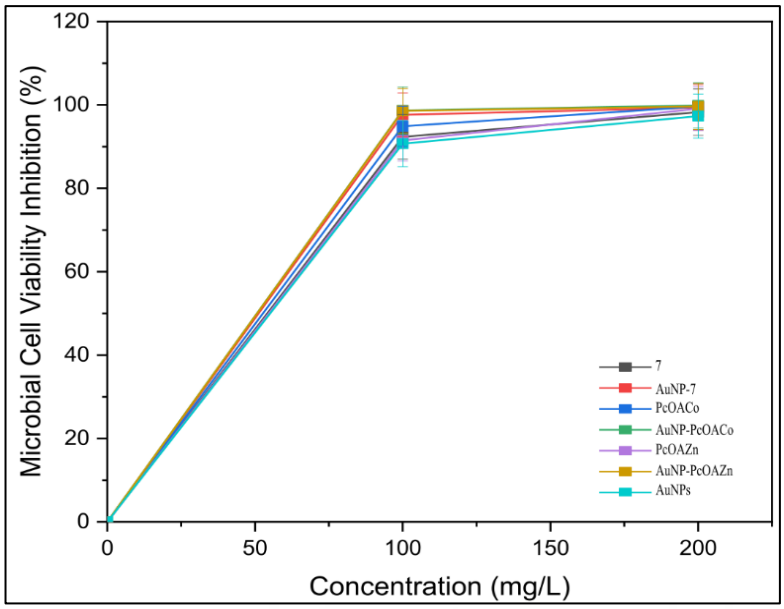

Figure 5.24 (b): Microbial cell viability inhibition of compounds **(7), AuNP-7, PcOACo&Zn, AuNP-PcOACo&Zn** and **AuNPs**.

Table 5.14: Microbial cell viability inhibition % of **(7), AuNP-7, PcOACo&Zn, AuNP-PcOACo&Zn** and **AuNPs**.

Compounds	100 mg/L	200 mg/L
(7)	92.34%	94.35%
AuNP-7	97.61%	98.84%
PcOACo	94.86%	98.65%
AuNP-PcOACo	98.67%	99.76%
PcOAZn	91.47%	94.69%
AuNP-PcOAZn	98.56%	99.42%
AuNPs	90.69%	95.54%

Antibacterial activity and photodynamic treatment properties of the examined chemicals were also explored in this research. The results are shown in Figure 5.25 (a) and (b). As indicated, all of the examined products' antibacterial PDT treatment activities were rather strong after 20 minutes of being exposed to LED light, and all of the tested compounds had 100% antimicrobial PDT treatment potential (Figure 5.25 b)

In past few years, photodynamic therapy (PDT) has emerged being one of the most effective antibacterial treatment approaches. The formation of reactive oxygen species (ROS) via the conversion of light energy is the basis of PDT's mechanism. Toxic chemicals called reactive oxygen species (ROS) invade the cellular membrane and lead to cell death (Kwiatkowski et al., 2018; Rajendran, 2016).

Nanoscience, on the contrary, is commonly applied in the domain of PDT applications

to improve clinical efficiency. Nanoparticles can also be used for a variety of reasons in nano medicine (Bhatia, 2016).

Similar research have been discussed in the literature. Nombona et al. created Zn phthalocyanine—polylysine conjugated metal nanoparticles and studied their photodynamic antibacterial properties. After photoluminescence, phthalocyanine–silver nanoparticles prevented 94 % microbiological growth and phthalocyanine–gold nanoparticles inhibited 86 % microbial growth. Furthermore, unconjugated phthalocyanines suppressed microbial growth by 83 % only (Nombona et al., 2012). The antibacterial photodynamic treatment activity of water-insoluble phthalocyanines-embedded silica nanoparticles against *S. Aureus* and *Candida albicans* was investigated by Baigorria et al. The in vitro studies of the antimicrobial photodynamic therapy activities MPcs indicated that they exhibited photo inactivation against *S. Aureus* and *C. albicans* (Baigorria et al., 2018). Giuliani et al. studied the antimicrobial photodynamic therapy (APDT) of cationic tetra-substituted Zn(II) phthalocyanines and they exhibited effective APDT killing efficacy (99.9%) against *S. Aureus* (Giuliani et al., 2010).

In comparison to the literature, the newly synthesized compounds **(7), PcOACo&Zn, AuNPs, AuNP-7** and **AuNP-PcOACo&Zn** can be used as photosensitizers in antimicrobial activity studies for different purposes.

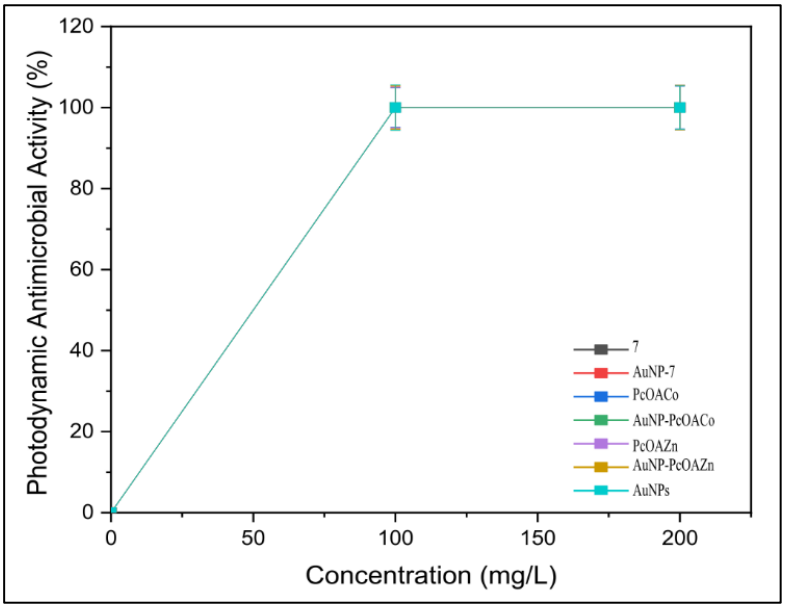

Figure 5.25 (a): Photodynamic antimicrobial activity of compounds **(7), AuNP-7, PcOACo&Zn, AuNP-PcOACo&Zn** and **AuNPs**

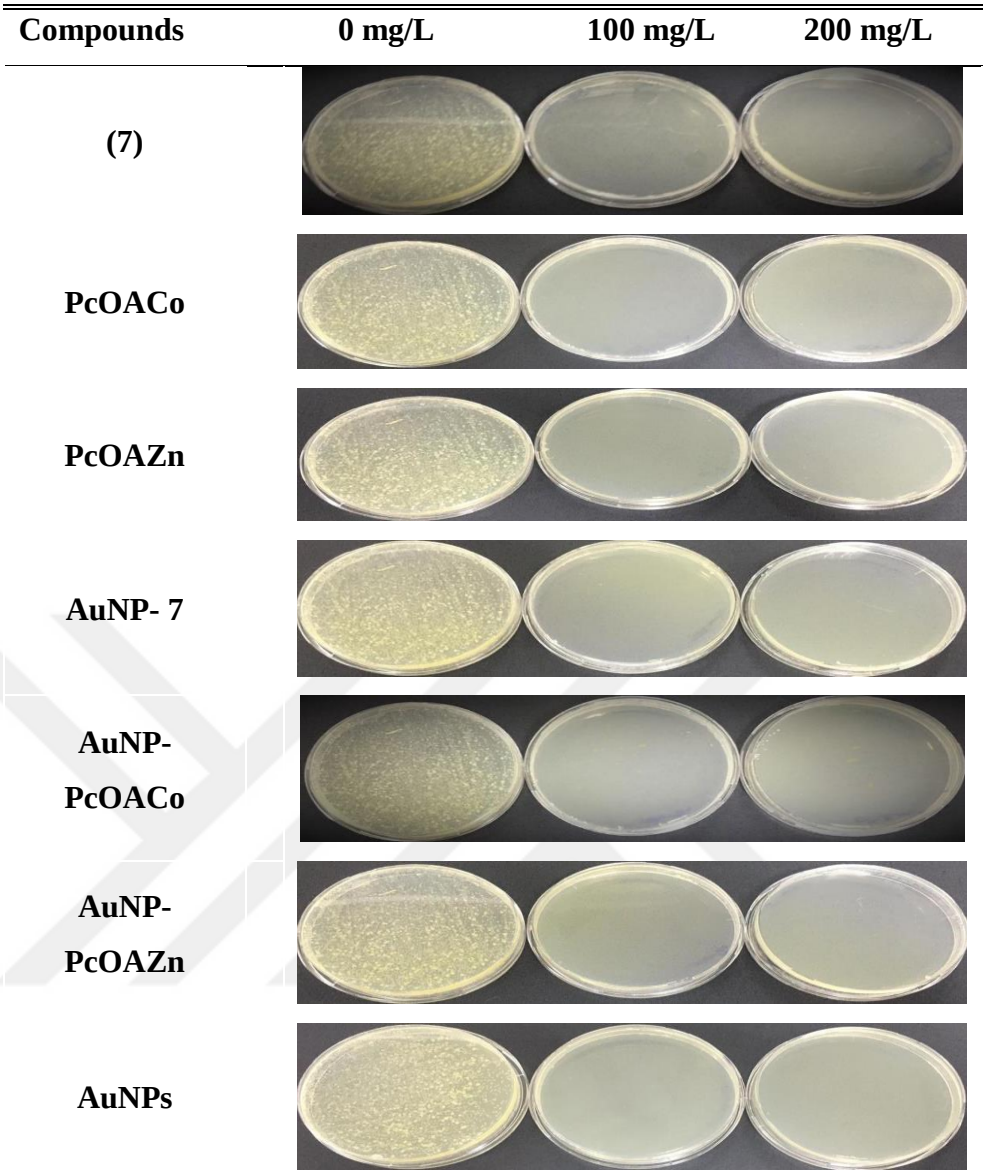

Figure 5.25 (b): Photodynamic antimicrobial activity of compounds **(7), AuNP-7, PcOACo&Zn, AuNP-PcOACo&Zn** and **AuNPs.**

5.4.3.5 Biofilm inhibition

The effects of various chemical concentrations of **(7), PcOACo&Zn, AuNPs, AuNP-7** and **AuNP-PcOACo&Zn** on *S. Aureus* and *P. Aeruginosa* biofilm inhibition were investigated in this study and are depicted in Table 5.15, Figures. 5.26 (a, b), Figure 5.27 (a, b) and Table 5.16 respectively. In general, all of the investigated substances inhibited the biofilm development of *P. Aeruginosa* more effectively than they inhibited the biofilm formation of *S. Aureus*. It was also discovered that compounds **AuNP-7** and **AuNP-PcOACo&Zn** inhibited biofilms more effectively than compounds **(7), PcOACo&Zn**, and **AuNPs**. At 125 mg L^{-1}, the biofilm inhibition activities of compounds. The maximum biofilm inhibition activity for **AuNP-7** was

92.41 percent against *S. Aureus*, while the highest biofilm inhibition activity for **AuNP-PcOAZn** was 96.68 percent against *P. Aeruginosa* at a concentration of 500 mg L^{-1}.

Some corresponding analysis have been described in the literature. Gao and co-workers studied the impact of zinc(II) phthalocyanine on S. Aureus biofilm inhibition and discovered anti-biofilm response (Gao et al., 2018). Lourenço et al. investigated the biofilm development limitation of cationic zinc(II) phthalocyanines and inhibited biofilm development in *E. coli* (Lourenço et al., 2019). When compared to previous studies, it became evident that compounds **(7), PcOACo&Zn** and particularly **AuNP-7** and **AuNP-PcOACo&Zn**, can be employed as anti-biofilm promoters in medicine and commercial microbiology.

Table 5.15: Biofilm inhibition % of compounds **(7), AuNP-7, PcOACo&Zn, AuNP-PcOACo&Zn** and **AuNPs** by using *S. Aureus*.

Compounds	125mg/L	250 mg/L	500 mg/L
(7)	64.38%	78.95%	91.05%
AuNP-7	72.73%	85.65%	92.41%
PcOACo	68.91%	79.86%	85.87%
AuNP-PcOACo	71.45%	82.36%	86.64%
PcOAZn	74.06%	78.54%	88.76%
AuNP-PcOAZn	84.51%	89.96%	87.15%
AuNPs	42.13%	58.86%	73.42%

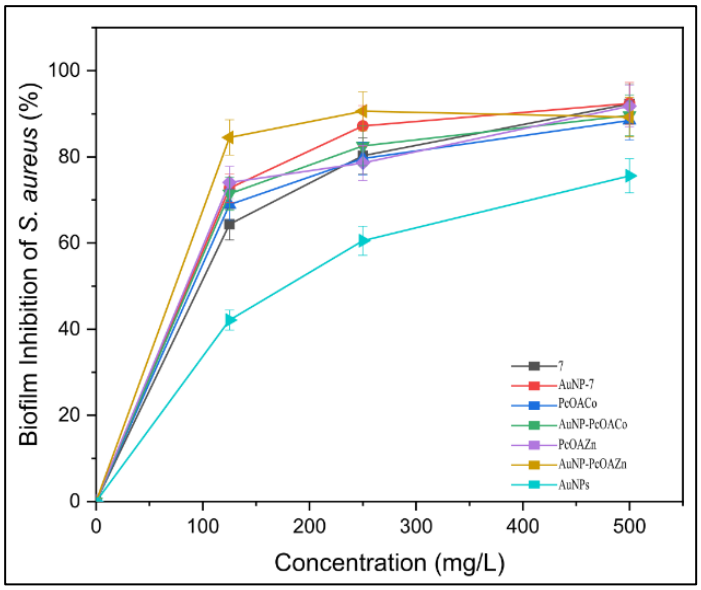

Figure 5.26 (a): Biofilm inhibition % of compounds **(7), AuNP-7, PcOACo&Zn, AuNP-PcOACo&Zn** and **AuNPs** by using *S. Aureus*.

Compounds	0 mg/L	500 mg/L	250 mg/L	125 mg/L
(7)				
PcOACo				
PcOAZn				
AuNP-7				
AuNP-PcOACo				
AuNP-PcOAZn				
AuNPs				

Figure 5.26 (b): Biofilm inhibition of **(7), AuNP-7, PcOACo&Zn, AuNP-PcOACo&Zn** and **AuNPs** by using *S. Aureus*.

Compounds	0 mg/L	500 mg/L	250 mg/L	125 mg/L
(7)	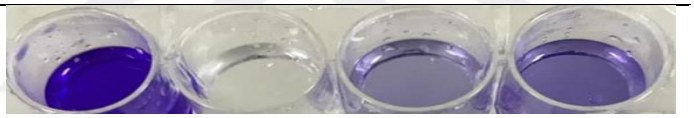			
PcOACo	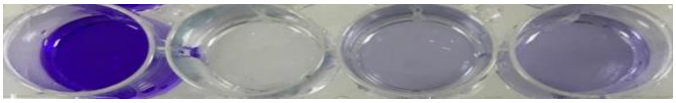			
PcOAZn				
AuNP-7				
AuNP-PcOACo				
AuNP-PcOAZn				
AuNPs				

Figure 5.27 (a): Biofilm inhibition of compounds **(7), AuNP-7, PcOACo&Zn, AuNP-PcOACo&Zn** and **AuNPs** by using *P. Aeruginosa*.

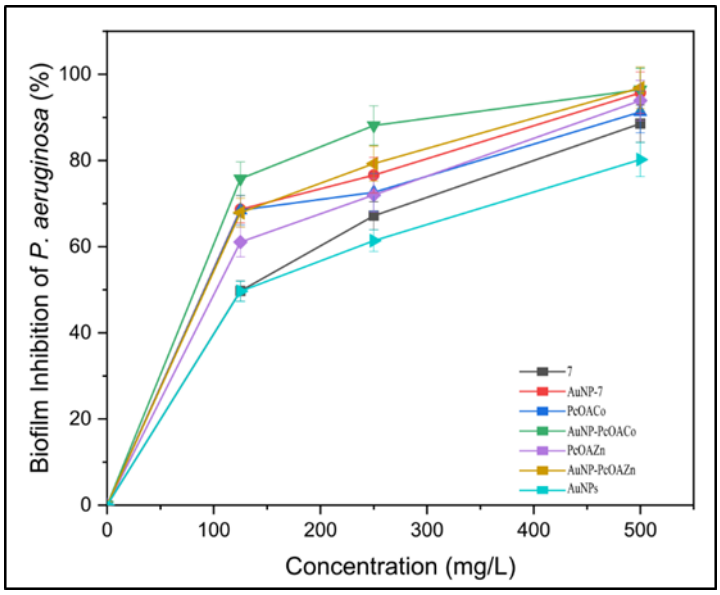

Figure 5.27 (b): Biofilm inhibition % of compounds **(7), AuNP-7, PcOACo&Zn, AuNP-PcOACo&Zn** and **AuNPs** by using *P. Aeruginosa*.

Table 5.16: Biofilm inhibition % of compounds **(7), AuNP-7, PcOACo&Zn, AuNP-PcOACo&Zn** and **AuNPs** by using *P. Aeruginosa*.

Compounds	125mg/L	250 mg/L	500 mg/L
(7)	49.7%	64.89%	81.84%
AuNP-7	68.67%	74.36%	92.87%
PcOACo	68.47%	70.03%	88.76%
AuNP-PcOACo	75.75%	86.74%	93.38%
PcOAZn	61.08%	70.15%	92.14%
AuNP-PcOAZn	67.89%	77.31%	96.68%
AuNPs	49.64%	59.75%	75.67%

5.4.4 UV-vis spectra of AuNPs-MPc conjugates of symmetrical octa-substituted metal-phthalocyanines of phthalonitrile derivative (7)

UV–vis spectra of AuNPs-MPc conjugates of phthalonitrile **(7)** and its phthalocyanine derivatives were conducted in DMSO at room temperature (Figure 5.28). The respective B, vibronic and Q-band values are illustrated in Table 5.17. As anticipated, the Q-bands of phthalocyanines conjugated to the gold nanoparticles' surface in nanoparticle hybrids **AuNP-PcOACo&Zn** exhibited shifts to the shorter wavelengths (hypsochromic shift) compared to those of **PcOACo&Zn** (Calladine et al., 2004).

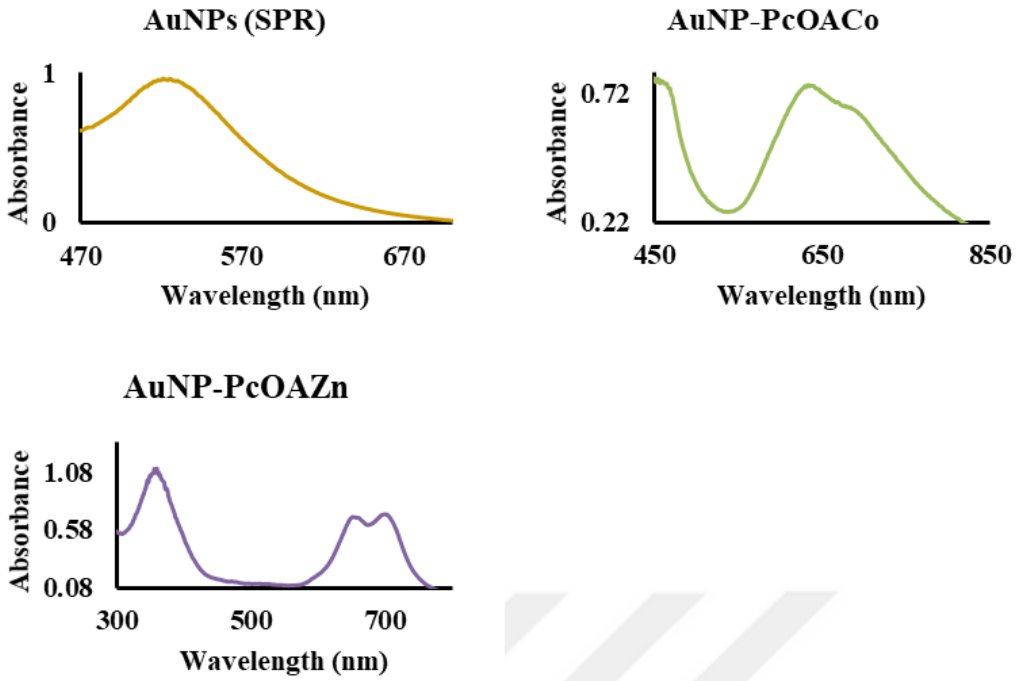

Figure 5.28: UV-vis spectra of AuNPs conjugates of symmetrical octa-substituted metal-phthalocyanines of phthalonitrile derivative **(7)**.

Table 5.17: UV-vis spectral values of AuNPs-MPc conjugates of symmetrical octa-substituted metal-phthalocyanines of phthalonitrile derivative **(7).**

Name of the Compound	B-Band λ_{max}(log Ɛ)	Vibronic Band λ_{max} (log Ɛ)	Q-Band λ_{max} (log Ɛ)
AuNPs	517nm (SPR)		
AuNP-PcOACo	453 (5.11)	-	631 (4.55)
AuNP- PcOAZn	356 (5.26)	649 (3.33)	694 (2.99)

5.4.5 TEM analysis of AuNPs-MPc conjugates of symmetrical octa-substituted metal-phthalocyanines of phthalonitrile derivative (7)

The conjugation of **AuNPs** to Metal Pcs (**PcOACo** and **Zn**) resulted in enlargement of the AuNPs (Ashjari et al. 2015; Moon, Tanaka, and Sekino 2010). TEM images of **AuNPs** and **AuNP-PcOAZn** are shown in TEM images of Figure 5.29 (a-e).

Figure 5.29 (a) confirmed the synthesized gold nanoparticles diameters in the range of 15nm that increased 5 nm after the conjugation with compound **PcOAZn** (Figure 5.29 b-e).

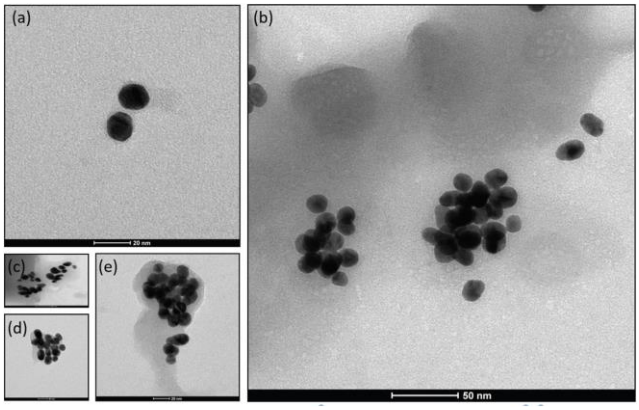

Figure 5.29: TEM images of **AuNPs** (a) **AuNP-PcOAZn** (b-e).

6. CONCLUSION

Within the span of this thesis, 5 phthalonitrile derivatives have been prepared. 4-[(4-pentylphenyl) ethynyl] **(2)**, 4-(thiophen-3-ylethynyl) **(3)** bearing phthalonitriles were employed to synthesize A_3B asymmetric Co and Zn phthalocyanines. 4-{[4-(dimethylamino)phenyl]ethynyl **(5)** entity containing phthalonitriles helped synthesizing tetra-substituted symmetrical MPcs of Co, Zn, Mn, Fe and Lu metals. Furthermore, symmetrical peripherally octa-substituted MPcs were synthesized utilizing phthalonitriles 4,5-bis{[3,5-bis(trifluoromethyl)phenyl]ethynyl} **(6)** (Co, Zn, Lu) and 4,5-bis[(4-(dimethylamino)phenyl)ethynyl] **(7)** (M=Co, Zn, Lu).

The structures of all synthesized phthalonitriles within the scope of the thesis were elucidated using spectral techniques such as FT-IR, ^{1}H-NMR and ^{13}C-NMR, whereas, all the 15 prepared MPcs structures were analyzed via UV-vis, FT-IR, MALDI-TOF and ^{1}H-NMR (excluding paramagnetic phthalocyanines).

Furthermore, the effect of concentration of phthalocyanine and solvent (THF) on the UV-vis spectra, solubility and aggregation properties of the newly synthesized Lu Pcs of phthalonitrile **(6)** were also examined.

Photoconductive properties inspection conducted through photovoltaic cells as ITO/PEDOT:PSS/Pc/Ag layers designed from synthesized Co and Zn asymmetric phthalocyanines of phthalonitrile **(2)** and **(3)** are also a part of this thesis.

Finally, in this thesis work gold nanoparticles **(AuNPs)** were synthesized using modified Turkevich method. Then, phthalonitriles **(5)** and **(7)** and their respective Co and Zn MPcs were conjugated with gold nano particles (AuNPs) through self-assembly process. Conjugational MPc-AuNP hybrids and synthesized AuNPs were assessed through TEM analysis revealing their size and shape.

Herein, the synthesized phthalonitrile **(5)** & **(7)** and all their MPc-AuNP hybrids together with their related Co and Zn MPcs and AuNPs were analyzed for several biological analyses namely anti-oxidant activity, DPPH activity, biofilm inhibition, anti- microbial and PDT activity, microbial cell viability inhibition and DNA clevage

ability. All these results deduced that using the MPc/AuNP hybrids gave higher efficiency for the examined biological properties as compared to when AuNPs were employed separately.

REFERENCES

Abbasi, E., Milani, M., Fekri Aval, S., Kouhi, M., Akbarzadeh, A., Tayefi Nasrabadi, H., ... Samiei, M. (2014). Silver nanoparticles: Synthesis methods, bio-applications and properties. *Critical Reviews in Microbiology*, 1–8. https://doi.org/10.3109/1040841X.2014.912200

Ağırtaş, M., Cabir, B., Yıldıko, Ü., Özdemir, S., & Gonca, S. (2021). Synthesis, antioxidant, DNA cleavage and antimicrobial properties of phthalocyanine complexes bearing the poly-hydroxyl groups. *Chemical Papers*, *75*(4), 1749–1760. https://doi.org/10.1007/s11696-020-01432-7

Ağırtaş, M. S., Güven, M. E., Gümüş, S., Özdemir, S., & Dündar, A. (2014). Metallo and metal free phthalocyanines bearing (4-(1(4-phenoxyphenyl)-1-phenylethyl)phenol substituents: Synthesis, characterization, aggregation behavior, electronic, antioxidant and antibacterial properties. *Synthetic Metals*, *195*(1), 177–184. https://doi.org/10.1016/j.synthmet.2014.06.004

Ali, F., Khan, S. B., Kamal, T., Anwar, Y., Alamry, K. A., & Asiri, A. M. (2017). Anti-bacterial chitosan/zinc phthalocyanine fibers supported metallic and bimetallic nanoparticles for the removal of organic pollutants. *Carbohydrate Polymers*, *173*, 676–689. https://doi.org/10.1016/j.carbpol.2017.05.074

Alvarez, S. (2020). Coordinating Ability of Anions, Solvents, Amino Acids, and Gases towards Alkaline and Alkaline-Earth Elements, Transition Metals, and Lanthanides. *Chemistry – A European Journal*, *26*(19), 4350–4377. https://doi.org/10.1002/chem.201905453

Amendola, V., & Meneghetti, M. (2009). Laser ablation synthesis in solution and size manipulation of noble metal nanoparticles. *Physical Chemistry Chemical Physics*, *11*(20), 3805. https://doi.org/10.1039/b900654k

Amitha, G. S., & Vasudevan, S. (2020). DNA binding and cleavage studies of novel Betti base substituted quaternary Cu(II) and Zn(II) phthalocyanines. *Polyhedron*, *190*, 114773. https://doi.org/10.1016/j.poly.2020.114773

Ashjari, M., Dehfuly, S., Fatehi, D., Shabani, R., & Koruji, M. (2015). Efficient functionalization of gold nanoparticles using cysteine conjugated protoporphyrin IX for singlet oxygen production in vitro. *RSC Advances*, *5*(127), 104621–104628. https://doi.org/10.1039/C5RA15862A

Ashokkumar, R., Kathiravan, A., & Ramamurthy, P. (2014). Zn-phthalocyanine-functionalized nanometal and nanometal–TiO2 hybrids: aggregation behavior and excited-state dynamics. *Physical Chemistry Chemical Physics*, *16*(27), 14139. https://doi.org/10.1039/c4cp00695j

Ayala, Y. M., Pantano, S., D'Ambrogio, A., Buratti, E., Brindisi, A., Marchetti, C., ... Baralle, F. E. (2005). Human, Drosophila, and C.elegans TDP43: Nucleic Acid Binding Properties and Splicing Regulatory Function. *Journal of Molecular Biology*, *348*(3), 575–588. https://doi.org/10.1016/j.jmb.2005.02.038

Aydın, M., Alıcı, E. H., Bilgiçli, A. T., Yarasir, M. N., & Arabaci, G. (2017). Synthesis, characterization, aggregation, fluorescence and antioxidant properties of bearing (4-(methylthio)phenylthio) tetra substituted phthalocyanines. *Inorganica Chimica Acta*, *464*, 1–10. https://doi.org/10.1016/j.ica.2017.04.038

Baigorria, E., Reynoso, E., Alvarez, M. G., Milanesio, M. E., & Durantini, E. N. (2018). Silica nanoparticles embedded with water insoluble phthalocyanines for the photoinactivation of microorganisms. *Photodiagnosis and Photodynamic Therapy*, *23*, 261–269. https://doi.org/10.1016/j.pdpdt.2018.06.020

Bala, M., Verma, P. K., Sharma, U., Kumar, N., & Singh, B. (2013). Iron phthalocyanine as an efficient and versatile catalyst for N-alkylation of heterocyclic amines with alcohols: one-pot synthesis of 2-substituted benzimidazoles, benzothiazoles and benzoxazoles. *Green Chemistry*, *15*(6), 1687. https://doi.org/10.1039/c3gc40137e

Bankole, O. M., & Nyokong, T. (2016). Comparative studies on photophysical and optical limiting characterizations of low symmetry phthalocyanine linked to Fe 3 O 4 –Ag core–shell or hybrid nanoparticles. *New Journal of Chemistry*, *40*(12), 10016–10027. https://doi.org/10.1039/C6NJ01511E

Bankole, O. M., & Nyokong, T. (2017). Azide-derivatized gold nanosphere "clicked" to indium and zinc phthalocyanines for improved nonlinear optical limiting. *Journal of Molecular Structure*, *1136*, 309–320. https://doi.org/10.1016/j.molstruc.2017.01.088

Bankole, O. M., Osifeko, O., & Nyokong, T. (2016). Enhanced nonlinear optical responses of zinc diaminopyrimidin-2-ylthio phthalocyanine conjugated to AgxAuy alloy nanoparticles. *Journal of Photochemistry and Photobiology A: Chemistry*, *329*, 155–166. https://doi.org/10.1016/j.jphotochem.2016.06.025

Barmin, R., Rudakovskaya, P., Gusliakova, O., Sindeeva, O., Prikhozhdenko, E., Maksimova, E., ... Gorin, D. (2021). Air-Filled Bubbles Stabilized by Gold Nanoparticle/Photodynamic Dye Hybrid Structures for Theranostics. *Nanomaterials*, *11*(2), 415. https://doi.org/10.3390/nano11020415

Barut, B., & Demirbaş, Ü. (2020). Synthesis, anti-cholinesterease, α-glucosidase inhibitory, antioxidant and DNA nuclease properties of non-peripheral triclosan substituted metal-free, copper(II), and nickel(II) phthalocyanines. *Journal of Organometallic Chemistry*, *923*, 121423. https://doi.org/10.1016/j.jorganchem.2020.121423

Baş, H., Barut, B., Biyiklioglu, Z., & Özel, A. (2019). Synthesis, DNA interaction, topoisomerase I, II inhibitory and cytotoxic effects of water soluble silicon (IV) phthalocyanine and napthalocyanines bearing 1-acetylpiperazine units. *Dyes and Pigments*, *160*, 136–144. https://doi.org/10.1016/j.dyepig.2018.08.005

Basova, T., Parkhomenko, R. G., Igumenov, I. K., Hassan, A., Durmuş, M., Gürek, A. G., & Ahsen, V. (2014). Composites of liquid crystalline nickel phthalocyanine with gold nanoparticles: Liquid crystalline behaviour and optical properties. *Dyes and Pigments*, *111*, 58–63. https://doi.org/10.1016/j.dyepig.2014.05.033

Basova, T. V., Hassan, A., & Morozova, N. B. (2019). Chemistry of gold(I, III) complexes with organic ligands as potential MOCVD precursors for fabrication of thin metallic films and nanoparticles. *Coordination Chemistry Reviews*, *380*, 58–82. https://doi.org/10.1016/j.ccr.2018.09.005

Bayır, Z. A. (2005). Synthesis and characterization of novel soluble octa-cationic phthalocyanines. *Dyes and Pigments*, *65*(3), 235–242. https://doi.org/10.1016/j.dyepig.2004.08.003

Beck, A., Mangold, K., & Hanack, M. (1991). Lösliche (Tetraethylphthalocyaninato)eisen(II)- und -cobalt(II)-Verbindungen. *Chemische Berichte*, *124*(10), 2315–2321. https://doi.org/10.1002/cber.19911241026

Bekaroğlu, Ö. (2001). Suprasüper Moleküller ve Bir Bilim Adamı. *Bilim ve Teknik Dergisi, Mayıs*.

Bhatia, S. (2016). Nanoparticles Types, Classification, Characterization, Fabrication Methods and Drug Delivery Applications. In *Natural Polymer Drug Delivery Systems* (pp. 33–93). Springer International Publishing. https://doi.org/10.1007/978-3-319-41129-3_2

Birsöz, B. (2013). *Tibbi uygulamalar için bor içeren ftalosiyaninler*. (Doktora Tezi), Istanbul Teknik Üniversitesi, Istanbul.

Boisselier, E., & Astruc, D. (2009). Gold nanoparticles in nanomedicine: preparations, imaging, diagnostics, therapies and toxicity. *Chemical Society Reviews*, *38*(6), 1759. https://doi.org/10.1039/b806051g

Braun, A., & Tcherniac, J. (1907). Über die Produkte der Einwirkung von Acetanhydrid auf Phthalamid. *Berichte Der Deutschen Chemischen Gesellschaft*, *40*(2), 2709–2714. https://doi.org/10.1002/cber.190704002202

Brechignac, C., Houdy, P., & Lahmani, M. (2007). *Nanomaterials and Nanochemistry* (C. Bréchignac, P. Houdy, & M. Lahmani (eds.)). Springer Berlin Heidelberg. https://doi.org/10.1007/978-3-540-72993-8

Broggi, A., Tomasi, I., Bianchi, L., Marrocchi, A., & Vaccaro, L. (2014). Small Molecular Aryl Acetylenes: Chemically Tailoring High-Efficiency Organic Semiconductors for Solar Cells and Field-Effect Transistors. *ChemPlusChem*, *79*(4), 486–507. https://doi.org/10.1002/cplu.201400001

Brust, M., Fink, J., Bethell, D., Schiffrin, D. J., & Kiely, C. (1995). Synthesis and reactions of functionalised gold nanoparticles. *Journal of the Chemical Society, Chemical Communications*, *16*, 1655. https://doi.org/10.1039/c39950001655

Calladine, C. R., Drew, H. R., Luisi, B. F., & Travers, A. A. (2004). *Understanding DNA The Molecule and How it Works* (3rd ed.). Elsevier. https://doi.org/10.1016/B978-012155089-9/50006-5

Camerin, M., Magaraggia, M., Soncin, M., Jori, G., Moreno, M., Chambrier, I., ... Russell, D. A. (2010). The in vivo efficacy of phthalocyanine–nanoparticle conjugates for the photodynamic therapy of amelanotic melanoma. *European Journal of Cancer*, *46*(10), 1910–1918. https://doi.org/10.1016/j.ejca.2010.02.037

Castro-Latorre, P., Miranda-Rojas, S., & Mendizabal, F. (2020). Theoretical exploration of the forces governing the interaction between gold–phthalocyanine and gold surface clusters. *RSC Advances*, *10*(7), 3895–3901. https://doi.org/10.1039/C9RA07959A

Cavalcante, L. L. R., Tedesco, A. C., Takahashi, L. A. U., Curylofo-Zotti, F. A., Souza-Gabriel, A. E., & Corona, S. A. M. (2020). Conjugate of chitosan nanoparticles with chloroaluminium phthalocyanine: Synthesis, characterization and photoinactivation of Streptococcus mutans biofilm. *Photodiagnosis and Photodynamic Therapy*, *30*, 101709. https://doi.org/10.1016/j.pdpdt.2020.101709

Chanteau, S. H., & Tour, J. M. (2001). Synthesis of potential molecular electronic devices containing pyridine units. *Tetrahedron Letters*, *42*(17), 3057–3060. https://doi.org/10.1016/S0040-4039(01)00394-X

Chauke, V., Durmuş, M., & Nyokong, T. (2007). Photochemistry, photophysics and nonlinear optical parameters of phenoxy and tert-butylphenoxy substituted indium(III) phthalocyanines. *Journal of Photochemistry and Photobiology A: Chemistry*, *192*(2–3), 179–187. https://doi.org/10.1016/j.jphotochem.2007.05.022

Cheng, H.-B., Li, X., Kwon, N., Fang, Y., Baek, G., & Yoon, J. (2019). Photoswitchable phthalocyanine-assembled nanoparticles for controlled "double-lock" photodynamic therapy. *Chemical Communications*, *55*(82), 12316–12319. https://doi.org/10.1039/C9CC03960K

Choi, C.-F., Tsang, P.-T., Huang, J.-D., Chan, E. Y. M., Ko, W.-H., Fong, W.-P., & Ng, D. K. P. (2004). Synthesis and in vitro photodynamic activity of new hexadeca-carboxy phthalocyanines. *Chemical Communications*, *19*, 2236. https://doi.org/10.1039/b405868b

Cong, F., Wei, Z., Huang, Z., Yu, F., Liu, H., Cui, J., ... Lai, J. (2015). Characteristic absorption band split of symmetrically tetra-octyloxy metal phthalocyanines. *Dyes and Pigments*, *120*, 1–7. https://doi.org/10.1016/j.dyepig.2015.03.034

Connor, E. E., Mwamuka, J., Gole, A., Murphy, C. J., & Wyatt, M. D. (2005). Gold Nanoparticles Are Taken Up by Human Cells but Do Not Cause Acute Cytotoxicity. *Small*, *1*(3), 325–327. https://doi.org/10.1002/smll.200400093

Costerton, J. W., Stewart, P. S., & Greenberg, E. P. (1999). Bacterial Biofilms: A Common Cause of Persistent Infections. *Science*, *284*(5418), 1318–1322. https://doi.org/10.1126/science.284.5418.1318

Culhane, P. J., & Woodward, G. E. (1927). 3-NITROPHTHALIC ACID. *Organic Syntheses*, *7*, 70. https://doi.org/10.15227/orgsyn.007.0070

D'Souza, S., Mashazi, P., Britton, J., & Nyokong, T. (2015). Effects of differently shaped silver nanoparticles on the photophysics of pyridylsulfanyl-substituted phthalocyanines. *Polyhedron*, *99*, 112–121. https://doi.org/10.1016/j.poly.2015.06.038

Daniel, M. C., & Astruc, D. (2004). Gold Nanoparticles: Assembly, Supramolecular Chemistry, Quantum-Size-Related Properties, and Applications toward Biology, Catalysis, and Nanotechnology. *Chemical Reviews*, *104*(1), 293–346. https://doi.org/DOI: 10.1021/cr030698+

Day, V. W., Marks, T. J., & Wachter, W. A. (1975). Large metal ion-centered template reactions. Uranyl complex of cyclopentakis(2-iminoisoindoline). *Journal of the American Chemical Society*, *97*(16), 4519–4527. https://doi.org/10.1021/ja00849a012

Díaz-Torres, R., & Alvarez, S. (2011). Coordinating ability of anions and solvents towards transition metals and lanthanides. *Dalton Transactions*, *40*(40), 10742. https://doi.org/10.1039/c1dt11000d

Diederich, F., Stang, P. J., & Tykwinski, R. R. (2005). *Acetylene Chemistry: Chemistry, biology and material science*. Weinheim: Wiley-VCH. http://public.eblib.com/choice/publicfullrecord.aspx?p=481516

Diesbach, H., & Von der Weid, E. (1927). Derivatives of cumidinic and pyromellitic acids. *Helvetica Chimica Acta*, *10*, 886.

Doron, S., & Gorbach, S. L. (2008). Bacterial Infections: Overview. In *International Encyclopedia of Public Health* (pp. 273–282). Elsevier. https://doi.org/10.1016/B978-012373960-5.00596-7

Doubrovsky, V. A., Yanina, I. Y., & Tuchin, V. V. (2010). *Inhomogeneity of photo-induced fat cell lipolysis* (V. V. Tuchin & E. A. Genina (eds.); p. 79990M). https://doi.org/10.1117/12.889326

Dube, E., Oluwole, D. O., Nwaji, N., & Nyokong, T. (2018). Glycosylated zinc phthalocyanine-gold nanoparticle conjugates for photodynamic therapy: Effect of nanoparticle shape. *Spectrochimica Acta Part A: Molecular and Biomolecular Spectroscopy*, *203*, 85–95. https://doi.org/10.1016/j.saa.2018.05.081

Dubinina, T. V., Tychinsky, P. I., Borisova, N. E., Krasovskii, V. I., Ivanov, A. S., Savilov, S. V., ... Tomilova, L. G. (2018). Lanthanide (III) complexes of 3-(ethylthio)phenyl-substituted phthalocyanines: Synthesis and physicochemical properties. *Dyes and Pigments*, *156*, 386–394. https://doi.org/10.1016/j.dyepig.2018.04.028

Durmuş, M., & Nyokong, T. (2007). Synthesis, photophysical and photochemical properties of tetra- and octa-substituted gallium and indium phthalocyanines. *Polyhedron*, *26*(13), 3323–3335. https://doi.org/10.1016/j.poly.2007.03.007

Durmuş, M., Yeşilot, S., & Ahsen, V. (2006). Separation and mesogenic properties of tetraalkoxy-substituted phthalocyanine isomers. *New J. Chem.*, *30*(5), 675–678. https://doi.org/10.1039/B600196C

Duruk, E. G., Yenilmez, H. Y., Koca, A., & Bayır, Z. A. (2015). Synthesis, electrochemical and spectroelectrochemical properties of thiazole-substituted phthalocyanines. *Synthetic Metals*, *209*, 361–368. https://doi.org/10.1016/j.synthmet.2015.08.013

Eberhardt, W., & Hanack, M. (1997). Synthesis of Hexadecaalkoxy-Substituted Nickel and Iron Phthalocyanines. *Synthesis*, *1997*(01), 95–100. https://doi.org/10.1055/s-1997-1495

Erdem, M., Korkmaz, E., Kösoğlu, G., Ahmetali, E., Farajzadeh, N., Eryürek, G., & Koçak, M. B. (2021). Nonlinear optical behavior and optical power limiting characteristics of peripheral symmetrical and non-symmetrical zinc phthalocyanines with nanosecond pulsed excitation. *Polyhedron*, *195*, 114975. https://doi.org/10.1016/j.poly.2020.114975

Erdoğmuş, A., & Nyokong, T. (2010). Novel, soluble, FluXoro functional substituted zinc phthalocyanines; synthesis, characterization and photophysicochemical properties. *Dyes and Pigments*, *86*(2), 174–181. https://doi.org/10.1016/j.dyepig.2010.01.001

Ertunç, B., Sevim, A. M., Durmuş, M., & Bayır, Z. A. (2015). Synthesis, photochemical and photophysical properties of zinc(II) and indium(III) phthalocyanines bearing fluoroalkynyl functionalized substituents. *Polyhedron*, *102*, 649–656. https://doi.org/10.1016/j.poly.2015.10.042

Fang, Y.-Z., Yang, S., & Wu, G. (2002). Free radicals, antioxidants, and nutrition. *Nutrition*, *18*(10), 872–879. https://doi.org/10.1016/S0899-9007(02)00916-4

Farajzadeh, N., Kösoğlu, G., Erdem, M., Eryürek, G., & Burkut Koçak, M. (2020). Nonlinear optical properties of peripheral symmetrically and non-symmetrically 4-(trifluoromethoxy)phenoxy substituted zinc phthalocyanines. *Synthetic Metals*, *266*, 116440. https://doi.org/10.1016/j.synthmet.2020.116440

Fashina, A., Antunes, E., & Nyokong, T. (2013). Characterization and photophysical behavior of phthalocyanines when grafted onto silica nanoparticles. *Polyhedron*, *53*, 278–285. https://doi.org/10.1016/j.poly.2013.01.037

Fleming, D., & Rumbaugh, K. (2017). Approaches to Dispersing Medical Biofilms. *Microorganisms*, *5*(2), 15. https://doi.org/10.3390/microorganisms5020015

Gao, Y., Ma, P., Chen, Y., Zhang, Y., Bian, Y., Li, X., ... Ma, C. (2009). Design, Synthesis, Characterization, and OFET Properties of Amphiphilic Heteroleptic Tris(phthalocyaninato) Europium(III) Complexes. The Effect of Crown Ether Hydrophilic Substituents. *Inorganic Chemistry*, *48*(1), 45–54. https://doi.org/10.1021/ic801040z

Gao, Y., Mai, B., Wang, A., Li, M., Wang, X., Zhang, K., ... Wang, P. (2018). Antimicrobial properties of a new type of photosensitizer derived from phthalocyanine against planktonic and biofilm forms of Staphylococcus aureus. *Photodiagnosis and Photodynamic Therapy*, *21*, 316–326. https://doi.org/10.1016/j.pdpdt.2018.01.003

George, R. D., & Snow, A. W. (1995). Synthesis of 3-nitrophthalonitrile and tetra-α-substituted phthalocyanines. *Journal of Heterocyclic Chemistry*, *32*(2), 495–498. https://doi.org/10.1002/jhet.5570320219

Geyer, M., Plenzig, F., Rauschnabel, J., Hanack, M., del Rey, B., Sastre, A., & Torres, T. (1996). Subphthalocyanines: Preparation, Reactivity and Physical Properties. *Synthesis*, *1996*(09), 1139–1151. https://doi.org/10.1055/s-1996-4349

Ghosh, C. K. (2017). Synthesis of Noble Metal Nanoparticles: Chemical and Physical Routes. In S. Roy, C. K. Ghosh, & C. K. Sarkar (Eds.), *Nanotechnology Synthesis to Applications* (pp. 106–108). CRC Press, Boca Raton. https://doi.org/10.1201/9781315116730

GHOSH, P., HAN, G., DE, M., KIM, C., & ROTELLO, V. (2008). Gold nanoparticles in delivery applications. *Advanced Drug Delivery Reviews*, *60*(11), 1307–1315. https://doi.org/10.1016/j.addr.2008.03.016

Giuliani, F., Martinelli, M., Cocchi, A., Arbia, D., Fantetti, L., & Roncucci, G. (2010). In Vitro Resistance Selection Studies of RLP068/Cl, a New Zn(II) Phthalocyanine Suitable for Antimicrobial Photodynamic Therapy. *Antimicrobial Agents and Chemotherapy*, *54*(2), 637–642. https://doi.org/10.1128/AAC.00603-09

Gouterman, M. (1978). Optical Spectra and Electronic Structure of Porphyrins and Related Rings. *The Porphyrins*, 1–165. https://doi.org/10.1016/B978-0-12-220103-5.50008-8

Gürek, A. G. (1996). *Tetratiya-makrohalkaları içeren yeni tip ftalosiyaninler*. Doctorate thesis, Istanbul Teknik Üniversitesi, Istanbul.

Güzel, E., Atsay, A., Nalbantoglu, S., Şaki, N., Dogan, A. L., Gül, A., & Koçak, M. B. (2013). Synthesis, characterization and photodynamic activity of a new amphiphilic zinc phthalocyanine. *Dyes and Pigments*, *97*(1), 238–243. https://doi.org/10.1016/j.dyepig.2012.12.027

Güzel, E., Günsel, A., Bilgiçli, A. T., Atmaca, G. Y., Erdoğmuş, A., & Yarasir, M. N. (2017). Synthesis and photophysicochemical properties of novel thiadiazole-substituted zinc (II), gallium (III) and silicon (IV) phthalocyanines for photodynamic therapy. *Inorganica Chimica Acta*, *467*, 169–176. https://doi.org/10.1016/j.ica.2017.07.058

Hanack, M., & Lang, M. (1994). Conducting Stacked Metallophthalocyanines and Related Compounds. *Advanced Materials*, *6*(11), 819–833. https://doi.org/10.1002/adma.19940061103

Hanack, M., Schmid, G., & Sommerauer, M. (1993). Chromatographic Separation of the Four Possible Structural Isomers of a Tetrasubstituted Phthalocyanine: Tetrakis(2-ethylhexyloxy)phthalocyaninatonickel(II). *Angewandte Chemie International Edition in English*, *32*(10), 1422–1424. https://doi.org/10.1002/anie.199314221

Hone, D. C., Walker, P. I., Evans-Gowing, R., FitzGerald, S., Beeby, A., Chambrier, I., ... Russell, D. A. (2002). Generation of Cytotoxic Singlet Oxygen via Phthalocyanine-Stabilized Gold Nanoparticles: A Potential Delivery Vehicle for Photodynamic Therapy. *Langmuir*, *18*(8), 2985–2987. https://doi.org/10.1021/la0256230

Hong, S.-M., Son, H., & Park, J. S. (2018). Preparation and electrochemical properties of cobalt-phthalocyanine-decorated Fe 3 O 4 nanoparticles. *Journal of Porphyrins and Phthalocyanines*, *22*(07), 611–618. https://doi.org/10.1142/S1088424618500827

Huang, L., Xuan, Y., Koide, Y., Zhiyentayev, T., Tanaka, M., & Hamblin, M. R. (2012). Type I and Type II mechanisms of antimicrobial photodynamic therapy: An in vitro study on gram-negative and gram-positive bacteria. *Lasers in Surgery and Medicine*, *44*(6), 490–499. https://doi.org/10.1002/lsm.22045

Inouye, M., Takahashi, K., & Nakazumi, H. (1999). Remarkably Strong, Uncharged Hydrogen-Bonding Interactions of Polypyridine-Macrocyclic Receptors for Deoxyribofuranosides. *Journal of the American Chemical Society*, *121*(2), 341–345. https://doi.org/10.1021/ja983539u

Jang, B., Park, J.-Y., Tung, C.-H., Kim, I.-H., & Choi, Y. (2011). Gold Nanorod−Photosensitizer Complex for Near-Infrared Fluorescence Imaging and Photodynamic/Photothermal Therapy In Vivo. *ACS Nano*, *5*(2), 1086–1094. https://doi.org/10.1021/nn102722z

Jia, X., & Jia, L. (2012). Nanoparticles Improve Biological Functions of Phthalocyanine Photosensitizers Used for Photodynamic Therapy. *Current Drug Metabolism*, *13*(8), 1119–1122. https://doi.org/10.2174/138920012802850074

Kadish, K., Guilard, R., & Smith, K. (2000). *The Porphyrin Handbook: Phthalocyanines: Properties and Materials*. Academic Press, San Diego.

Kadish, K. M., Smith, K. M., & Guilard, R. (2003). The Porphyrin Handbook. In *The Porphyrin Handbook* (Vol. 18). Elsevier. https://doi.org/10.1016/C2009-0-22714-0

Kalkan, A., Koca, A., & Bayır, Z. A. (2004). Unsymmetrical phthalocyanines with alkynyl substituents. *Polyhedron*, *23*(18), 3155–3162. https://doi.org/10.1016/j.poly.2004.09.021

Kalska-Szostko, B. (2012). Electrochemical Methods in Nanomaterials Preparation. In U. K. Su (Ed.), *Recent Trend in Electrochemical Science and Technology* (p. 261). InTech. https://doi.org/10.5772/33662

Karaoğlu, H. R. P., Koca, A., & Koçak, M. B. (2012). Synthesis, electrochemical and spectroelectrochemical characterization of novel soluble phthalocyanines bearing chloro and quaternizable bulky substituents on peripheral positions. *Dyes and Pigments*, *92*(3), 1005–1017. https://doi.org/10.1016/j.dyepig.2011.07.021

Karaoğlu, H. R. P., Yenilmez, H. Y., & Koçak, M. B. (2018). Phthalocyanines formed from several precursors: synthesis, characterization, and comparative fluorescence and quinone quenching. *Journal of Coordination Chemistry*, *71*(15), 2340–2357. https://doi.org/10.1080/00958972.2018.1471686

Kessel, D., & Lier, J. E. V. (1990). *Photodynamic Therapy of Neoplastic Disease, Volume I*. CRC Press, Boca Raton, FL.

Kharisov, B. I., Ortiz Méndez, U., Almaraz Garza, J. L., & Almaguer Rodríguez, J. R. (2005). Synthesis of non-substituted phthalocyanines by standard and non-standard techniques. Influence of solvent nature in phthalocyanine preparation at low temperature by UV-treatment of the reaction system. *New Journal of Chemistry*, *29*(5), 686. https://doi.org/10.1039/b415712p

Khlebtsov, N. G., & Dykman, L. A. (2010). Optical properties and biomedical applications of plasmonic nanoparticles. *Journal of Quantitative Spectroscopy and Radiative Transfer*, *111*(1), 1–35. https://doi.org/10.1016/j.jqsrt.2009.07.012

Khoza, P., & Nyokong, T. (2014). Photocatalytic behavior of phthalocyanine-silver nanoparticle conjugates supported on polystyrene fibers. *Journal of Molecular Catalysis A: Chemical*, *395*, 34–41. https://doi.org/10.1016/j.molcata.2014.07.031

Kim, C., Cho, E. C., Chen, J., Song, K. H., Au, L., Favazza, C., ... Wang, L. V. (2010). In Vivo Molecular Photoacoustic Tomography of Melanomas Targeted by Bioconjugated Gold Nanocages. *ACS Nano*, *4*(8), 4559–4564. https://doi.org/10.1021/nn100736c

Klyamer, D., Sukhikh, A., Nikolaeva, N., Morozova, N., & Basova, T. (2020). Vanadyl Phthalocyanine Films and Their Hybrid Structures with Pd Nanoparticles: Structure and Sensing Properties. *Sensors*, *20*(7), 1893. https://doi.org/10.3390/s20071893

Kobayashi, N., Kondo, R., Nakajima, S., & Osa, T. (1990). New route to unsymmetrical phthalocyanine analogs by the use of structurally distorted subphthalocyanines. *Journal of the American Chemical Society*, *112*(26), 9640–9641. https://doi.org/10.1021/ja00182a034

Koçak, D., & Gonca, E. (2010). Synthesis, structural and spectral properties of novel octakis(3,5-bis-trifluoromethyl-benzylthio) substituted porphyrazine derivatives. *Journal of Fluorine Chemistry*, *131*(12), 1322–1326. https://doi.org/10.1016/j.jfluchem.2010.09.002

Koçak, M. B., Cihan, A., Gürsoy, S., Okur, A. İ., Gül, A., & Bekaroğlu, Ö. (2003). A New Double-Decker Lu(III) Diphthalocyanine with Eight Peripheral Benzo(15-crown-5) Units. *Synthesis and Reactivity in Inorganic and Metal-Organic Chemistry*, *33*(9), 1527–1533. https://doi.org/10.1081/SIM-120025438

Korkut, S. E., Ahmetali, E., Bilgi, M., Karataş, Ö., Yerli, Y., Peksel, A., & Şener, M. K. (2021). Synthesis and antioxidant activity of zinc(II) phthalocyanine tetranitroxide. *Polyhedron*, *197*, 115045. https://doi.org/10.1016/j.poly.2021.115045

Kumari, Y., Kaur, G., Kumar, R., Singh, S. K., Gulati, M., Khursheed, R., ... Porwal, O. (2019). Gold nanoparticles: New routes across old boundaries. *Advances in Colloid and Interface Science*, *274*, 102037. https://doi.org/10.1016/j.cis.2019.102037

Kumral, E., Yenilmez, H. Y., Albayrak, S., Şahin, A. N., Altındal, A., & Bayır, Z. A. (2020). Investigation of the photoconductive properties of thiophene substituted metallo-phthalocyanines. *Dalton Transactions*, *49*(27), 9385–9392. https://doi.org/10.1039/D0DT01129K

Kurt, Ö., Koca, A., Gül, A., & Burkut Koçak, M. (2015). Synthesis, electrochemistry and in situ spectroelectrochemistry of novel hexadeca-substituted phthalocyanines with three different groups. *Synthetic Metals*, *206*, 72–83. https://doi.org/10.1016/j.synthmet.2015.05.012

Kurt, Ö., Özçeşmeci, İ., Şebnem Sesalan, B., & Burkut Koçak, M. (2015). The synthesis and investigation of binding properties of a new water soluble hexadeca zinc(II) phthalocyanine with bovine serum albumin and DNA. *New Journal of Chemistry*, *39*(7), 5767–5775. https://doi.org/10.1039/C5NJ00933B

Kwiatkowski, S., Knap, B., Przystupski, D., Saczko, J., Kędzierska, E., Knap-Czop, K., ... Kulbacka, J. (2018). Photodynamic therapy – mechanisms, photosensitizers and combinations. *Biomedicine & Pharmacotherapy*, *106*, 1098–1107. https://doi.org/10.1016/j.biopha.2018.07.049

Lee, J. E., Lee, N., Kim, T., Kim, J., & Hyeon, T. (2011). Multifunctional Mesoporous Silica Nanocomposite Nanoparticles for Theranostic Applications. *Accounts of Chemical Research*, *44*(10), 893–902. https://doi.org/10.1021/ar2000259

Lei, Y., Lu, J., Luo, X., Wu, T., Du, P., Zhang, X., ... Amine, K. (2013). Synthesis of Porous Carbon Supported Palladium Nanoparticle Catalysts by Atomic Layer Deposition: Application for Rechargeable Lithium–O 2 Battery. *Nano Letters*, *13*(9), 4182–4189. https://doi.org/10.1021/nl401833p

Leznoff, C. C., & Hall, T. W. (1982). The synthesis of a soluble, unsymmetrical phthalocyanine on a polymer support. *Tetrahedron Letters*, *23*(30), 3023–3026. https://doi.org/10.1016/S0040-4039(00)87523-1

Leznoff, C. C., & Lever, A. B. P. (1989). *Phthalocyanines: Properties and Applications*, (Vols. 1–4). VCH, New York.

Leznoff, C., & Lever, A. B. *Phthalocyanines: Properties and applications, volume 1-4, VCH Publishers Inc., New York (1989, 1992, 1993, 1996)*. https://doi.org/10.1002/adma.19930051218

Li, C., Shuford, K. L., Chen, M., Lee, E. J., & Cho, S. O. (2008). A Facile Polyol Route to Uniform Gold Octahedra with Tailorable Size and Their Optical Properties. *ACS Nano*, *2*(9), 1760–1769. https://doi.org/10.1021/nn800264q

Li, L., Chen, J.-Y., Wu, X., Wang, P.-N., & Peng, Q. (2010). Plasmonic Gold Nanorods Can Carry Sulfonated Aluminum Phthalocyanine To Improve Photodynamic Detection and Therapy of Cancers. *The Journal of Physical Chemistry B*, *114*(51), 17194–17200. https://doi.org/10.1021/jp109363n

Li, L., Zhang, N., He, H., Zhang, G., Song, L., & Qiu, W. (2019). Shape-controlled synthesis of Pd nanocrystals with exposed {110} facets and their catalytic applications. *Catalysis Today*, *327*, 28–36. https://doi.org/10.1016/j.cattod.2018.07.038

Linares-Flores, C., Mendizabal, F., Arratia-Pérez, R., Inostroza, N., & Orellana, C. (2015). Substituents role in zinc phthalocyanine derivatives used as dye-sensitized solar cells. A theoretical study using Density Functional Theory. *Chemical Physics Letters*, *639*, 172–177. https://doi.org/10.1016/j.cplett.2015.09.025

Liu, L., & Corma, A. (2018). Metal Catalysts for Heterogeneous Catalysis: From Single Atoms to Nanoclusters and Nanoparticles. *Chemical Reviews*, *118*(10), 4981–5079. https://doi.org/10.1021/acs.chemrev.7b00776

Liu, M., & Guyot-Sionnest, P. (2005). Mechanism of Silver(I)-Assisted Growth of Gold Nanorods and Bipyramids. *The Journal of Physical Chemistry B*, *109*(47), 22192–22200. https://doi.org/10.1021/jp054808n

Lokesh, K. S., Narayanan, V., & Sampath, S. (2009). Phthalocyanine macrocycle as stabilizer for gold and silver nanoparticles. *Microchimica Acta*, *167*(1–2), 97–102. https://doi.org/10.1007/s00604-009-0226-3

Loosli, C., Jia, C., Liu, S.-X., Haas, M., Dias, M., Levillain, E., ... Decurtins, S. (2005). Synthesis and Electrochemical and Photophysical Studies of Tetrathiafulvalene-Annulated Phthalocyanines. *The Journal of Organic Chemistry*, *70*(13), 4988–4992. https://doi.org/10.1021/jo0501801

Lourenço, L. M. O., Rocha, D. M. G. C., Ramos, C. I. V., Gomes, M. C., Almeida, A., Faustino, M. A. F., ... Tomé, J. P. C. (2019). Photoinactivation of Planktonic and Biofilm Forms of Escherichia coli through the Action of Cationic Zinc(II) Phthalocyanines. *ChemPhotoChem*, *3*(5), 251–260. https://doi.org/10.1002/cptc.201900020

Ma, C., Du, G., Cao, Y., Yu, S., Cheng, C., Jiang, W., ... Yu, H. (2007). Synthesis and electrochemistry of a substituted phthalocyaninatozinc. *Dyes and Pigments*, *72*(2), 267–270. https://doi.org/10.1016/j.dyepig.2005.08.024

Magro, N. A. A., Eastham, G. R., & Cole-Hamilton, D. J. (2007). The synthesis of amines by the homogeneous hydrogenation of secondary and primary amides. *Chemical Communications*, *30*, 3154. https://doi.org/10.1039/b706635j

Mah, T.-F. (2012). Biofilm-specific antibiotic resistance. *Future Microbiology*, *7*(9), 1061–1072. https://doi.org/10.2217/fmb.12.76

Majeed, S. A., Sekhosana, K. E., & Tuhl, A. (2020). Progress on phthalocyanine-conjugated Ag and Au nanoparticles: Synthesis, characterization, and photo-physicochemical properties. *Arabian Journal of Chemistry*, *13*(12), 8848–8887. https://doi.org/10.1016/j.arabjc.2020.10.014

Malekzad, H., Sahandi Zangabad, P., Mirshekari, H., Karimi, M., & Hamblin, M. R. (2017). Noble metal nanoparticles in biosensors: recent studies and applications. *Nanotechnology Reviews*, *6*(3), 301–329. https://doi.org/10.1515/ntrev-2016-0014

Maliszewska, I., Wanarska, E., & Tylus, W. (2020). Sulfonated hydroxyaluminum phthalocyanine-biogenic Au/Ag alloy nanoparticles mixtures for effective photo-eradication of Candida albicans. *Photodiagnosis and Photodynamic Therapy*, *32*, 102016. https://doi.org/10.1016/j.pdpdt.2020.102016

Manthe, R. L., Foy, S. P., Krishnamurthy, N., Sharma, B., & Labhasetwar, V. (2010). Tumor Ablation and Nanotechnology. *Molecular Pharmaceutics*, *7*(6), 1880–1898. https://doi.org/10.1021/mp1001944

Mapukata, S., Britton, J., Osifeko, O. L., & Nyokong, T. (2021). The improved antibacterial efficiency of a zinc phthalocyanine when embedded on silver nanoparticle modified silica nanofibers. *Photodiagnosis and Photodynamic Therapy*, *33*, 102100. https://doi.org/10.1016/j.pdpdt.2020.102100

Mapukata, S., Nwahara, N., & Nyokong, T. (2020). The photodynamic antimicrobial chemotherapy of Stapphylococcus aureus using an asymmetrical zinc phthalocyanine conjugated to silver and iron oxide based nanoparticles. *Journal of Photochemistry and Photobiology A: Chemistry*, *402*, 112813. https://doi.org/10.1016/j.jphotochem.2020.112813

Marcinkiewicz, J., Strus, M., & Pasich, E. (2013). Antibiotic resistance: a "dark side" of biofilm-associated chronic infections. *Polish Archives of Internal Medicine*, *123*(6), 309–313. https://doi.org/10.20452/pamw.1780

Marks, T. J., & Stojakovic, D. R. (1978). Large metal ion-centered template reactions. Chemical and spectral studies of the "superphthalocyanine" dioxocyclopentakis(1-iminoisoindolinato)uranium(VI) and its derivatives. *Journal of the American Chemical Society*, *100*(6), 1695–1705. https://doi.org/10.1021/ja00474a009

Matlou, G. G., Managa, M., & Nyokong, T. (2019). Effect of symmetry and metal nanoparticles on the photophysicochemical and photodynamic therapy properties of cinnamic acid zinc phthalocyanine. *Spectrochimica Acta Part A: Molecular and Biomolecular Spectroscopy*, *214*, 49–57. https://doi.org/10.1016/j.saa.2019.02.005

Maya, E. M., García, C., García-Frutos, E. M., Vázquez, P., & Torres, T. (2000). Synthesis of Novel Push−Pull Unsymmetrically Substituted Alkynyl Phthalocyanines. *The Journal of Organic Chemistry*, *65*(9), 2733–2739. https://doi.org/10.1021/jo991843f

Mckeown, N. (1998). *Phthalocyanine materials: synthesis, structure, and function,*. U.K.: Cambridge University Press, Cambridge.

McKeown, N. B. (1983). *Phthalocyanine vol 1-2*. CRC, Boca Raton, Florida.

McKeown, N. B., Chambrier, I., & Cook, M. J. (1990). Synthesis and characterisation of some 1,4,8,11,15,18,22,25-octa-alkyl- and 1,4,8,11,15,18-hexa-alkyl-22,25-bis(carboxypropyl)phthalocyanines. *Journal of the Chemical Society, Perkin Transactions 1*, *4*, 1169. https://doi.org/10.1039/p19900001169

Mohajer, F., Heravi, M. M., Zadsirjan, V., & Poormohammad, N. (2021). Copper-free Sonogashira cross-coupling reactions: an overview. *RSC Advances*, *11*(12), 6885–6925. https://doi.org/10.1039/D0RA10575A

Mondal, D., & Bera, S. (2014). Porphyrins and phthalocyanines: promising molecules for light-triggered antibacterial nanoparticles. *Advances in Natural Sciences: Nanoscience and Nanotechnology*, *5*(3), 033002. https://doi.org/10.1088/2043-6262/5/3/033002

Moon, S. Y., Tanaka, S., & Sekino, T. (2010). Crystal Growth of Thiol-Stabilized Gold Nanoparticles by Heat-Induced Coalescence. *Nanoscale Research Letters*, *5*(5), 813–817. https://doi.org/10.1007/s11671-010-9565-6

Morachevskii, A. G., & Beloglazov, I. N. (2006). Poole, C.P., Jr. and Owens, F.J., Introduction to Nanotechnology. *Russian Journal of Applied Chemistry*, *79*(7), 1213–1214. https://doi.org/10.1134/S1070427206070366

Moser, F. . H., & Thomas, A. L. (1983). *The Phthalocyanines: Manufacture and applications* (Volume II). CRC Press.

Mpeta, L. S., Sekhosana, K. E., & Nyokong, T. (2020). Nonlinear optical response and electrocatalytic activity of cobalt phthalocyanine clicked zinc oxide nanoparticles. *Inorganica Chimica Acta*, *509*, 119661. https://doi.org/10.1016/j.ica.2020.119661

Mphuthi, N. G., Adekunle, A. S., Fayemi, O. E., Olasunkanmi, L. O., & Ebenso, E. E. (2017). Phthalocyanine Doped Metal Oxide Nanoparticles on Multiwalled Carbon Nanotubes Platform for the detection of Dopamine. *Scientific Reports*, *7*(1), 43181. https://doi.org/10.1038/srep43181

Mthethwa, T., & Nyokong, T. (2015). Fluorescence behavior and singlet oxygen generating abilities of aluminum phthalocyanine in the presence of anisotropic gold nanoparticles. *Journal of Luminescence*, *157*, 207–214. https://doi.org/10.1016/j.jlumin.2014.09.005

Mukherjee, P., Ahmad, A., Mandal, D., Senapati, S., Sainkar, S. R., Khan, M. I., ... Kumar, R. (2001). Bioreduction of AuCl4− Ions by the Fungus, Verticillium sp. and Surface Trapping of the Gold Nanoparticles Formed D.M. and S.S. thank the Council of Scientific and Industrial Research (CSIR), Government of India, for financial assistance. *Angewandte Chemie International Edition*, *40*(19), 3585. https://doi.org/10.1002/1521-3773(20011001)40:19<3585::AID-ANIE3585>3.0.CO;2-K

Murphy, C. J., Thompson, L. B., Chernak, D. J., Yang, J. A., Sivapalan, S. T., Boulos, S. P., ... Sisco, P. N. (2011). Gold nanorod crystal growth: From seed-mediated synthesis to nanoscale sculpting. *Current Opinion in Colloid & Interface Science*, *16*(2), 128–134. https://doi.org/10.1016/j.cocis.2011.01.001

Nalwa, H. (2001). Handbook of Surfaces and Interfaces of Materials: zeolites. *Handbook of Surfaces and Interfaces of Materials*, *2*, 495–522. http://www.sciencedirect.com/science/article/pii/B9780125139106500694

Nar, I., Atsay, A., Altındal, A., Hamuryudan, E., Koçak, M. B., & Gül, A. (2018). Ferrocenyl Phthalocyanine as Donor in Non-Poly(3-hexylthiophen-2,5-diyl) Bulk Heterojunction Solar Cell. *Chemistry - A European Journal*, *24*(27), 6946–6949. https://doi.org/10.1002/chem.201801340

Nehl, C. L., Liao, H., & Hafner, J. H. (2006). Optical Properties of Star-Shaped Gold Nanoparticles. *Nano Letters*, *6*(4), 683–688. https://doi.org/10.1021/nl052409y

Nemykin, V. N., Dudkin, S. V., Dumoulin, F., Hirel, C., Gürek, A. G., & Ahsen, V. (2014). Synthetic approaches to asymmetric phthalocyanines and their analogues. *Arkivoc*, *2014*(1), 142–204. https://doi.org/10.3998/ark.5550190.p008.412

Nguyen, D. T., Kim, D.-J., & Kim, K.-S. (2011). Controlled synthesis and biomolecular probe application of gold nanoparticles. *Micron*, *42*(3), 207–227. https://doi.org/https://doi.org/10.1016/j.micron.2010.09.008.

Nicolet, B. H., & Bender, J. A. (1927). 3-NITROPHTHALIC ANHYDRIDE. *Organic Syntheses*, *7*, 74. https://doi.org/10.15227/orgsyn.007.0074

Nombona, N., Antunes, E., Chidawanyika, W., Kleyi, P., Tshentu, Z., & Nyokong, T. (2012). Synthesis, photophysics and photochemistry of phthalocyanine-ε-polylysine conjugates in the presence of metal nanoparticles against Staphylococcus aureus. *Journal of Photochemistry and Photobiology A: Chemistry*, *233*, 24–33. https://doi.org/10.1016/j.jphotochem.2012.02.012

Nwaji, N., Mack, J., & Nyokong, T. (2017). 4-Bis(4-aminophenoxy)phenoxy derivitized phthalocyanine conjugated to metallic nanoparticles: searching for enhanced optical limiting materials. *New Journal of Chemistry*, *41*(23), 14351–14363. https://doi.org/10.1039/C7NJ02718D

Nwaji, N., Mack, J., & Nyokong, T. (2018). Photophysical and strong optical limiting properties of ball-type phthalocyanines dimers and their monomeric analogues. *Journal of Photochemistry and Photobiology A: Chemistry*, *352*, 73–85. https://doi.org/10.1016/j.jphotochem.2017.10.045

Nwaji, N., & Nyokong, T. (2017). Nanosecond optical nonlinearities in low symmetry phthalocyanine nanoconjugates studied using the Z-scan technique. *Journal of Luminescence*, *192*, 1167–1179. https://doi.org/10.1016/j.jlumin.2017.08.053

Nyokong, T., & Antunes, E. (2013). Influence of nanoparticle materials on the photophysical behavior of phthalocyanines. *Coordination Chemistry Reviews*, *257*(15–16), 2401–2418. https://doi.org/10.1016/j.ccr.2013.03.016

Ogunsipe, A., Durmuş, M., Atilla, D., Gürek, A. G., Ahsen, V., & Nyokong, T. (2008). Synthesis, photophysical and photochemical studies on long chain zinc phthalocyanine derivatives. *Synthetic Metals*, *158*(21–24), 839–847. https://doi.org/10.1016/j.synthmet.2008.06.007

Ogunsipe, A., Nyokong, T., & Durmuş, M. (2007). Photophysical, photochemical and bovine serum albumin binding studies on water-soluble gallium(III) phthalocyanine derivatives. *Journal of Porphyrins and Phthalocyanines*, *11*(09), 635–644. https://doi.org/10.1142/S1088424607000746

Oluwole, D. O., Ngxeke, S. M., Britton, J., & Nyokong, T. (2017). The effect of point of substitution and silver based nanoparticles on the photophysical and optical nonlinearity of indium carboxyphenoxy phthalocyanine. *Journal of Photochemistry and Photobiology A: Chemistry*, *347*, 146–159. https://doi.org/10.1016/j.jphotochem.2017.07.032

Oluwole, D. O., Prinsloo, E., & Nyokong, T. (2016). Photophysicochemical properties of nanoconjugates of zinc(II) 2(3)-mono-2-(4-oxy)phenoxy)acetic acid phthalocyanine with cysteamine capped silver and silver–gold nanoparticles. *Polyhedron*, *119*, 434–444. https://doi.org/10.1016/j.poly.2016.09.034

Openda, Y. I., & Nyokong, T. (2021). Enhanced photo-ablation effect of positively charged phthalocyanines-detonation nanodiamonds nanoplatforms for the suppression of Staphylococcus aureus and Escherichia coli planktonic cells and biofilms. *Journal of Photochemistry and Photobiology A: Chemistry*, *411*, 113200. https://doi.org/10.1016/j.jphotochem.2021.113200

Özçeşmeci, İ., Burat, A. K., İpek, Y., Koca, A., & Bayır, Z. A. (2013). Synthesis, electrochemical and spectroelectrochemical properties of phthalocyanines having extended π-electrons conjugation. *Electrochimica Acta*, *89*, 270–277. https://doi.org/10.1016/j.electacta.2012.11.015

Ozturk, F., AÇIK, L., ŞENER, İ., KARCI, F., & KILIÇ, E. (2012). Antimicrobial properties and DNA interactions studies of 3-hetarylazoquinoline-2,4-diol compounds. *TURKISH JOURNAL OF CHEMISTRY*, *36*(2), 293–302. https://doi.org/10.3906/kim-1107-14

Packiavathy, I. A. S. V., Priya, S., Pandian, S. K., & Ravi, A. V. (2014). Inhibition of biofilm development of uropathogens by curcumin – An anti-quorum sensing agent from Curcuma longa. *Food Chemistry*, *148*, 453–460. https://doi.org/10.1016/j.foodchem.2012.08.002

Park, J.-W., & Shumaker-Parry, J. S. (2014). Structural Study of Citrate Layers on Gold Nanoparticles: Role of Intermolecular Interactions in Stabilizing Nanoparticles. *Journal of the American Chemical Society*, *136*(5), 1907–1921. https://doi.org/10.1021/ja4097384

Patra, J. K., Kim, S. H., & Baek, K.-H. (2015). Antioxidant and Free Radical-Scavenging Potential of Essential Oil from E nteromorpha linza L. Prepared by Microwave-Assisted Hydrodistillation. *Journal of Food Biochemistry*, *39*(1), 80–90. https://doi.org/10.1111/jfbc.12110

Pekbelgin Karaoğlu, H. R., Gül, A., & Koçak, M. B. (2008). Synthesis and characterization of a new tetracationic phthalocyanine. *Dyes and Pigments*, *76*(1), 231–235. https://doi.org/10.1016/j.dyepig.2006.08.032

Pereira, R. M. S., Borges, J., Smirnov, G. V., Vaz, F., & Vasilevskiy, M. I. (2019). Surface Plasmon Resonance in a Metallic Nanoparticle Embedded in a Semiconductor Matrix: Exciton–Plasmon Coupling. *ACS Photonics*, *6*(1), 204–210. https://doi.org/10.1021/acsphotonics.8b01430

Poole Jr., C. P., & Owens, F. (2003). *Introduction to Nanotechnology*. John Wiley & Sons, Inc., Hoboken.

Prior, R. L., & Cao, G. (1999). In vivo total antioxidant capacity: comparison of different analytical methods1. *Free Radical Biology and Medicine*, *27*(11–12), 1173–1181. https://doi.org/10.1016/S0891-5849(99)00203-8

Rahman, T., Hosen, I., Islam, M. M. T., & Shekhar, H. U. (2012). Oxidative stress and human health. *Advances in Bioscience and Biotechnology*, *03*(07), 997–1019. https://doi.org/10.4236/abb.2012.327123

Rajendran, M. (2016). Quinones as photosensitizer for photodynamic therapy: ROS generation, mechanism and detection methods. *Photodiagnosis and Photodynamic Therapy*, *13*, 175–187. https://doi.org/10.1016/j.pdpdt.2015.07.177

Rawal, I., & Kaur, A. (2013). Synthesis of mesoporous polypyrrole nanowires/nanoparticles for ammonia gas sensing application. *Sensors and Actuators A: Physical*, *203*, 92–102. https://doi.org/10.1016/j.sna.2013.08.023

S. A. Lawrence. (2004). Amines: Synthesis, Properties and Applications. In *Organic Process Research & Development*. Cambridge University Press: Cambridge. https://doi.org/10.1021/op0501390

Saki, N., Akin, M., Atsay, A., Pekbelgin Karaoglu, H. R., & Kocak, M. B. (2018). Synthesis and characterization of novel quaternized 2, 3-(diethylmethylamino)phenoxy tetrasubstituted Indium and Gallium phthalocyanines and comparison of their antimicrobial and antioxidant properties with different phthalocyanines. *Inorganic Chemistry Communications*, *95*, 122–129. https://doi.org/10.1016/j.inoche.2018.07.010

Sardar, R., Funston, A. M., Mulvaney, P., & Murray, R. W. (2009). Gold Nanoparticles: Past, Present, and Future. *Langmuir*, *25*(24), 13840–13851. https://doi.org/10.1021/la9019475

Sastre, A., Torres, T., & Hanack, M. (1995). Synthesis of novel unsymmetrical monoaminated phthalocyanines. *Tetrahedron Letters*, *36*(46), 8501–8504. https://doi.org/10.1016/0040-4039(95)01781-C

Schaffer, A. M., Gouterman, M., & Davidson, E. R. (1973). Porphyrins XXVIII. Extended Hückel calculations on metal phthalocyanines and tetrazaporphins. *Theoretica Chimica Acta*, *30*(1), 9–30. https://doi.org/10.1007/BF00527632

Schultz, H., Lehmann, H., Rein, M., & Hanack, M. (1990). *Phthalocyaninatometal and related complexes with special electrical and optical properties* (pp. 41–146). https://doi.org/10.1007/3-540-52899-7_2

Schulz, F., Homolka, T., Bastús, N. G., Puntes, V., Weller, H., & Vossmeyer, T. (2014). Little Adjustments Significantly Improve the Turkevich Synthesis of Gold Nanoparticles. *Langmuir*, *30*(35), 10779–10784. https://doi.org/10.1021/la503209b

Seayad, A., Ahmed, M., Klein, H., Jackstell, R., Gross, T., & Beller, M. (2002). Internal Olefins to Linear Amines. *Science*, *297*(5587), 1676–1678. https://doi.org/10.1126/science.1074801

Sen, P., Managa, M., & Nyokong, T. (2019). New type of metal-free and Zinc(II), In(III), Ga(III) phthalocyanines carrying biologically active substituents: Synthesis and photophysicochemical properties and photodynamic therapy activity. *Inorganica Chimica Acta*, *491*, 1–8. https://doi.org/10.1016/j.ica.2019.03.010

Sevim, A. M., Yenilmez, H. Y., & Bayır, Z. A. (2013). Synthesis and photophysical properties of novel (trifluoromethyl)phenylethynyl-substituted metallophthalocyanines. *Polyhedron*, *62*, 120–125. https://doi.org/10.1016/j.poly.2013.06.037

Shankar, S. S., Rai, A., Ahmad, A., & Sastry, M. (2004). Rapid synthesis of Au, Ag, and bimetallic Au core–Ag shell nanoparticles using Neem (Azadirachta indica) leaf broth. *Journal of Colloid and Interface Science*, *275*(2), 496–502. https://doi.org/10.1016/j.jcis.2004.03.003

Sharman, W. M., & Van Lier, J. E. (2003). Phthalocyanines: Synthesis. In K. M. Kadish, K. M. Smith, & R. Guilard (Eds.), *The porphyrin handbook Vol-15* (pp. 11–13). Academic Press, San Diego.

Słota, R., & Dyrda, G. (2003). UV Photostability of Metal Phthalocyanines in Organic Solvents. *Inorganic Chemistry*, *42*(18), 5743–5750. https://doi.org/10.1021/ic0260217

Snow, A. W. (2003). 109-Phthalocyanine Aggregation. In K. M. Kadish, K. M. Smith, & R. Guilard (Eds.), *The Porphyrin Handbook* (pp. 129–176). Academic Press, Amsterdam.

Sonogashira, K. (2002). Development of Pd–Cu catalyzed cross-coupling of terminal acetylenes with sp2-carbon halides. *Journal of Organometallic Chemistry*, *653*(1–2), 46–49. https://doi.org/10.1016/S0022-328X(02)01158-0

Soppok, R. (1979). Ullmans Enzyclöpedia der technischen Chemie. *Urban & Schwarzenberg München, Bd*, 18, p.501.

Sperling, R. A., Rivera Gil, P., Zhang, F., Zanella, M., & Parak, W. J. (2008). Biological applications of gold nanoparticles. *Chemical Society Reviews*, *37*(9), 1896. https://doi.org/10.1039/b712170a

Stuchinskaya, T., Moreno, M., Cook, M. J., Edwards, D. R., & Russell, D. A. (2011). Targeted photodynamic therapy of breast cancer cells using antibody–phthalocyanine–gold nanoparticle conjugates. *Photochemical & Photobiological Sciences*, *10*(5), 822. https://doi.org/10.1039/c1pp05014a

Suriati, G., Mariatti, M., & Azizan, A. (2014). SYNTHESIS OF SILVER NANOPARTICLES BY CHEMICAL REDUCTION METHOD: EFFECT OF REDUCING AGENT AND SURFACTANT CONCENTRATION. *International Journal of Automotive and Mechanical Engineering*, *10*, 1920–1927. https://doi.org/10.15282/ijame.10.2014.9.0160

Tabassum, S., Ahmad, M., Afzal, M., Zaki, M., & Bharadwaj, P. K. (2014). Synthesis and structure elucidation of a copper(II) Schiff-base complex: In vitro DNA binding, pBR322 plasmid cleavage and HSA binding studies. *Journal of Photochemistry and Photobiology B: Biology*, *140*, 321–331. https://doi.org/10.1016/j.jphotobiol.2014.08.015

Tau, P., & Nyokong, T. (2006). Synthesis, electrochemical and photophysical properties of phthalocyaninato oxotitanium(iv) complexes tetra-substituted at the ? and ? positions with arylthio groups. *Dalton Transactions*, *37*, 4482. https://doi.org/10.1039/b607538j

Templeton, D. H., Fischer, M. S., Zalkin, A., & Calvin, M. (1971). Structure and chemistry of the porphyrins. Crystal and molecular structure of the monohydrated dipyridinated magnesium phthalocyanine complex. *Journal of the American Chemical Society*, *93*(11), 2622–2628. https://doi.org/10.1021/ja00740a008

Thomas, A. (1990). *Phthalocyanine Research and Applications* (1st Ed.). CRC Press.

Thompson, J. A., Murata, K., Miller, D. C., Stanton, J. L., Broderick, W. E., Hoffman, B. M., & Ibers, J. A. (1993). Synthesis of high-purity phthalocyanines (pc): high intrinsic conductivities in the molecular conductors H2(pc)I and Ni(pc)I. *Inorganic Chemistry*, *32*(16), 3546–3553. https://doi.org/10.1021/ic00068a027

Torre, G., Bottari, G., & Hahn, U. (2010). *Functional Phthalocyanine Molecular Materials* (J. Jihang (ed.)). Springer-Verlag Berlin Heidelberg.

Turkevich, J., Stevenson, P. C., & Hillier, J. (1951). A study of the nucleation and growth processes in the synthesis of colloidal gold. *Discussions of the Faraday Society*, *11*, 55. https://doi.org/10.1039/df9511100055

Turkevich, J., Stevenson, P. C., & Hillier, J. (1953). The Formation of Colloidal Gold. *The Journal of Physical Chemistry*, *57*(7), 670–673. https://doi.org/10.1021/j150508a015

Uppal, M. A., Kafizas, A., Ewing, M. B., & Parkin, I. P. (2010). The effect of initiation method on the size, monodispersity and shape of gold nanoparticles formed by the Turkevich method. *New Journal of Chemistry*, *34*(12), 2906. https://doi.org/10.1039/c0nj00505c

Valko, M., Rhodes, C. J., Moncol, J., Izakovic, M., & Mazur, M. (2006). Free radicals, metals and antioxidants in oxidative stress-induced cancer. *Chemico-Biological Interactions*, *160*(1), 1–40. https://doi.org/10.1016/j.cbi.2005.12.009

Vollhardt, K. P. C., & Schore, N. E. (1999). *Organic chemistry: Structure and Function* (3rd ed.). New York: W.H. Freeman.

Voronina, A. A., Filippova, A. A., Znoiko, S. A., Vashurin, A. S., & Maizlish, V. E. (2015). Effect of the solvation properties of the solvent on the formation of associated structures of water-soluble Co(II) phthalocyanines. *Russian Journal of Inorganic Chemistry*, *60*(11), 1407–1414. https://doi.org/10.1134/S0036023615110236

Westerlund, F., & Bjørnholm, T. (2009). Directed assembly of gold nanoparticles. *Current Opinion in Colloid & Interface Science*, *14*(2), 126–134. https://doi.org/10.1016/j.cocis.2008.07.002

Whitesides, G. (2005). Nanoscience, Nanotechnology, and Chemistry. *Small*, *1*(2), 172–179. https://doi.org/10.1002/smll.200400130

Wieder, M. E., Hone, D. C., Cook, M. J., Handsley, M. M., Gavrilovic, J., & Russell, D. A. (2006). Intracellular photodynamic therapy with photosensitizer-nanoparticle conjugates: cancer therapy using a 'Trojan horse.' *Photochem. Photobiol. Sci.*, *5*(8), 727–734. https://doi.org/10.1039/B602830F

Wöhrle, D., Eskes, M., Shigehara, K., & Yamada, A. (1993). A Simple Synthesis of 4,5-Disubstituted 1,2-Dicyanobenzenes and 2,3,9,10,16,17,23,24-Octasubstituted Phthalocyanines. *Synthesis*, *1993*(02), 194–196. https://doi.org/10.1055/s-1993-25825

Xiao, W., Guan, X., Huang, B., Ye, Q., Zhang, T., Chen, K., ... Fu, F. (2021). Fluorinated dendritic silicon (IV) phthalocyanines nanoparticles: Synthesis, photoinduced intramolecular energy transfer and DNA interaction. *Dyes and Pigments*, *186*, 109013. https://doi.org/10.1016/j.dyepig.2020.109013

Yalazan, H., Barut, B., Ertem, B., Yalçın, C. Ö., Ünver, Y., Özel, A., ... Kantekin, H. (2020). DNA interaction and anticancer properties of new peripheral phthalocyanines carrying tosylated 4-morpholinoaniline units. *Polyhedron*, *177*, 114319. https://doi.org/10.1016/j.poly.2019.114319

Yang, L., Guo, L., Chen, Q., Sun, H., Liu, J., Zhang, X., ... Dai, S. (2012). Theoretical design and screening of panchromatic phthalocyanine sensitizers derived from TT1 for dye-sensitized solar cells. *Journal of Molecular Graphics and Modelling*, *34*, 1–9. https://doi.org/10.1016/j.jmgm.2011.12.001

Ye, J., Van Dorpe, P., Van Roy, W., Borghs, G., & Maes, G. (2009). Fabrication, Characterization, and Optical Properties of Gold Nanobowl Submonolayer Structures. *Langmuir*, *25*(3), 1822–1827. https://doi.org/10.1021/la803768y

Yenilmez, H. Y., Şahin, A. N., Altındal, A., & Bayır, Z. A. (2021). Photosensitive field effect transistor based on metallo-phthalocyanines containing (4-pentylphenyl) ethynyl moieties. *Synthetic Metals*, *273*, 116690. https://doi.org/10.1016/j.synthmet.2020.116690

Yıldırım, N., Bilgiçli, A. T., Alici, E. H., Arabacı, G., & Yarasir, M. N. (2017). Formation, characterization, aggregation, fluorescence and antioxidant properties of novel tetrasubstituted metal-free and metallophthalocyanines bearing (4-(methylthio)phenoxy) moieties. *Journal of Molecular Structure*, *1144*, 66–79. https://doi.org/10.1016/j.molstruc.2017.05.006

Young, J. G., & Onyebuagu, W. (1990). Synthesis and characterization of di-disubstituted phthalocyanines. *The Journal of Organic Chemistry*, *55*(7), 2155–2159. https://doi.org/10.1021/jo00294a032

Zagal, J. H. (1992). Metallophthalocyanines as catalysts in electrochemical reactions. *Coordination Chemistry Reviews*, *119*, 89–136. https://doi.org/10.1016/0010-8545(92)80031-L

Zagal, J. H., Griveau, S., Silva, J. F., Nyokong, T., & Bedioui, F. (2010). Metallophthalocyanine-based molecular materials as catalysts for electrochemical reactions. *Coordination Chemistry Reviews*, *254*(23–24), 2755–2791. https://doi.org/10.1016/j.ccr.2010.05.001

Zasedatelev, A. V., Dubinina, T. V., Krichevsky, D. M., Krasovskii, V. I., Gak, V. Y., Pushkarev, V. E., T ..... Chistyakov, A. A. (2016). Plasmon-Induced Light Absorption of Phthalocyanine Layer in Hybrid Nanoparticles: Enhancement Factor and Effective Spectra. *The Journal of Physical Chemistry C*, *120*(3), 1816–1823. https://doi.org/10.1021/acs.jpcc.5b08804

Zhou, Z.-F., Menna, M., Cai, Y.-S., & Guo, Y.-W. (2015). Polyacetylenes of Marine Origin: Chemistry and Bioactivity. *Chemical Reviews*, *115*(3), 1543–1596. https://doi.org/10.1021/cr4006507

Zijlstra, P., Chon, J. W. M., & Gu, M. (2009). Five-dimensional optical recording mediated by surface plasmons in gold nanorods. *Nature*, *459*(7245), 410–413. https://doi.org/10.1038/nature08053

APPENDICES

APPENDIX A: Spectra

APPENDIX A: Spectra

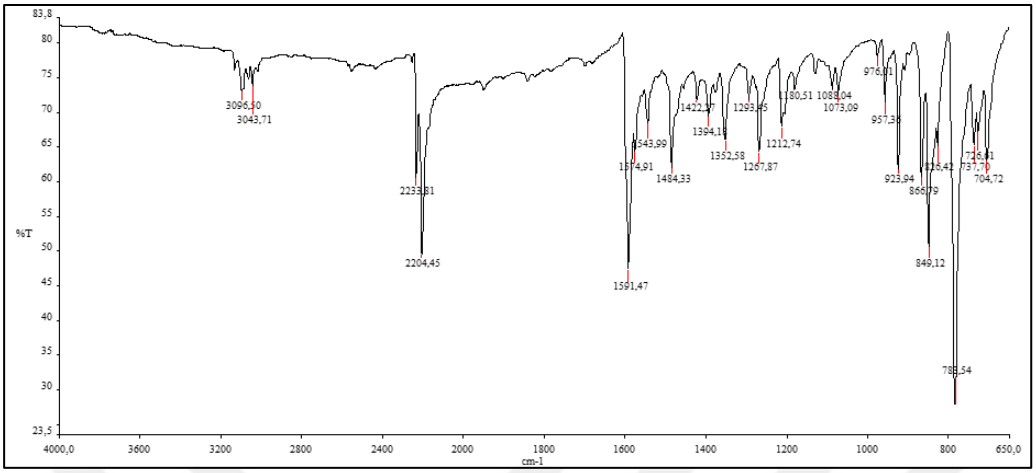

Figure A.1: FT-IR spectrum of phthalonitrile compound **(2)**.

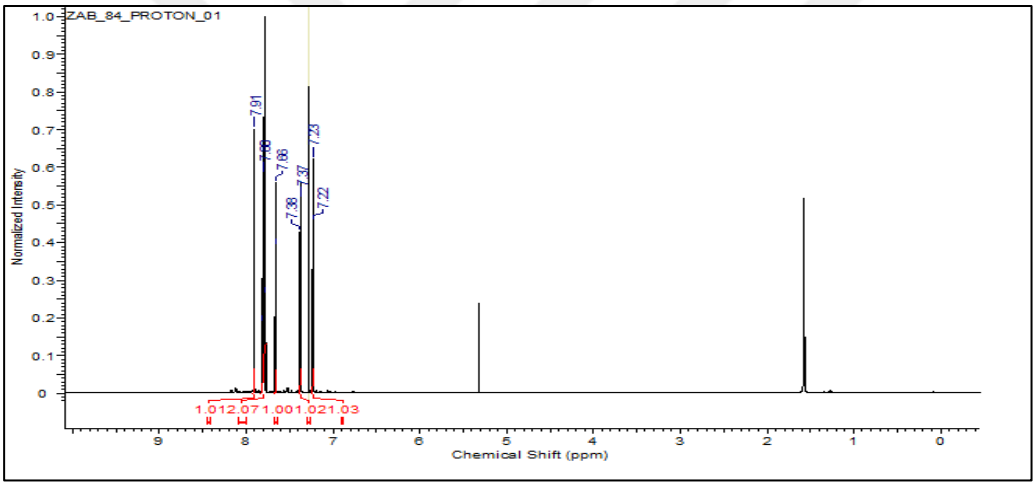

Figure A.2: ^{1}H-NMR spectrum of phthalonitrile compound **(2).**

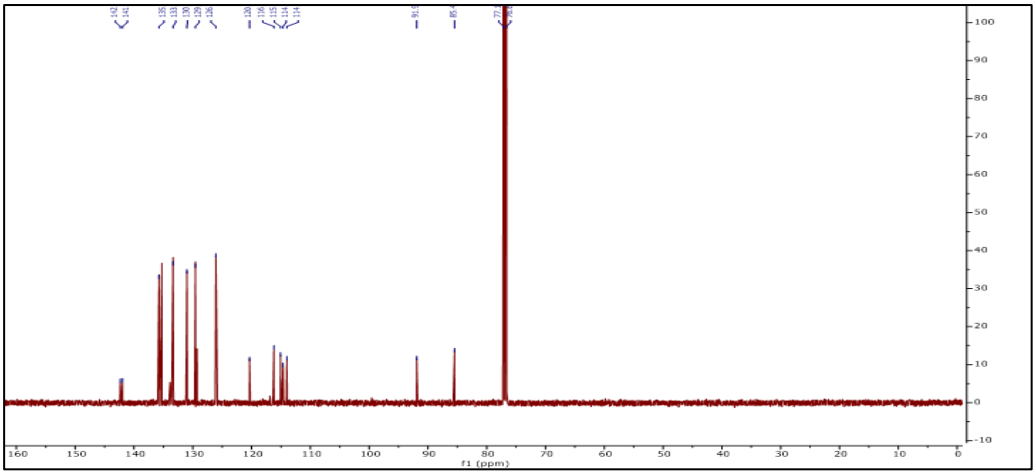

Figure A.3: ^{13}C-NMR spectrum of phthalonitrile compound **(2)**.

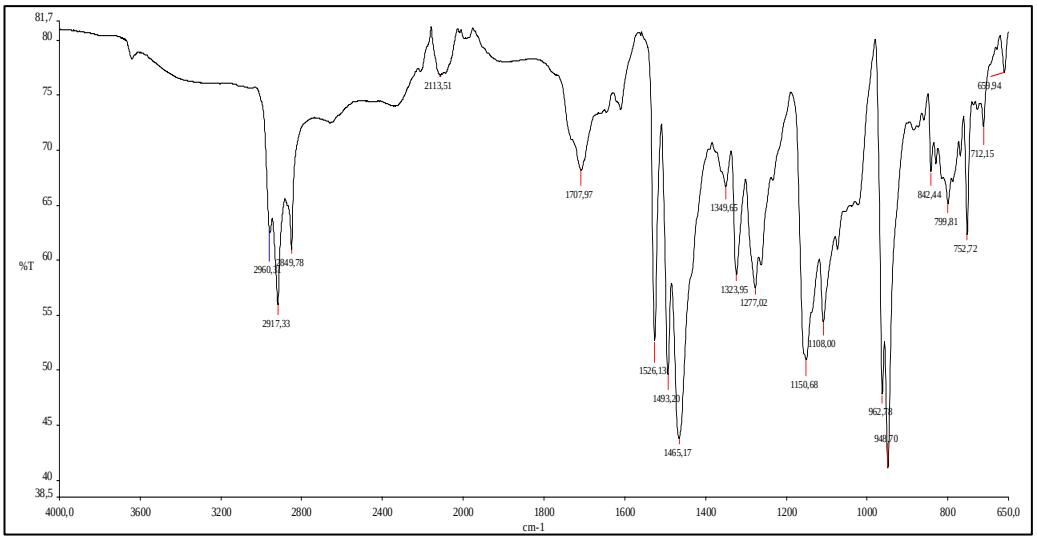

Figure A.4: FT-IR spectrum of compound **PcAsCo-1**.

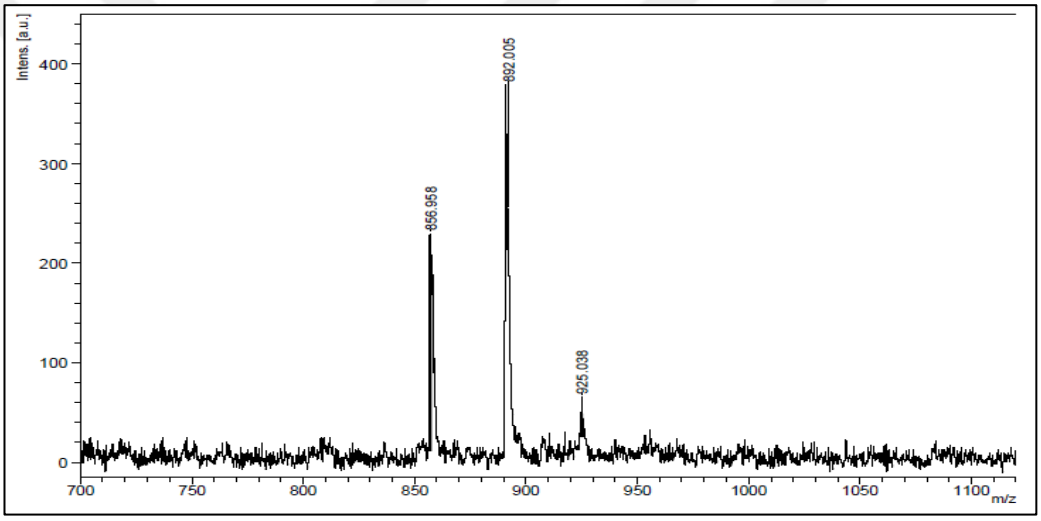

Figure A.5: Mass spectrum of compound **PcAsCo-1**.

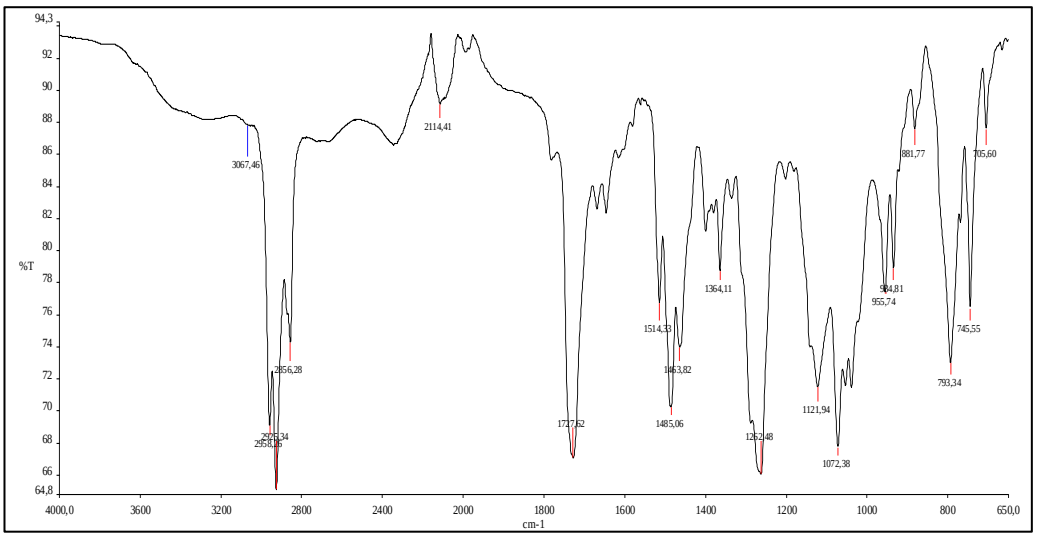

Figure A.6: FT-IR of compound **PcAsZn-1**.

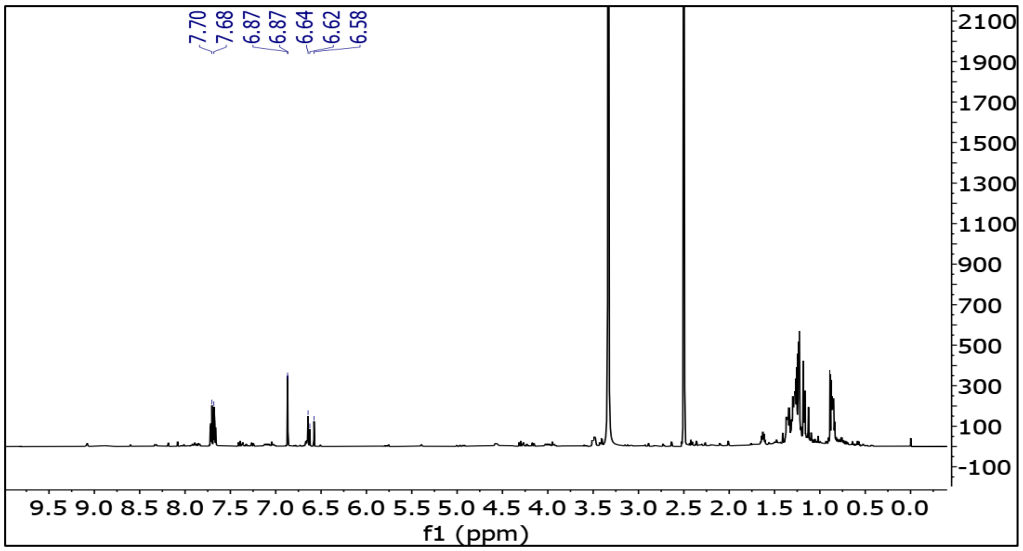

Figure A.7: ^{1}H-NMR spectrum of compound **PcAsZn-1**.

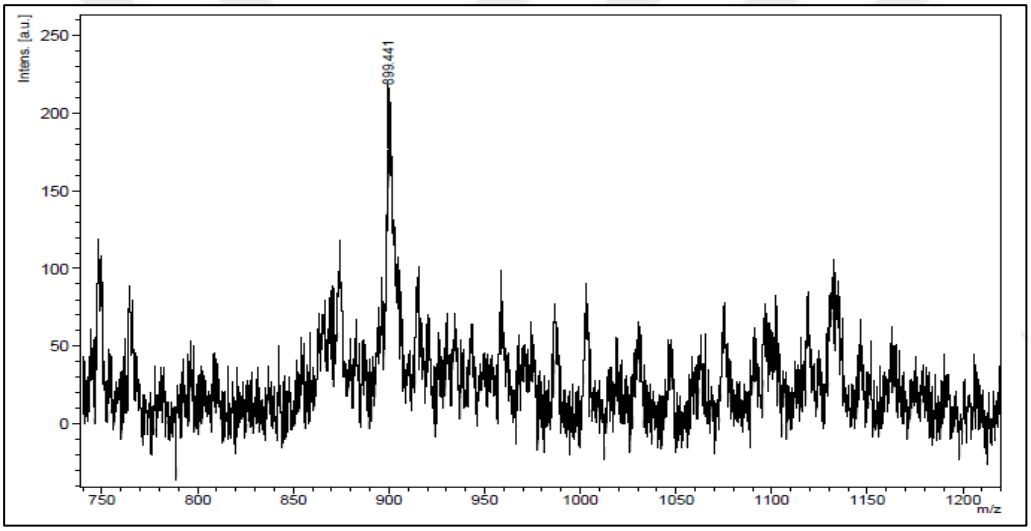

Figure A.8: Mass spectrum of compound **PcAsZn-1**.

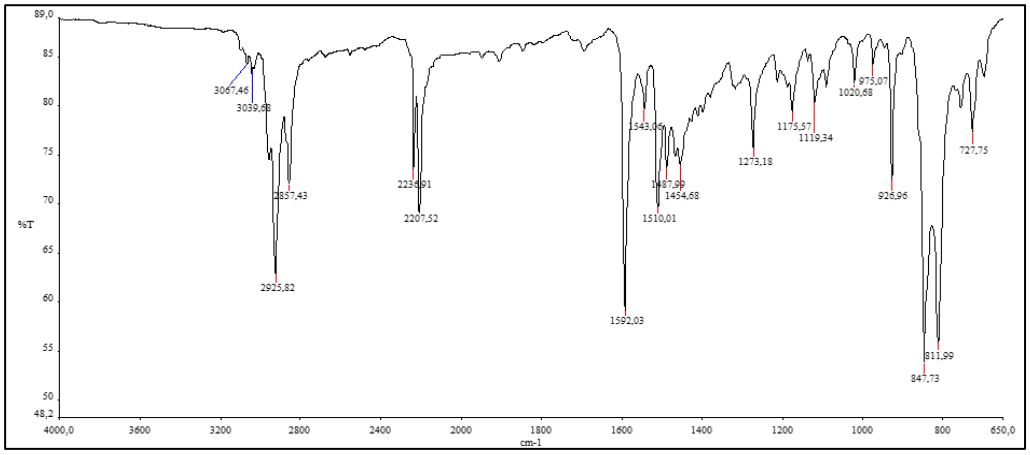

Figure A.9: FT-IR spectrum of phthalonitrile compound **(3)**.

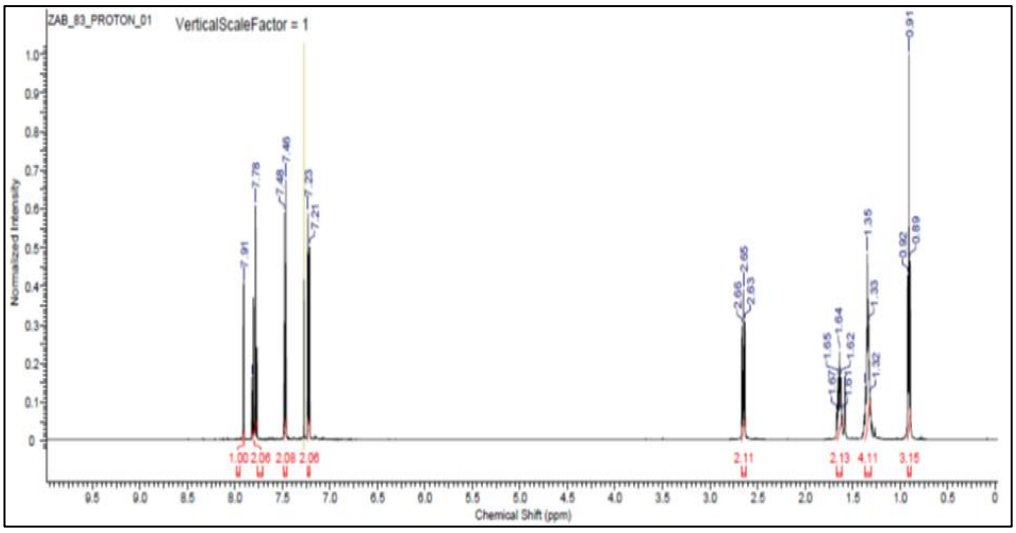

Figure A.10: ^{1}H-NMR spectrum of phthalonitrile compound **(3)**.

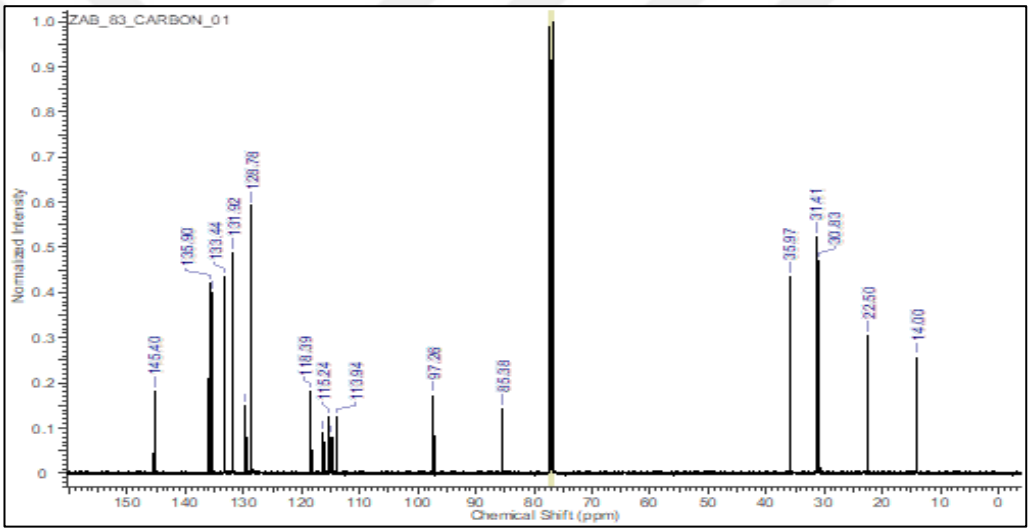

Figure A.11: ^{13}C-NMR spectrum of phthalonitrile compound **(3).**

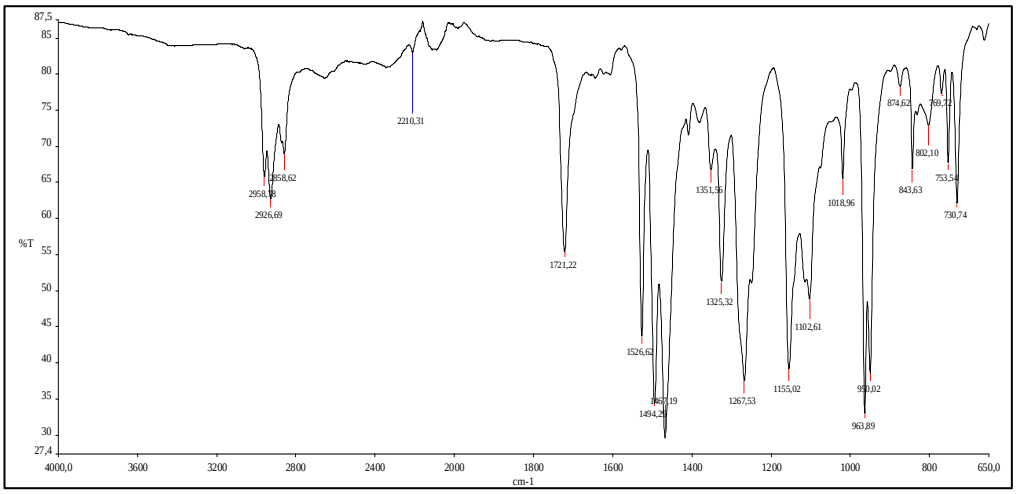

Figure A.12: FT-IR spectrum of compound **PcAsCo-2**.

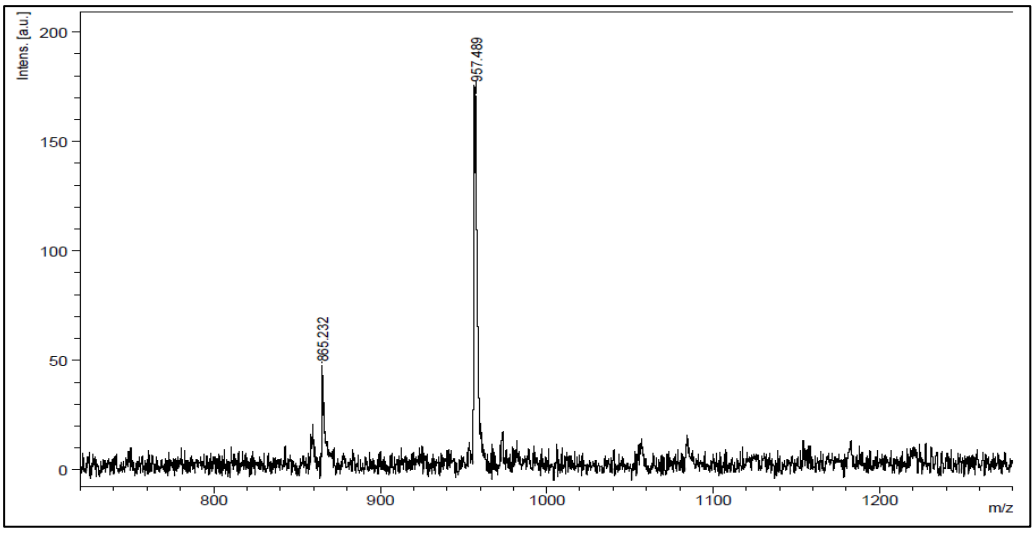

Figure A.13: Mass spectrum of compound **PcAsCo-2**.

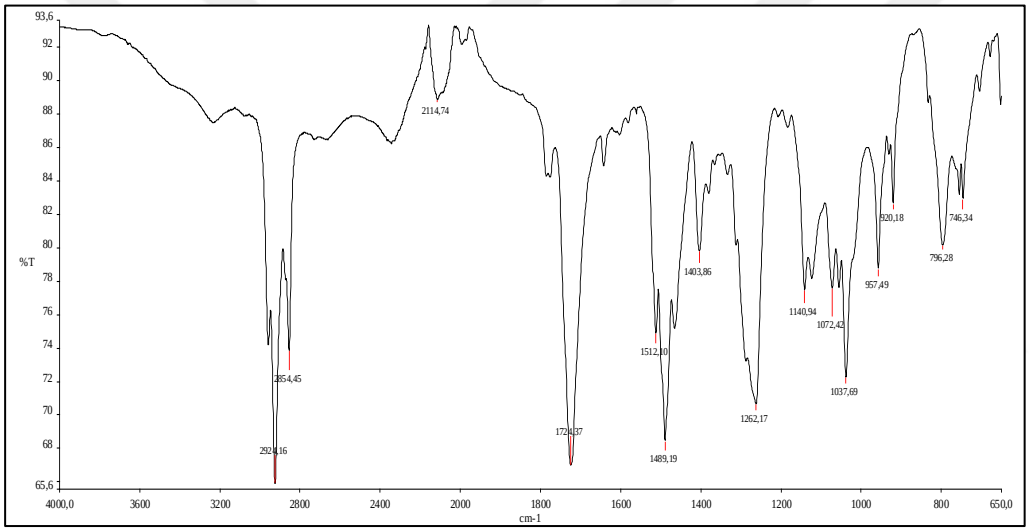

Figure A.14: FT-IR spectrum of compound **PcAsZn-2**.

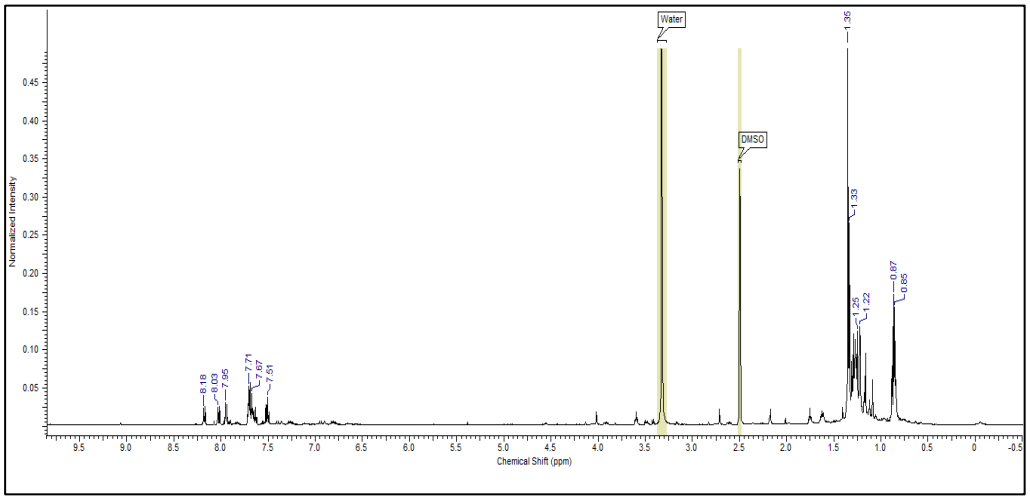

Figure A.15: ^{1}H-NMR spectrum of compound **PcAsZn-2**.

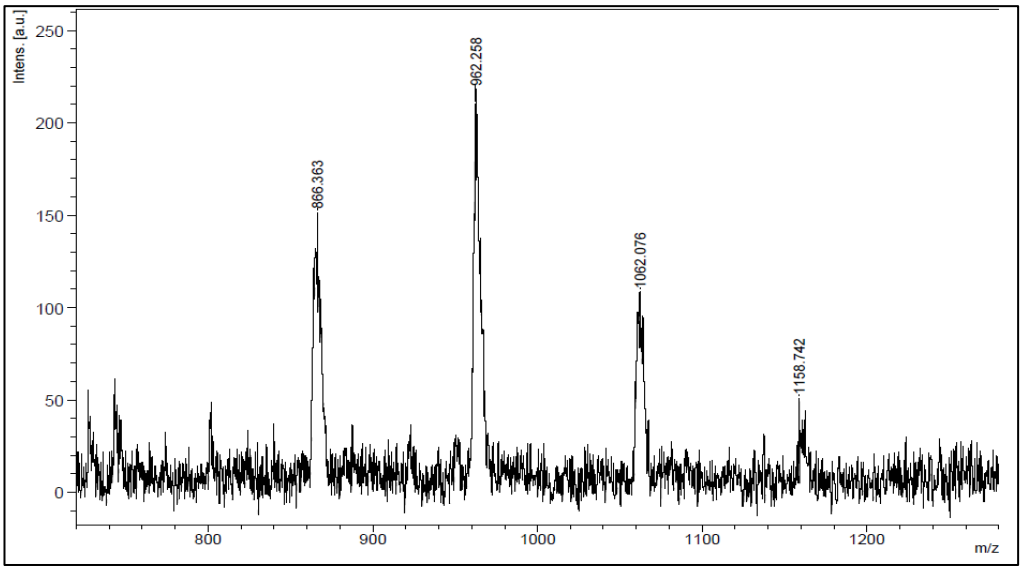

Figure A.16: Mass spectrum of compound **PcAsZn-2**.

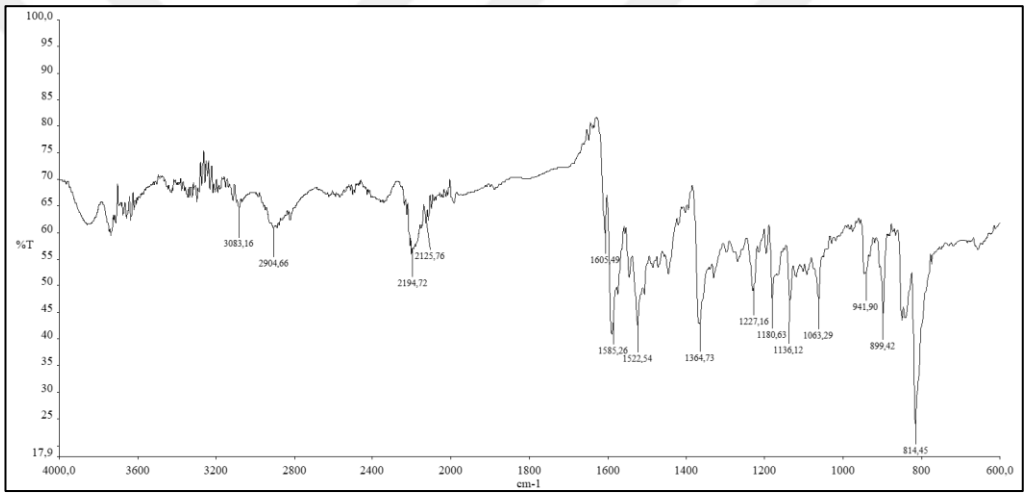

Figure A.17: FT-IR spectrum of phthalonitrile compound **(5)**.

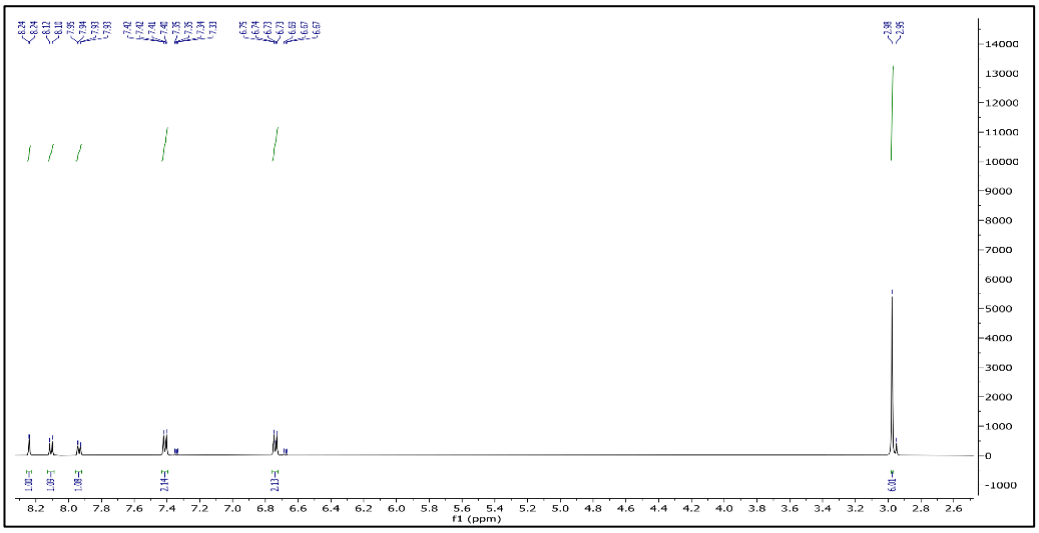

Figure A.18: ^{1}H-NMR spectrum of phthalonitrile compound **(5)**.

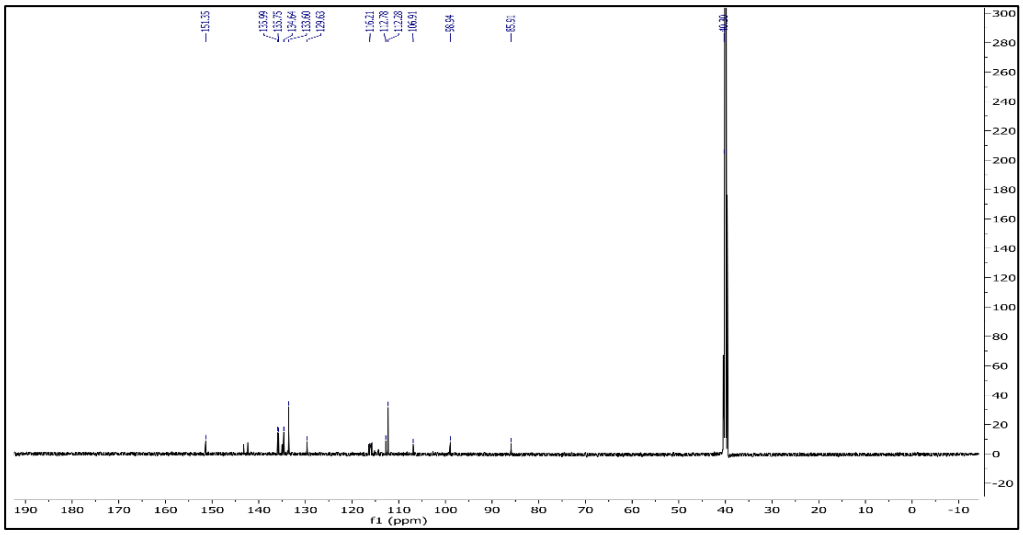

Figure A.19: ^{13}C-NMR spectrum of phthalonitrile compound **(5)**.

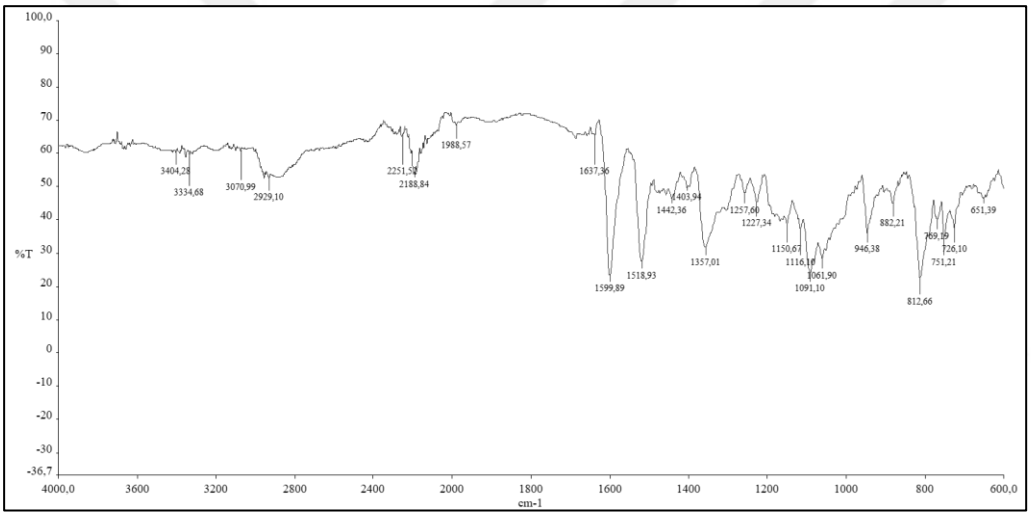

Figure A.20: FT-IR spectrum of compound **PcTACo**.

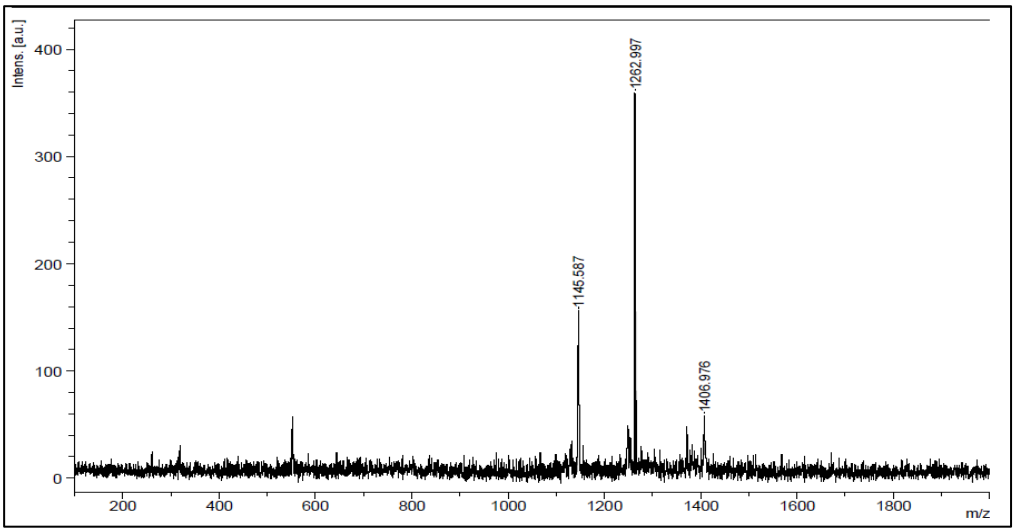

Figure A.21: Mass spectrum of compound **PcTACo**.

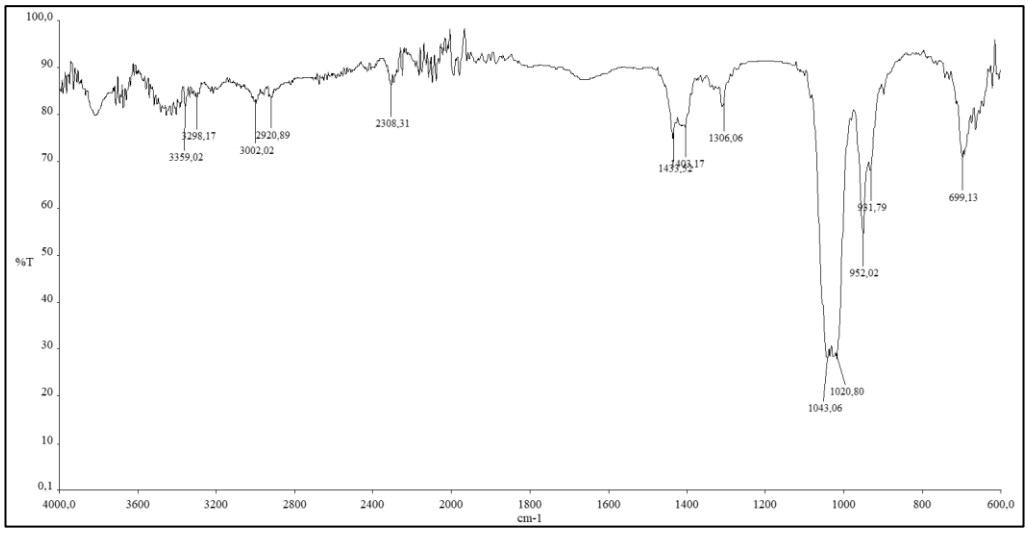

Figure A.21: FT-IR spectrum of compound **PcTAZn.**

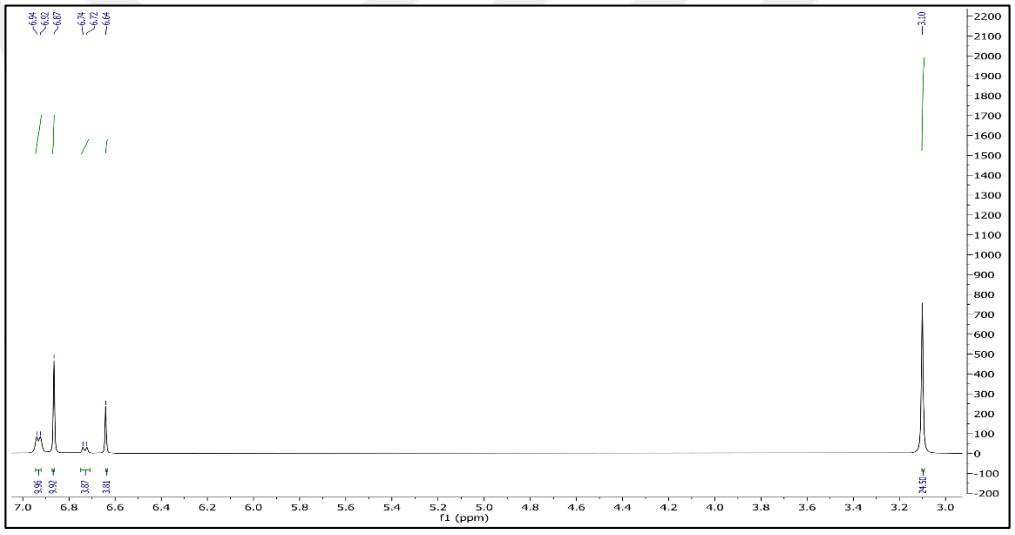

Figure A.23: ^{1}H-NMR spectrum of compound **PcTAZn**.

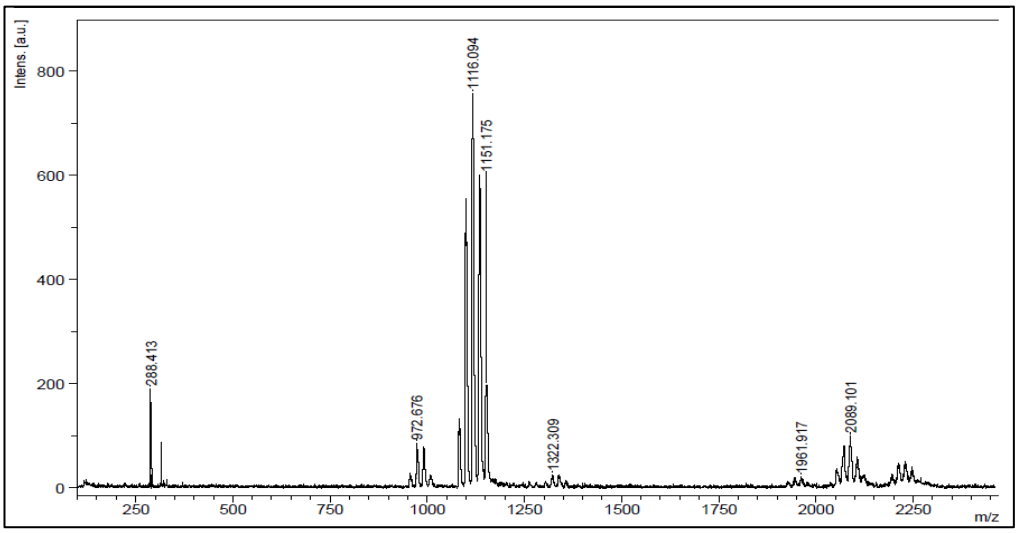

Figure A.24: Mass spectrum of compound **PcTAZn**.

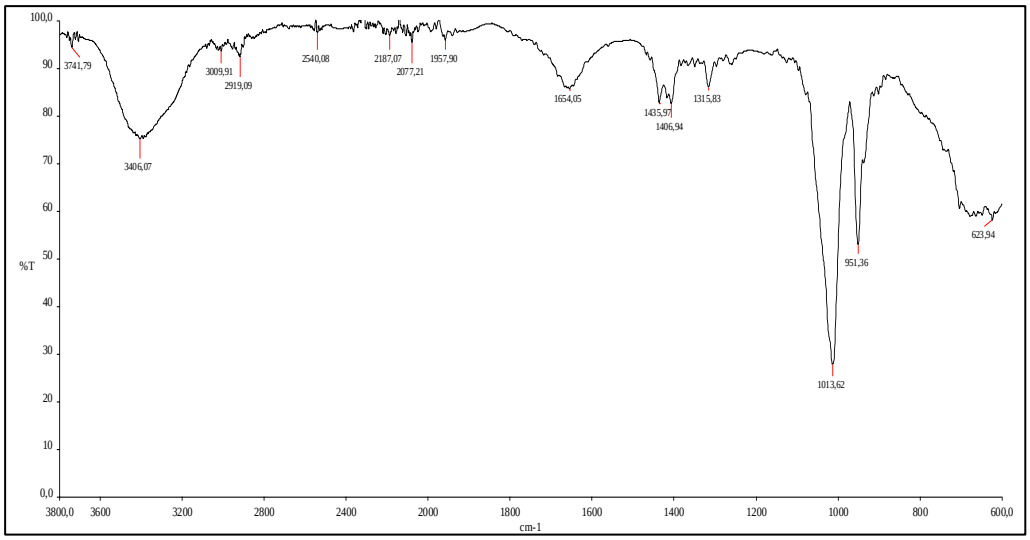

Figure A.25: FT-IR spectrum of compound **PcTAFe.**

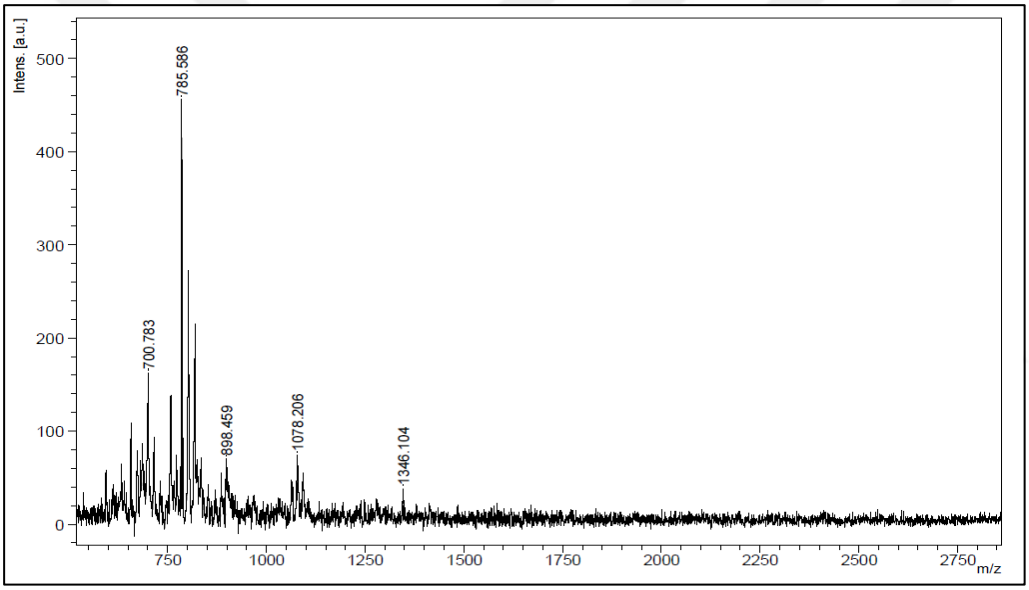

Figure A.26: Mass spectrum of compound **PcTAFe**.

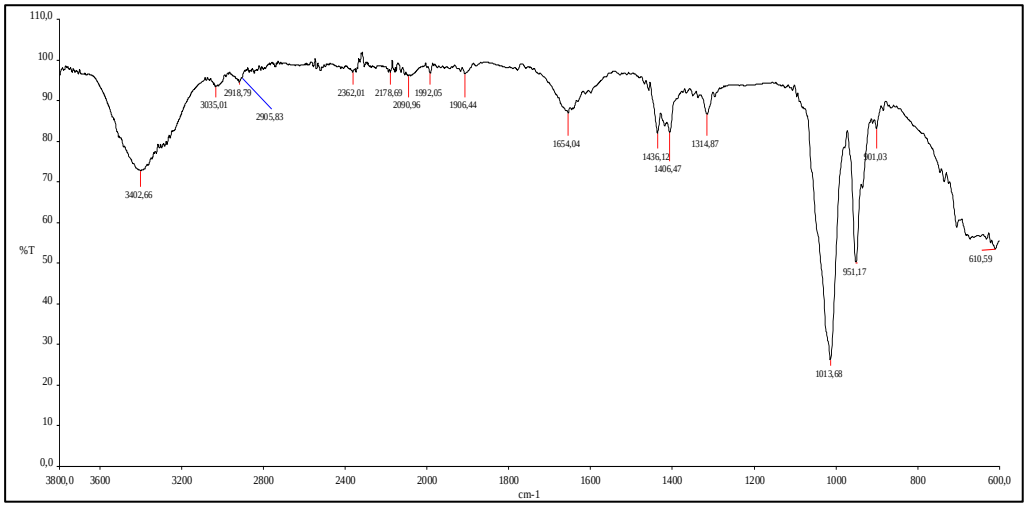

Figure A.27: FT-IR spectrum of compound **PcTAMn**.

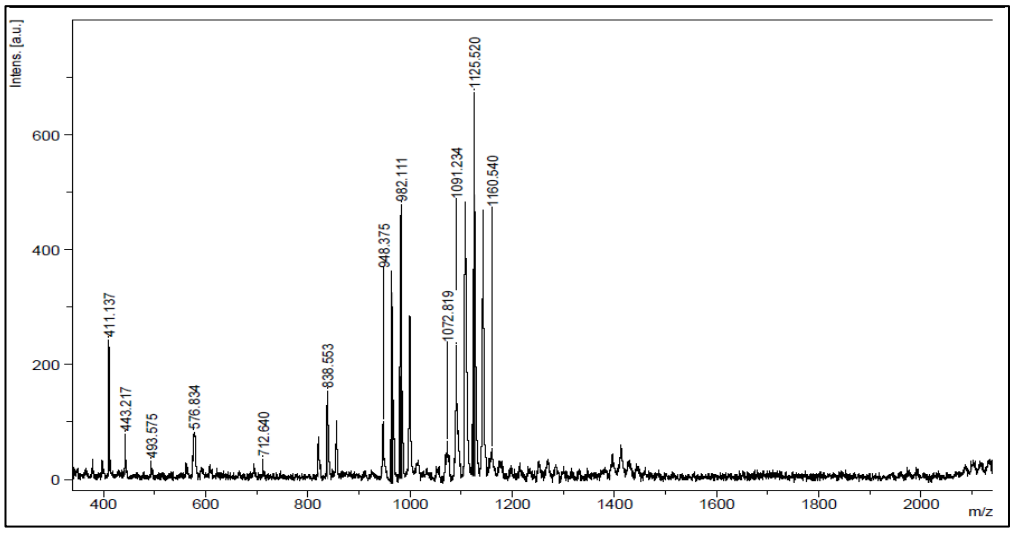

Figure A.28: Mass spectrum of compound **PcTAMn**.

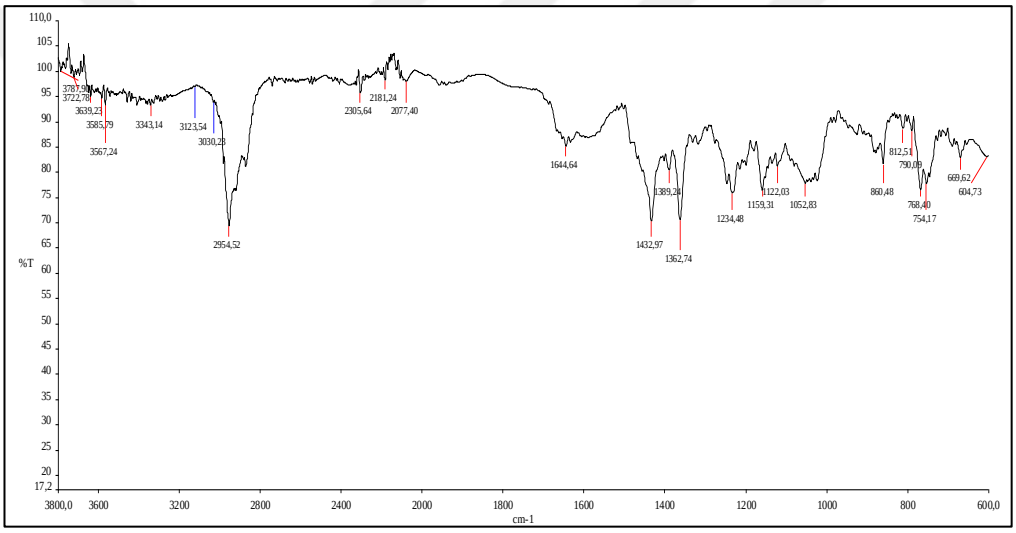

Figure A.29: FT-IR spectrum of compound **PcTALu′**.

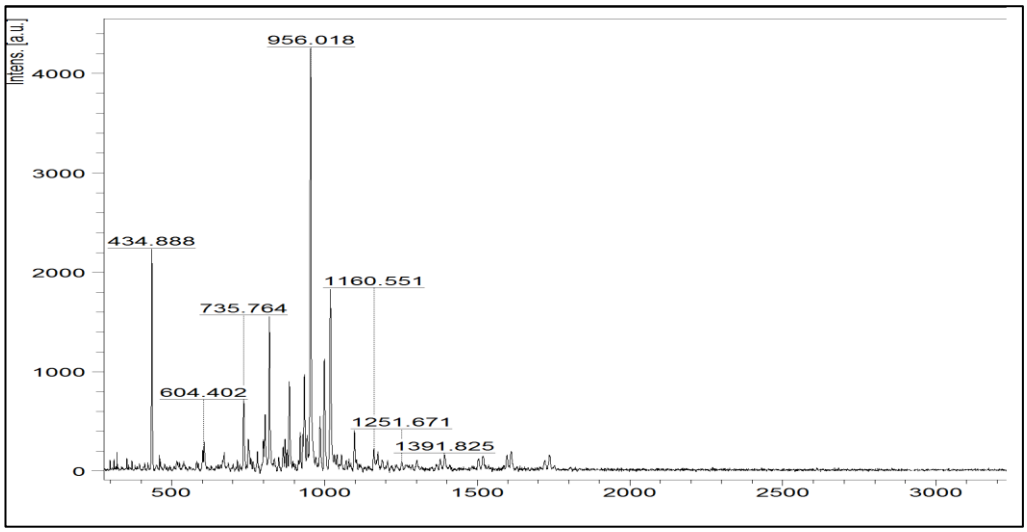

Figure A.30: Mass spectrum of compound **PcTALu′**.

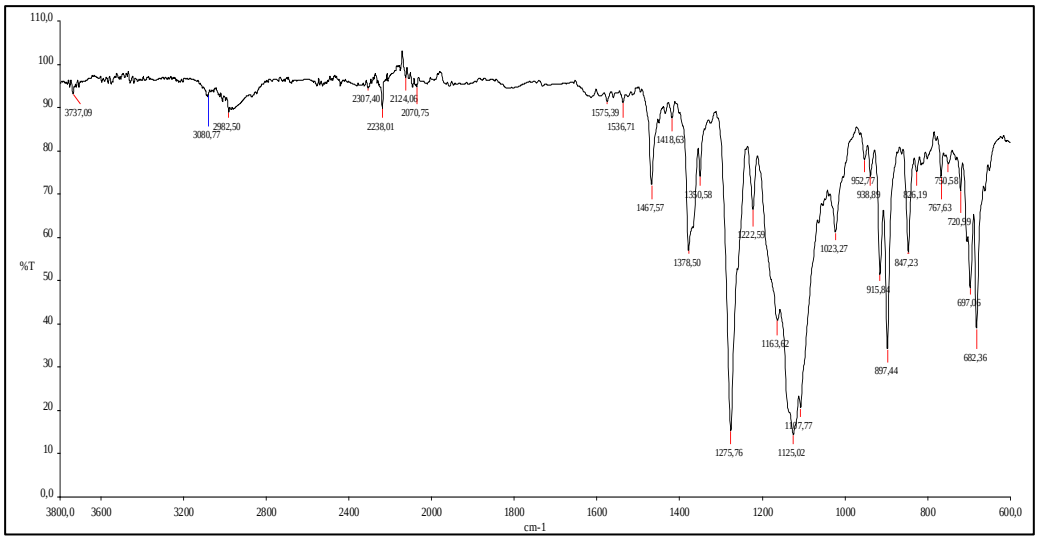

Figure A.31: FT-IR of phthalonitrile compound **(6)**.

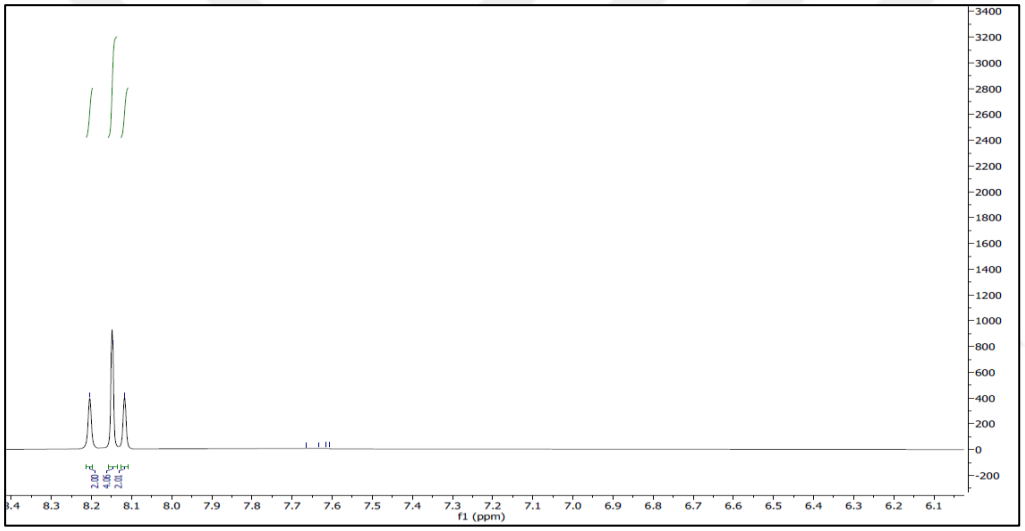

Figure A.32: ^{1}H-NMR of phthalonitrile compound **(6)**.

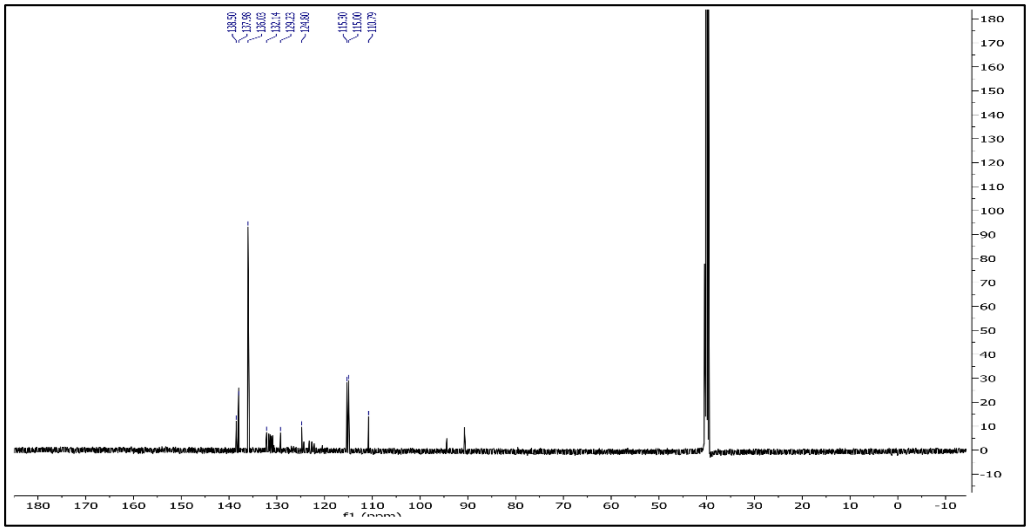

Figure A.33: ^{13}C-NMR of phthalonitrile compound **(6)**.

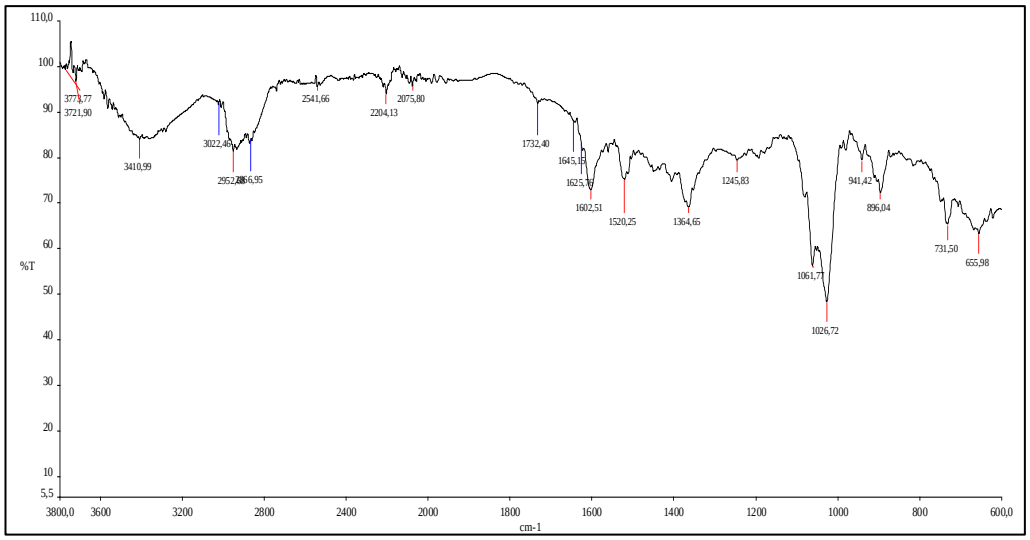

Figure A.34: FT-IR spectrum of compound **PcOFCo**.

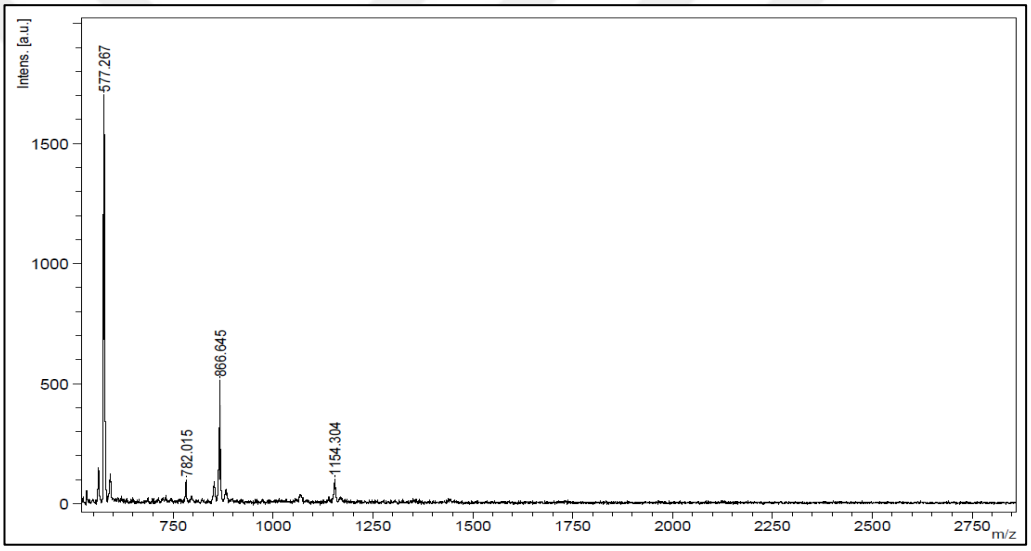

Figure A.35: Mass spectrum of compound **PcOFCo**.

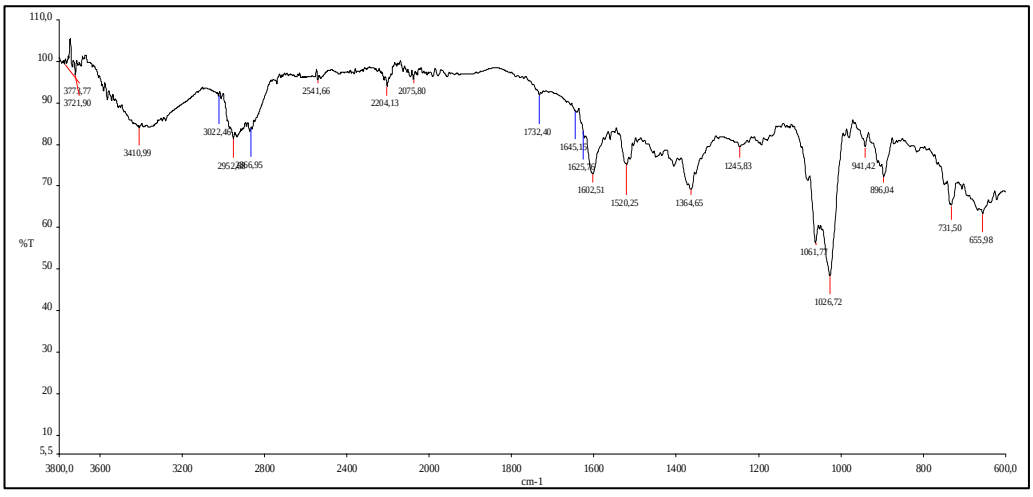

Figure A.36: FT-IR spectrum of compound **PcOFZn**.

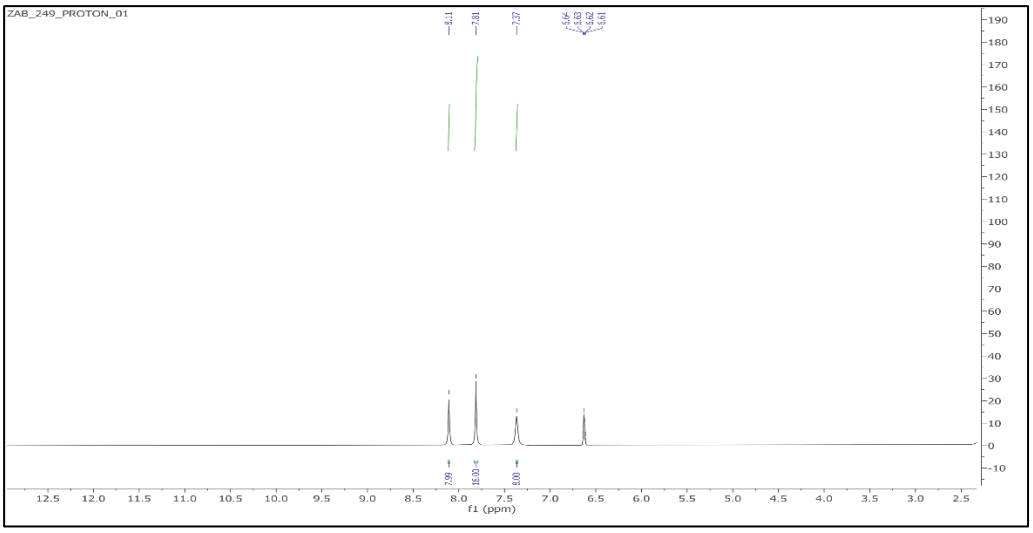

Figure A.37: ^{1}H-NMR spectrum of compound **PcOFZn**.

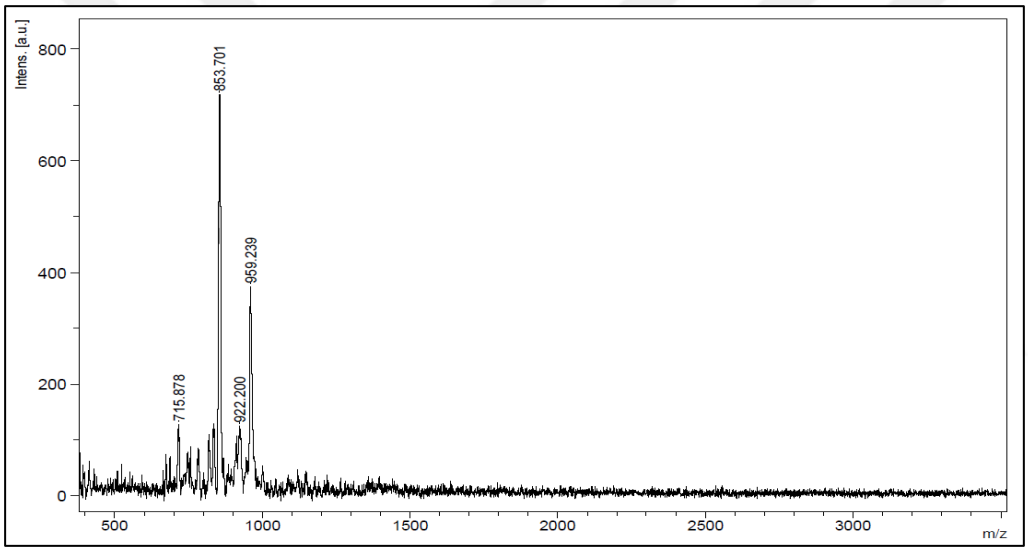

Figure A.38: Mass spectrum of compound **PcOFZn**.

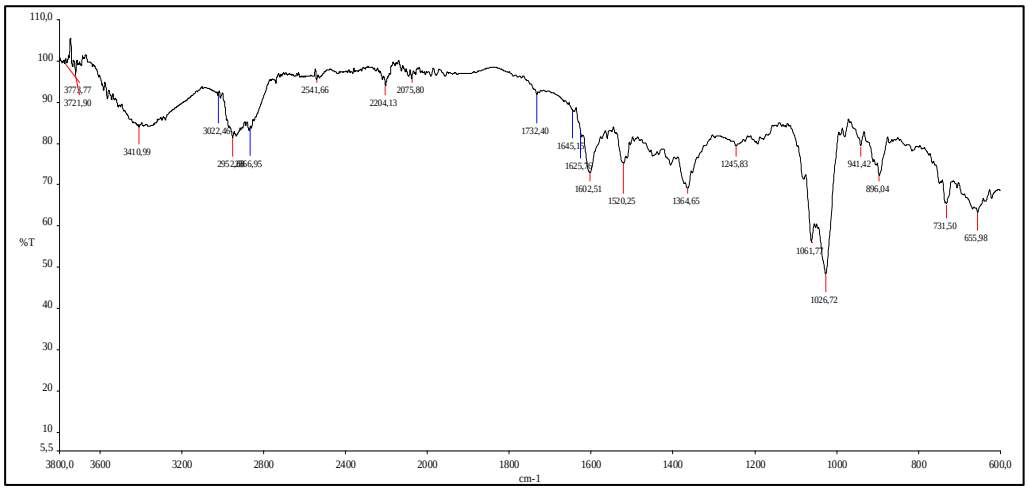

Figure A.39: FT-IR spectrum of compound **PcOFLu.**

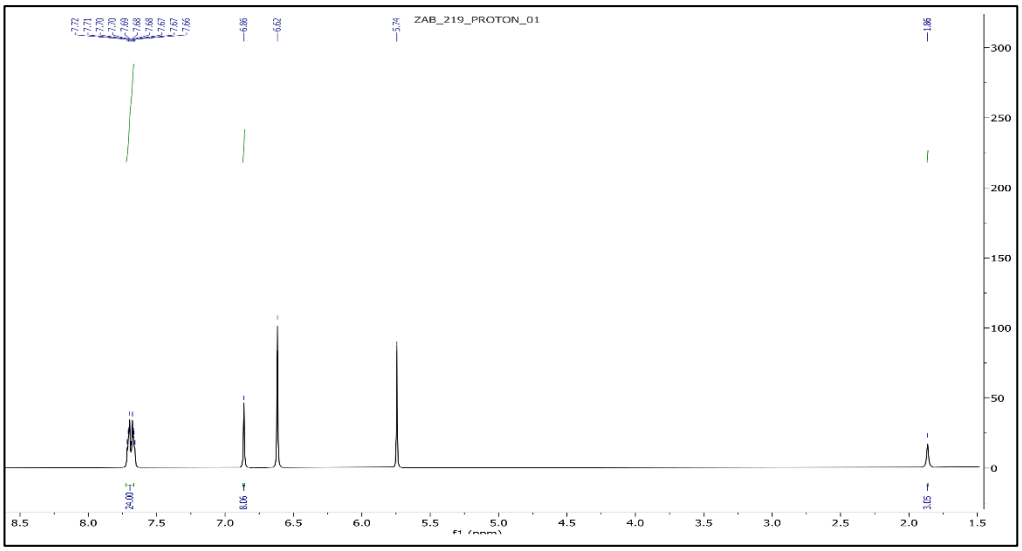

Figure A.40: ^{1}H-NMR spectrum of compound **PcOFLu**.

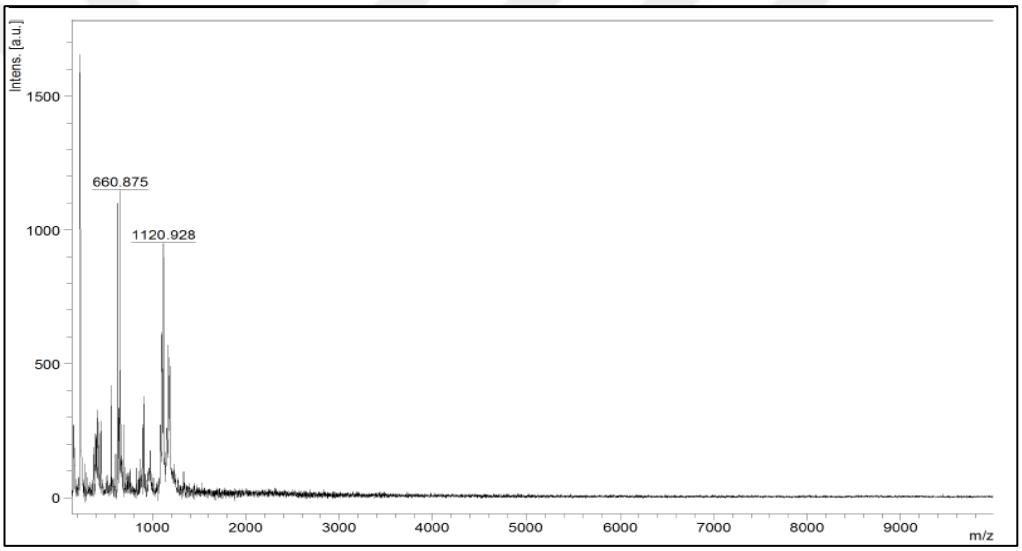

Figure A.41: Mass spectrum of compound **PcOFLu**.

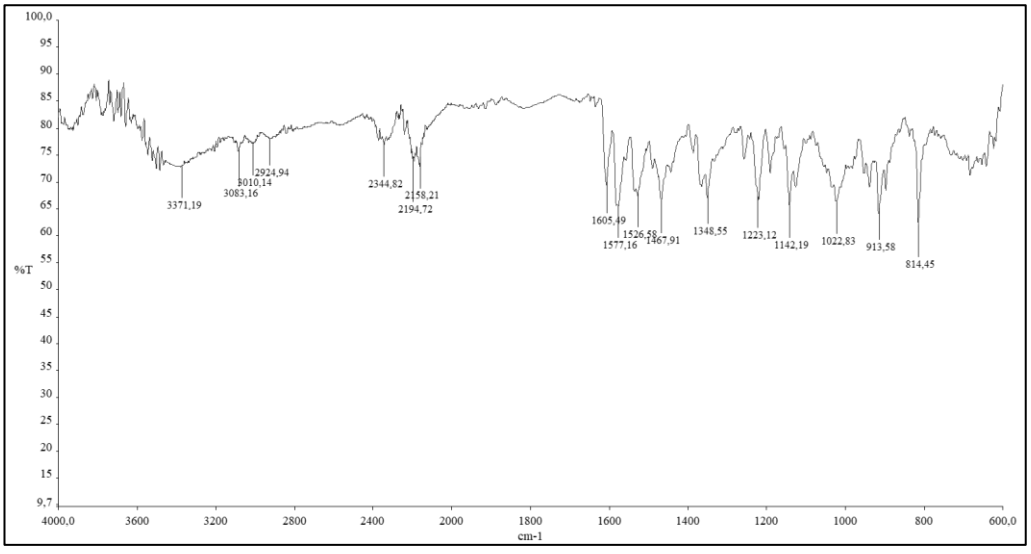

Figure A.42: FT-IR spectrum of phthalonitrile compound **(7)**.

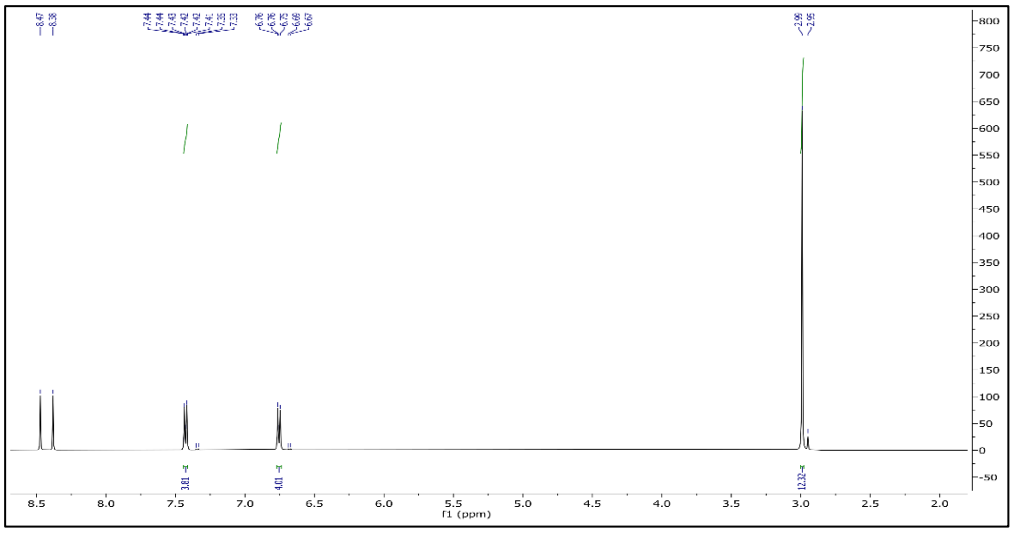

Figure A.43: ^{1}H-NMR spectrum of phthalonitrile compound **(7)**.

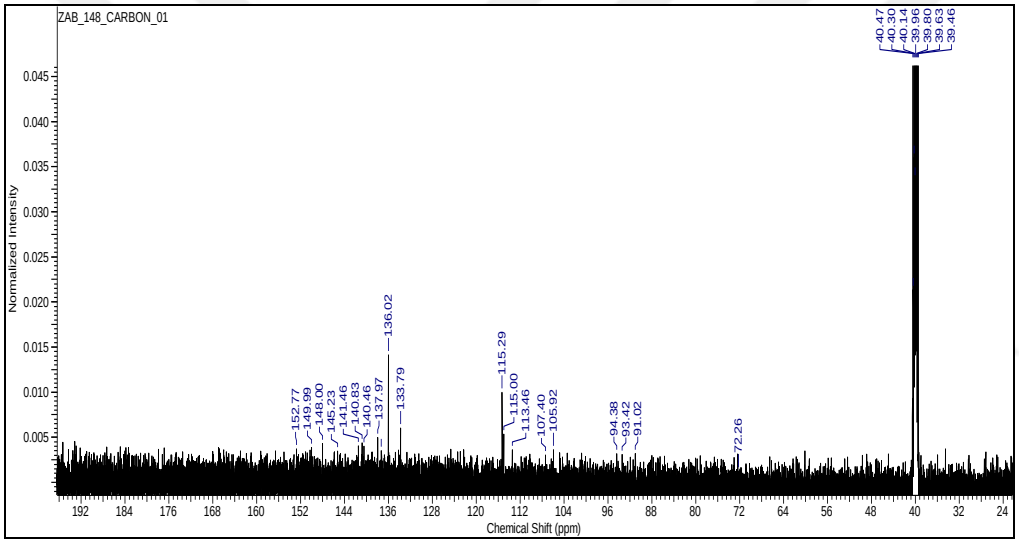

Figure A.44: ^{13}C-NMR spectrum of phthalonitrile compound **(7)**.

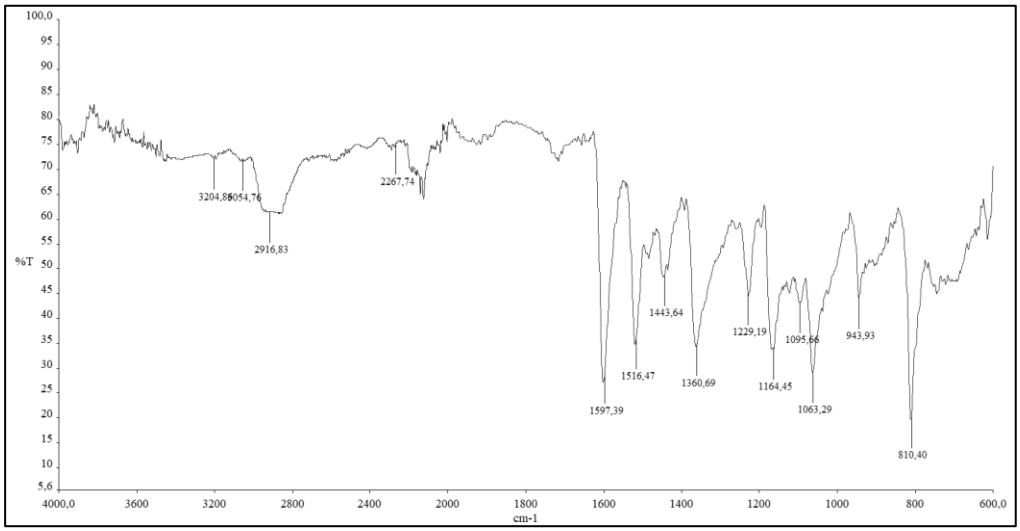

Figure A.45: FT-IR spectrum of compound **PcOACo**.

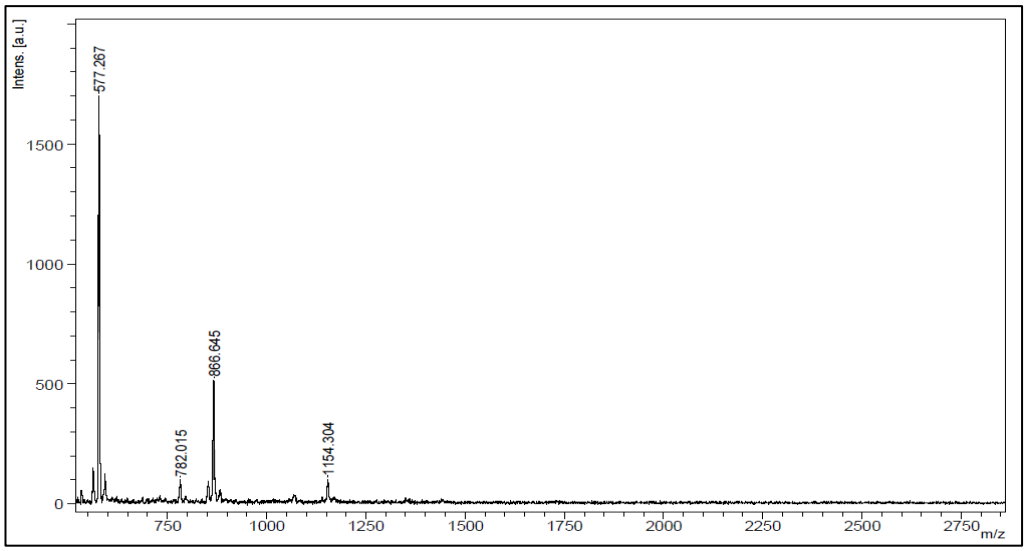

Figure A.46: Mass spectrum of compound **PcOACo**.

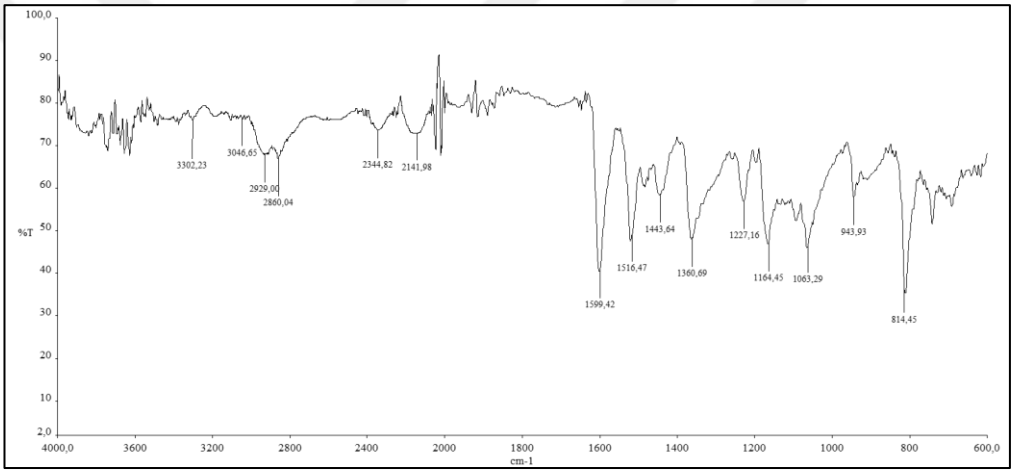

Figure A.47: FT-IR spectrum of compound **PcOAZn**.

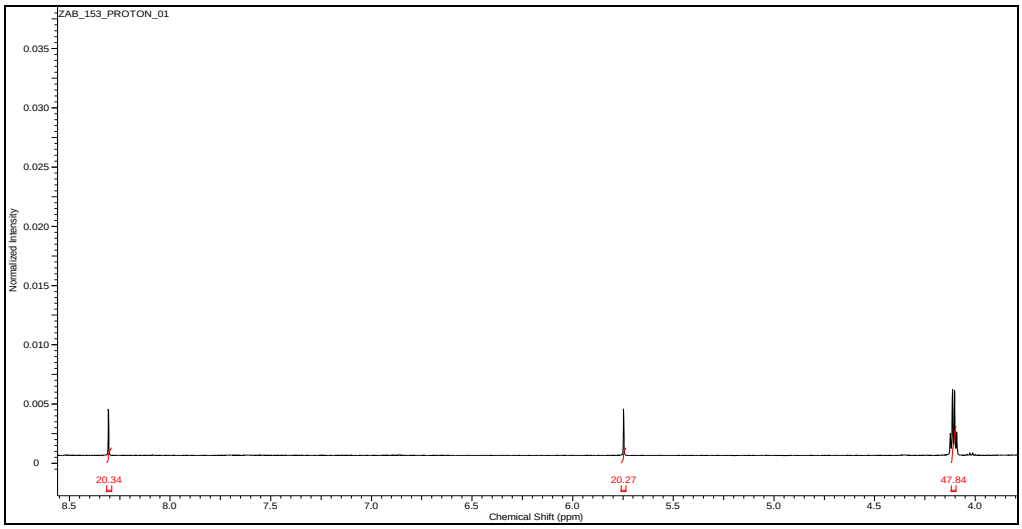

Figure A.48: ^{1}H-NMR spectrum of compound **PcOAZn**.

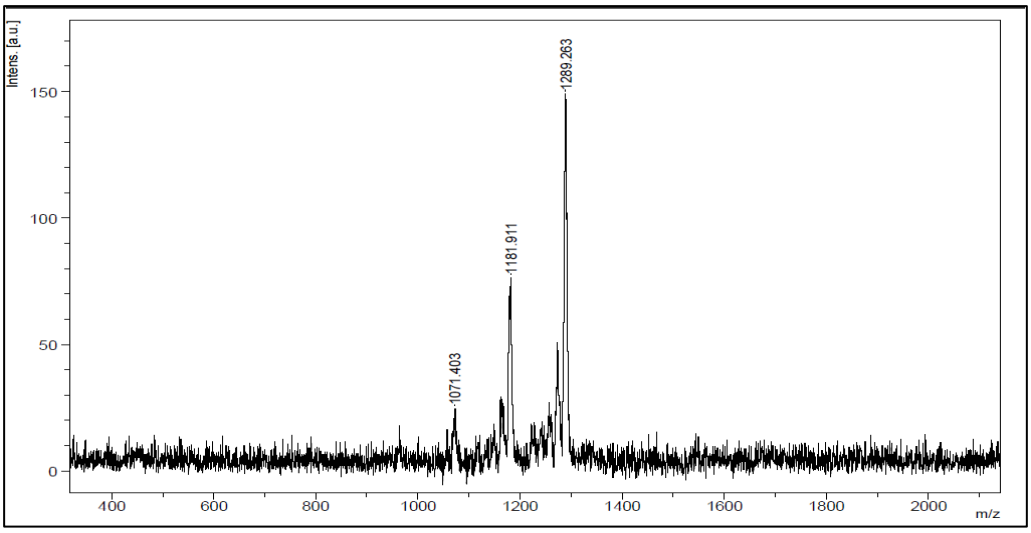

Figure A.49: Mass spectrum of compound **PcOAZn**.

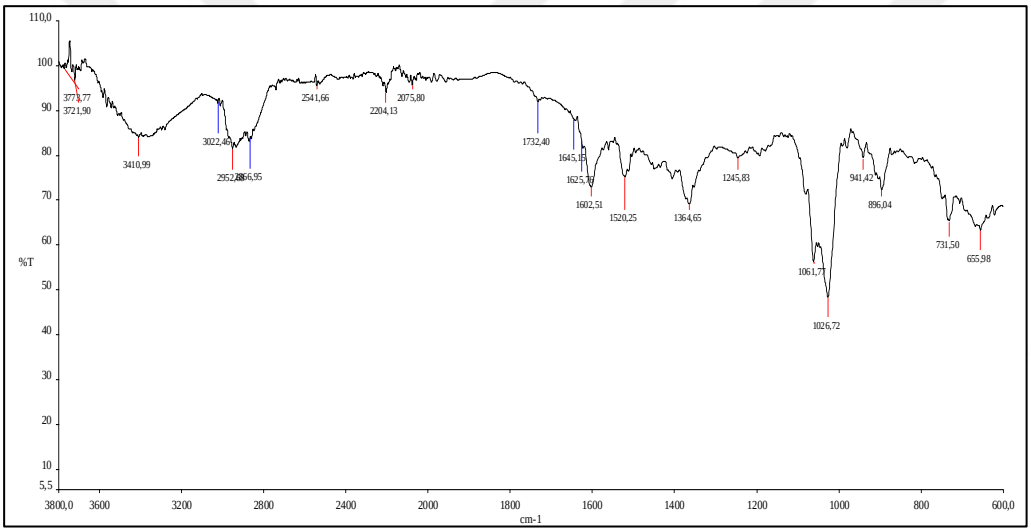

Figure A.50: FT-IR spectrum of compound **PcOALu**.

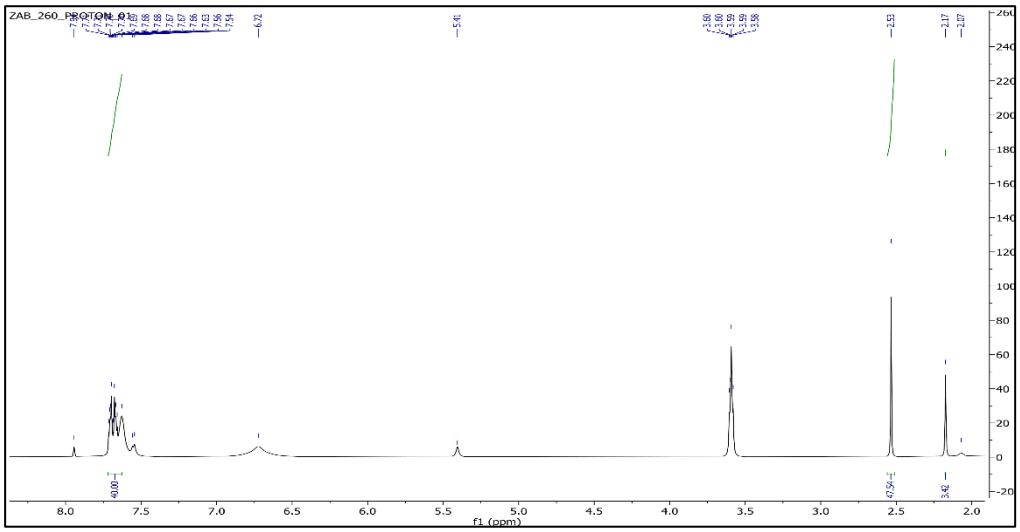

Figure A.51: ^{1}H-NMR spectrum of compound **PcOALu**.

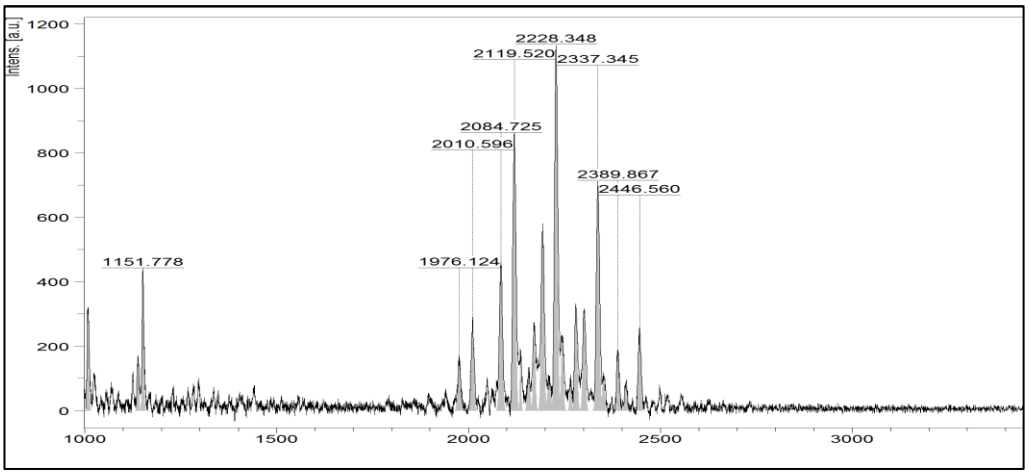

Figure A.52: Mass spectrum of compound **PcOALu.**

CURRICULUM VITAE

Name Surname **:** Javaria AFTAB

EDUCATION **:**

- **BSc.** **:** 2015, Lahore College for Women University, Chemistry
- **MSc.** **:** 2018, Istanbul Technical University, Lisansüstü Enstitüsü, Kimya

PROFESSIONAL EXPERIENCE AND REWARDS:

- 2019-2021 worked as a scholarship Ph.D. student in the TÜBİTAK project (Project no.: 118Z731) at Istanbul Technical University Research Laboratories.
- 2021-2022 worked as a scholarship Ph.D. student in the BAP project (Project no.: TDK-2021-42932) at Istanbul Technical University Research Laboratories

PUBLICATIONS, PRESENTATIONS AND PATENTS ON THE THESIS:

- **Aftab, J.,** Farajzadeh, N., Yenilmez, Y. H., Özdemir, S., Gonca, S., and Bayır, Z. A. New phthalonitrile/metal phthalocyanine–gold nanoparticle conjugates for biological applications, Dalton Trans., 2022, 51, 4466-4476, https://doi.org/10.1039/D2DT00041E
- Farajzadeh, N., **Aftab, J.,** Yenilmez, Y. H., Özdemir, S., Gonca, S., and Bayır, Z. A. The design and synthesis of metallophthalocyanine–gold nanoparticle hybrids as biological agents, New J. Chem., 2022, 46, 5374-5384, https://doi.org/10.1039/D2NJ00484D

OTHER PUBLICATIONS, PRESENTATIONS AND PATENTS:

- Rasheed, J., Jamil, A., Hameed, A. A., Aftab, U., **Aftab, J.,** Shah, S. A., and Draheim, D. A survey on artificial intelligence approaches in supporting frontline workers and decision makers for the COVID-19 pandemic, Chaos, Solitons & Fractals, Volume 141, 2020, 110337, ISSN 0960-0779,(SCIE, IF:3.764), https://doi.org/10.1016/j.chaos.2020.110337
- **Aftab, J.,** Kalaycıoğlu, Z., Kolaylı, Z., and Erim, F. B. Sample stacking–Capillary electrophoretic determination of nitrate and nitrite contents as nitric oxide

metabolites in honey varieties originated from Anatolia, Acta Alimentaria, Volume 50: Issue 4, 2021, https://doi.org/10.1556/066.2021.00125

- **Aftab, J.,** Kalaycıoğlu, Z., and Erim, F. B. A Capillary Electrophoresis Method for the Determination of Nitrate and Nitrite Contents in Anatolian Honeys (Oral Presentation). 26th-28th October, 2017, Konya/ Turkey, 4th International Turk Park Conference On Chemical Sciences